AN INTEGRATED FINITE ELEMENT ANALYSIS OF CFRP LAMINATES: FROM LOW-VELOCITY IMPACT TO CAI STRENGTH PREDICTION

CHRISTABELLE LI SIXUAN

B.Eng. (Hons.), NUS

A THESIS SUBMITTED

FOR THE DEGREE OF DOCTOR OF PHILOSOPHY

DEPARTMENT OF MECHANICAL ENGINEERING

NATIONAL UNIVERSITY OF SINGAPORE

2013

DECLARATION

I hereby declare that the thesis is my original work and it has been written by me in its entirety. I have duly acknowledged all the sources of information which have been used in the thesis.

This thesis has also not been submitted for any degree in any university previously.

Christabelle Li Sixuan

30 May 2013

ACKNOWLEDGEMENTS

Apart from Jesus, I can do nothing; yet I can do all things through Christ who strengthens me. (John 15:5, Philippians 4:13)

It has been my privilege and honor to be under the supervision of Prof. Tay Tong Earn throughout the course of my research. While knowledge is the prerequisite to being a professor, Prof. Tay has been one professor who is not only knowledgeable but who also abounds in wisdom, and I have gained a lot from him. Despite his busy schedule, he always has time for his students.

I would also like to extend my gratitude to the post docs and research students in the lab, particularly Ridha, Boyang and Zhou Cheng. I have the propensity for asking stupid questions, and they have the patience to hold countless discussions with me. This research would not have been possible without their help.

To my granddad-You were the one who taught a little girl that she could dream big dreams.

To my parents, especially my mum-Everyone needs someone who believes in them even when they stop believing in themselves, someone who understands them more than they could ever understand themselves, someone who encourages them in anything they choose to undertake, someone who loves them even when they're most unlovable. I'm blessed to have found that someone in you.

From one belle to the other-You're the ding to my dong. How could I have kept my sanity without having a sister to go crazy with and to laugh with, like we had not a care in the world?

To Benaiah-You are to me a great encourager, a constant support, a reliable companion, my best friend. Thank you for the patience and understanding you've extended to me throughout the years of research and months of thesis writing. I would not have been able to complete this thesis without you and the humor that you inject into every situation.

CONTENTS

PRESENTATION

Composites Durability Workshop (CDW-15)
Kanazawa Institute Technology, Kanazawa Japan
October 17-20, 2010

SUMMARY

Carbon fiber-reinforced plastic (CFRP) laminates have gained increasing usage especially in the aerospace industry due to its high strength and stiffness, coupled with its lightweight properties. In the 1980s, only 3% by weight of the Boeing 767 was made of CFRP. Today, this percentage has increased to 50% in the Boeing 787. Some modern military aircrafts contain 70% by weight of CFRP.

In the assessment of damage tolerance of a composite structure, the most critical source of damage has to be considered. Low-velocity impact that could be caused by dropped tools or runway debris has been found to be the most critical source of damage in composite laminates due to a lack of fiber reinforcement in the out-of-plane direction. Low-velocity impact loading is considered to be potentially dangerous because it causes Barely Visible Impact Damage (BVID) on composite materials such as embedded matrix cracks, delaminations and fiber failure. Such impact damage has been found to affect the residual compressive strength to the greatest extent due to buckling in the delaminated areas. As such, Compression After Impact (CAI) strength is of particular concern, and is adopted by industries to be an important measure of damage tolerance of composite materials.

Extensive experimental research has been performed on the topic of low-velocity impact of CFRP laminates and its consequent CAI strength. Industries have also integrated FE simulation into part of their design process in order to minimize design costs and to achieve higher efficiency, thereby promoting extensive Finite Element (FE) analyses that have been performed to study the damage pattern on CFRP laminates arising from low-velocity impact, and to predict the CAI strength of impact damaged composites. The impact event and CAI test are two separate topics, often studied separately. In FE simulation models aimed at predicting the

resultant CAI strength due to low-velocity impact damage, a very approximate damage is usually pre-modeled into the FE model, neglecting matrix cracks and fiber failure. However, experimental studies have shown that the reduction in compressive strength due to impact damage is caused not solely by delaminations, but a complex interaction of matrix cracks, fiber breakage and delaminations. It is hence evident that there still exists a gap between experimental findings and the current capability of accurately emulating the findings in a computational model.

With the purpose of bridging this existing gap, the overarching aim of this research is to devise an integrated FE simulation for the prediction of impact damage initiation and progression due to low-velocity impact and subsequently predict the residual CAI strength using the same damaged model. Such an integrated approach has the potential to be developed into a convenient design tool into which design engineers can input both the impact and composite plate parameters, and obtain the CAI strength value.

This research is conducted in three stages:

Stage	Objectives
I: Low-velocity impact	To build a finite element model for the prediction of impact damage initiation and progression. The finite element model is validated by comparison with experimental results obtained from literature.
II: CAI test	To build a finite element model with pre-included damage (including both delaminations and matrix cracks) for the prediction of residual CAI strength from a given damage pattern.
III: Integrated approach	To integrate stages I and II into a single FE simulation such that CAI strength can be predicted directly from the impact damaged model, without having to pre-include an approximate damage for the purpose of CAI strength prediction.

Overview of Research

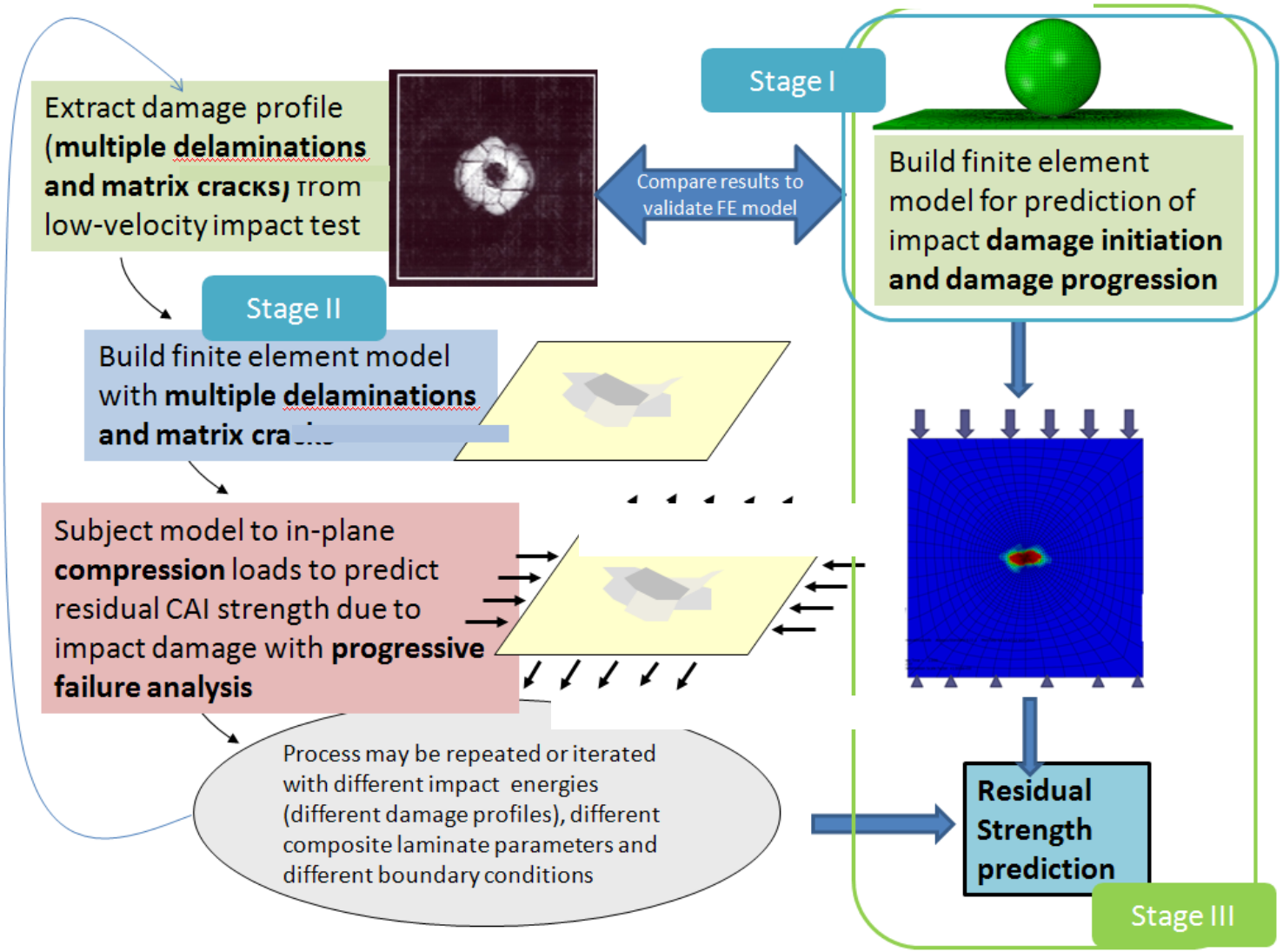

Figure 1 Overview of research

LIST OF FIGURES

LIST OF TABLES

LIST OF SYMBOLS

E_1, E_2, E_3	Young's moduli
G_{12}, G_{13}, G_{23}	Shear moduli
G_{fc}^{+}	In-plane fracture toughness in fiber direction under tension
G_{fc}^{-}	In-plane fracture toughness in fiber direction under compression
G_{mc}	Mixed-mode fracture energy
G_{nc}	Mode I critical fracture energy
G_{sc}	Mode II critical fracture energy
K_{nn}, K_{ss}, K_{tt}	Cohesive elements stiffnesses
N	Normal strength of cohesive elements
S	Shear strength of cohesive elements
$S_{12}, S_{13}, S_{23},$	Shear strength
T	Effective traction of cohesive elements
T_o	Original thickness of cohesive elements
X_C	Compressive strength in the fiber direction
X_T	Tensile strength in the fiber direction
Y_C	Compressive strength in the transverse direction
Y_T	Tensile strength in the transverse direction
d_f	Degradation factor for fiber dominated damage
d_m	Degradation factor for matrix dominated damage

d^{inst}	Instantaneous values of the degradation factors
$\delta_n, \delta_s, \delta_t$	Displacement components for cohesive elements
ϵ_{ij}	Strain components
ϵ_{eff}	Effective strain
ϵ^o	Strain at onset of failure
ϵ^f	Strain at final failure
$\epsilon_n, \epsilon_s, \epsilon_t$	Strain components of cohesive elements
l_c	Characteristic length of an element
$\boldsymbol{\eta}$	Material parameter in the B-K criterion
σ_{ij}	Stress components
σ_{eff}	Effective stress
t_n	Normal traction for cohesive elements
t_s , t_t	Shear tractions for cohesive elements
$\nu_{12}, \nu_{13}, \nu_{23}$	Poisson's ratios

CHAPTER 1

INTRODUCTION

Carbon Fiber Reinforced Plastics (CFRP) have found increasing applications in light-weight structural members, in fields of aerospace, automobile and marine due to their high performance index such as their high strength-to-weight and stiffness-to-weight ratios. CFRPs are significantly lighter than aluminum, yet they can be as strong and as stiff as steel. However, the damage mechanisms of FRP are still not very well understood.

The main inhibiting factor that prevents the use of CFRPs from being more prevalent in industries is its susceptibility to impact damage due to low-velocity impact. The likelihood at which the body of an aircraft is exposed to low-velocity impact is very high, because low-velocity impact can be caused by seemingly trivial events such as the dropping of tools on the body of the aircraft during maintenance or by the impact of runway debris during takeoff or landing. Barely visible impact damage (BVID) arising from the low-velocity impact of CFRPs, namely matrix cracks, fiber breakage and delaminations interact with each other, leading to the complex nature of damage mechanisms in CFRP. It is known that BVID will cause a significant reduction in compressive strength of the composite [1, 2]. Industries have thus adopted compression after impact (CAI) strength as a consideration in designing composite structures. With the increasing popularity of CFRP in industries, it is imperative that we predict the CAI strength of impact damaged composites as accurately as possible.

Many experimental studies have been performed over the years with the common goal of better understanding the impact and CAI behavior of FRP [3-8]. These experimental studies have formed the basis of our current understanding of impact behavior, including the impact-damage characterization and the resulting impact-induced reduction of compressive strength. It is from this basis that numerical, analytical and finite element analyses are formulated with the aim of CAI strength prediction [2, 9-11].

Industries have integrated simulation into part of their design process in order to minimize design costs and to achieve higher efficiency, thereby promoting extensive studies that have been performed to better predict the CAI strength of impact damaged composites. These studies have contributed to the knowledge base of CAI strength prediction. The difficulty in modeling low-velocity impact on composite plates and its residual CAI strength prediction arises from the complexities of low-velocity impact damage. For the same incident energy, different combinations of impactor mass and velocities can have different effects on the impact response [12]. Furthermore, different sizes and layups of the composite plates would display different damage patterns. The differences in damage patterns in turn lead to differing residual compressive strength, or CAI strength.

To the author's knowledge, there is currently no CAI strength prediction model that allows for the user to obtain a predicted CAI strength value by specifying the impact energy, together with the composite laminate parameters and boundary conditions. In most CAI strength prediction models, the impact damage as observed from impact tests has to be manually included into the model. Through such a process, some damage details are inevitably lost. For example, in most CAI strength prediction efforts, only delaminations are modeled. Delamination growth is assumed to be the sole cause of compressive strength reduction on the account that delamination is the dominant damage mode causing compressive failure [10, 13-15].

Furthermore, the delaminations modeled are generally assumed to take on simple circular or elliptical shapes. However, it has been found through experimental studies that the reduction of compressive strength due to impact damage is not caused solely by delamination, but by a complex interaction of matrix cracks, fiber breakage and delamination [16-20]. Studies investigating the interaction between the different damage modes resulting from impact are also relatively scarce.

1.1 Objectives of study

Although extensive experimental results exist to contribute to our current understanding of low-velocity impact damage and CAI behavior, there still exists a gap between experimental findings and the current capability of accurately emulating the experimental findings in a computational model.

With the motive of bridging this existing gap, the overarching aim of this research is to devise an integrated FE simulation for the prediction of impact damage initiation and progression due to low-velocity impact and subsequently predict the residual CAI strength using the same damaged model. The main rationale guiding this research is to avoid over-simplification of the finite element models such that the predictions obtained are inaccurate, yet also to avoid having to model to an impractical and excessive level of accuracy such that the method loses its efficiency.

With this main objective in mind, the research is broken down into three stages, each stage bearing its own objective leading towards the main objective:

Stage	Objectives
I: Low-velocity impact	To build a finite element model for the prediction of impact damage initiation and progression. The finite element model will be validated by comparison of the FE results with experimental results obtained from literature. An FE model capable of accurately predicting the impact damage sequence and extent of damage for different impact and composite laminate parameters is crucial for the accurate prediction of residual CAI strength.
II: CAI test	To build a finite element model with pre-included damage (including both delaminations and matrix cracks) for the prediction of residual CAI strength from a given damage pattern.
III: Integrated approach	To integrate stages I and II into a single FE simulation such that CAI strength can be predicted directly from the impact damaged model, without having to pre-include an approximate damage for the purpose of CAI strength prediction

1.2 Chapters overview

Chapter 2 of this thesis covers the background knowledge required in this research, including the definitions of low-velocity impact and BVID, impact damage mechanisms of CFRP, and a literature review of selected studies relating to low-velocity impact and CAI strength prediction. Chapter 3 details the finite element model formulated for this research. The chapter starts with a brief review of selected failure criteria and damage modeling techniques available, followed by a description of the modeling strategy adopted in the finite element model formulation of this research.

Chapter 4 presents stage I of the research, where the finite element model is used to simulate low-velocity impact and to study low velocity impact damage initiation and progression. The purpose of this stage of the research is to predict the impact damage sequence and the locations, sizes and shapes of delaminations, matrix cracks and fiber failure as observed in experiments to an acceptable accuracy. Additionally, results from the various parametric studies conducted to investigate the influence of parameters such as ply thickness and ply angle variation on impact damage are presented in this chapter.

Chapter 5 presents stage II of the research, where damage due to low-velocity impact is approximately pre-modeled into the finite element model for the prediction of residual CAI strength. In this study, a combination of two different damage modes, namely matrix cracks and delaminations were included, and different damage shapes, sizes and locations were pre-modeled into the finite element model. The purpose of this stage of the research is to determine the dominant damage modes that have an influence on the residual CAI strength. To confirm the efficacy of this modeling technique, damage patterns of an impacted composite plate as observed from an experimental study were also modeled into the finite element model, and the

residual strength obtained from the finite element simulation was compared with the experimental value.

Chapter 6 details the integrated approach in which CAI strength is predicted using the exact damage information obtained from the finite element simulations of low-velocity impact. Finally, chapter 7 presents the conclusions of the research and recommendations for future direction of research.

CHAPTER 2

BACKGROUND OF RESEARCH AND LITERATURE REVIEW

As stated in chapter one, the overarching aim of this research is to devise an integrated FE simulation for the prediction of impact damage initiation and progression due to low-velocity impact and subsequently predict the residual CAI strength using the same damaged model. In the first portion of this chapter, the background information required for this research is expounded. Such background information includes the definition of various important terms involved in this research such as "low-velocity impact" and "barely visible impact damage (BVID)", the various low-velocity impact damage mechanisms in CFRP materials and the importance of CAI strength as a damage tolerance measure.

It has also been stated in chapter one that the main rationale guiding this research is to avoid the over-simplification of the finite element models such that the predictions obtained are inaccurate, yet also to avoid having to model to such an impractical and excessive level of accuracy such that the method loses its efficiency. To achieve this, a good understanding of the different computational modeling methods for low-velocity impact tests and CAI tests of CFRP materials adopted by other researchers is necessary. The second portion of this chapter contains a literature review focusing on the computational modeling of low-velocity impact tests and CAI tests.

2.1 Background

2.1.1 Fiber-Reinforced Composites

Structural materials are generally divided into four basic categories- metals, ceramics, polymers and composites. Composite materials consist of at least two constituent materials from the other three categories combined in a macroscopic structural unit. Composites are advantageous because they demonstrate desirable properties that are not achievable by either of their constituent materials acting alone [21]. However, the presence of two constituent materials having different material properties causes the material property of the composite laminate to be dependent on the direction and location of its individual plies, rendering it anisotropic and inhomogeneous unlike typical materials such as metals.

A common example of composite materials is the Fiber Reinforced Plastic (FRP), which is made of reinforcing fibers embedded in a matrix material. The material of focus in this study is polymer-matrix composite laminates reinforced by unidirectional carbon fibers, also known as Carbon Fiber Reinforced Plastics (CFRP).

CFRP has found widespread application especially in the aerospace industry, but the main concern of aircraft designers and airworthiness regulators is usually impact damage in the composite airframe components because of the high likelihood at which the body of an aircraft is exposed to low-velocity impact such as bird strikes or ice impacts during its flight and the impact of runway debris during takeoff or landing. During the maintenance of the aircraft, tool drops are also a source of low-velocity impact. Figure 2 provides the impact energy levels for a variety of different dropped tools.

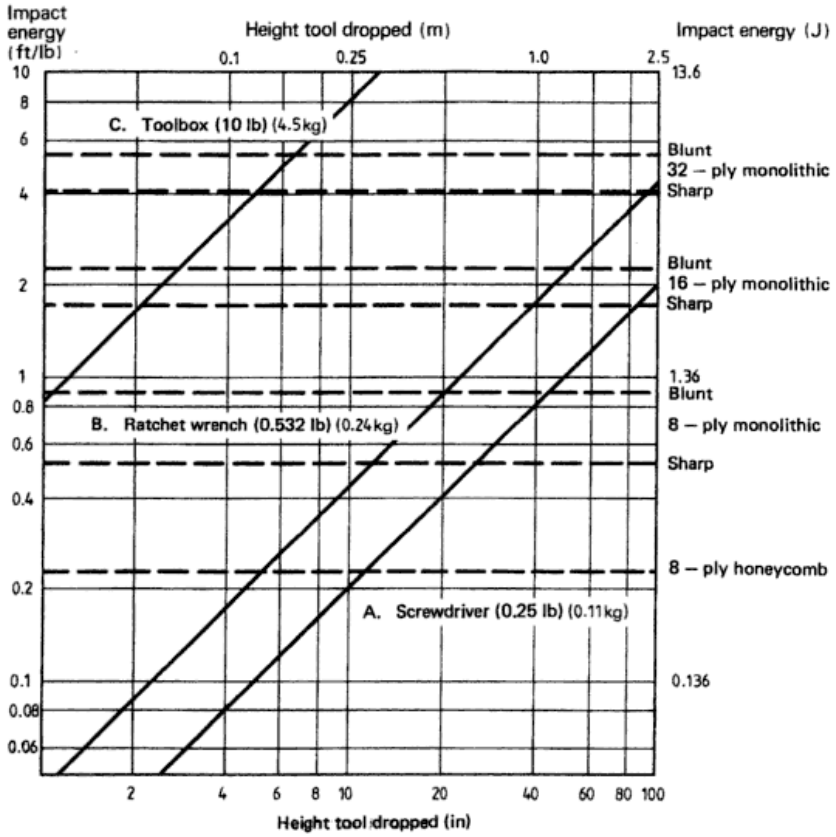

Figure 2 Impact energy of dropped tools [22]

In order for engineers to design the components of the airplane such as the fuselage or the wing in a manner that makes use of CFRP efficiently, it is important that the failure mechanism of CFRP under low-velocity impact loading is relatively well understood.

Low-velocity impact is not a threat to metal structures due to the ductile nature of metals allowing for large amounts of impact energy to be absorbed. When metals are impacted at lower incident energies, the energy is absorbed through both elastic and plastic deformation. The resultant permanent structural deformation has relatively insignificant effect on the load-carrying capability of the metal component because the local work-

hardening is increased [23, 24]. Low-velocity impact is, however, a threat to brittle composite materials, causing barely visible impact damage (BVID) in the composite materials. When composite materials are subject to impact, the incident impact energy is absorbed mainly via elastic deformation and their various damage mechanisms, but not plastic deformation. The damage mechanisms such as matrix cracks, delaminations [25] and fiber fracture significantly reduce the strength and stiffness of the damaged composite structure. As such, low-velocity impact can cause the compressive strength of the CFRP laminate to be severely compromised.

Figure 3 shows the strength comparisons between aluminum alloy and CFRP laminates. As seen in the comparison, the out-of-plane tensile strength obtained from unidirectional tensile tests in the out-of-plane direction of CFRP laminates is drastically lower than that of aluminum alloy, rendering low-velocity impact a threat to CFRP laminates.

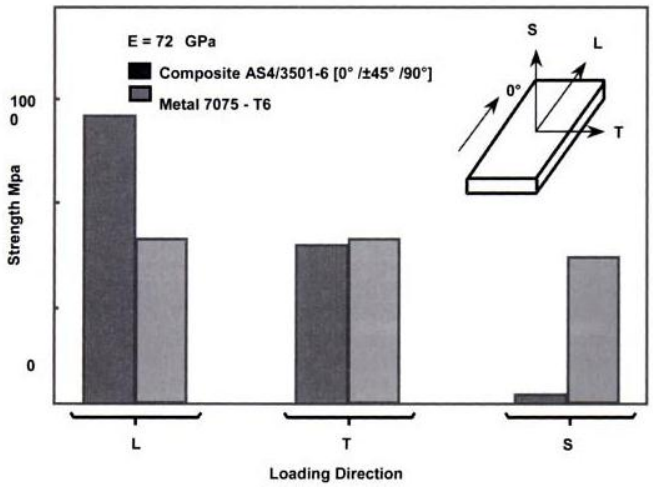

Figure 3 Comparisons of tensile strength obtained from unidirectional tensile tests of aluminum alloy and CFRP laminates in three different loading directions- S, L and T, as depicted in the figure [22]

The low-velocity impact damage mechanisms of composite materials are interdependent on each other. The various damage modes interact with each other, causing the prediction of post-impact load-bearing capability to be a challenge. Unlike impact on metals, where damage due to the impact is easily detected on the impact surface, impact on CFRP induces damage on the non-impacted face and internally in the form of delamination between plies. Such Barely Visible Impact Damage (BVID), which occurs in composite materials, can severely degrade the structural integrity of the composite structure.

Different ways of determining the occurrence of BVID can be found in literature. This is because visibility is difficult to quantify since it is dependent on variables such as light conditions and the differences in human perception [22]. Boeing [26] has defined BVID to be small damages that may not be discovered during heavy maintenance, where general visual inspections using typical lighting conditions takes place from a distance of five feet. Such BVID is noted to have a typical dent depth of 0.01 to 0.02 inches (or 0.254 to 0.508mm). Baker [22] described BVID as damage with indentations of up to 0.1mm, while de Freitas [27] determined that in BVID, indentations of up to 0.3mm can be accepted. In general, BVID is a term used to refer to damage that is embedded within the composite laminate such as interply delaminations and matrix cracks, and can be loosely defined as damage occurring in low-velocity impact cases where there is a significant loss in laminate strength even though damage is not clearly visible.

2.1.2 Low-Velocity Impact

During a typical low-velocity impact, the impactor velocity at the point of impact is gradually reduced as its movement is opposed by the deforming composite specimen. This deceleration is associated with a reaction force on the impactor. The kinetic energy is transferred to the laminate and temporarily stored as elastic strain energy. If the local strength of the material is reached, part of this energy starts to be dissipated through irreversible damage. The impactor velocity is reduced to zero as the penetration reaches a maximum, and thereafter the major part of the accumulated elastic strain energy is transferred back to the impactor. The impactor accelerates away from the specimen at an energy lower than the impact energy. Part of the accumulated energy is kept in the form of panel vibrations and eventually dissipated by damping. Another part corresponds to the energy dissipated by material damage, namely matrix cracks, delaminations, fiber fracture and total peforation.

Low and high velocity impact have been observed to induce different structural responses in the composite material [28]. In low-velocity impact, the contact duration between the projectile and the target are long enough to cause the whole structure to respond to the impact. This enables kinetic energy to be accommodated at points well away from the point of impact. Hence, the geometrical configuration of the target would determine its energy-absorbing capability. On the other hand, high velocity impact loading induces a more localized form of target response, since its relatively short duration does not allow for the material to have sufficient time to respond in flexural or shear modes. This results in the dissipation of energy over a comparatively small region, with the main consideration being whether complete penetration occurs[29].

There are various definitions of low-velocity impact found in literature. Cantwell et. al. [23] classified any impact velocity lower than

$10ms^{-1}$ as low-velocity impact, taking into consideration the typical test techniques used to simulate the low-velocity impact event such as the instrumented drop-weight test, the Charpy pendulum and the Izod test. Abrate [30], however, determined that low-velocity impact occurs at impactor speeds of less than $100ms^{-1}$. Other researchers such as Liu et. al. [16] suggest that impact should be classified according to the type of damage incurred, especially when damage is of utmost concern. They hence defined low-velocity impact as one in which no penetration occurs in the specimen such that damage is dominated by matrix cracks and delamination rather than fiber fracture. On the other hand, Soutis et. al. [2] noted that low-velocity impact results in both delamination and fiber fracture.

Mishra et. al. classified impact into two broad categories- boundary-controlled impact and wave-controlled impact [12]. In boundary-controlled cases, the time of contact between the projectile and the target are relatively long and the whole structure responds, enabling kinetic energy to be accommodated at points away from the impact point. The contact time is much longer than the period of lowest vibration mode, and the entire plate is deformed during the impact. The contact force and plate response are in phase. Boundary-controlled cases are named as such because the geometrical configuration of the target would determine its energy absorbing capability. Boundary-controlled cases may be analyzed using quasi-static methods. In wave-controlled cases the plate response is more localized, resulting in energy dissipation over a comparatively small region. The contact force and plate response are not in phase and the plate deformation is localized to a region around the impact point. Such response is dependent on impactor velocity and mass, and plate dimensions and properties. In other words, according to Mishra et. al. [12], boundary-controlled cases result from low-velocity impact while wave-controlled cases result from high-velocity impact.

However Mishra et. al. did not indicate the range of impact velocities that would give rise to these two categories of impact.

In this present research, the definition of low-velocity impact as stipulated by Mishra et. al. [12] is adopted. Low-velocity impact is considered to be quasi-static, and impact tests are simulated in this research by prescribing a displacement instead of a velocity to the impactor in the FE model. In adopting Mishra's definition of low-velocity impact, the definition by Liu et. al. [16] is indirectly adopted as well, because damage induced by quasi-static load has been observed to be dominated by matrix cracks and delaminations rather than fiber fracture.

2.1.3 Low-velocity impact damage mechanisms

Failure in composite materials is an ill-defined term, because composite materials usually undergo various local failures before final rupture into two or more distinct parts. The initiation of failure, also known as 'first failure' in composite laminates, does not necessarily correspond to 'final failure' as there can be failure accumulation within the composite laminates before final failure occurs. The local failures occuring within the composite laminates before final failure is usually refered to as 'damage'.

The internal damage, or BVID, that is caused by low-velocity impact on composite laminates generally consists of two types at the micro level, namely interlaminar damage, also known as delaminations, and intralaminar damage. Intralaminar damage, which refers to damage within a single ply, can further be subdivided into two categories: Intralaminar damage between fibers such as matrix cracks and intralaminar damage involving fiber fracture [31]. There is generally no penetration of the composite laminate under low-velocity impact.

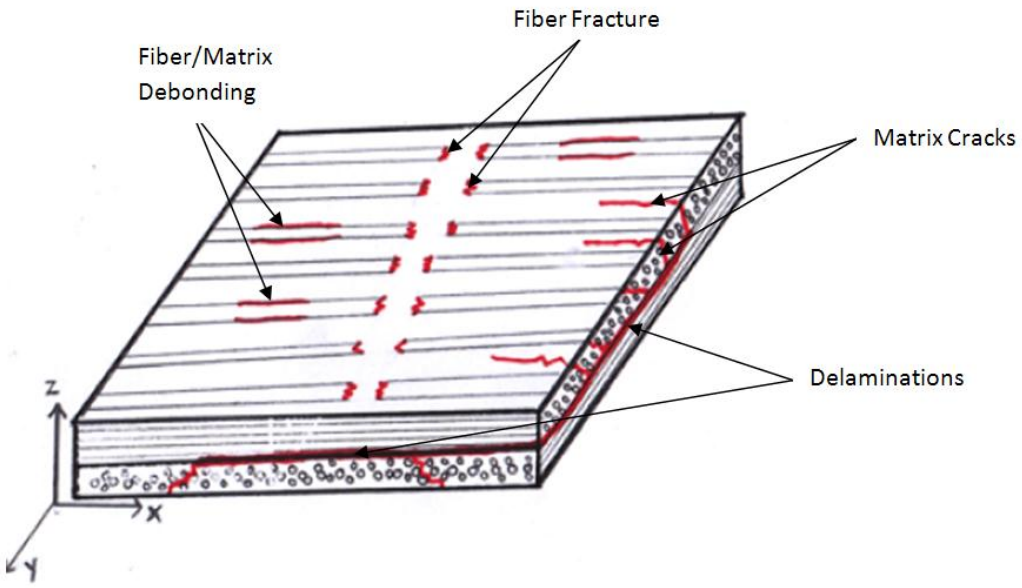

Figure 4 3D representation of damage mechanisms

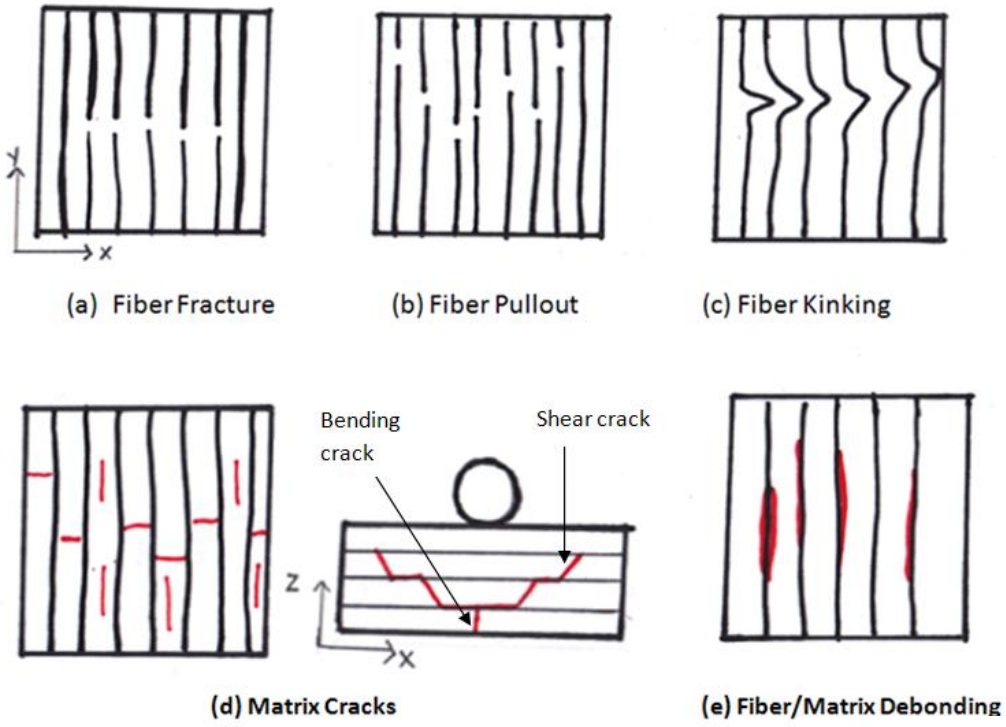

Figure 5 2D representation of damage mechanisms

Fiber fracture, or the breaking of a continuous fiber into two or more distinct parts (Figure 4 and Figure 5a), is the most severe of all failure mechanisms with the potential of leading to catastrophic failure. This is because in composite laminates, fibers typically act as the primary load-carrying component. Fiber fracture is caused when the fracture strain limit of the fiber is reached. It can occur under tensile loading, when the maximum allowable tensile stress or strain of the fiber is exceeded. Under compressive loading, fiber micro-buckling, crushing or kinking occurs. The critical buckling stress of a fiber embedded in a matrix is found to be influenced by the properties of the fiber and the matrix, which provides lateral support to the fiber [21].

Fiber pullout (Figure 5b) is observed when fiber fracture occurs simultaneously with fiber/matrix debonding. Fiber kinking (Figure 5c) has been observed to be initiated by local microstructural defects like fiber misalignments and longitudinal cracks (matrix and interfacial cracks). An initial fiber-misalignment will trigger failure due to further rotation of the fibers during compressive loading [32]. Kink bands induce high shear stresses in the matrix phase. In composite materials with high fiber-volume-fraction, kink band formations are normally the failure mechanism involved in compressive failure due to stress in the fiber direction [17].

Under low-velocity impact, fiber failure occurs much later in the damage progression as compared to matrix cracking and delamination. Fiber failure tends to be observed right under the impactor on the impact face, and is caused by the high local stresses and indentation of the impact face. Failure in the fiber mode is the precursor to catastrophic failure by penetration.

In low-velocity impact where the impact energy is low, matrix cracks are usually observed to be the first failure mechanism to occur. Fiber/matrix debonding is sometimes observed to be the first failure mode in low-velocity impact as well. The polymer matrices used in CFRP are usually brittle; they undergo a limited deformation before fracture and hence absorb an insignificant amount of impact energy.

Matrix cracks (Figure 4 and Figure 5d) occur in planes parallel to the fibers within unidirectional layers [33] when the strength of the matrix is exceeded. They can be caused by tension, compression or shear. Matrix cracks can also be caused by stress concentrations at the fiber-matrix interface due to a mismatch in mechanical properties between the matrix and fiber, which leads to fiber-matrix debonding (Figure 4 and Figure 5e).

Matrix cracks resulting from low-velocity impact can be classified into bending cracks and shear cracks, named after the dominant stress causing the cracks [34]. Shear matrix cracks form in the upper and middle layers of the composite laminate under the edges of the impactor due to the high transverse shear stress through the laminate. As seen in Figure 5d, these cracks are inclined at an angle of approximately 45^0. Bending cracks form on the bottom layers due to the high tensile bending stresses and, as seen in Figure 5d, are typically vertical.

The stiffness of the laminate plays an important role in the way damage due to impact develops [18], as it is an important parameter controlling the mode of matrix fracture of the composite laminate. Under low-velocity impact, a more flexible structure such as long and thin specimens will tend to respond by bending. This produces high tensile stresses in the lower plies, leading to the formation of bending cracks in the lower layers, as depicted in Figure 6a. On the other hand, for a stiffer structure such as short and thick specimens, damage occurs mainly as

transverse shear cracks near the impact surface due to high contact stresses, as shown in Figure 6b.

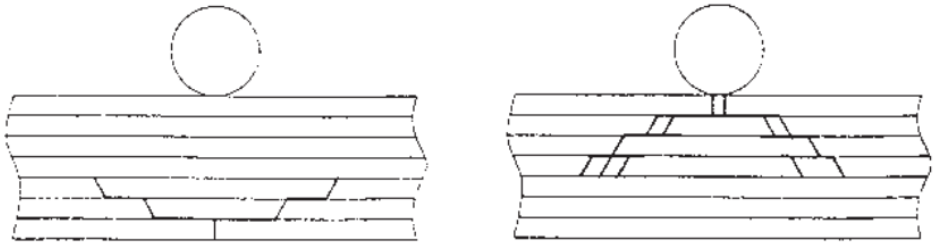

(a) (b)

Figure 6 Matrix cracks development in (a) flexible and (b) rigid structures [18]

Delaminations, as shown in Figure 4, are cracks that occur preferentially within the resin-rich layer between plies of different fiber orientations due to a bending stiffness mismatch at the ply interface. Their planes lie parallel to the surface of the structure. Generally, they do not occur between plies of the same fiber orientation [18, 35, 36]. Composite laminates are particularly susceptible to delamination as a form of failure when subject to external loads that generate high through-thickness shear and normal stresses, such as low-velocity impact, because of their weak interlaminar strengths [37]. Delamination can absorb a significant amount of impact energy, and from experiments conducted, it has been established that the delamination areas are influenced directly by impact energy [27, 38-40].

Bouvet et al. [41] reported the physical explanation for the interaction between matrix cracks and delamination proposed by Renault. Renault suggested that the development of matrix cracks is a precursor to the development of delaminations. To illustrate the explanation proposed by Renault, a [-45/0/45] layup, which is not representative of an entire laminate but can be part of any laminate layup, is presented in Figure 7. In each

composite ply, matrix cracks would initiate and propagate along the fiber direction. This would lead to the creation of disjointed strips in each composite ply as seen in Figure 7(b). Under impact load in the thickness direction of the composite laminate, the disjointed strips would be displaced in the thickness direction as well. The displacement of the disjointed strips would lead to an interlaminar zone of tension stress at interfaces of plies with differing orientations, and delaminations would form within these zones. As clearly illustrated in Figure 7, the zones that are susceptible to the formation of delaminations are triangular in shape at interfaces in which the fiber orientations change by 45^{o}, and the direction of propagation follows the fiber direction of the ply below the interface, away from impact face. This idea has been widely accepted and adopted [29, 42].

Another widely accepted explanation for the matrix crack and delamination interaction is reported by Nguyen et. al. [18]. When a matrix crack propagating through a ply reaches the ply interface where the orientation of the adjacent ply is different, the crack is arrested. High shear stress in the matrix causes the crack to start growing along the ply interface, resulting in delamination [18]. It has been observed that delamination only occurs in the presence of a matrix crack. The results obtained from the modeling work done during the course of this research concur with the explanation reported by Nguyen et. al. but not the explanation proposed by Renault. The FE results showed that delamination was initiated due to high shear stresses, while 'zones of interlaminar tension stress' as proposed by Renault was not observed.

In low-velocity impact damage, the size and locations of the external matrix cracks would provide a good gauge of the size and location of the internal delaminations. This is because in general, the size and locations of the internal delaminations would correspond to that of the external matrix cracks.

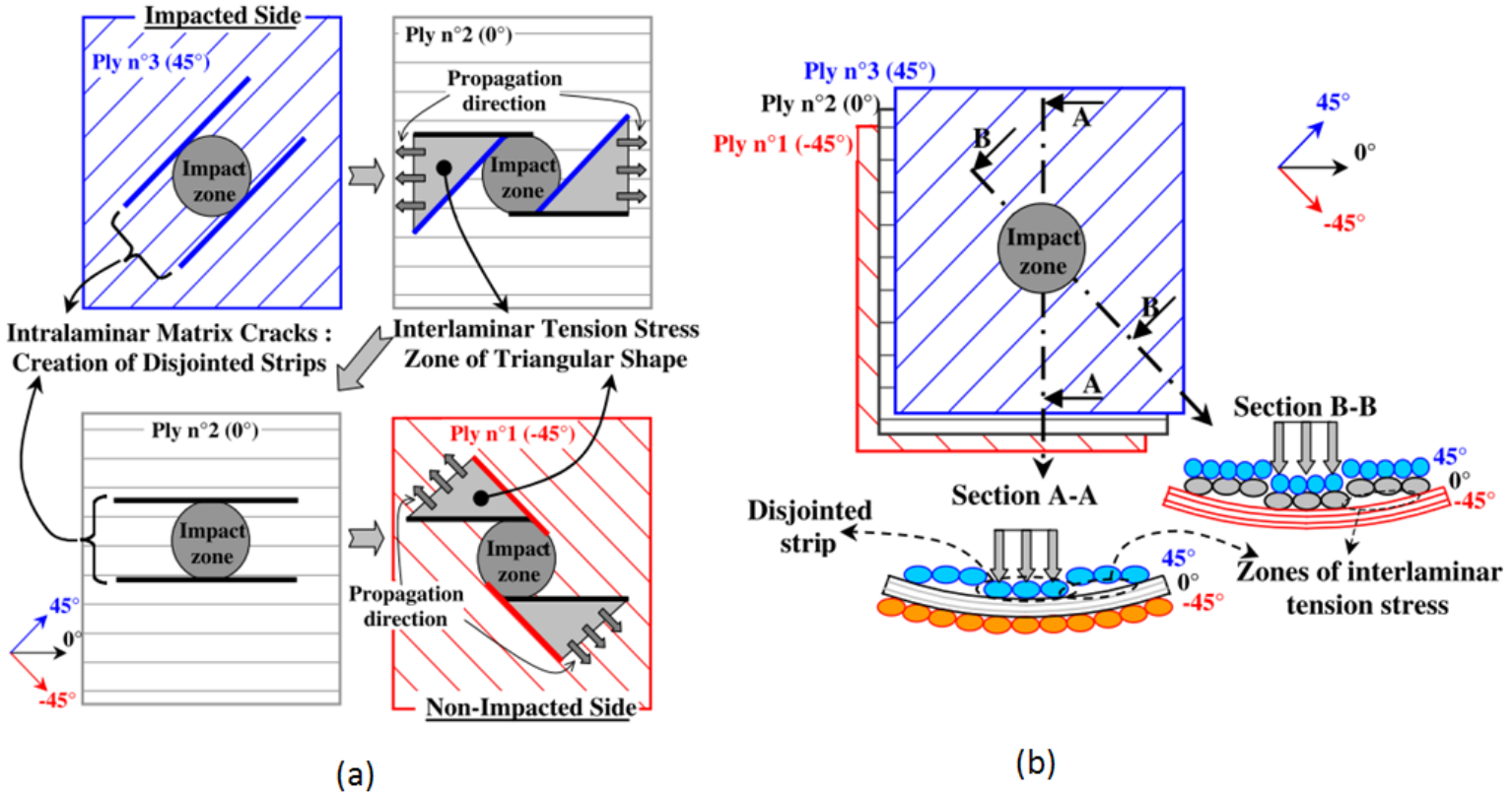

Figure 7 (a) Delamination formation mechanism and (b) interface tension stress zones, obtained from [41]

2.2 Literature Review

The low-velocity impact event and CAI test are two separate topics, often studied separately. Damage resistance of a material can be defined as the ability of the material not to undergo a permanent change due to a loading event [33], while damage tolerance relates to the capacity of the material to maintain its function after a permanent change has occurred in the material [43]. In the assessment of the damage tolerance of a composite structure, the most critical source of damage has to be considered. Localized low-velocity impact has been found to be the most critical source of damage in composite laminates, inducing delaminations within the laminates that can cause reductions in the residual compressive strength of up to 65% of the undamaged compressive strength [44]. Compression After Impact (CAI) strength is thus of particular concern, and is an important measure of the damage tolerance of composite materials.

The damage tolerance assessment of composite material generally involves two main steps [45]. First, the tolerance assessment of composite materials starts with a damage generation and characterization process, usually achieved through performing impact tests and damage characterization methods which includes destructive deply and cross-sectional microscopy techniques, and non-destructive methods such as ultrasonic scanning. The second step of the tolerance assessment of composite materials involves a determination of the residual compressive strength of the impact-damaged laminates, or the CAI strength. In studying the low-velocity impact event, the impact damage characterization requires a variety of information such as the through-thickness location and distribution of matrix cracks, delaminations, fiber fracture and their respective shapes and sizes [46-48]. These characteristics are dependent on parameters such as the diameter, mass and incident velocity of the impactor and the dimensions, stacking sequence and boundary conditions of the

laminates [12, 49-51]. In the determination of the CAI strength, the compressive behavior of thin laminates is generally characterized by prebuckling, buckling and finally post-buckling, with impact damage affecting the behavior of the composite laminate under compression. Both the low-velocity impact damage characteristics and the response of the composite laminate under compressive load would affect the damage tolerance of the composite laminate.

2.2.1 Studies on low-velocity impact damage

Many researchers have contributed to the extensive studies performed on the topic of low-velocity impact of CFRP laminates. Due to the complex failure modes that exist in composite structures, extensive testing of CFRP structures is necessary, taking into consideration different parameters such as loading conditions and geometry of the structure. There are various disadvantages of experimental testing of CFRP structures. The extensive testing required before a component can be certified safe would lead to exorbitant costs. Davies and Ankersen [52] approximated that the cost of structural testing would add up to approximately $40 million for a new aircraft variant. Such extensive experimental testing is also arduous. Experimental testing has its limitations, such as the inability to capture the internal impact damage progression, which is important in BVID.

To supplement experimental testing, researchers have turned to analytical and numerical modeling. There are numerous papers published on analytical studies for impact damage [53-56]. However, the complexity of the low-velocity impact event, which includes loading, contact, friction, damage followed by failure often results in the oversimplification of analytical models. Analytical solutions are thus generally formed for particular impact cases where variables such as impactor size, boundary conditions or plate

geometries have to be fixed, rendering the analytical solution strategy to be a very limited one [28].

The numerical modeling approach is an approach that can be used to supplement experimental testing and provide insight into the mechanisms of damage. FE analyses that are based on accurate constitutive models have been deemed to be the method able to provide the most detailed information on the damage distribution throughout the impact process [57]. As such, numerical modeling, such as finite element analysis, has become a widely adopted approach in both industrial and research environments. Researchers can choose from a selection of commercially available finite element codes such as Abaqus/Standard, Abaqus/Explicit and LS-Dyna to study the topic of impact damage of composite materials. Such codes have the capability to deal with a wide range of contact problems and allow for the implementation of user defined subroutines which can be customized for various applications [28]. This is an important capability because the accuracy to which impact damage can be predicted is dependent on the material model which controls the extent of damage, energy absorbed, stiffness reduction and structural behavior of the composite laminate.

In the paper "Virtual testing of realistic aerospace composite structures" [52], Davies and Ankersen studied in great detail the feasibility of relying on simulations to test composite structures to failure and concluded that simulations are rapidly evolving into a viable design tool.

As discussed in Section 2.1.3, low-velocity impact damage consists of various damage mechanisms. In studies on low-velocity impact damage, an area of interest is the interaction between the various damage mechanisms, as a better understanding of how the different damage mode interacts with each other would deepen our current understanding of low-velocity impact damage.

The first report of interaction between delamination cracks and transverse matrix cracks is found in [20], where Malvern et. al. performed microscopic observations of impacted cross-ply glass-epoxy composite laminates and noticed the interactions between these two damage modes. Liu and Malvern [16] went on to study and compile detailed interactions between delaminations and matrix cracks for various layups of composite laminates. In [36], Liu established the major cause of delamination to be bending-induced stresses because both experiment and analysis showed that the composite laminate tends to bend concave in the fiber direction and convex in the transverse direction. He then attributed the formation of delaminations to the mismatch of bending stiffness between adjacent layers due to varying fiber orientations between the layers, and defined a bending mismatch coefficient between the adjacent layers. He reported a direct relationship between the bending stiffness mismatch and the size of delamination; the greater the mismatch, with cross-ply having the greatest mismatch, the greater the size of delamination.

From experimental studies conducted, Liu [36] also reported that delamination areas were generally elongated, with their major axis coinciding with the fiber orientation of the layer below (away from impact face) the interface (Figure 8).

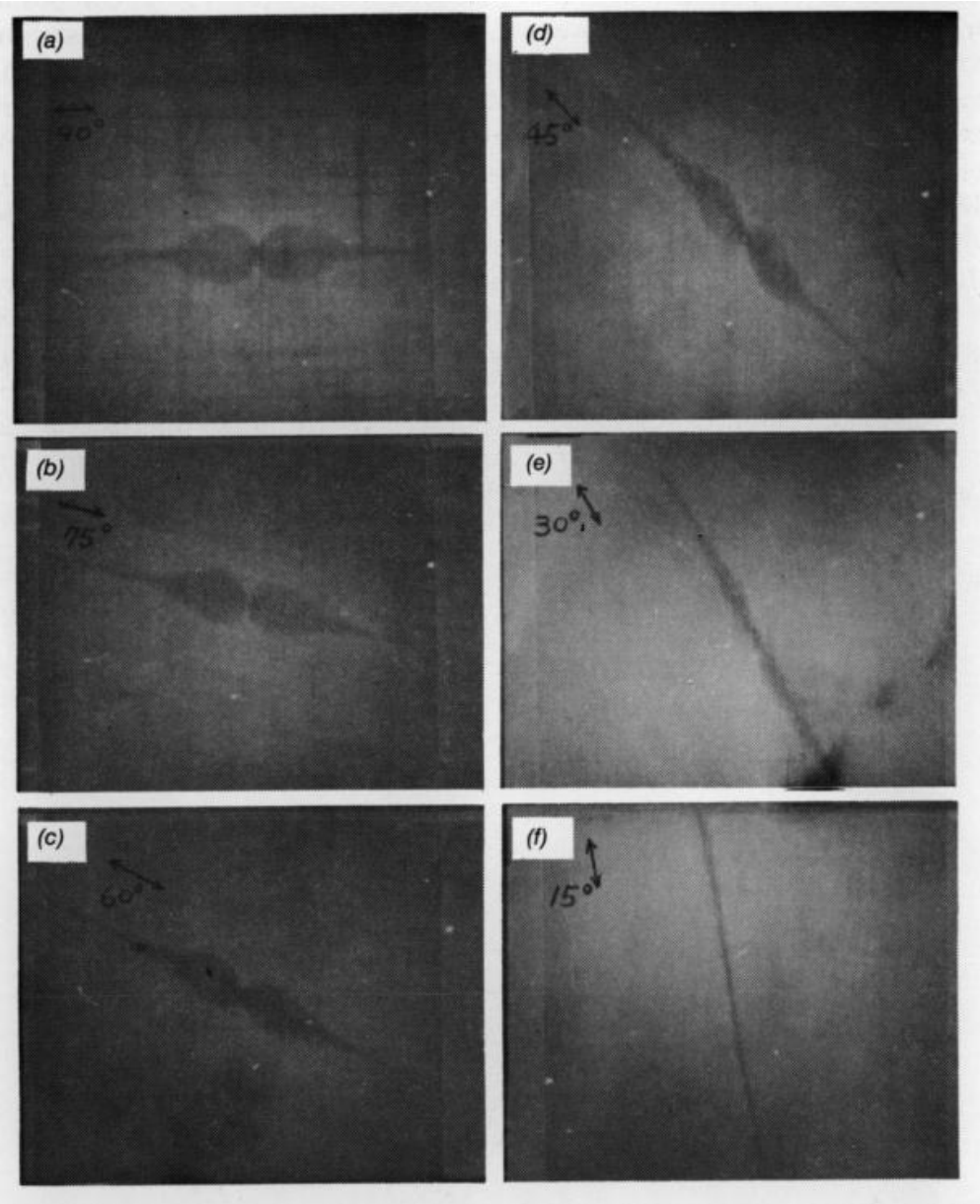

Figure 8 Delaminations in the impacted plates: (a) $[0_4/90_4]$, (b) $[0_4/75_4]$, (c) $[0_4/60_4]$, (d) $[0_4/45_4]$, (e) $[0_4/30_4]$, (f) $[0_4/15_4]$, obtained from [36]. Impact direction is into the plane of the paper.

Many studies have since been performed, confirming the results as reported by Liu and Malvern. An example is the detailed study performed by Finn et al. [58, 59] that measures the locations and geometries of delaminations induced by an impact load. In their study, they reported that peanut-shaped delaminations were induced in all cross-ply laminates. It was also reported that delaminations do not occur at interfaces between plies of the same fiber orientation. Finn et al. [58] performed a parametric study in which the effects of parameters including the plate thickness, impactor mass and thickness of the back ply group on the impact damage was investigated. Delamination sizes were observed to increase with increasing plate thickness, as seen in Figure 9. The increase in delamination sizes with increasing plate thickness was attributed to the increase in back ply group thickness, which leads to an increased strain energy in the back ply group made available for the formation of delamination. Delamination sizes were also observed to increase with increasing impactor mass, which corresponds to an increase in impact energy and maximum force applied to the composite laminate. With an increase in impact energy, more strain energy is present in the plate, leading to more energy being available to cause delamination. Finn et. al. [58, 59] also reported that the dimensions of the impactor does not have an effect on delamination sizes because the contact area between the impactor and the composite laminate is usually of an order of magnitude smaller than the delamination sizes, which typically ranges from 5mm to 50mm for low-velocity impact cases. Delamination sizes were also observed to increase with an increasing number of plies in the back ply group, away from the impact face. They attributed this to the increase in energy stored in the back ply group as the number of plies increases, hence availing more stored strain energy for delamination formation.

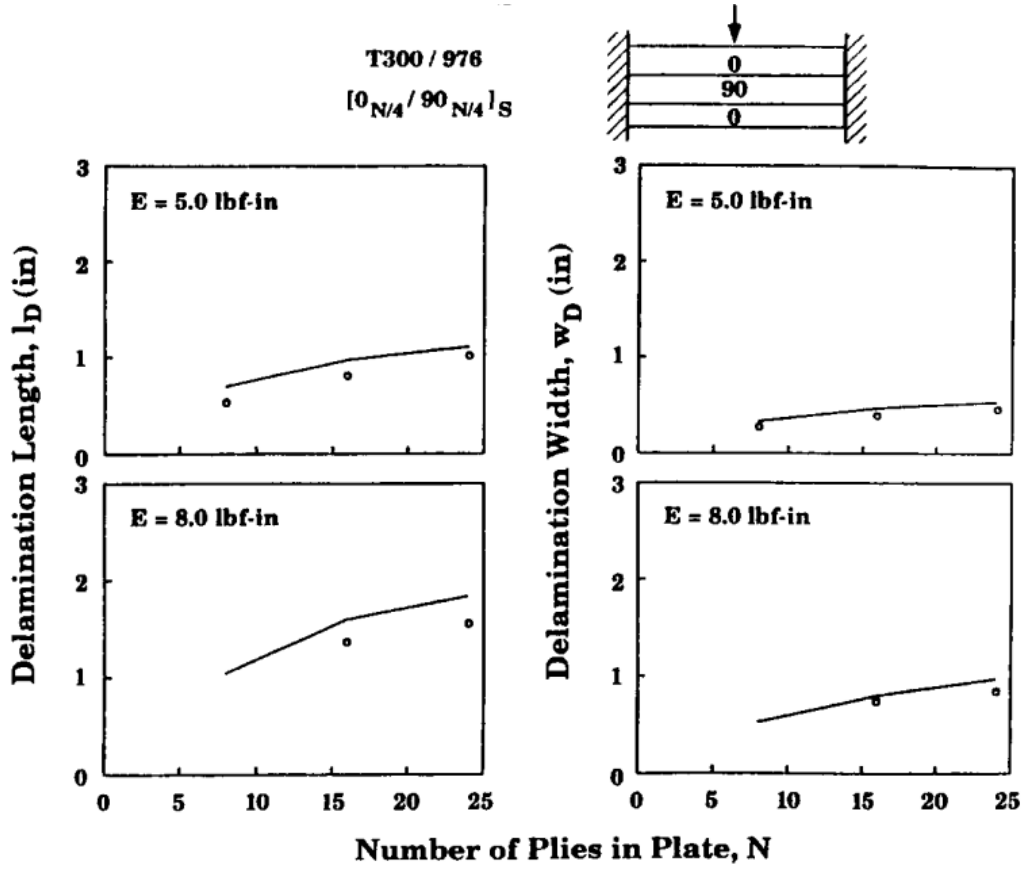

Figure 9 Delamination lengths and widths in plates subjected to static loads as functions of the total number of plies N in the plate, with plate dimensions 3in by 4in (1in=25.4mm), obtained from [58]

De Moura et. al. [60] conducted low-velocity impact tests on two different laminate layups, $[0_4/90_4]_s$ and $[0_2/\pm45_2/90_2]_s$, using a drop-weight testing machine. They then performed damage characterization using X-ray radiography and the deply technique. The interaction between matrix cracks and delamination was also reported by the researchers, who noted that delaminations were generated by the transverse cracks in the plies adjacent to the delamination interface. It was also reported that delaminations occurred only at interfaces where the adjacent plies were of differing fiber orientations, and has a characteristic two-lobed shape with the major axis

oriented in the same direction as the fiber orientation of the ply below the interface. De Moura et. al noted that the internal damage due to low-velocity impact was characterized by delamination and transverse cracking.

Low-velocity impact damage sequence was studied by Choi et. al. [61, 62] in their investigations involving low-velocity line-loading impact . A line-nosed impactor which could produce a uniformly distributed and transient dynamic load across the specimen width was used. The researchers observed matrix cracking to be the first failure mode of impact damage in laminated composites, which in turn lead to the formation of delaminations and micro-cracks. The matrix cracks that induce the formation of delaminations are termed 'critical matrix cracks'. It was reported that delaminations are always accompanied by a critical matrix crack. There exists a threshold impact energy, below which the critical matrix crack does not form, and no damage is observed. After the critical matrix crack is formed, stresses in the out-of-plane normal direction and interlaminar shear stresses are found to be the dominant stresses causing the initiation and propagation of delaminations. As delaminations propagate the in-plane transverse tensile stresses and interlaminar shear stresses in the vicinity of the critical matrix cracks then causes the formation of micro-cracks. Choi et. al. also found that the stacking sequence of the composite laminates have an effect on the impact resistance of the composites.

It has also been reported in a study conducted by Saito et al. [63] that there exists a minimum ply thickness in order for critical matrix cracks to initiate and propagate. In their study, they calculated the strain energy release rate at the matrix crack tip by means of the virtual crack closure method and found that critical cracks propagated only when the strain energy release rate exceeded $40J/m^2$. Such an energy release rate could not be attained in composite layers of thickness less than 0.04mm. Saito et al. also reported that the strain energy at the crack tip of a particular crack

length would be at its maximum when the crack length was approximately three-quarter of the ply thickness of the composite layer in which the crack exists. As such, with a decrease in ply thickness, the maximum strain energy that could exist at the crack tip decreased accordingly. In the event that the maximum strain energy at the crack tip does not exceed the strain energy required for critical crack propagation, crack propagation would not occur, and delaminations would not form.

The difficulty of modeling low-velocity impact on composite plates arises from the complexities of low-velocity impact damage. For the same incident energy, different combinations of impactor mass and velocities can have different effects on the impact response [12]. Furthermore, different sizes and layups of the composite plates would display different damage patterns. The differences in damage patterns in turn lead to differing residual compressive strength, or CAI strength. Nguyen et al. [18] did a review on the capability of finite element softwares for composite impact damage analysis, comparing three commercial explicit FE analysis packages, Pam-Shock, LS-Dyna and MSC.Dytran, on their ability to model the damage arising from the impact load. The comparison is conducted by determining the suitability of the explicit FE analysis packages in constructing an FE model of a composite laminate, predicting the BVID, and retrieving the results. The results retrieved for BVID were then compared with experimental results. It was concluded that all three packages were capable of creating a composite damage model and solving for damage and degradation. They were also capable of post processing the damage information. Nguyen et al. [18] noted that an important capability of the use of these FE packages in the study of low-velocity impact damage was the ability to view the damage in each individual ply.

Following their experimental studies, Lopes et al. [64] conducted numerical simulations for the prediction of impact damage using the

commercially available finite element analysis software, ABAQUS/Explicit. Continuum damage mechanics is used in their numerical simulations to predict the quasi-brittle process of failure of composites. In their model, the LaRC04 failure criteria is used for the prediction of the onset of matrix cracking and fiber fracture under both tensile and compressive loads. A cohesive damage model is used to account for delamination. The FE model created simulates several physical processes which occur during low-velocity impacts on composite laminates, including the correct geometrical representation of the structural system, loads, boundary conditions, material behavior and contact conditions between the two bodies involved. The material studied in this research was AS4/8552. The dimensions of the FE model used were 150mm by 100mm, and 4.36mm thick, with 24 plies in the thickness direction. More details on the geometry and boundary conditions used for the simulation are found in Figure 10. The impactor was modeled as a rigid body and has a spherical shape with diameter 16mm. In this FE model, each laminate ply was modeled using C3D8R solid elements behaving according to a continuum damage model, with one element in the thickness direction. The resin-rich interface between each ply was modeled using COH3D8 cohesive elements, with its behavior described by a traction-separation law. Lopes et al. [64] concluded that the simulations are computationally expensive due to the large number of elements required. However, Lopes et al. deemed that the large computational cost is acceptable because the model predicts the maximum impact force and the maximum impactor displacements, delamination location and size, as well as matrix cracks and fiber damage with acceptable accuracy as compared to their experimental results reported in [65]. However, the stiffness of the specimen is higher than predicted by the model. The authors attribute the under-predicted stiffness to the prediction of delamination initiation to be at a lower load than observed in experiments. The model was also unable to predict the impact indentation.

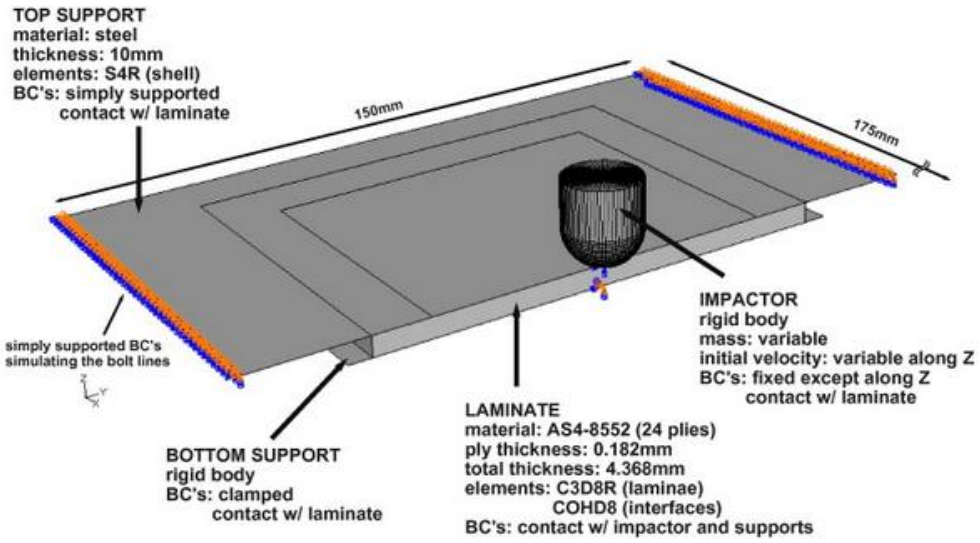

Figure 10 Geometry and boundary conditions for the simulation of an impact event on a 24-ply laminate, with only half the structure represented, obtained from [64]

Faggiani et al. [66] built a similar model for predicting low-velocity impact damage on a stiffened composite panel. In this model, continuum damage mechanics was used in the composite damage model as well. The model had dimensions 450mm by 375mm, and the center region of dimensions 60mm by 60mm corresponding to the site of impact was modeled using a finer mesh. Clamped boundary conditions were defined at the edges of the FE model. It is reported that this model is able to predict the rate of energy absorption by the panel, the maximum average impactor force, and the post-impact permanent indentation. However, the prediction of the size, shape and location of the delaminations could not be verified as no experiments were performed. In Figure 11, it could be seen that the most extensive delamination was predicted to occur in the 90/90 interface. This is inaccurate, as it has been proven in many studies that delaminations do not occur between plies of the same fiber orientation [35, 36].

In the modeling of low-velocity impact, many researchers have approximated the low-velocity impact event using quasi-static indentation

[12, 67]. In [68], the same results were obtained from low-velocity impact test and quasi-static indentation test. In [69], it was also shown that a quasi-static indentation analytical model provided good agreement with the experimental results obtained from low-velocity impact tests. A low-velocity impact event could be approximated using quasi-static indentation because of the analogous impact and boundary conditions. One advantage of modeling a low-velocity impact event as quasi-static indentation is that it allows for in-depth study of the damage mechanisms at different stages of the damage progression during the impact event [70].

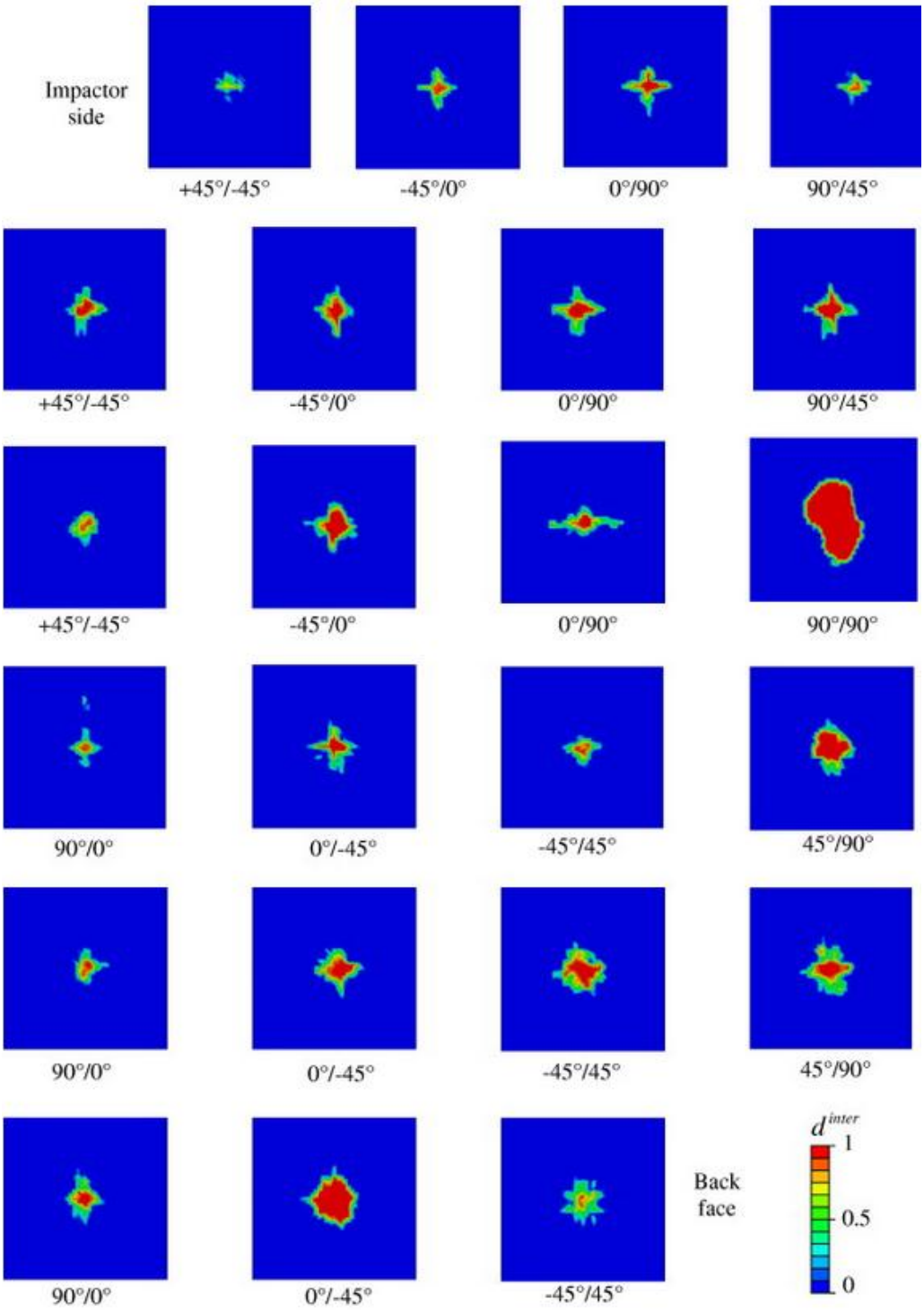

Figure 11 Ply delaminations at each interface of the impacted composite panel, obtained from [66]

2.2.2 Studies on compression after impact (CAI) strength

The CAI test is performed to evaluate the consequence of impact damage on the compressive strength of the material. Delaminations have little effect on the tensile strength of the composite laminate, but significantly reduce the compressive strength because when a composite laminate is subject to tension after impact, the delamination simply closes up. However, under compression, the sublaminates can buckle locally at the area of delamination as demonstrated in Figure 12b below. The CAI test is a test method used to characterize damage due to impact. It consists of a specific impact event followed by an in-plane compression loading to failure.

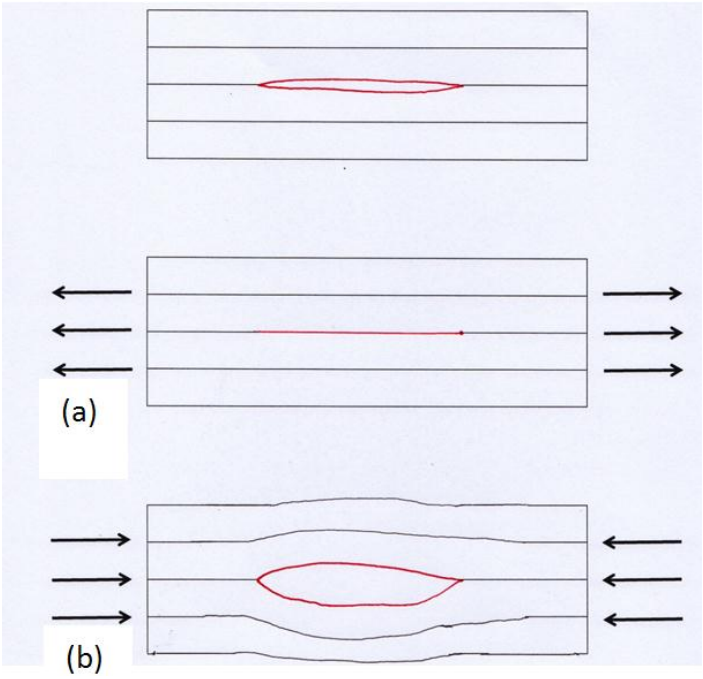

Figure 12 Delamination (a) closes up under tension and (b) buckles locally under compression

Most attempts at predicting the residual CAI strength [71-74] make two erroneous asuumptions: Firstly, delamination shapes are assumed to be uniform in each interface, simplified to be either circular or elliptical in shape.

Secondly, in most of these studies, delamination, which leads to the loss of stability of sublaminates, was deemed to be the main contributing factor causing the reduced compressive strength of the impact damaged laminate. The effect of delamination on the residual CAI strength of composite laminates has been well studied [9, 75-80].

Various models have been proposed for the prediction of CAI strength. In the model proposed by Dost et al. [76] for the prediction of CAI strength, the impact damaged region in the composite laminate was treated as a soft inclusion with reduced stiffness. CAI tests have shown that under compression, the sublaminate furthest from the impact surface will buckle first. Subsequently, the other sublaminates in the damaged region buckles as well. The buckling of the sublaminates causes the elastic moduli of the material in the damaged region to be reduced, hence the material in the damaged region could be treated as a soft inclusion embedded in the laminate. A load-redistribution in which higher loads are transferred to the undamaged region of the laminate results in a stress concentration at the edge of the delaminations, causing a reduced compressive strength. The maximum strain failure criterion was used in this prediction model. This is a model that has been widely adopted by various other researchers because of its simplicity. However, one shortfall of this model is that it does not account for the out-of-plane deformation of the sublaminate and assymetrical layups.

Xiong et al. [9] then modified the model proposed by Dost et al, to account for the out-of-plane deformation of the sublaminate and assymetrical layups. The method proposed by Xiong et al. [9] includes a sublaminate buckling analysis using the Rayleigh-Ritz method. A rectangular laminate containing an embedded elliptical delamination was subject to uniaxial compression, and the stress at which buckling occurs is calculated using the Rayleigh-Ritz method. Secondly, the material within the damaged region is degraded by a reduction of its moduli. In the analysis proposed by

Xiong et al. [9], the laminate assumes a linear stress-strain relationship until the first sublaminate buckles. The load carried by the buckled sublaminate then remains constant, as in Euler buckling. The axial modulus of material in the damaged region would decrease as compressive strain increases in its post-buckled state. This is caused by the load redistribution within the damaged region, and delamination growth followed by the buckling of the next sublaminate occurs subsequently. This process repeats until all the sublaminate in the damaged region buckles as strain is increased, and the entire damaged region is now considered a soft inclusion; the damaged laminate can now be simulated by a similar plate containing a soft inclusion. The third step in this CAI strength prediction model is stress redistribution in the damaged laminate in which the complex variable method is used to calculate the in-plane stresses of the laminate containing an elliptical soft inclusion. In the method proposed by Xiong et al. [9], three failure criteria were used. The point stress failure criterion was used to predict the laminate failure strength, while the maximum stress and Tsai-Wu failure criteria were used to predict first ply failure. Avery et al. [78] proposed a semi-discrete approach for the prediction of CAI strength, which makes use of fully coupled partial differential equations for anisotropic elasticity in the calculation of the buckling load of the sublaminate. This is opposed to the method used by Dost et al. [76] which modified the analysis of Shivakumar et al. [77] to account for the reduced bending stiffness in unsymmetric sublaminates.

Another modeling technique for the prediction of CAI strength was proposed by Kassapoglou [79], in which the impact site was treated as a region of stress concentration. The stress concentration factor was calculated using semi-empirical methods. Gottesman et al. [80] proposed a method for CAI strength prediction which considers the competing failure modes of local delamination buckling and compression failure. In this method, the sublaminates were checked for two possible failure modes- the

compressive mode and the buckling mode. The failure criterion used to check for the compressive failure mode was the first ply fiber failure mode, while the buckling failure mode was checked using the classical buckling theory of orthotropic plates. Soutis et al. [2] proposed that there is great similarity between the failure patterns in CFRP laminates containing an open-hole and an impact damaged composite. In their work, a fracture toughness model which was originally proposed for an open-hole plate was used to predict residual CAI strength.

There are a few striking similarities between the CAI strength prediction models described above, and their main features include an impact damage characterization where information on the delamination shape, sizes and location is determined, a sublaminate stability analysis, a soft inclusion modeling of the impact damage in which the material contained in the damaged region is simulated by reducing the moduli of the material and finally a stress redistribution and failure criterion.

Even though the sublaminate stability based method as discussed above has been widely adopted in CAI strength prediction models and have been successfully used to predict CAI strength of composite laminates, there are still various shortfalls of this model such as the inability to simulate the real deformation of the damage zone when the laminate is subject to compression, and impact induced fiber breakage was ignored. Furthermore, the effective reduced moduli for the material contained within the damaged region were calculated at failure by ensuring strain compatibility at the boundaries of the undamaged and damaged material. However, strain compatibility cannot be satisfied even at failure. To overcome these shortfalls, Chen et al. [81] proposed a method for the prediction of CAI strength based on an equivalent hole model. In this model, the impact damaged region was simplified and approximated to be an open hole. A technique for determining the shape and size of the equivalent hole was also proposed. Chen et al. [81]

concluded that the predictions obtained from the equivalent hole model were in good agreement with experimental results.

Craven et al. [75] performed a finite element study in which 'peanut delaminations' were modeled, instead of the usual circular or elliptical delaminations, and found that the peanut shaped delaminations led to significant stiffness reduction as compared to matrix or fiber damage. Fiber fracture cracks were also included in the model, but these were reported to demonstrate minimum effect on further stiffness reduction. Matrix cracks were simulated in this model by degrading the transverse properties of each ply by a nominal amount of 60%, and the effect on stiffness was found to be negligible, hence the effect of matrix cracking was pursued no further, and only peanut shaped delaminations were taken into account in their study.

Most studies involving impact damage of composite laminates and its resultant CAI strength consider central impact on flat composite laminates. However, a few researchers have investigated the effect of near-edge and on-edge impact and found that such impact might be more detrimental to a composite laminate subjected to after impact compression than a central impact [82, 83]. Some researchers have also investigated the effect of impact on the resultant CAI strength of curved composite laminates [84-87]. However, the focus of this thesis would be on the central impact damage and resultant CAI strength of flat CFRP laminates.

2.3 Review of failure criteria used in this study

Failure initiation occurring in a ply within the composite laminate, or first-ply failure, can be predicted by means of an appropriate failure criterion [88, 89]. Subsequently, failure prediction requires an understanding of the different damage modes and damage accumulation and the effect they have on the mechanical behavior of the composite laminate. Many failure criteria have been proposed with the purpose of predicting failure initiation and their progression.

Failure criteria for composite materials can be classified into two groups [90]: theories with independent failure modes, and theories without independent failure modes, or polynomial failure theories.

One of the earliest and most widely used failure criteria with independent failure modes is the Maximum Stress Criterion for orthotropic laminates. It was suggested by Jenkins [91] as an extension of the Maximum Normal Stress Theory, or Rankine's Theory, for isotropic materials. According to the Maximum Stress Criterion, failure is predicted to occur when any stress component in the principle material axes reaches or exceeds the corresponding individual strength value.

In order to avoid failure, according to the Maximum Stress Criterion, the following inequalities musts be satisfied:

$$-X_C < \sigma_{11} < X_T \quad (1)$$

$$-Y_C < \sigma_{22} < Y_T \quad (2)$$

$$-S_{12} < \tau_{12} < S_{12} \quad (3)$$

Where X_C refers to the compressive strength in the fiber direction

X_T refers to the tensile strength in the fiber direction

Y_C refers to the compressive strength in the transverse direction

Y_T refers to the tensile strength in the transverse direction

S_{12} refers to the in-plane shear strength

An alternative to the Maximum Stress Criterion is the Maximum Strain Criterion for orthotropic laminae, which was proposed by Waddoups [92] as an extension of the Maximum Normal Strain Theory, or Saint Venant's Theory for isotropic materials. As opposed to the Maximum Stress Criterion, failure predicted by the Maximum Strain Criterion is based on strain components instead. According to this criterion, failure occurs when any strain component in the principle material axes reaches or exceeds the corresponding ultimate strain value.

A limitation of these two criteria is that they do not account for interactions between different stress components in the failure mechanism, since these two theories make use of noninteractive stress or strain limits to characterize failure. In spite of such a limitation, these failure criteria are still widely used because of their simplicity and ease of application. [93, 94]

Polynomial failure criteria were subsequently proposed to account for the interaction between the stress or strain components. Unlike the Maximum Stress and Strain Criteria, these criteria include terms that account for the interaction between stress components. Hill [95] proposed a criterion as an extension of the von Mises yield criterion for isotropic materials to anisotropic plastic materials with equal strengths in tension and compression. Tsai and Azzi [96] later extended Hill's criterion to orthotropic fiber composites by proposing a relation between the coefficients of Hill's polynomial failure criterion to the longitudinal, transverse and shear strengths of the composites. The resultant failure criterion has been named the Tsai-Hill failure criterion, which has the capability of accounting for

materials with different tensile and compressive strengths. One limitation of these polynomial failure criteria is the assumption that hydrostatic stresses do not contribute to failure. Such an assumption is incorrect, as shear coupling would cause a hydrostatic state of stress in an anisotropic material to produce shear strains that lead to failure. Hoffman [97] derived an equation that could predict failure under a hydrostatic state of stress.

A more general polynomial failure criterion is the Tsai-Wu failure criterion. The Tsai-Wu failure criterion [98] was proposed in 1971 by Tsai and Wu as a simplified and improved version of a tensor polynomial failure theory for anisotropic materials derived by Gol'denblat and Kopnov [99].

In the Tsai-Wu failure criterion, the failure surface in the stress space is described by the following tensor polynomial:

$$F_i\sigma_i + F_{ij}\sigma_i\sigma_j = 1 \tag{4}$$

where i,j = 1,2,...6 and F_i and F_{ij} are experimentally derived strength tensors in the second and fourth rank respectively. A vector notation for the strength tensor is adopted as follows: $\sigma_1 = \sigma_{11}, \sigma_2 = \sigma_{22}, \sigma_3 = \sigma_{33}, \sigma_4 = \tau_{23}, \sigma_5 = \tau_{31}, \sigma_6 = \tau_{12}$.

Expanded, Equation (4) becomes:

$$\begin{aligned} &F_1\sigma_1 + F_2\sigma_2 + F_3\sigma_3 + F_4\sigma_4 + F_5\sigma_5 + F_6\sigma_6 \\ &+F_{11}\sigma_1^2 + 2F_{12}\sigma_1\sigma_2 + 2F_{13}\sigma_1\sigma_3 + 2F_{14}\sigma_1\sigma_4 + 2F_{15}\sigma_1\sigma_5 + 2F_{16}\sigma_1\sigma_6 \\ &+F_{22}\sigma_2^2 + 2F_{23}\sigma_2\sigma_3 + 2F_{24}\sigma_2\sigma_4 + 2F_{25}\sigma_2\sigma_5 + 2F_{26}\sigma_2\sigma_6 \\ &+F_{33}\sigma_3^2 + 2F_{34}\sigma_3\sigma_4 + 2F_{35}\sigma_3\sigma_5 + 2F_{36}\sigma_3\sigma_6 \\ &+F_{44}\sigma_4^2 + 2F_{45}\sigma_4\sigma_5 + 2F_{46}\sigma_4\sigma_6 \\ &+F_{55}\sigma_5^2 + 2F_{56}\sigma_5\sigma_6 \\ &+F_{66}\sigma_6^2 = 1 \end{aligned} \tag{5}$$

For the case of plane stress,

$$\sigma_3 = \sigma_{33} = 0, \qquad \sigma_4 = \tau_{23} = 0, \qquad \sigma_5 = \tau_{31} = 0$$

Hence Equation (5) is reduced to:

$$F_1\sigma_1 + F_2\sigma_2 + F_{66}\tau_{12}^2 + F_{11}\sigma_1^2 + 2F_{12}\sigma_1\sigma_2 + F_{22}\sigma_2^2 = 1 \qquad (6)$$

The linear terms in the shear stress $\sigma_6 = \tau_{12}$ has been removed from Equation (6) because the shear strength along the principal material axes is not affected by the sign of the shear stress. Only a quadratic term in the shear stress σ_6 remains in the equation. The linear terms in the normal stresses $\sigma_1 = \sigma_{11}$ and $\sigma_2 = \sigma_{22}$ are retained because they take into account the different strengths in tension and compression. Finally, the term $2F_{12}\sigma_1\sigma_2$ takes into account the interaction between the normal stresses.

The strength tensors F_1, F_2, F_{11}, F_{22} and F_{66} are derived by considering uniaxial test cases and solving the equations obtained simultaneously. They can be expressed in terms of the uniaxial and shear strengths as follows:

$$F_1 = \frac{1}{X_T} + \frac{1}{X_C}$$

$$F_{11} = -\frac{1}{X_T X_C}$$

$$F_2 = \frac{1}{Y_T} + \frac{1}{Y_C}$$

$$F_{22} = -\frac{1}{Y_T Y_C}$$

$$F_{66} = \frac{1}{S_{12}^2}$$

The interaction parameter F_{12} is found using a biaxial test involving both σ_1 and σ_2. There exists four different values for F_{12} since there can be four different failure pairs of σ_1 and σ_2 [100]. Wu [101] has suggested that the biaxial ratio $B = \frac{\sigma_1}{\sigma_2}$ has to be optimized to account for the sensitivity of F_{12} to experimental scatter, so that F_{12} can be determined more accurately.

An expression for F_{12} that is commonly employed was proposed by Tsai and Hahn [102]:

$$F_{12} = -\frac{\sqrt{F_{11}F_{22}}}{2}$$

A limitation of the Tsai-Wu failure criterion is that the mode of failure is not indicated by this method.

Mechanism-based failure criteria were later developed to account for specific modes of failure at the micro-scale. The Hashin failure criterion [100, 103-105] is one such mechanism-based failure criterion that takes into account the specific modes of failure at the macro-scale. Based on this failure criterion, matrix and fiber failure of composites are distinguished through the use of independent sub-criteria. Damage is deemed to have initiated once any of the following sub-criteria that make up the Hashin failure criterion is met:

Tensile fiber failure (where $\sigma_{11} > 0$)

$$\left(\frac{\sigma_{11}}{X_T}\right)^2 + \frac{\sigma_{12}^2}{S_{12}^2} = 1 \qquad (7)$$

Compressive fiber failure (where $\sigma_{11} < 0$)

$$\left(\frac{\sigma_{11}}{X_C}\right)^2 = 1 \qquad (8)$$

Tensile matrix (transverse direction) failure (where $\sigma_{22} > 0$)

$$\frac{{\sigma_{22}}^2}{Y_T^2} + \frac{\sigma_{12}^2}{S^2} = 1 \tag{9}$$

Compressive matrix failure (where $\sigma_{22} < 0$)

$$\left[\left(\frac{Y_c}{2S_{23}}\right)^2 - 1\right]\frac{\sigma_{22}}{Y_C^2} + \frac{{\sigma_{22}}^2}{4S_{23}^2} + \frac{\sigma_{12}^2}{S_{12}^2} = 1 \tag{10}$$

Although the Hashin failure criterion is able to differentiate between the different failure modes, it considers each failure mode as independent sub-criteria, not accounting for the interaction between tensile and compressive stresses in cases of multi-axial loads. In this research, the Tsai-Wu and Hashin failure criteria were chosen because the damage prediction obtained have demonstrated good agreement with experimental results, coupled with the ease of implementation into the FE model.

While the use of stress components in the prediction of failure in composites is most common, there exist other failure criteria that make use of strain energy [106-108] and dissipated energy [109].

2.4 Review of damage modeling techniques used in this study

2.4.1 In-plane damage modeling techniques

After the initiation of failure has been predicted by an appropriate failure criterion, the effect that the damage has on the load-carrying capability of the material is described by the application of an appropriate damage modeling technique. Researchers have proposed various different techniques for modeling damage in composites materials, including the modification of the reduced stiffness matrix [110, 111], fracture mechanics method [112], element-delete method [113], the material property

degradation method (MPDM) [114-117] and the Continuum Damage Mechanics (CDM) method [118], among which the CDM is one of the most widely-used approach.

The material property degradation method (MPDM) and Continuum Damage Mechanics (CDM) approach is based on the idea that a damaged material can be described by degrading the material properties of the same undamaged material. In the application of MPDM, once damage has initiated as deemed by the failure criterion used, the damaged material is replaced with an equivalent material with degraded material properties. The simplest and most conservative version of MPDM is the ply discount method, where it is applied at the ply level. In the ply discount method, as the applied load is increased, a failure criterion is used to identify the first ply in which the first transverse crack appears, or first-ply failure. The Young's modulus in the transverse direction, E_2, and the shear modulus, G_{12}, of that entire ply in which failure is first observed are then degraded. A new stress analysis of the composite laminate with degraded ply properties is carried out to identify subsequent failure occurrence. The ply discount method in which the material properties of the ply are completely degraded to zero is called the total ply discount method [119]. The total ply discount method is based on the assumption that once failure has initiated, the ply is deemed to have totally failed and is no longer capable of sustaining further load. This method is widely used by researchers [115, 116, 120] because of its ease of implementation. It is evident that the total ply discount method is overly conservative because in reality, the damaged material would still be able to withstand a certain amount of load after initial failure. This method underestimates laminate strength, and fails to recognize that ply failure is localized and that the stiffness of a failed ply might not be zero.

To improve on the total ply discount method, the material properties of the failed plies could be degraded by a degradation factor other than zero,

and material properties could be degraded selectively depending on the failure mechanisms responsible for the ply failure [121].

A less conservation damage modeling method is when MPDM is applied at the element level rather than at the ply level. A stress analysis is performed in the finite element model to identify where damage has initiated in each ply, and the material properties of these damaged elements are degraded. A stress analysis with the updated material properties is then carried out to identify subsequent locations of failure initiation, and degrading the material properties of the elements in which failure has initiated. This process is repeated until final damage.

Many researchers have used MPDM in their studies involving progressive failure. An example of such an application of MPDM is found in the investigation performed by Reddy and Reddy [122], where two different degradation approaches were used: the degradation of only the elastic modulus and Poisson's ratios, and the simultaneous degradation of elastic and shear moduli and Poisson's ratio. However, the degradation parameters used were the same regardless of failure modes. Tan and Perez, in their investigation of the progressive failure of laminates containing holes under in-plane tensile and compressive loading, used different degradation parameters, D_1, D_2 and D_6 for longitudinal modulus and for transverse and shear moduli to account for fiber breakage and matrix failure respectively [114, 117]:

$$E_{11} = D_1 E_{11}^0$$

$$E_{22} = D_2 E_{22}^0$$

$$G_{12} = D_6 G_{12}^0$$

The degradation factors have values less than unity when damage has occurred. Estimates of their values are proposed in [123]. The above

degradation method does not differentiate between compressive and tensile failure.

Shokrieh and Lessard [124] proposed a degradation model which accounted for the difference in compressive and tensile failure. In this model, seven different failure modes are considered- fiber tension, fiber compression, fiber-matrix shearing, matrix tension, matrix compression, out-of-plane tension and out-of-plane compression. Suitable stress-based failure criteria for detecting the individual failure modes under a multi-axial state of stress are used together with a suitable set of degradation factors for each failure mode. For example, when fiber failure is detected, all the material properties are degraded based on the assumption that fiber failure would cause the material to be unable to withstand further stress. When matrix failure is detected, only transverse properties are degraded, while fiber direction properties remain unchanged. They later validated their model with experiments [125].

Tserpes et. al. [126] also implemented a 3D MPDM model with the ability to differentiate between different damage modes. In this study, the Hashin failure criterion was used to predict the different damage modes in composites, namely fiber tensile and compressive failure, matrix tensile and compressive cracking, fiber-matrix shear-out and delamination in tension and compression.

When matrix damage is predicted, the matrix is assumed to be unable to carry further load and the material properties of the failed ply in the matrix direction such as the Young's modulus in the in-plane transverse direction and Poisson's ratio v_{12} is degraded to zero. Table 1 below summarizes the degradation scheme used in this study for the various damage modes accounted for.

No failure	Fiber failure	Matrix cracking	Fiber-matrix shear-out	Delamination
E_{11}	0	E_{11}	E_{11}	E_{11}
E_{22}	0	0	E_{22}	E_{22}
E_{33}	0	E_{33}	E_{33}	0
G_{12},	0	0	0	ν_{12}
ν_{23}	0	ν_{23}	ν_{23}	0
ν_{13}	0	ν_{13}	ν_{13}	0
G_{12}	0	G_{12}	0	G_{12}
G_{23}	0	G_{23}	G_{23}	0
G_{13}	0	G_{13}	G_{13}	0

Table 1 Degradation scheme employed by Tserpes et. al. [126]in the modeling of progressive damage

Reddy et. al. [127] noted that in most degradation schemes, selected stiffness properties of the failed elements are reduced either to zero, or reduced using a step-wise unloading scheme. This is inaccurate because in reality, damage induced stiffness reduction occurs gradually instead of in steps. To address this inaccuracy, Reddy et. al. proposed a gradual stiffness reduction scheme by reducing the stiffness properties of an element in which failure has been indicated by the failure criterion of choice to a level at which the failure criterion is no longer satisfied. Such a scheme allows for the same element to undergo repeated failures, simulating the accumulation of damage in the element.

Continuum damage mechanics (CDM) models have also been proposed by various researchers for damage propagation modeling, and are generally considered to be a more realistic approach as they can feature internal variables representing the damage characterization [118]. In such

models, a constitutive model of the damage states of composites is applied together with a damage evolution criterion to predict progressive damage. The constitutive model of the damage states is described by a set of internal state variables that carry information on crack geometry and fracture modes. The key assumption of CDM is that a microcrack growth can be treated at a macro level by treating the damage as a continuum over a representative volume [57].

One of the first applications of CDM to composite laminates was performed by Talreja [128] where he proposed two damage variables for both the matrix and fiber damage. He then used his model to predict the stiffness reduction in various angle-ply laminates, demonstrating good agreement with experimentally measured stiffness loss [129]. A commonly adopted CDM model is the model proposed by Ladeveze et. al. [130] in which fiber and matrix behavior are considered separately, and many researchers have adopted Ladeveze's model in their implementation of CDM to more specific cases involving different types of composite materials [131, 132]. Williams et al. [133] addressed the physical significance of the damage parameters used in their CDM model by using experimental observations of damage growth and of the effects that damage has on the material response in their derivation of the mathematical formulation. The formulation proposed by Williams et al. [133] was based on the sub-laminate response, in recognition that the laminate response is driven by ply interactions through the stacking sequence and damage growth instead of being driven simply by the lamina properties. Pinho et al. [118, 134] incorporated a smeared formulation in their CDM model in an attempt to avoid problems of strain localization leading to mesh dependency. Strain localization occurs when narrow and highly strained zones emerge prior to failure. In the smeared formulation proposed by Pinho et al. [118], the fracture energy is distributed, or smeared, over the entire volume of the element. This smeared formulation

method is implemented in the FE models used in the current research, and more details on the smeared formulation method is found in Section 3.1.1.2. A detailed review of CDM models can be found in [57].

2.4.2 Delamination modeling techniques

In the modeling of delamination, the fracture mechanics approach and the cohesive and interface models are commonly applied. Delamination in composites can be accounted for as matrix cracks occurring between plies. The Virtual Crack-Closure Technique (VCCT) has traditionally been the most common approach used for the simulation of delamination in composites [135]. This technique is based on the assumption that the energy released during the propagation of delamination is equals to the work required to close the crack to its original position. The components of the energy release rate are hence computed from the nodal forces and relative displacements, and delamination growth is predicted to occur when a combination of the components of the energy release rate equate a critical value. A restrictive limitation of such a fracture-mechanics based approach is that a pre-existing delamination has to be assumed. In other words, such a method is unable to predict delamination initiation; it is only able to predict delamination propagation. In many cases, the determination of the precise location of delamination initiation might be challenging [136]. Furthermore, the VCCT assumes self-similar crack growth, which is contradictory to experimental observations where delaminations are observed not to remain straight under propagation [137].

Cohesive and interface models which make use of a combination of strength-based analysis for the prediction of delamination initiation and fracture mechanics for the prediction of delamination propagation have been adopted as a technique used to better predict delamination onset and

propagation without having to assume a pre-existing crack. The cohesive element method is also better able to track delamination growth because failure in cohesive elements is explicitly modeled. Cohesive zone models are based on the Dugdale [138] and Barenblatt [139] cohesive zone approach, and can be related to Griffith's theory of fracture when the cohesive zone size is negligible in comparison with other characteristic dimensions. The main concept of cohesive models is the inclusion of a thin cohesive or interface layer between surfaces where delamination might occur. The interface layer follows a linear or non-linear shear stress-strain response, and has to be stiff enough in compression to prevent the penetration of damaged layers [140]. The most important aspect of a cohesive model is its constitutive law, and a widely adopted law is the assumption of a linear softening response [141].

Cui et. al. [35] noted that stress-based criteria are more suited for the prediction of delaminations in cases where no macroscopic singularity is present, while fracture-based criteria are more suited for cases where macroscopic singularities exist. To overcome both the cumber of requiring different failure criteria in different situations and of having to determine the possible fracture location in advance, they then presented an interface model that could predict the onset and growth of delamination in both situations, regardless of whether singularities are present. In this 2D model, horizontal and vertical non-linear spring elements were included between plies. The initial stiffness of the springs were stipulated to be high, and when a threshold force was reached the spring stiffness was reduced to physically represent delamination.

Collombet et. al. [142] used node-pairs in the modeling of the interface where the node pairs were initially connected. When a failure criterion was met to signal the initiation of delamination, the node pairs were then separated, simulating the propagation of delamination. In a two-dimensional study, Lo et. al. [143] devised non-linear interface elements and

used the interface elements to study delamination growth from a matrix crack tip in thick composite laminates subjected to low-velocity impact. Other cohesive methods such as the point cohesive method and the line cohesive methods were also proposed [144].

Wisheart et. al. [145] employed zero-thickness interface elements with variable tractions and relative displacements between node-pairs in their study of impact induced delaminations. They verified their model under mode I, mode II and mixed-mode loadings and their model predicted delamination shapes that demonstrated good agreement with experimental results. A detailed overview of delamination characterization is provided by Tay in [140]. A detailed overview of delamination modeling techniques is provided by Bouvet et. al. in [41] with the conclusion that interface elements are required to simulate the initiation of delaminations and the degradation caused by delaminations accurately.

2.5 Brief review of types of elements, implicit and explicit analyses and non-linear analyses [146]

The elements available in the element library of Abaqus are generally characterized by considering its family (Continuum, shell, membrane, beam, truss etc.), its number of nodes which is determined by the element shape and geometric order, the degrees of freedom (displacements, rotations, temperature etc.), its formulation (the mathematical theory used to define an element's behavior) and its integration. In the Abaqus element library there are different elements available to provide a complete geometric modelling capability. Numerical integration is used in all elements, allowing for complete generality in the material behaviour. In shell and beam elements, the element properties can either be defined as general section behaviours, or the cross section of each element can be integrated numerically such that

the non-linear response can be obtained. The elements can be broadly classified into two different categories- full integration elements which include all triangular and tetrahedral elements or reduced integration elements. In full integration elements, there are sufficient integration points such that the virtual work expression can be integrated exactly. On the other hand, reduced integration elements have sufficient integration points to integrate the contributions of the strain field of one order less than the order of interpolation. Advantages of using reduced integration elements include lesser computational time, and allowing for the computation of strains and stresses at points which provide optimal accuracy. However the disadvantages of using reduced integration elements include the possibility of hourglassing, in which there is no strain at the integration points and inaccurate distortions of the mesh occur. The main difference between continuum shell elements and solid continuum elements is their formulation- Continuum shell elements make use of the shell theory in formulation, and the displacement in the z-direction (thickness direction), w, is assumed to be constant across the thickness of the shell. In this case, the displacements in the x and y direction, u and v respectively, can be derived from the curvature using: $u = u_o - z(dw/dx)$ and $v = v_o - z(dw/dy)$ where u_o and v_o are the displacements of the mid-plane of the shell. At the mid-plane of the shell, z=0. These assumptions are not made in the formulation of solid continuum elements. For the purpose of modelling bending, 2D or 3D fully integrated linear isoparametric continuum elements are unsuitable because they are overly stiff and pose the problem of shear locking in which very large shear strain energy inaccurately increases the flexural rigidity of the model. Continuum shell elements can be employed as a means to overcome the problem of shear locking, and are suitable for the modelling of thin models in which bending is dominant. Continuum shell elements are more suitable for the modeling of thin structures, in which bending is dominant. In continuum shells, the transverse shear has parabolic distribution through the thickness.

However for continuum solid elements, the transverse shear has a linear distribution through the thickness, and more continuum solid elements has to be included in the thickness direction to match the accuracy of shell elements. Hence, the use of continuum shells would allow for a more accurate transverse shear stress response which is important in the case of impact because these stresses are responsible for delamination. More detailed information on the elements available in Abaqus can be found in the Abaqus manual [146].

In Abaqus, there exist Abaqus/Standard, a general-purpose finite element program, and Abaqus/Explicit, an explicit dynamic finite element program. In Abaqus/Standard, the displacement is not a function of time. The solution of a problem using Abaqus/Standard involves the inversion of the stiffness matrix. In Abaqus/Explicit, the displacement is a function of time, and velocity and acceleration can be considered. The stiffness matrix also does not have to be inversed. However, such an analysis is unstable and very small time steps are required to ensure that the solution is conditionally stable. For the purpose of modelling low-velocity impact, both Abaqus/Standard and Abaqus/Explicit could be employed. Each method has its advantages and disadvantages. The modelling of low-velocity impact using Abaqus/Standard involves the assumption that the low-velocity impact event is a quasi-static event, and impact is simulated by prescribing a displacement to the impactor. On the other hand, the use of Abaqus/Explicit in the modelling of low-velocity impact allows for the assignment of an initial velocity to the impactor. To ensure stability, Abaqus/Explicit uses very small time increments of order 1e-9s. However a low-velocity impact event is considered long in time, of the order 5e-3s. A large amount of increments are hence required before the simulation is complete, resulting in a significantly longer simulation runtime when Abaqus/Explicit is used as compared to Abaqus/Standard. An advantage of the use of Abaqus/Explicit in the

modelling of low-velocity impact is that it allows for a more detailed study of the impact event such as the impact force versus time curve, and the energy dissipated in relation to each different damage mode occurring in the laminate due to the impact event. More detailed information on the differences between Abaqus/Standard and Abaqus/Explicit could be found in the Abaqus manual [146].

Material non-linearity and geometric non-linearity can exist in stress analysis problems. A range of non-linear material behaviors which are mainly history dependent are offered in Abaqus. In these materials, the material's response at a particular time is dependent on what the material underwent at previous time steps. However in the analysis of low-velocity impact of CFRP laminates, material non-linearity need not be taken into account since carbon-epoxy composites are brittle. To account for geometric non-linearity, Abaqus has a 'Nlgeom' setting that is turned off by default for Abaqus/Standard steps and turned on by default for Abaqus/Explicit steps. This setting can be turned on or off for each individual step in the finite element analysis in Abaqus/Standard. When the 'Nlgeom' setting is turned off, the problem is defined as a small displacement analysis in which non-linearity is ignored and the kinematic relationships in the element calculations are linear. In this case, the elements are formulated in their reference configurations using their reference nodal coordinates. When the 'Nlgeom' setting is turned on, the problem is defined to include the effects of large displacements, and the elements are formulated in their current configurations using their current nodal coordinates. For the purpose of modelling low-velocity impact and CAI test in CFRP laminates, geometric non-linearity is included to account for the large rotations especially during the CAI test.

2.6 Conclusion

In this chapter, the background information required for this research such as the definitions of low-velocity impact and barely visible impact damage have been presented. The importance of CAI strength as a damage tolerance measure has also been explained. In the literature review section of this chapter, different computational modelling methods for low-velocity impact tests and CAI tests of CFRP materials adopted by other researchers have been presented. This information is useful for the research because a good understanding of the different computational modelling methods employed and the results achieved is necessary for fulfilling one of the objectives of this research: To avoid the over-simplification of the FE models such that the predictions obtained and inaccurate, yet also to avoid having to model to such an impractical and excessive level of accuracy such that the method loses its efficacy. The various low-velocity impact damage mechanisms in CFRP materials, such as the mechanisms of matrix cracking and the mechanisms of the interaction between matrix cracks and delaminations have been expounded in this chapter. This information would be useful in the discussions in Chapter 4 of this thesis.

CHAPTER 3

FINITE ELEMENT MODEL

Progressive failure analysis of composite structures generally involves a stress analysis, where the stress and strain distributions in the laminates due to a prescribed load and boundary conditions are analyzed, and a failure analysis, where damage accumulation in the laminates is evaluated by a proposed failure criterion to detect failure initiation combined with a proposed material property degradation model to simulate a loss in the load-carrying capability of the element in which failure has initiated [147]. Some of the challenges faced in the performance of progressive failure analysis include convergence issues, mesh dependency issues and the selection of an appropriate material softening law.

In the finite element simulation of progressive failure due to low-velocity impact, the implementation of a suitable failure criterion and material property degradation model that describes the material behavior appropriately is essential. This is because the material model plays the very important role of determining factors such as the damage extent, amount of stiffness reduction and the final structural behavior [28].

3.1 Modeling strategy

There exist different modes of damage in a composite laminate, and these different modes of damage accumulate and interact with each other, leading ultimately to final failure of the composite laminate. A progressive damage model should have the capability of capturing the different damage modes. There exist a large number of failure criteria and damage modeling techniques. In the current study, two different constitutive models are used [148] to model the in-plane damage progression and interlaminar delamination. The continuum mechanics (CDM) method is used to model the in-plane damage progression. This model used is based on a hybrid maximum-stress and Tsai-Wu or Hashin failure criteria written into an Abaqus user-defined subroutine (UMAT) [146] for use with 3D continuum shell elements. Delaminations are modeled using the cohesive elements available in Abaqus.

3.1.1 In-plane damage modeling

3.1.1.1 Damage initiation

Hybrid Maximum-Stress and Tsai-Wu failure criterion

As explained in Section 2.3 above, the Tsai-Wu failure criterion is incapable of differentiating between the different modes of failure. To overcome this limitation, the Maximum Stress failure criterion is used in conjunction with the Tsai-Wu failure criterion, where the former is used to detect and model fiber-dominated failure initiation, and the latter to detect and model matrix-dominated failure initiation [148, 149].

Fiber dominated damage initiation is determined using the following maximum stress criterion in the fiber direction:

Tensile fiber failure: $\frac{\sigma_{11}}{X_T} = 1$ (11)

Compressive fiber failure: $\frac{\sigma_{11}}{X_C} = -1$ (12)

Matrix dominated damage initiation is determined using the following Tsai-Wu failure criterion:

$$F_1\sigma_1 + F_2\sigma_2 + F_{66}\tau_{12}^2 + F_{11}\sigma_1^2 + 2F_{12}\sigma_1\sigma_2 + F_{22}\sigma_2^2 = 1 \quad (6)$$

$$F_1 = \frac{1}{X_T} + \frac{1}{X_C}, \quad F_{11} = -\frac{1}{X_T X_C}, \quad F_2 = \frac{1}{Y_T} + \frac{1}{Y_C},$$

$$F_{22} = -\frac{1}{Y_T Y_C}, \quad F_{44} = F_{66} = \frac{1}{S_{12}^2}, \quad F_{12} = -\frac{\sqrt{F_{11}F_{22}}}{2}$$

Hashin failure criterion

The Hashin failure criterion was also used to model failure initiation for both fiber and matrix dominated damage in a separate FE code. Damage is deemed to have initiated once any of the following sub-criteria that make up the Hashin failure criterion is met:

Tensile fiber failure (where $\sigma_{11} > 0$)

$$\left(\frac{\sigma_{11}}{X_T}\right)^2 + \frac{\sigma_{12}^2}{S_{12}^2} = 1 \tag{13}$$

Compressive fiber failure (where $\sigma_{11} < 0$)

$$\left(\frac{\sigma_{11}}{X_C}\right)^2 = 1 \tag{14}$$

Tensile matrix (transverse direction) failure (where $\sigma_{22} > 0$)

$$\frac{{\sigma_{22}}^2}{Y_T^2} + \frac{\sigma_{12}^2}{S_{12}^2} = 1 \tag{15}$$

Compressive matrix failure (where $\sigma_{22} < 0$)

$$\left[\left(\frac{Y_c}{2S_{23}}\right)^2 - 1\right]\frac{\sigma_{22}}{Y_C^2} + \frac{{\sigma_{22}}^2}{4S_{23}^2} + \frac{\sigma_{12}^2}{S_{12}^2} = 1 \tag{16}$$

3.1.1.2 Damage progression

After damage is deemed to have initiated, damage progression is modeled using a stress-softening model to capture the energy dissipation process. A smeared formulation as proposed by Pinho et al. [118] is used, in order to avoid strain localization which would in turn lead to mesh dependency. Strain localization occurs when narrow and highly strained zones emerge prior to failure. In the smeared formulation, cracks are not explicitly modeled; rather, fracture energy is distributed or smeared over the entire element volume. As a result, a length parameter with dimensions relative to the element dimensions and runs perpendicular to the fracture plane, also known as characteristic length of the element, is introduced into the constitutive law. A characteristic length is an averaging length that is a function of geometry and material properties [150]. The reason for the introduction of a length parameter into the constitutive law is demonstrated in the following example, as explained in [118]:

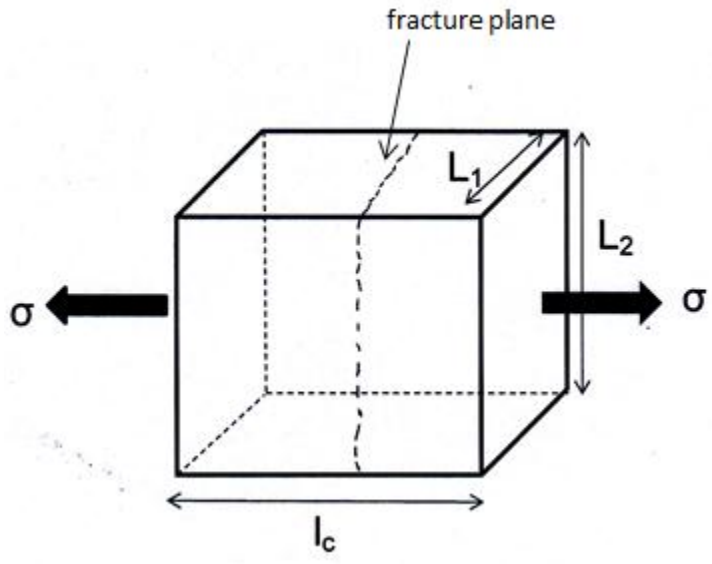

Figure 13 Example of an element loaded in tension up to final fracture

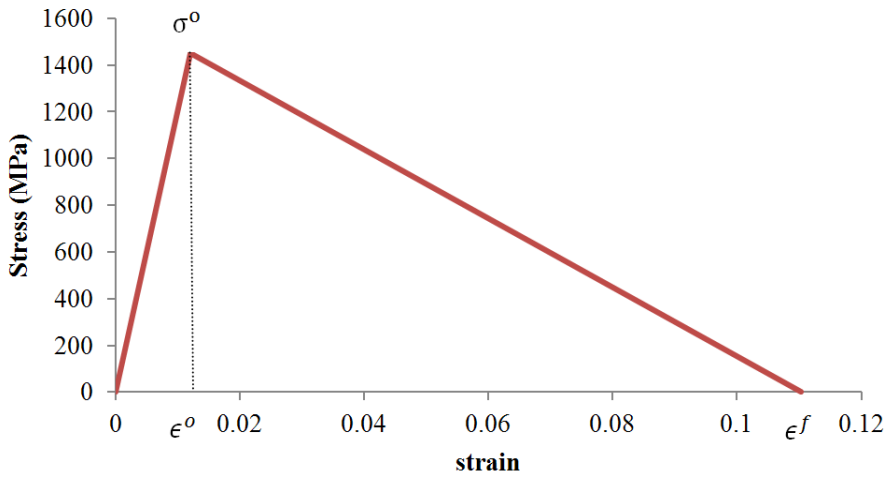

Figure 14 Linear softening applied to simulate material degradation

Consider an element shown in Figure 13, with dimensions L_1 by L_2 by l_c, failed along a fracture plane. The energy absorbed by the element after complete fracture, U, is given by:

$$U = V \frac{\sigma^o \epsilon^f}{2} = L_1 L_2 l_c \frac{\sigma^o \epsilon^f}{2} \quad (17)$$

Where V refers to the volume of the element, and V= $L_1 L_2 l_c$,

σ^o refers to the material strength and

ϵ^f refers to the maximum strain as demonstrated in Figure 14.

The energy per unit area, G_{fc} in the case of fiber dominated damage and G_{mc} in the case of matrix dominated damage, when multiplied by the corresponding area given by $L_1 L_2$, would give us the total energy absorbed by the fractured element, U.

Taking the example of fiber dominated damage,

$$\mathrm{U} = G_{fc}\, L_1 L_2 \tag{18}$$

Equating equations (17) and (18), we obtain the maximum strain ϵ^f as follows:

$$\epsilon^f = \frac{2G_{fc}}{\sigma^o l_c} \tag{19}$$

As seen in equation (19), the characteristic length l_c has been introduced into the constitutive law.

The basis of such a softening law is the assumption that the total energy required to create a crack that passes through the element is the same as the energy required to fail the element. The strain energy released by an element undergoing failure can be determined from the area under the stress-strain curve (Figure 14), multiplied by the characteristic length of the element, l_c. In Abaqus [146] l_c is defined as the square root of the area of a continuum shell element. This strain energy released by the element undergoing failure is then equated to the critical energy release rate, or the fracture toughness, of the composite material in the fiber direction, G_{fc}, as summarized in Equation (20):

$$\int \sigma_{11}\, \mathrm{d}\epsilon_{11}\, l_c = G_{fc} \tag{20}$$

Where $\epsilon_{11} l_c$ is the effective displacement for this failure mode.

Equation (20) is used to simulate damage progression after fiber dominated damage predicted by the Maximum stress failure criterion has initiated. Damage progression is modeled by degrading E_{11}, E_{22} and G_{12}, together with the Poisson's ratio ν_{12} using a linear softening law. The stress of the ply decreases linearly with strain, as shown in Figure 14. Similarly, after matrix dominated damage initiation is predicted by the Tsai-Wu failure criterion, matrix damage progression is modeled using a linear softening law,

in which the transverse stiffness E_{22}, shear stiffness G_{12} and Poission's ratio ν_{12} in the elements are degraded.

For matrix dominated damage progression, mixed-mode failure has to be considered since matrix dominated damage involves both the normal stress σ_{22} and the shear stress τ_{12}. In this case, the linear softening law is defined based on the following energy criterion:

$$\int \sigma_{eff} \mathrm{d}\epsilon_{eff} l_c = G_{mc} \tag{21}$$

Where

$$\sigma_{eff} = \sqrt{{\sigma_{22}}^2 + \tau_{12}^2} \tag{22}$$

$$\epsilon_{eff} = \sqrt{{\epsilon_{22}}^2 + \gamma_{12}^2} \tag{23}$$

σ_{eff} refers to the effective stress,

ϵ_{eff} refers to the effective strain,

G_{mc} refers to the mixed-mode fracture toughness under combined Mode I and Mode II loading

G_{mc} is assumed to follow the mixed-mode fracture enery criterion developed by Benzeggagh and Kenane [151]:

$$G_{mc} = G_{sc} + (G_{sc} - G_{nc})B^{\eta} \tag{24}$$

Where G_{nc} refers to the mode I critical fracture energy,

G_{sc} refers to the mode II critical fracture energy,

$$B = \frac{G_S}{G_N + G_S}$$

$$G_N = \frac{1}{2}\langle\sigma_{22}\rangle\langle\epsilon_{22}\rangle l_c$$

$$G_S = \frac{1}{2}\tau_{12}\gamma_{12} l_c$$

η is a material property obtained from mixed mode bending tests at different mode ratios. The value used here is 1.39.

A combination of fiber and matrix dominated damage is considered in the model using the following degradation methods:

$$E_{11} = (1 - d_f)E_{11_0} \tag{25}$$

$$E_{22} = (1 - d_f)(1 - d_m)E_{22_0} \tag{26}$$

$$G_{12} = (1 - d_f)(1 - d_m)G_{12_0} \tag{27}$$

$$\nu_{12} = (1 - d_f)(1 - d_m)\nu_{12_0} \tag{28}$$

Where the subscript 0 indicates undamaged material properties,
d_f refers to the degradation factor for fiber dominated damage,
d_m refers to the degradation factor for matrix dominated damage.

The degradation factors are defined in such a way that they degrade the relevant material properties linearly to zero. The degradation factors take on the value of 0 at the onset of failure (when $\epsilon = \epsilon^o$ as shown in Figure 14) and a value of 1 at final failure, when $\epsilon = \epsilon^f$. After failure initiation is predicted by a failure criterion, damage progression is modelled by multiplying the relevant material parameters to be degraded by (1-*d*) in each time-step of the simulation. This ensures that the material parameters are progressively and linearly degraded to zero without any discontinuity.

The instantaneous value of the degradation factors d_f and d_m can be obtained from equations (20) and (21), together with Figure 14, and is defined by Pinho et al. [118] to be:

$$d^{inst} = \max[0, \min\left[1, \epsilon^f \frac{\epsilon - \epsilon^o}{\epsilon(\epsilon^f - \epsilon^o)}\right]] \tag{29}$$

When tensile fiber dominated damage is predicted by the Hashin failure criterion, the effective stress and displacements have to be considered

before the fiber dominated degradation law is applied because in such a case, both the tensile and shear stresses σ_{11} and τ_{12} are involved. The following are expressions for the effective stress and displacement in fiber dominated failure:

$$\sigma_{efib} = \sqrt{\sigma_{11} + \tau_{12}^2} \tag{30}$$

$$d_{efib} = l_c \sqrt{{\epsilon_{11}}^2 + \gamma_{12}^2} \tag{31}$$

The effective stress and strain in matrix-dominated failure are given in Equations (22) and (23).

The mixed-mode energy criterion used for this model in which damage initiation is predicted by the Hashin failure criterion is the Benzeggagh and Kenane criterion [151] (Equation (24)).

3.1.2 Delamination modeling

In this model, damage at the ply interface, or delaminations, are modeled using cohesive elements available in Abaqus. Layers of cohesive elements are included in between composite plies with different orientations. This can be done to reduce computational time because it is known that delamination only occurs mainly between plies with different fiber orientations under impact loading [29].

The damage in the cohesive elements is described by a traction separation law available in Abaqus. Before damage initiation, elastic behavior is assumed. The elastic behavior is described by the stress-strain relationship of the elements, where the stresses t_n, t_s and t_t are obtained by dividing the force components over the original area at each integration point, and the strains ϵ_n, ϵ_s and ϵ_t are obtained by dividing the separations or displacements δ_n, δ_s and δ_t by the original thickness, T_o, of the cohesive

elements at each integration point. The following expression describes the relationship between the cohesive stresses and strains:

$$\begin{bmatrix} t_n \\ t_s \\ t_t \end{bmatrix} = \begin{bmatrix} K_{nn} & & \\ & K_{ss} & \\ & & K_{tt} \end{bmatrix} \begin{bmatrix} \epsilon_n \\ \epsilon_s \\ \epsilon_t \end{bmatrix} \quad (32)$$

Where t_n refers to the normal traction

t_s and t_t refers to the two shear tractions

K_{nn}, K_{ss} and K_{tt} refers to the cohesive stiffness

ϵ_n, ϵ_s and ϵ_t refers to the normal and shear strains

$\epsilon_n = \frac{\delta_n}{T_o}$, $\epsilon_s = \frac{\delta_s}{T_o}$, $\epsilon_t = \frac{\delta_t}{T_o}$

T_o refers to the original thickness of the cohesive element

δ_n refers to the normal displacement

δ_s and δ_t refers to the two shear displacements.

According to the traction-separation law, delamination is assumed to initiate once the following stress-based quadratic failure criteria proposed by Brewer et. al. [152] is satisfied:

$$\frac{{t_n}^2}{N^2} + \frac{t_s^2}{S^2} + \frac{t_t^2}{S^2} = 1 \quad (33)$$

Where N refers to the normal strength of the interface and

S refers to the shear strength of the interface.

Delamination growth is then modelled using an energy-based linear softening traction-separation law:

$$\int T d\delta = G_{if} \quad (34)$$

where G_{if} refers to the mixed mode fracture energy

(based on the Benzeggagh and Kenane criterion [151])

T refers to the effective traction,

$$T = \sqrt{t_n^2 + t_s^2 + t_t^2} \tag{35}$$

δ refers to the displacement

$$\delta = \sqrt{\delta_n^2 + \delta_s^2 + \delta_t^2} \tag{36}$$

3.1.3 Control of finite element instabilities

The implementation of the material softening or stiffness degradation method described in sections 3.1.1.2 and 3.1.2 above might lead to numerical instabilities and non-convergence in the finite element analysis. Graça-e-Costa et al [153] proposed a non-iterative approach to overcome convergence difficulties. This approach is used in approximating the linear-softening curve in the stress-strain relationship by a zig-zagging curve (Figure 15) to overcome convergence problems in this current study. The stiffness of the the damaged element is degraded in a stepwise manner (which also means that the degradation factor is increased in a piecewise manner) while the stress deviation from the linear curve is kept at less than 5% of the strength. Such a zig-zag degradation ensures that a positive tangent modulus exists most of the simulation time, and a converged solution for the stiffness can be attained faster when the stiffness is piecewise constant with respect to strain and simulation time.

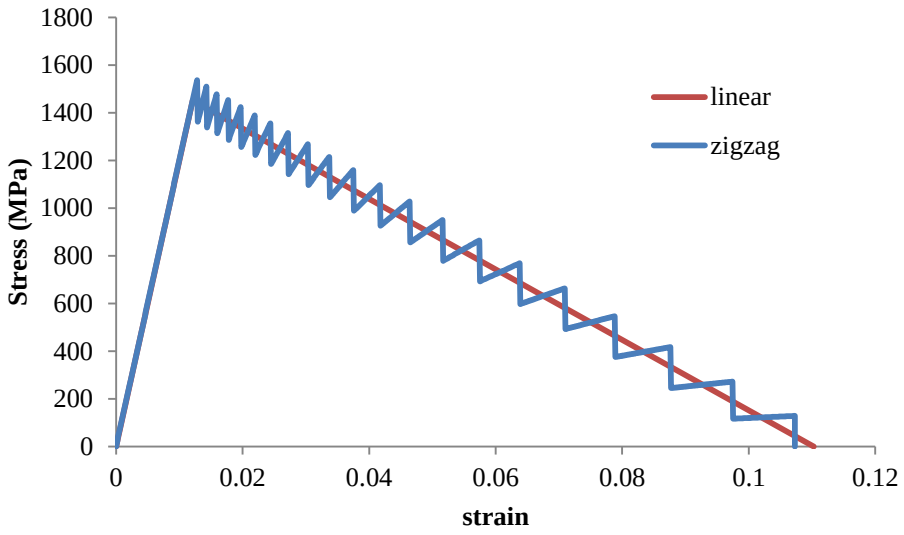

Figure 15 Zig-zag approximation of the linear softening law for in-plane material stiffness degradation [148]

This zig-zag approximation is implemented in all the linear softening laws used for the simulation of damage progression described in sections 3.3.1.2 and 3.3.2 above.

3.2 Development of FE model

The commercially available finite element analysis software Abaqus/Standard version 6.11 was used in this current study. In the first analysis perfomed, a simple 8-ply laminate with $[0/45/90/-45]_s$ layup was chosen to be used in the impact FE simulations. Such a laminate stacking sequence can be considered the most common stacking sequence used in many applications. This layup would continue to be the reference layup for the parametric studies conducted and reported in Section 4.2. Throughout this study, the 0^o fiber direction is defined to be horizontal, and angle is increased by rotating the positive x-axis in the positive y-direction. Figure 16 is a pictorial representation of the way fiber orientations is defined in this study.

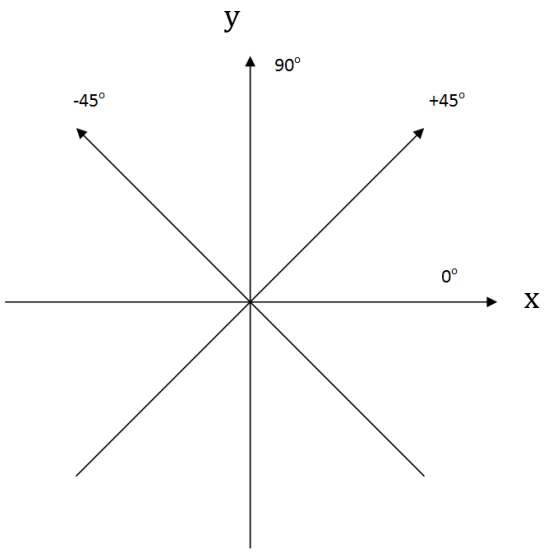

Figure 16 Fiber orientations

The FE model of the composite plies was modeled using the eight-node quadrilateral 3D continuum shell elements SC8R with one element per ply in the thickness direction. The intralaminar damage model described in

Section 3.1.1 is assigned to the continuum shell elements within the composite plies by means of the implementation of a user-defined material subroutine UMAT. Each interface was modeled with one cohesive element in the thickness direction, and the intralaminar damage model described in Section 3.1.2 is used.

Continuum shell elements are chosen in this model because they allow for more accurate contact modeling than conventional shell elements, with consideration for two-sided contact and changes in thickness. Continuum shell elements can also model the stacking of different angled plies in a composite laminate better as they capture the through-thickness response more accurately than other element types [146].

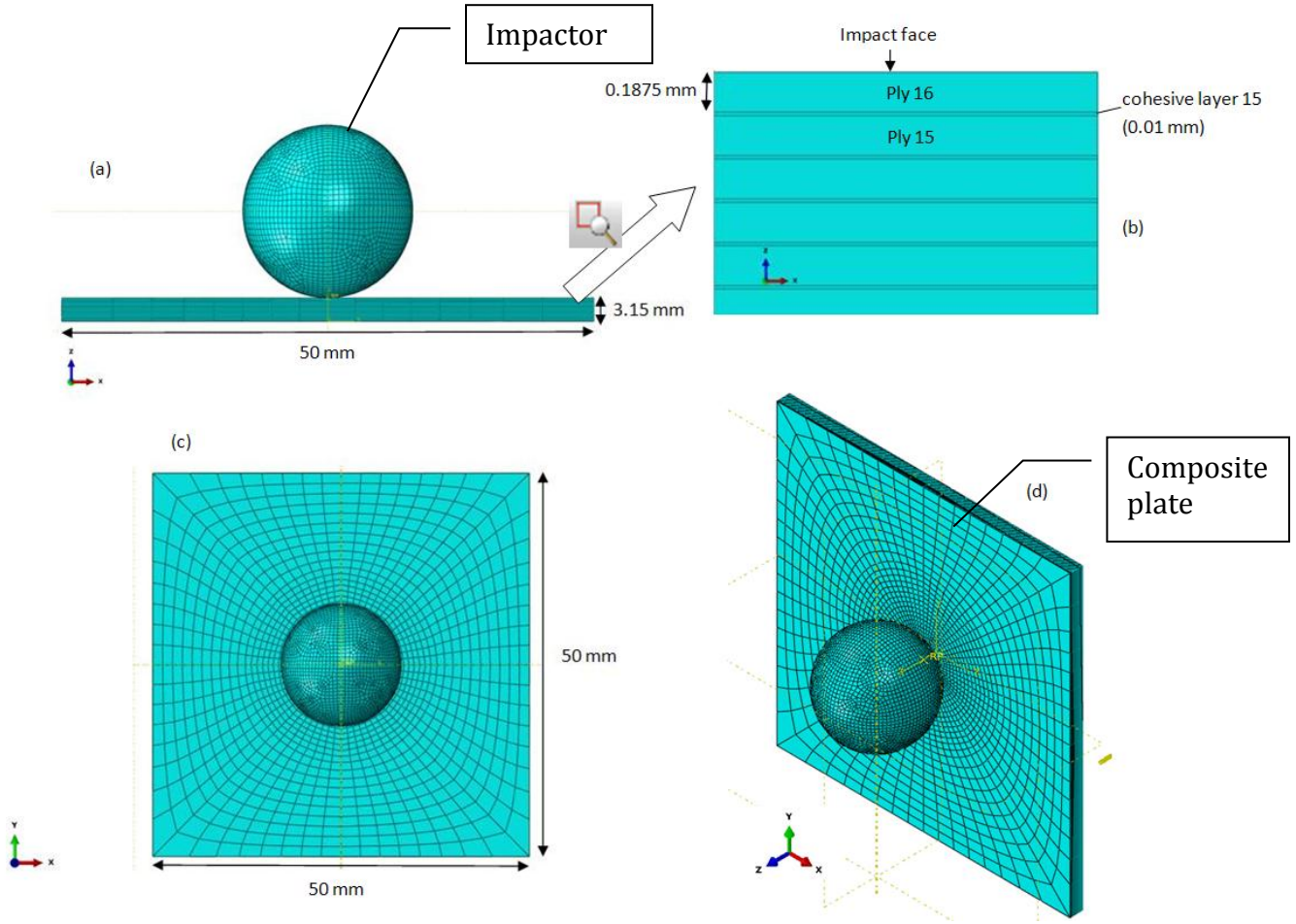

Figure 17 (a) x-z view of the impact FE model, (b) Magnified x-z view, showing the ply and cohesive numbering and dimensions, (c) x-y view and (d) isometric view

The dimensions of the FE model are chosen to be 50mm by 50mm for convenience of modeling and meshing. Each composite ply was 0.1875mm thick, and each cohesive element used to model the interface was modeled to be 0.01mm thick. The thickness of the cohesive elements should be at least 10 times smaller than the composite elements [154]. The cohesive layers used in this FE model are about 20 times thinner than the composite plies. In this study, the bottom most ply away from the impact face is named "Composite Ply 1", and the interface ply between composite plies one and two is named "Interface 1", or "Cohesive 1". In this manner, the composite ply on the impact face will be numbered the same number as the total number of plies the composite laminate is composed of, as illustrated in Figure 17.

The material properties used in the FE model are those of T800S/3900-2B (high strength graphite/toughened epoxy, Toray, Japan) [155, 156] and are summarized in Table 2 below, while the interface properties are summarized in Table 3. These material properties are chosen to compare the simulation results with the experimental results of Kimpara et al. [3].

Elastic Property	**Value**
Modulus in the fiber direction E_{11} (GPa)	138.5
Transverse modulus E_{22} (GPa)	8.76
Transverse modulus E_{33} (GPa)	8.76
Shear modulus G_{12} (GPa)	4.57
Shear modulus G_{13} (GPa)	4.57
Shear modulus G_{23} (GPa)	3.40
Poisson's ratio ν_{12}	0.324
Poisson's ratio ν_{13}	0.324
Poisson's ratio ν_{23}	0.45
Ply Strength	**Value**
Longitudinal tensile X_t(MPa)	2960
Longitudinal compression X_c (MPa)	1500
Transverse tensile Y_t(MPa)	26
Transverse compression Y_c(MPa)	146
Longitudinal shear S_{12}(MPa)	75
Transverse shear S_{23}(MPa)	75
Fracture Toughness	**Value**
Longitudinal toughness in tension G_{fc}^{+} (kJ/m^2)	152
Longitudinal toughness in compression G_{fc}^{-} (kJ/m^2)	79
Transverse normal toughness G_{nc} (kJ/m^2)	0.71
Transverse shear toughness G_{sc} (kJ/m^2)	2.176

Table 2 Material properties of composite plies

Property	Value
Normal strength N (MPa)	26
Shear strength S (MPa)	75
Normal toughness G_n (kJ/m^2)	0.71
Shear toughness G_s (kJ/m^2)	2.176

Table 3 Material properties of cohesive elements

The initial stiffnesses and interface strengths of cohesive elements are necessary input parameters. The initial stiffness values in Equation (32) are calculated from the thickness of the cohesive elements and modulus of the composite plies in the following equation [157]:

$$K_{nn} = K_{ss} = K_{tt} = \frac{\alpha E_3}{T_o} \tag{37}$$

Where α is a parameter much larger than 1; $\alpha \gg 1$

Turon et. al. [157] determined that an interface stiffness should be sufficiently large to model a reasonable stiffness value, yet small enough to reduce risks of numerical problems such as spurious oscillations of the tractions in an element. Turon et. al. also determined that the loss of stiffness of the composite laminate due to the presence of an interface is less than 2% when the value of α is chosen to be greater than 50. They thus proposed a cohesive stiffness value of 4.43MN/mm^3 for a sublaminate of thickness 0.125mm. Camanho et. al. [158] proposed a stiffness value of 1MN/mm^3 for all sublaminate thicknesses. In the FE models used in this research, the interface modulus E_3 in Equation (37) is assumed to be that of the matrix material #3900-2B produced by Toray, with a value of 3.5GPa, and the value of α was chosen to be 50.

For the prediction of delamination initiation in Equation (33), the values for cohesive strength parameters N and S have to be specified. Brewer et. al. [152] determined that the transverse tensile strength and shear strengths of a unidirectional composite provide good estimations for the interlaminar normal and shear strengths N and S. Hence, the values of N and S are assumed to be 26MPa and 75MPa in this study respectively. The value of the shear toughness G_s is obtained from ENF tests performed on five T800S-3900-2B specimens by Davidson et. al [156]. The value of the normal toughness $G_n$is obtained from Mode I interlaminar fracture toughness tests [159] performed by Hojo et al.

There are two different ways of modeling the connection between the composite and cohesive plies. In the first method, both the composite and cohesive plies share the same in-plane mesh size such that the nodes at each layer are shared with the adjacent layers. The second method involves connecting the different plies through the use of *Tie Constraints*, a capability within Abaqus. Tie constraints serves to bond the surfaces of the plies together permanently, ensuring that the translational and rotational movements are the same for the connecting surfaces. Both methods were employed in this study, and it was found that the first method was about two times more computationally efficient than the method of using tie constraints.

The impactor is modeled as a rigid body with infinite stiffness, and is constrained to move only in the z-direction. The impact process is modeled by prescribing a displacement instead of a velocity to the impactor, as low-velocity impact can be considered a quasi-static process [12, 41]. In impact experiments, impact energy is varied by varying the mass of the impactor and height from which the impactor is dropped. The impact energy can be calculated from the standard formula for potential energy, E=mgh. In this FE model, the impact energy is obtained from the area under the force-displacement curve plotted from the FE results.

The first impact model was meshed in the simplest way with identical elements of the same size (Mesh 1), shown in Figure 18. Impact was simulated using a displacement of 5mm in the thickness direction. The edges of the laminate were fully clamped. However the use of identical elements throughout the entire model is unnecessarily computationally expensive as elements around the locus of the point of impact has to be sufficiently small in order to capture the impact damage accurately, while coarser elements can be used nearer the edge of the impacted CFRP laminate where damage is not expected to occur. A second mesh (Mesh 2) (Figure 18) is then generated using hex-dominated elements with advancing front algorithm based on local seed placement with enhanced hourglass control. This algorithm allows for the generation of a biased mesh with variable element sizes- one that is denser in the middle where impact occurs, and coarser towards the edges of the laminate. Furthermore, Mesh 2 is designed such that the elements are arranged in a circular manner outward [160]. This is advantageous to the modeling of quasi-isotropic composite laminates because having the edges of the elements aligned in the fiber direction would improve the prediction of matrix crack paths [161]. Figure 18 shows that both meshes are capable of predicting similar impact damage induced, while Table 4 demonstrates the significant computational time savings achieved in using Mesh 2 instead of Mesh 1.

To shorten the computational time even further, a partial cohesive model as shown in Figure 19 is built. In this model, cohesive interfaces are included only in the center portion of the CFRP laminate model with a radius of 30mm (Figure 19c). The edge of the laminate where damage is not likely to occur does not contain cohesive elements. This is shown in Figure 19(a) and (b), and can be built using just one element through the entire laminate thickness. The variation in angles of each ply is specified using the composite layup module built in Abaqus.

Comparing the FE results obtained from the partial cohesive model with the results obtained from the models with Mesh 1 and Mesh 2, the partial cohesive model is proven to be capable of predicting similar impact damage induced from low-velocity impact Figure 18. The impact damage sequence predicted by both models is also the same. Hence this method of modeling is a viable method of modeling low-velocity impact, while reducing the total number of elements contained in the laminate model and subsequently reducing the total CPU time by approximately two times as reported in Table 4. This reduction in CPU time would be of significant impact especially in thicker laminates composed of a larger number of plies.

	Number of elements per ply	Total CPU time (h)
Mesh 1 (Uniform element size)	19600	47.7
Mesh 2	1056	19.4
Partial cohesive model	840	8.3

Table 4 Total CPU time required to complete a low-velocity impact simulation on a 16 ply laminate with $[0/45/90/-45]_{2s}$ layup

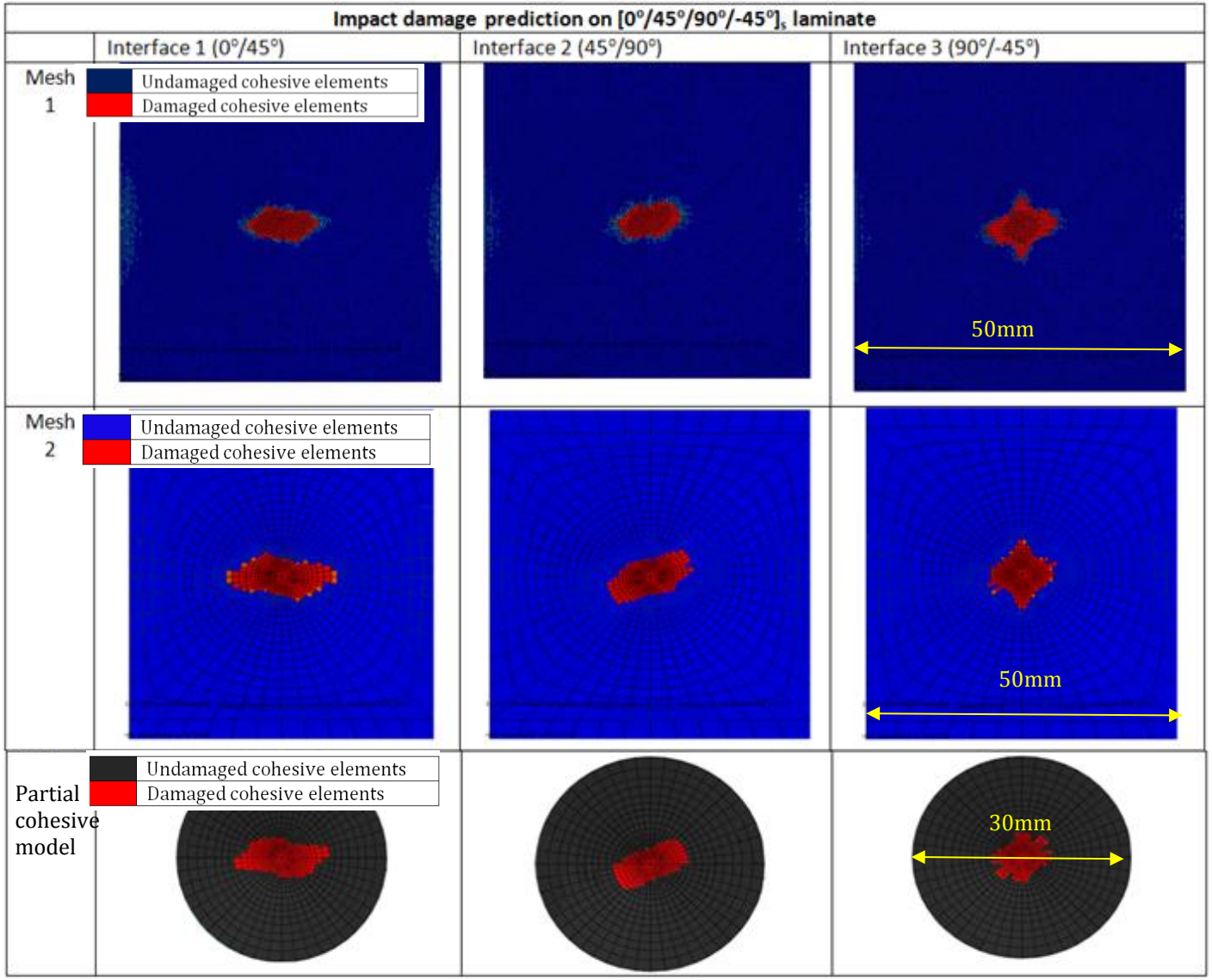

a

b

c

Figure 18 Low-velocity impact damage prediction for a [0/45/90/-45]s laminate obtained from (a) Mesh 1 (composed of uniform elements-the mesh is too dense to see the individual elements clearly), (b) Mesh 2 (composed of smaller elements around the point of impact and larger elements towards the edge of the laminate) and (c) Partial cohesive model

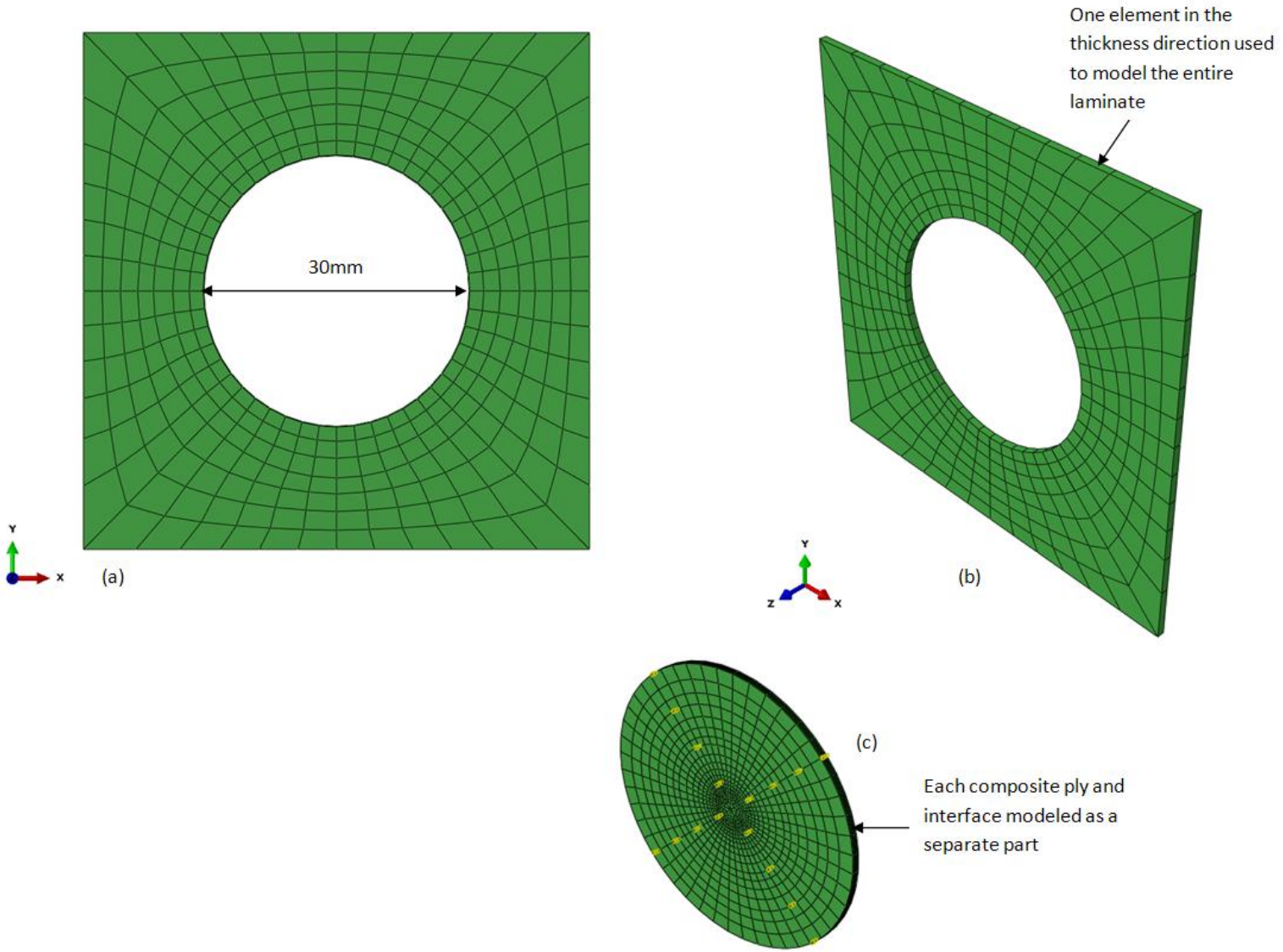

Figure 19 (a) x-y view of the part without cohesive interfaces

(b) isometric view of the part without cohesive interfaces

(c) isometric view of the part containing cohesive interfaces

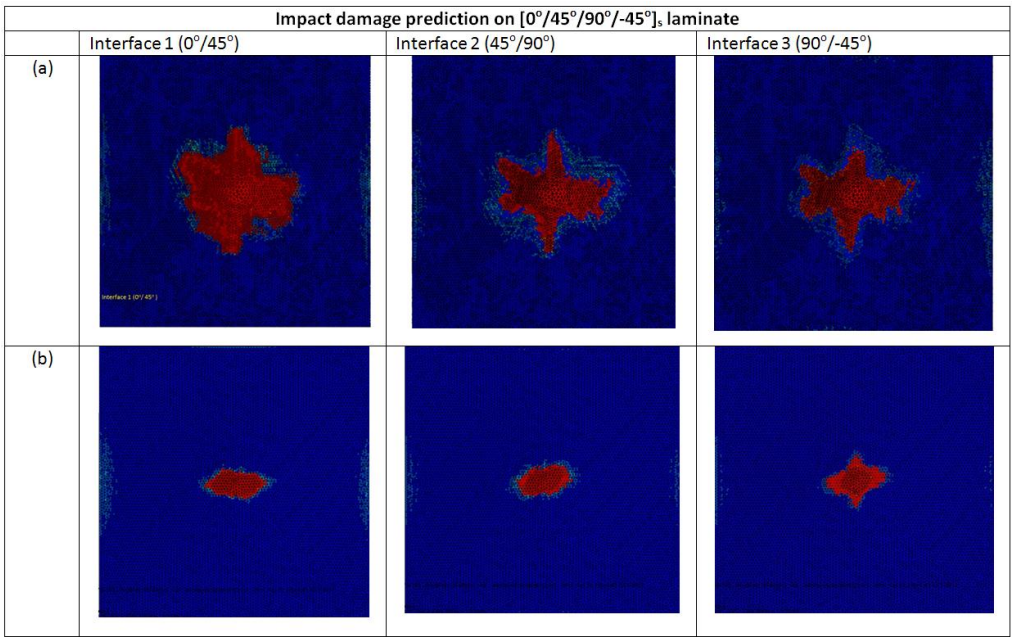

Figure 20 Low-velocity impact damage prediction for a [0/45/90/-45]s laminate with (a) immediate degradation and (b) gradual degradation according to the linear law in Figure 21

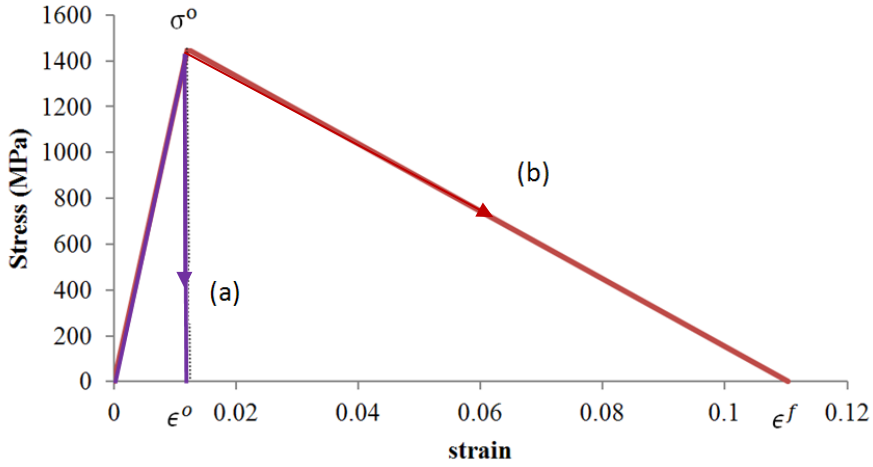

Figure 21 (a) Immediate stress degradation to zero after damage initiation (b) Linear softening law simulating damage progression

In Section 3.1.1.2, a degradation model which incorporates a linear-softening law used in the FE analysis is detailed. The results from the low-velocity impact FE simulation depicted in Figure 20 illustrate the necessity of implementing such a softening model. As seen in Figure 20(a), the low-velocity impact induced delaminations are predicted to be of approximately the same shape and size at every interface when the linear softening law is not incorporated into the material degradation, and the stress is instantly reduced to zero after damage initiation (Figure 21(a)). It has however been widely observed in experimental studies that delaminations caused by low-velocity impact are generally elongated, with their major axis coinciding with the fiber orientation of the layer below the interface where the delamination occurs [36, 58-60]. Figure 20(b) shows that with the linear softening law incorporated into the damage progression model, the delaminations predicted are elongated in the direction of the fiber orientation of the ply below the interface where the delaminations occur. This is in concordance with the experimentally observed delaminations, signifying that a stress-softening model is necessary for the accurate prediction of impact damage.

3.3 Conclusions

The following lists the main points that have been established in this chapter, and will be adopted in the FE models used in this entire study:

1. It has been shown through FE studies conducted and presented in Figure 20 that a linear softening law for material stiffness degradation is necessary for the prediction of the correct qualitative shape of the delaminations. Such a softening law is hence incorporated into the damage model used in this study.
2. To control finite element instabilities and to promote easier convergence of the FE simulations, it is necessary to use a zig-zagging curve to approximate the linear softening curve.
3. Cohesive elements are employed for the purpose of modeling delamination and the material degradation caused by the delaminations. The interface elements also allow for the study of damage progression because the shape and size of the individual delamination at each interface can be studied at any intermediate step throughout the impact process.
4. A partial cohesive model with cohesive elements included only in the region nearer the point of impact has been found to reduce computational time by approximately half, while predicting similar impact damage results.
5. A mesh that is composed of smaller elements around the point of impact and larger elements towards the edge of the model has been proven to be computationally more efficient than a mesh composed of uniform elements. Henceforth, such a mesh would be used for the rest of this study.

Chapter 4

FINITE ELEMENT SIMULATIONS OF LOW-VELOCITY IMPACT

The difficulty in modeling low-velocity impact arises from the complexities of low-velocity impact damage. For the same incident energy, different combinations of impactor mass and velocities can have different effects on the impact response [12]. Furthermore, different sizes and layups of the composite plates would display different damage patterns. The differences in damage patterns in turn lead to differing residual compressive strength, or CAI strength.

The aim of this stage of the research is to predict the correct damage sequence as observed in experiments on impact damage and to predict the location and sizes of matrix cracks and fiber fracture, and the location, sizes and shapes of the delamination in each inter-layer to an acceptable accuracy. It is important to predict the actual through-thickness location, shape and size of individual delaminations instead of the total projected delamination area, because the post-impact strength of each specimen is dependent on the location, shape and size of the delaminations [75]. It is also important to predict the location and sizes of the matrix cracks because during compression, the delaminations and cracks interact, thereby cooperatively reducing the compressive strength of the composite. The CAI strength is dependent on both the delaminations and the cracks. An FE model capable of accurately predicting the impact damage sequence and extent of damage for different impact and laminate parameters is crucial for the accurate prediction of residual CAI strength.

4.1 Verification of FE model for low-velocity impact

To verify the reliability of the FE model in the prediction of low-velocity impact damage, three experimental studies on low-velocity impact damage are referenced. The first involves a simple cross-ply laminate of layup $[0^{o}_{2}/90^{o}_{6}/0^{o}_{2}]$ performed by Li et. al. [162]. The other two experimental studies are impact studies on 16-ply quasi-isotropic laminates. One is performed by Kimpara et. al. [3] and the other is performed by Aboissiere and reported by Bouvet et. al. [41]. In the experimental studies reported by Kimpara et al. [3] and Bouvet et al. [41], a detailed report of the matrix and fiber damage in each composite ply and the delamination geometry in each interface is reported. These experimental results are the benchmarks for the computational modeling work done in this research.

4.1.1 Cross-Ply laminate of layup $[0^{o}_{2}/90^{o}_{6}/0^{o}_{2}]$

Low-velocity impact damage on cross-ply laminates is widely researched due to the relative simplicity of the impact damage pattern compared to other laminate layups. The low-velocity impact test performed on a cross-ply laminate by Li et. al. [162] is chosen as one of the cases of the impact damage studied in this current research. The laminate has the layup $[0^{o}_{2}/90^{o}_{6}/0^{o}_{2}]$, and the resultant low-velocity impact damage is shown in Figure 22 below.

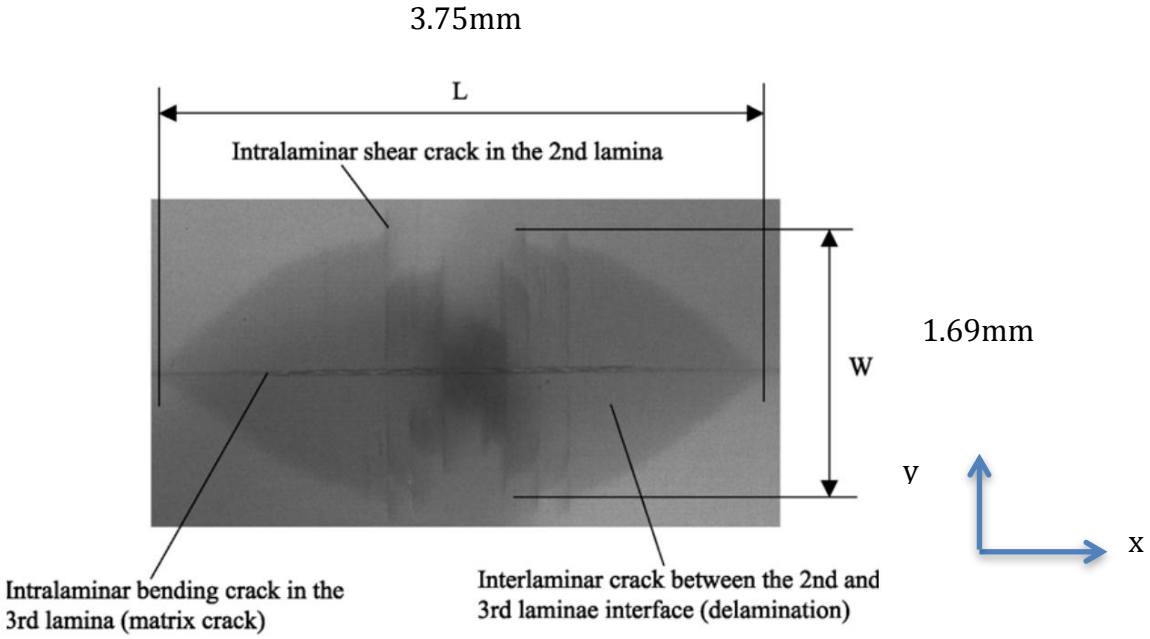

Figure 22 Damage in a $[0^{o}_{2}/90^{o}_{6}/0^{o}_{2}]$ cross-ply laminate under low-velocity impact

Impact damage on a [0°2/90°6/0°2] laminate

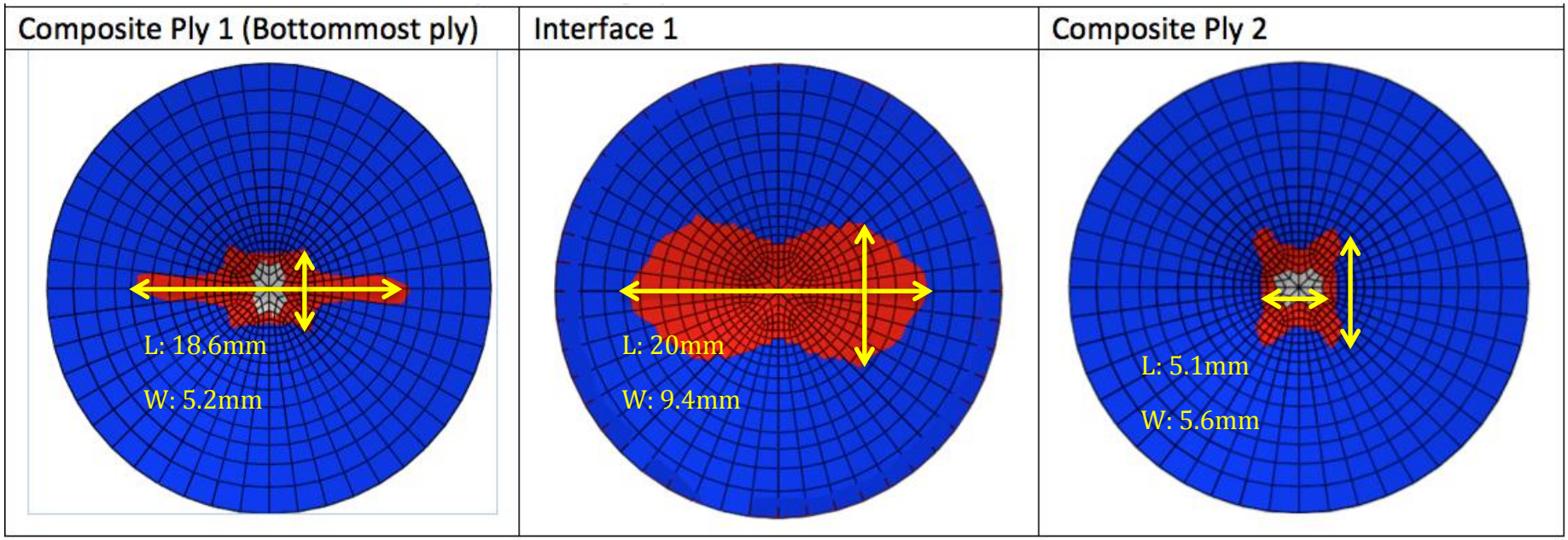

	Undamaged
	Matrix damage in composite elements Delamination in cohesive elements
	Fiber failure in composite elements

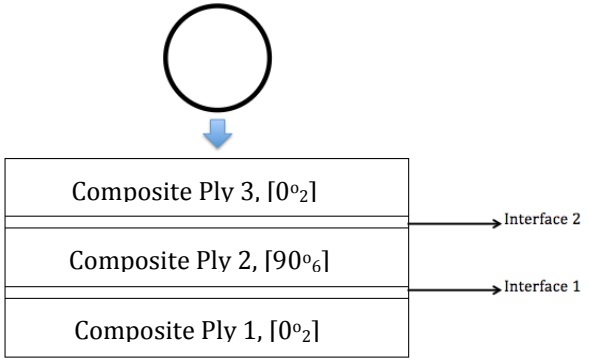

Figure 23 Damage prediction in a [0°2/90°6/0°2] cross-ply laminate under low-velocity impact

Since no information was provided on the material properties, impact boundary conditions or the dimensions of the laminate used by Li et al. [162] for the impact experiment, the material properties used in this FE model is assumed the same as that presented in Table 2 and Table 3, and the dimensions used are the same as that prescribed in Figure 17. All four edges of the laminate are assumed fully clamped i.e. the displacements in the x, y and z directions are restricted and the rotations in the x, y and z directions are restricted. Although the material properties, laminate geometry and boundary conditions of the FE model might differ from that of the laminate used in the impact test, the general damage pattern predicted by the FE model should still be similar to the experimental result shown in Figure 22 because the most prominent impact damage in a cross-ply laminate is the peanut-shaped delamination like that of Figure 22. Many different researchers have performed experimental impact tests on cross-ply laminates made of different material with different geometries and boundary conditions, and have reported similar peanut shaped delamination [36, 58, 60].

The finite element results for impact damage on $[0^{o}_{2}/90^{o}_{6}/0^{o}_{2}]$ cross-ply laminate show strong correlation with the experimental results. As seen in Figure 23, a long matrix crack is predicted in the bottommost ply, or Ply 1 in the FE model. The same long intralaminar bending crack was observed in the bottommost ply named 3rd lamina in the experiment as seen in Figure 22. In Ply 2, the 90^{o} ply in the FE model, short vertical matrix cracks are predicted, similar to that observed in the experiment. Finally the FE model was also able to predict the peanut-shaped delamination in Interface 1, with the lobes elongated in the 0^{o} direction.

Towards the end of the simulation, fiber failure was predicted by the FE model to occur in Ply 1 and Ply 2 directly below the point of impact. Comparing the finite element results obtained from the low-velocity impact

simulation on the cross-ply laminate of layup $[0^o_2/90^o_6/0^o_2]$ with the experimental results reported on a laminate of the same layup by Li et al. [162], it can be concluded that the FE model is capable of predicting the low-velocity impact damage sequence and damage pattern accurately. However, since the dimensions of the laminate that was used in the experimental study and the size of damage were not reported, the size of the damage obtained from the FE prediction could not be compared with experimental results to further verify the reliability of the FE model.

4.1.2 16-ply quasi-isotropic laminate of layup $[-45^o/0^o/45^o/90^o]_{2s}$

In this experimental study conducted by I. Kimpara and H. Saito [3], a detailed damage characterization of CFRP laminates due to low-velocity impact was mapped, and the residual CAI strength was reported. The aim is to compare the low-velocity impact damage predicted by the FE model with the low-velocity impact damage obtained in the experimental study conducted by I. Kimpara and H. Saito.

The dimensions of the FE model and the material properties input replicate that of the dimensions and material properties of the composite laminate used by I. Kimpara and H. Saito [3] in their experimental study of residual CAI strength as closely as possible.

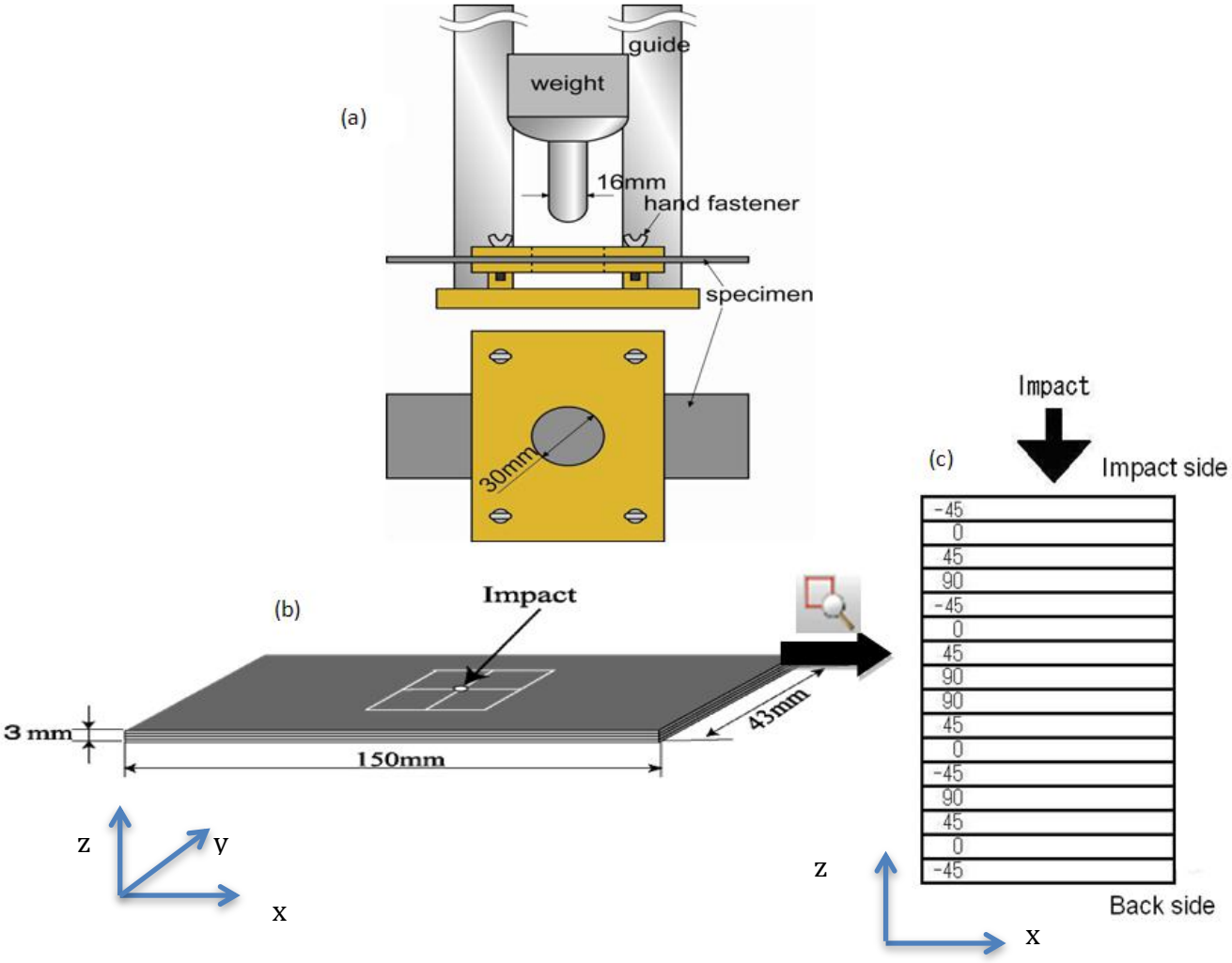

Figure 24 (a) Experimental set up for low-velocity impact test (b) Dimensions of CFRP laminate (c) Magnified x-z view showing sequence of layup. Pictures are obtained from [3]

The experimental set up is illustrated in Figure 24. The material used in this experiment is T800S/3900-2B, and the material properties are summarized in Table 2. These same material properties are used for the FE model. The quasi-isotropic CFRP laminate used for this experiment bears a stacking sequence of $[-45/0/45/90]_{2s}$. The specimen has a thickness of 3mm, a width of 43mm and a length of 150mm. The thickness of each composite ply is 0.1875mm. The gauge length, which is the distance along the specimen upon which contraction calculations are made during the CAI test, is 50mm. The gauge length can also be taken to be the distance between the grips on the specimen during the CAI test. During the low-velocity impact experiment, the composite laminate is clamped between two plates containing a circular hollow of diameter 30mm, as seen in Figure 24.

In the FE model, each composite ply was modeled to be 0.1875mm thick, replicating that of the CFRP laminate used in the experiment. The dimensions of the FE model and experiment are shown in Figure 17 and Figure 24 above. The dimensions of the FE model are chosen to be 50mm by 50mm for convenience of modeling and meshing. Although these dimensions are different from that of the laminate used in the referenced experiment, the effect of the difference in dimensions on the low-velocity impact damage is expected to be negligible since the boundary conditions used for the impact test as shown in Figure 24(a) is a 30mm diameter circular opening. In the FE model, the boundary conditions imposed on the laminate as shown in Figure 25 approximates that of the boundary conditions used in the experiment.

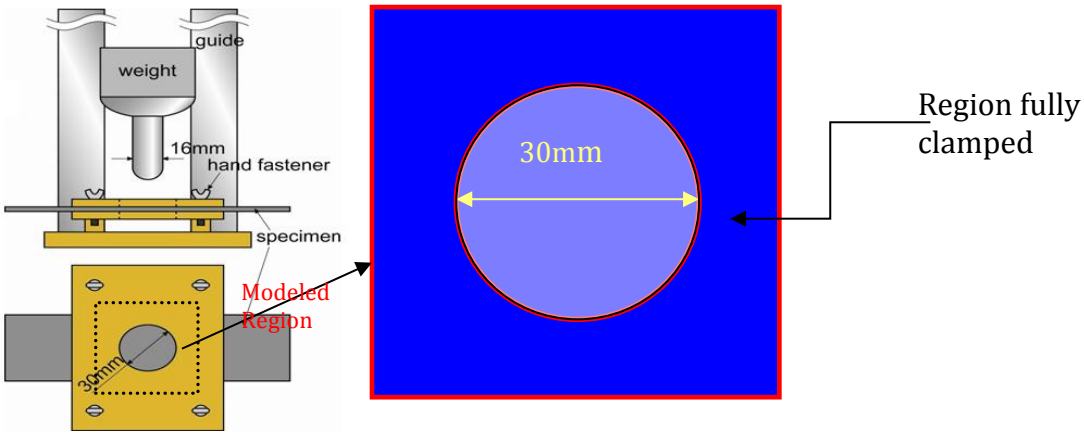

Figure 25 Boundary conditions imposed on FE model

In the low-velocity impact experiment, an impactor of mass 1113.5g and 16mm in diameter was used to achieve an impact energy of 2J/mm, which typically results in barely visible impact damage. No information was provided on the drop height or impact velocity. For the composite laminate considered, the thickness of 3mm means that the total impact energy applied was 6J. Impact energy is specified in units of 'J/mm', or Joules per unit thickness, instead of units of 'J' in order to facilitate comparison of the impact damage across different experiments. Specifying impact energy in units of 'J/mm' serves to normalize the impact energy such that regardless of plate thickness, the impact energy and the subsequent impact damage can be compared. The normalization of impact energy has to be performed because for the same absolute impact energy, different plate thickness would exhibit a different damage extent. When composite plates of different thicknesses are subject to the same absolute impact energy, the damage incurred in

thinner laminates would be more extensive than the damage incurred in thicker laminates. This is because thinner laminates have fewer plies to absorb the dissipated impact energy.

In the experiment performed by Kimpara et al. [3], the delamination and crack profile of the impact damaged laminate was extracted in two steps (Figure 26): Firstly, the laminate was scanned with an ultrasonic scanning device. This allows for a non-intrusive evaluation and provides information of delamination in each interface in the x-y plane. This information was accumulated in the z-direction. Secondly, the specimen is cut into pieces of 1mm thickness as shown in Figure 26, and direct observation with an optical microscope was used to obtain information on delaminations and transverse crack in the y-z plane. This information was accumulated in the x-direction. From these evaluations, a 3D map of damage distribution is obtained, as shown in Figure 27. Figure 28 shows the detailed delamination damage map obtained in this experiment. In Figure 28, only half of the specimen is shown because the delamination is rotationally symmetrical about the line passing through the impact point in the z-axis direction.

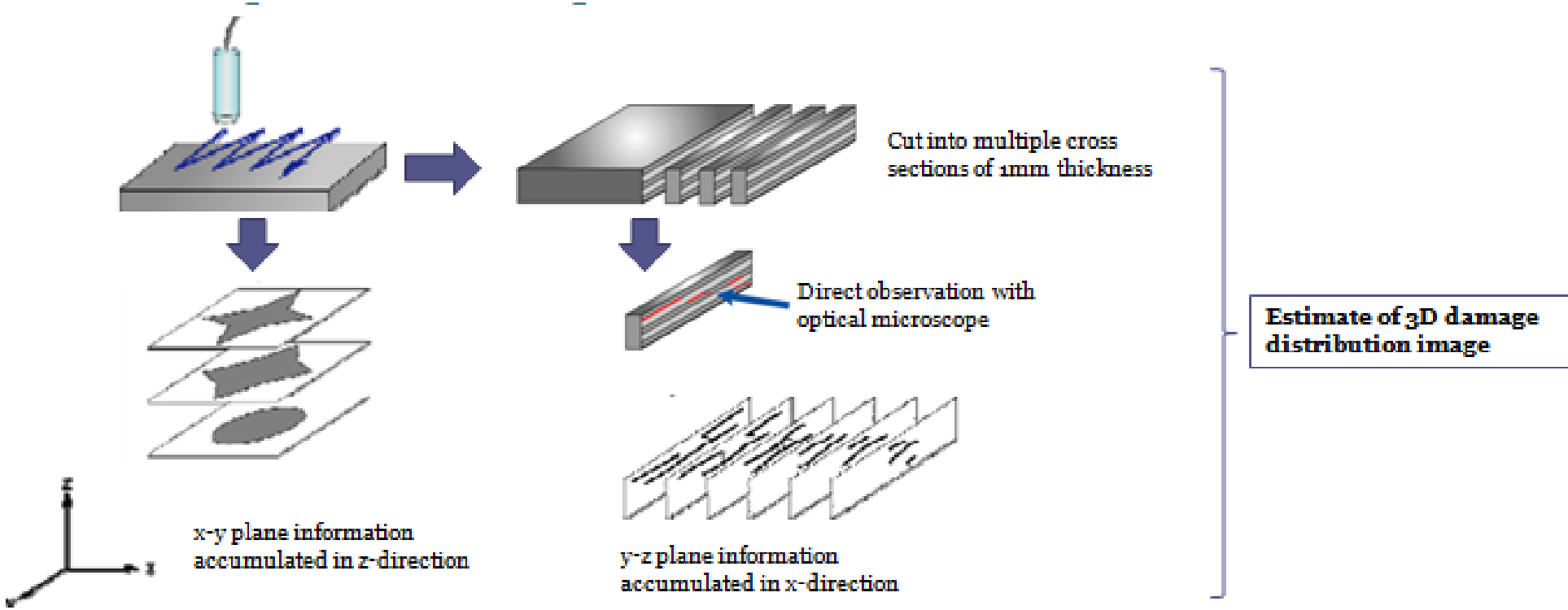

Figure 26 Methodology of 3D characterization of impact damage in laminate, obtained from [3]

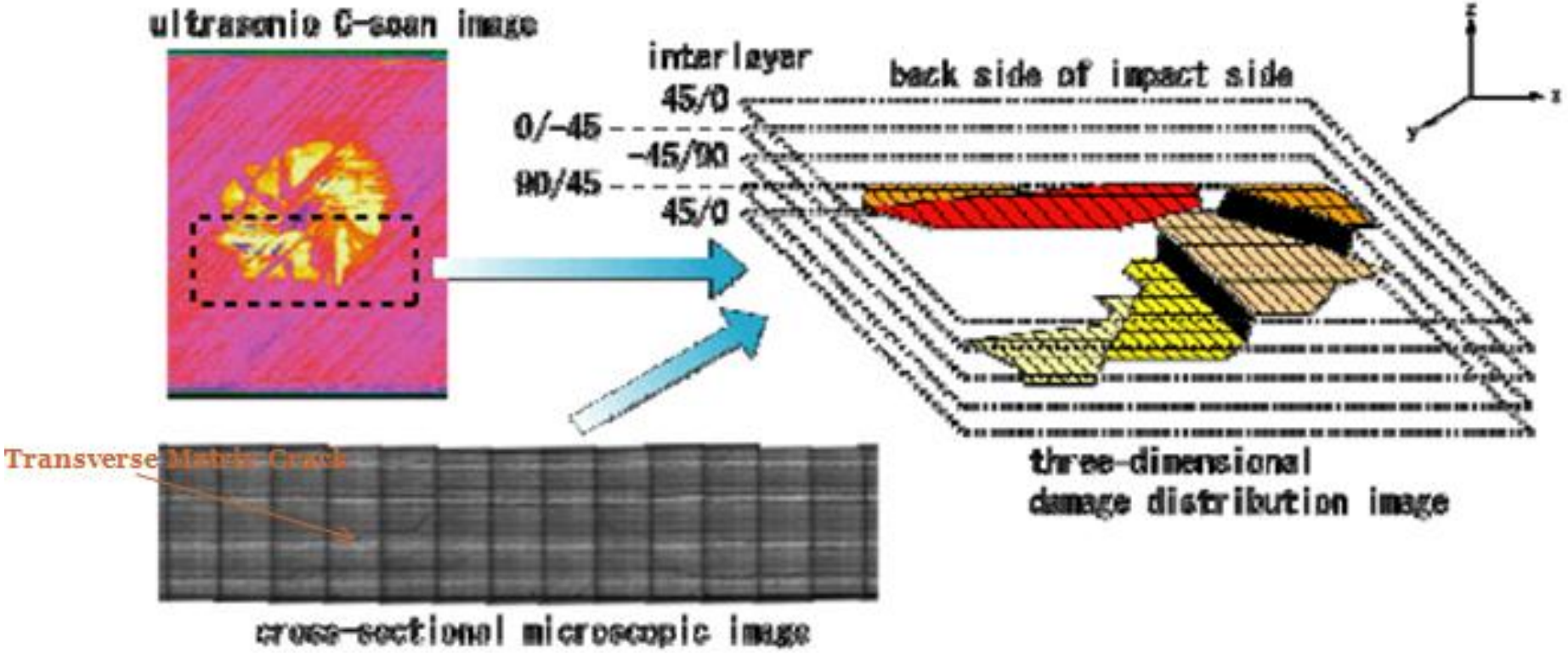

Figure 27 Damage distribution image for the impacted $[-45/0/45/90]_{2s}$ laminate obtained from the 3D damage characterization method illustrated in Figure 26 [3]

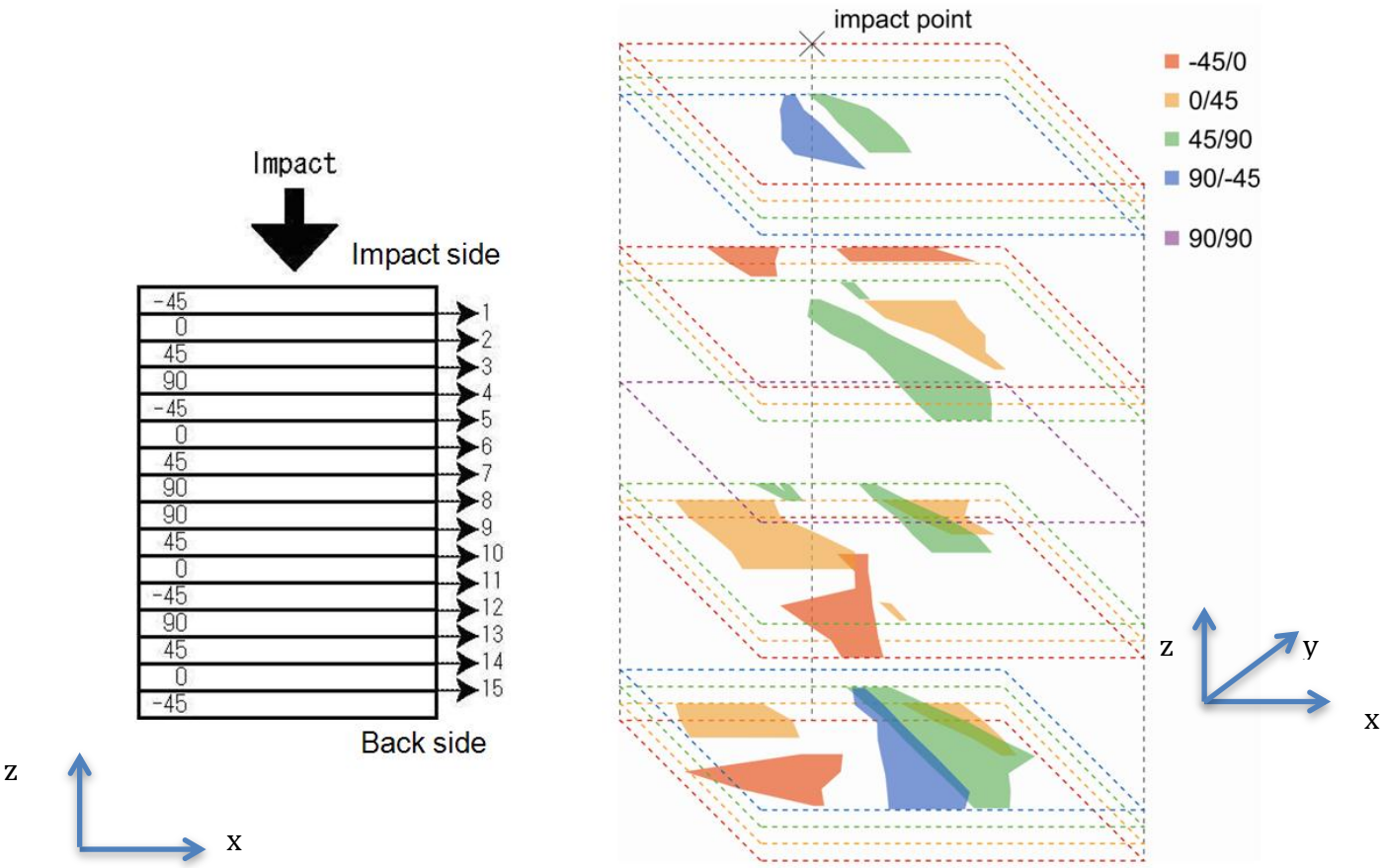

Figure 28 Detailed delamination distribution map for the impacted $[-45/0/45/90]_{2s}$ laminate. Only half the specimen is shown because the delamination is rotationally symmetrical about the line passing through the impact point in the z-axis direction. [3] Opposite numbering of ply is shown here because such a numbering system is used by the researchers who conducted the experiment.

In this experiment, Kimpara et. al. defined the 0^o ply to be oriented in the vertical direction (Figure 29). Hence the $[-45^o/0^o/45^o/90^o]_{2s}$ layup in the experiment is equivalent to a $[-45^o/90^o/45^o/0^o]_{2s}$ layup in the FE model (Figure 16).

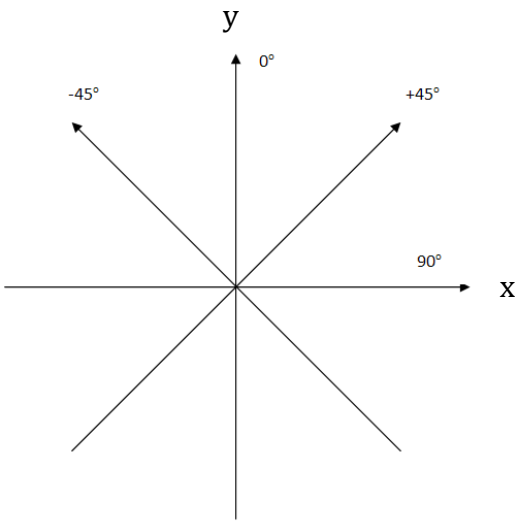

Figure 29 Fiber orientations for the experiment conducted by Kimpara et al. [3]

Figure 30 presents the delamination profiles extracted from the experiments by I. Kimpara and H. Saito. Figure 30(b) was included to emphasize the fact that the delaminations progress in a direction that is the same as the fiber orientation of the ply below the interface. Figure 31 shows the low-velocity impact delaminations on the $[-45^o/0^o/45^o/90^o]_{2s}$ laminate as predicted by the FE model.

The absolute delamination sizes obtained from the experiment conducted by Kimpara et al. [3] as shown in Figure 30 cannot be compared directly with the absolute delamination sizes predicted by the FE model as shown in Figure 31 because the experimental impact energy was 6J, while the impact energy prescribed to the FE model was 1.2J. This is due to a shortfall of the current impact FE model. In this current impact FE model, the

simulation will not converge once a drop in force is experienced, and it is found that the maximum impact energy that can be prescribed to the model to ensure convergence is 1.2J. The inability of the FE simulation to converge is due to an out-of-plane hourglassing effect, in which the elements distort in a manner where the strains calculated at all integration points are zero, leading to an uncontrolled distortion of the mesh without stresses to resist the distortion. Details on how this problem can be solved are found in Section 6.2. Nevertheless, even with smaller impact energy of 1.2J, the low velocity impact damage predicted by the FE model was found to have good agreement with the experimental results reported by Kimpara et al. in terms of the damage sequence, delamination shapes and the relative delamination sizes in each interface. The absolute delamination sizes predicted by the FE model are smaller than the experimental delamination sizes because the impact energy in the FE model is smaller than that in the experiment.

In Figure 30, it could be seen that the smallest experimental delamination occurred in Interface 3 (8.8mm), and the second smallest experimental delamination occurred in Interface 4 (11mm). The same trend is predicted by the FE model (Figure 31)- the smallest delamination is predicted to occur in Interface 3 (6.2mm) and the second smallest delamination is predicted to occur in Interface 4 (8.8mm). By visual inspection of the experimental delaminations in Figure 30, it is obvious that the delamination occurring in Interface 10 is of the largest size in spite of the fact that its length is reported to be 15.3mm, smaller than the length of the delamination found in Interface 11 which has a length of 19.1mm. This is because it has the largest width of 6.7mm, which is double the width of the delamination found in Interface 11 (3.3mm). While the FE result reported in Figure 31 was incapable of predicting the lengths and widths of the delamination accurately, it also predicted the largest delamination to occur in Interface 10.

The direction of delamination progression has also been well predicted by the FE model, in that the direction of delamination progression follows that of the fiber orientation of the ply below the interface.

An interesting observation is related to the delamination at interface 10. It has been observed from the experimental results [3] in Figure 30(a) that interface 10 contains two small delaminations separate from the main delamination area, such that the delamination at interface 11 is flanked by a small and a big delamination occurring at interface 10. Such a phenomenon has also been predicted by the FE model, as seen in Figure 31.

In view of the above results, it can be concluded that the FE model created in this study is capable of qualitatively predicting low-velocity impact damage.

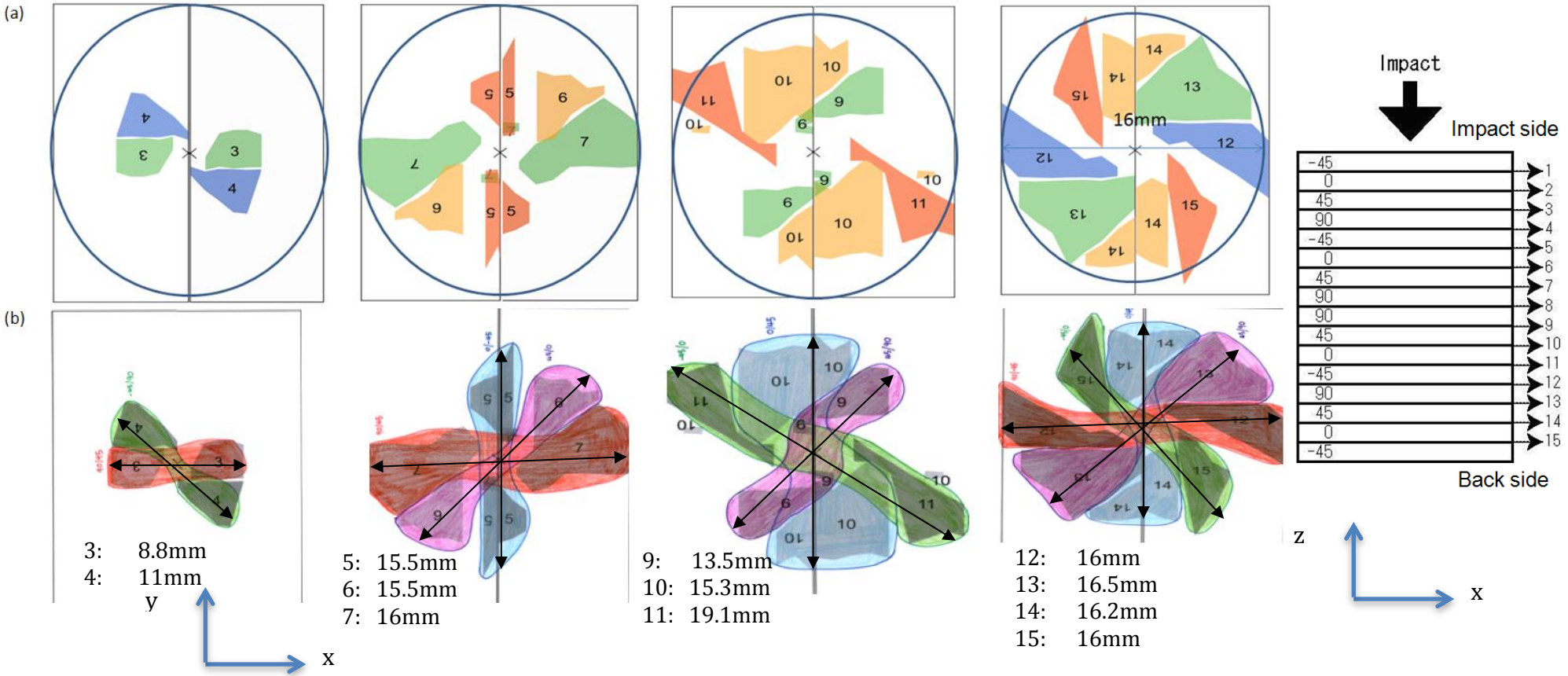

Figure 30 Delamination profile obtained from experiments. (a) Delamination profile provided by I. Kimpara and H. Saito. [3] (b) Delamination profile as intepreted in current thesis, showing the lengths of the delaminations.

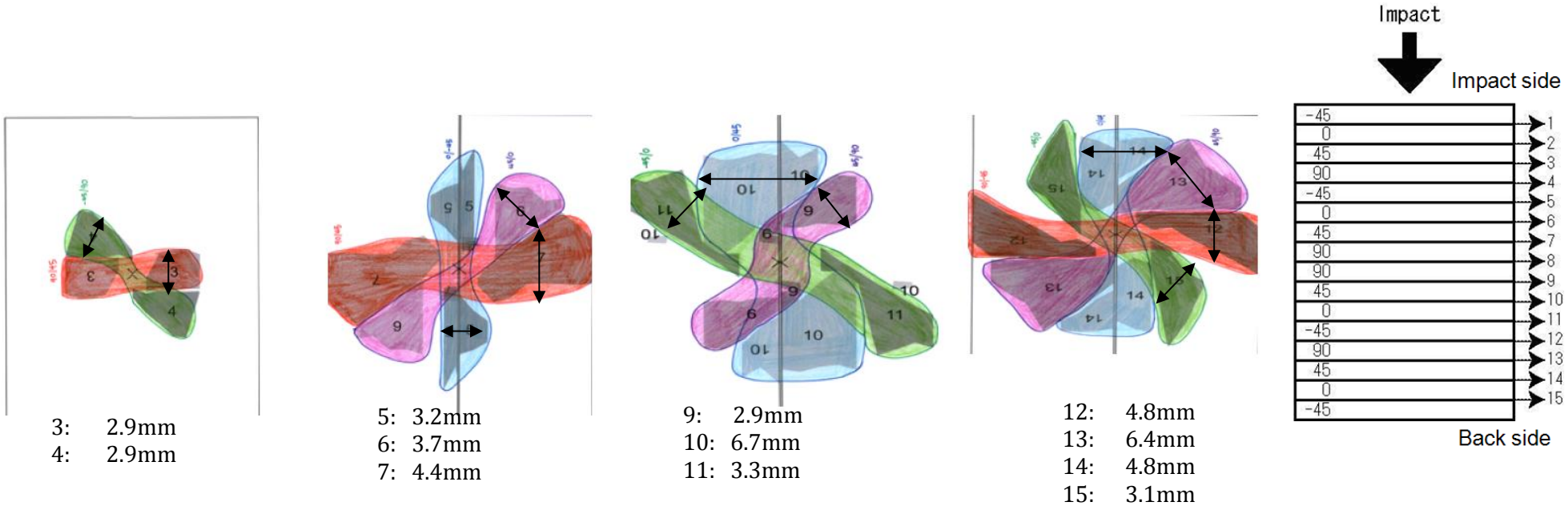

Figure 30(c) Delamination profile as intepreted in current thesis, showing the widths of the delaminations.

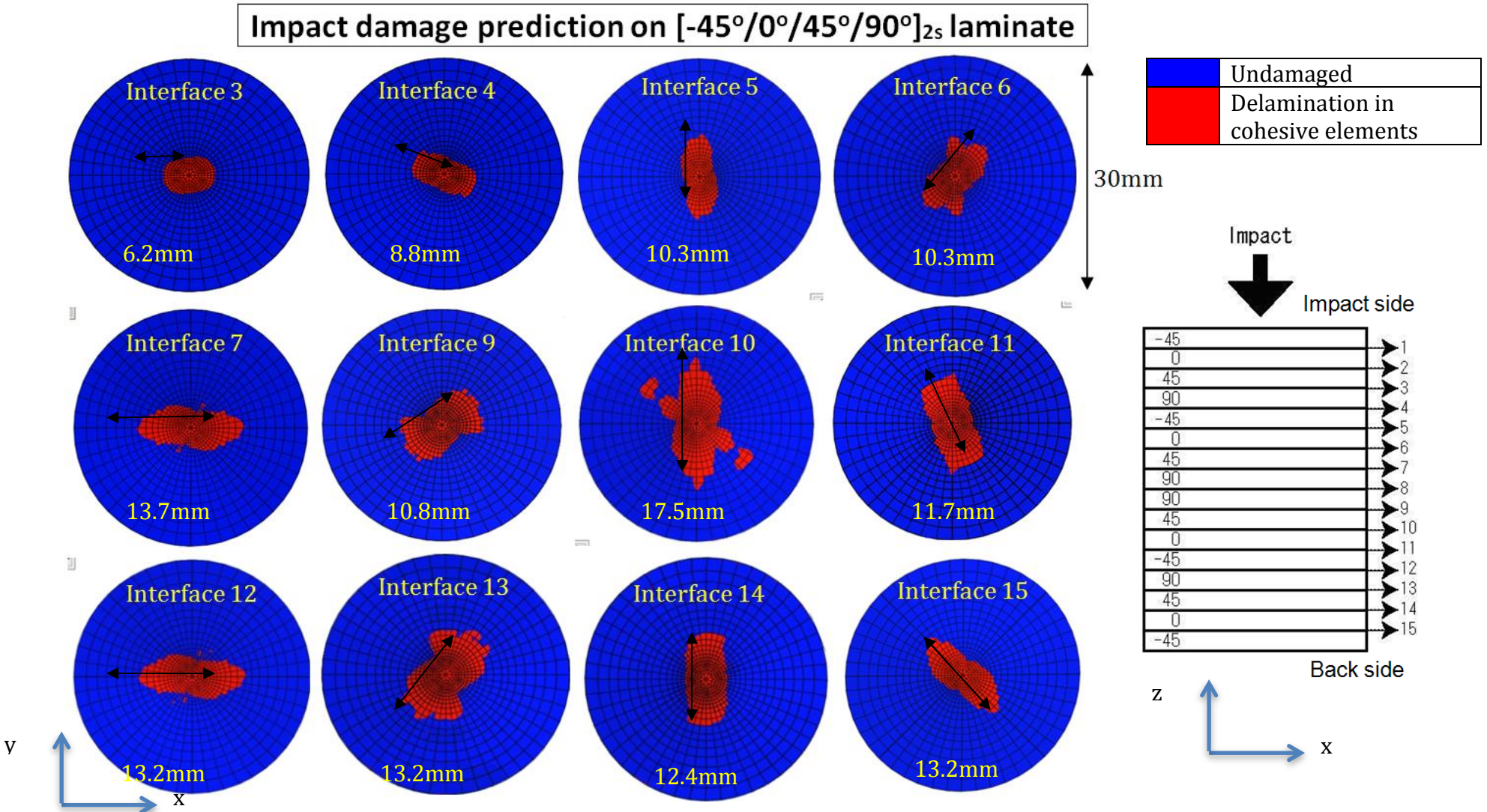

Figure 31(a) Low-velocity impact delaminations on a $[-45^{o}/0^{o}/45^{o}/90^{o}]_{2s}$ laminate predicted by the FE model, showing the lengths of the delaminations

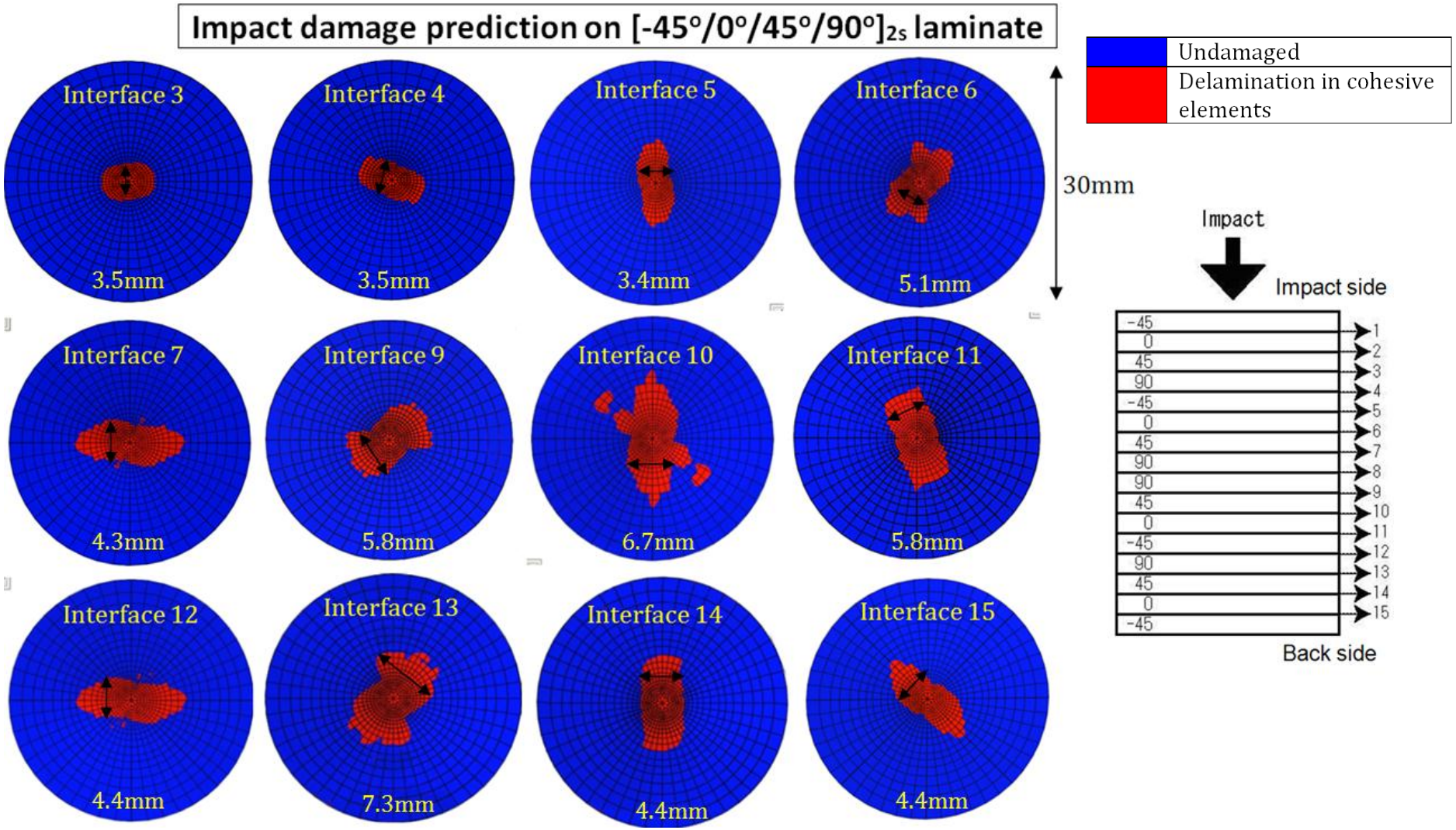

Figure 31(b) Low-velocity impact delaminations on a $[-45^o/0^o/45^o/90^o]_{2s}$ laminate predicted by the FE model, showing the widths of the delaminations

4.1.3 16-ply quasi-isotropic laminate of layup $[0^o_2/45^o_2/90^o_2/-45^o_2]_s$

Finally, low-velocity impact simulations was run on an FE model with layup $[0^o_2/45^o_2/90^o_2/-45^o_2]_s$ and the simulation results were compared with the results obtained by Bouvet et al. [41] to verify the reliability of the FE model devised in this research. Low-velocity impact experiments on $[0^o_2/45^o_2/90^o_2/-45^o_2]_s$ laminates were carried out by Aboissiere and reported by Bouvet et al. in [41], where the researchers also studied the low-velocity impact modeling in laminate composite panels with discrete interface elements. Here, Bouvet et al. compared the FE results obtained from their model with the experimental results from experimental tests performed by Aboissiere, and concluded that 'a very good match has been found' (Figure 32).

Impact is simulated on the current FE model using the same layup. In both Bouvet's FE model [41] and the current FE model, the diameter of the impactor is 16mm, and low-velocity impact was simulated using a prescribed displacement in the z-direction to the impactor. In both FE models, all four edges of the laminate are simply supported i.e. the displacements in the x, y and z directions are constrained. The key differences between Bouvet's [41] FE model and the current FE model are the material properties used, dimensions of the laminate and the impact energy. Bouvet et al. did not provide the material properties used in their model, hence the properties used in this current FE model is that of the material T800S/39002B, as listed in Table 2. The laminate in Bouvet's model is 125mm in length and 75mm in width while the laminate in the current FE model is 75mm in length and 75mm in width. In Bouvet's model, the impact energy was 28J, while the impact energy used in the current model was very much lower, at 1.2J.

A qualitative comparison of the results obtained from the current FE model with that of the FE results obtained by Bouvet et al. is presented in Figure 33. Due to the lower impact energy prescribed to the FE model used in this research, the damage sizes are very much smaller than that predicted by Bouvet's model, with the exception of the delamination size in Interfaces 3 and 6. This might be due to the differences in the interface stiffness prescribed to the model, and the way in which the stiffness is degraded once damage has initiated. Nevertheless, the matrix cracks orientation, delamination shapes and delamination orientation predicted by the current FE model are generally in good agreement with that reported by Bouvet et al.

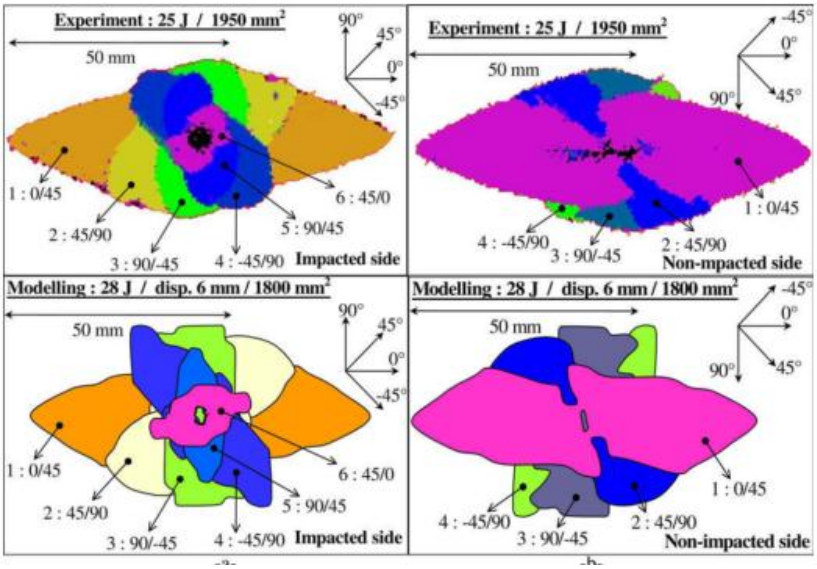

Figure 32 Experimental and modeling delamination in the impacted and non-impacted side, obtained from [41]

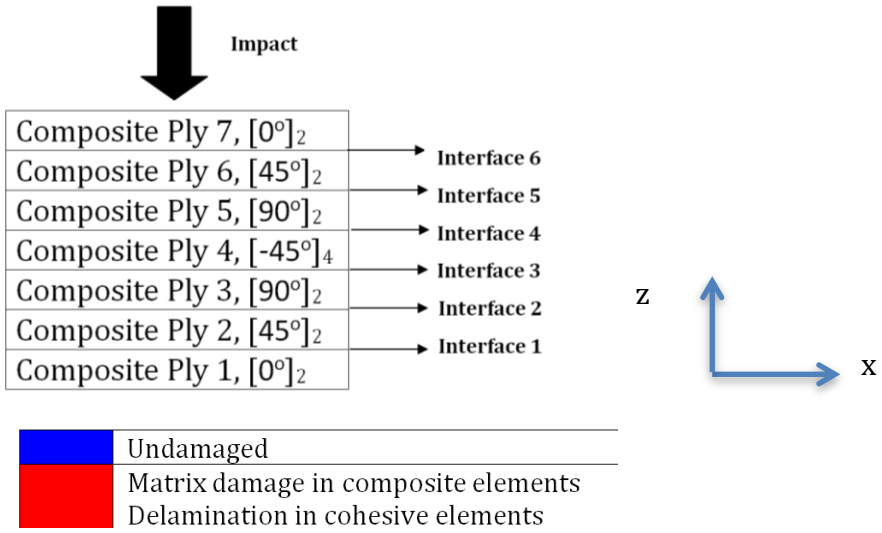

Figure 33(a) Legend for the low-velocity impact FE simulation on a $[0^{o}_{2}/45^{o}_{2}/90^{o}_{2}/-45^{o}_{2}]_{s}$ laminate

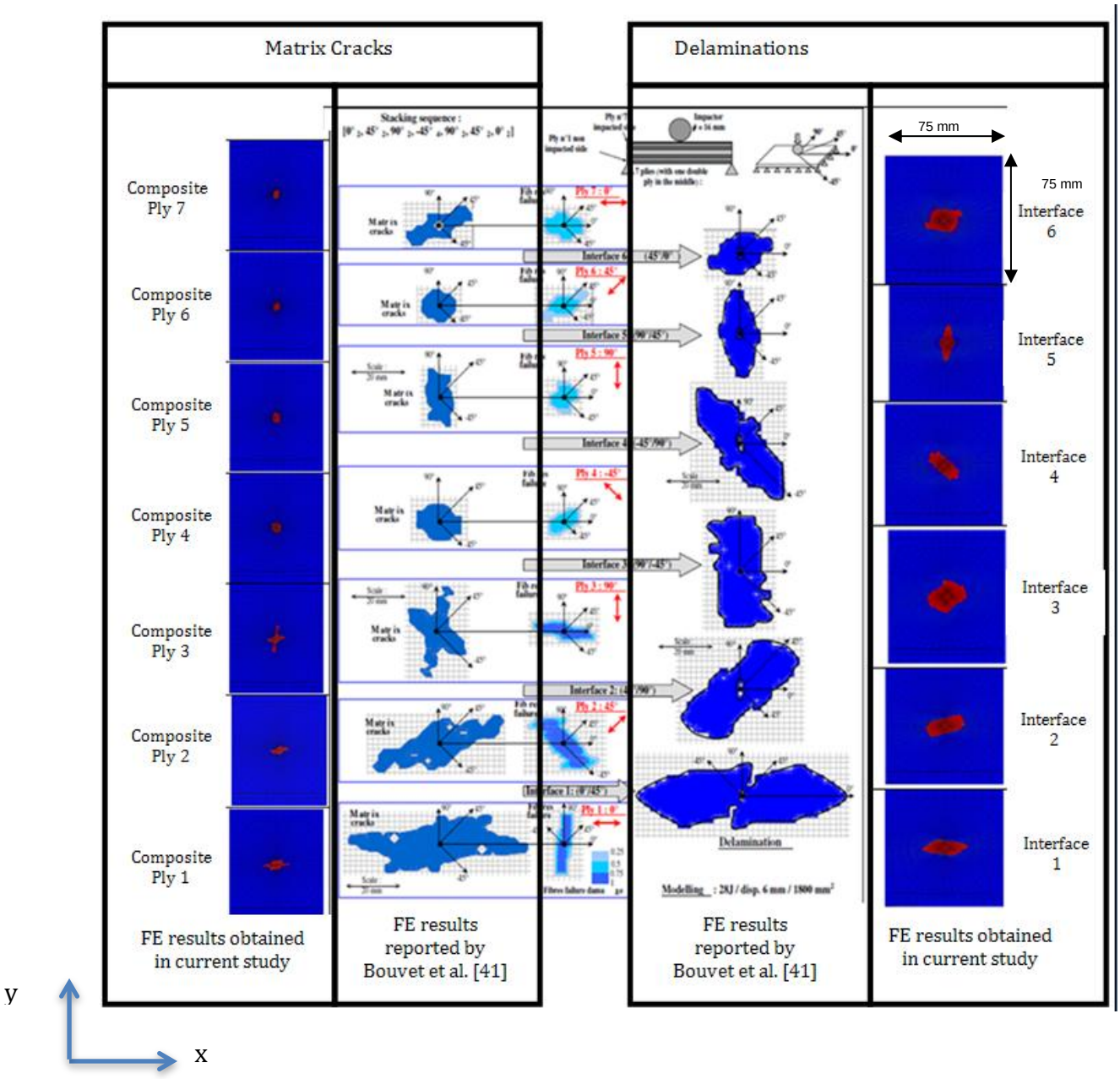

Figure 33 (b) A detailed comparison of the delaminations observed in an experiment with the delaminations predicted by the FE model

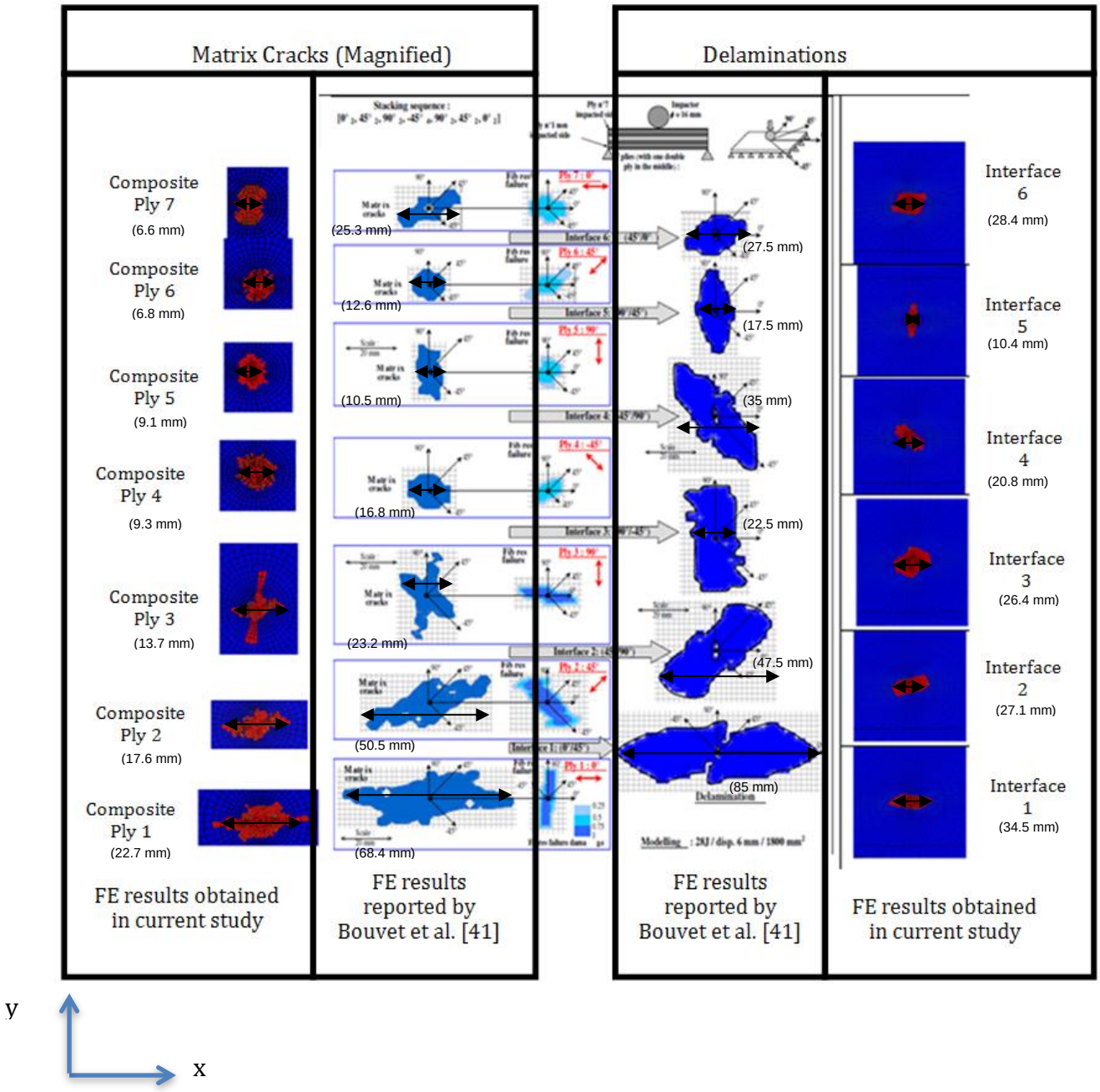

Figure 33 (c) A detailed comparison of the delaminations observed in an experiment with the delaminations predicted by the FE model with magnified view of matrix cracks

4.2 FE study of low-velocity impact on a $[0^o/45^o/90^o/-45^o]_s$ laminate (Reference case- Model A)

An eight-ply quasi-isotropic laminate with a stacking sequence of $[0^o/45^o/90^o/-45^o]_s$ is chosen to be the reference laminate used in this study, and is the basis of comparison for the parametric studies that are conducted and presented later in Section 4.3 of this thesis. This is chosen as a reference case because low-velocity impact FE simulation on an 8-ply laminate is not too computationally demanding, with an average computational time of approximately 20 hours.

The dimensions of this reference laminate are 50mm by 50mm with a total thickness of 1.07mm. Each composite ply is modeled to be 0.125mm in thickness, and each cohesive ply is modeled to be 0.01mm in thickness. A fully clamped boundary condition is imposed on all four edges of the laminate by stipulating the displacements at all four edges in the x, y and z directions and the rotation about the x, y and z directions to be zero. The results are presented in Figure 34.

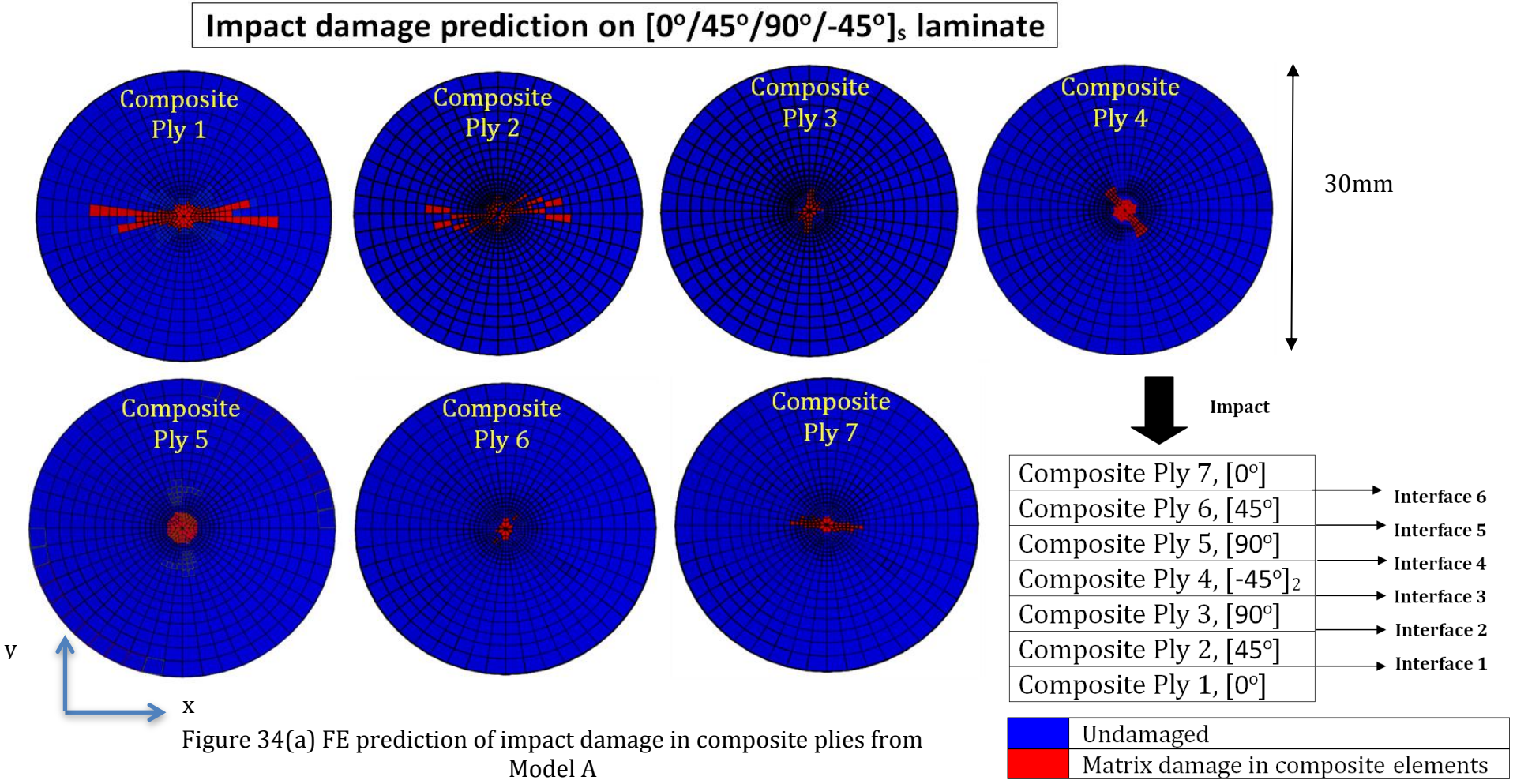

Figure 34(a) FE prediction of impact damage in composite plies from Model A

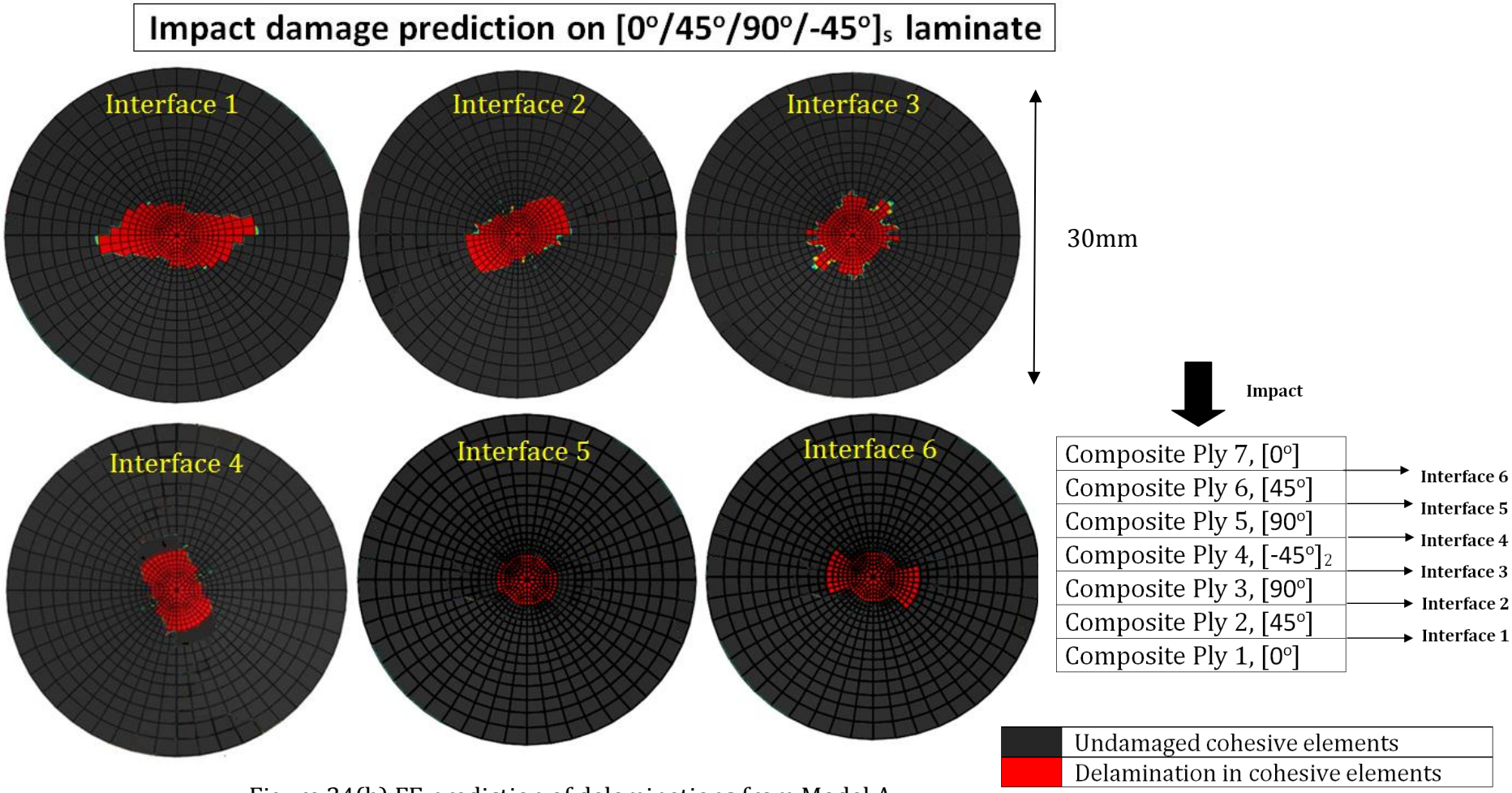

Figure 34(b) FE prediction of delaminations from Model A

The following observations can be made from the impact damage prediction obtained from Model A:

- The first sign of damage due to impact is the initiation of matrix cracks in Composite Ply 1, the ply furthest away from the impact face. This occurred at increment 24 of the FE simulation (Figure 36). Soon after, delamination initiated in every interface at almost the same time. Matrix cracks then initiated in Composite Ply 2.
- From Figure 34(a), it is observed that matrix cracks generally propagate in the direction of the fiber orientation for the ply. The matrix cracks in Composite Ply 1 are the most extensive.
- The major direction of delamination growth is observed in Figure 34(b) to be oriented parallel to the fibers of the ply below the interface at which the delaminations occur.
- As seen in Figure 34(b), delamination area is the largest at interface 1, and tends to decrease towards the impact face.
- There exists a correlation between the size of a matrix cracks and the size of the delamination at the interface above the matrix cracks, as observed in Figure 35.

These observations made are in good agreement with experimental results found in literature [58, 65, 163].

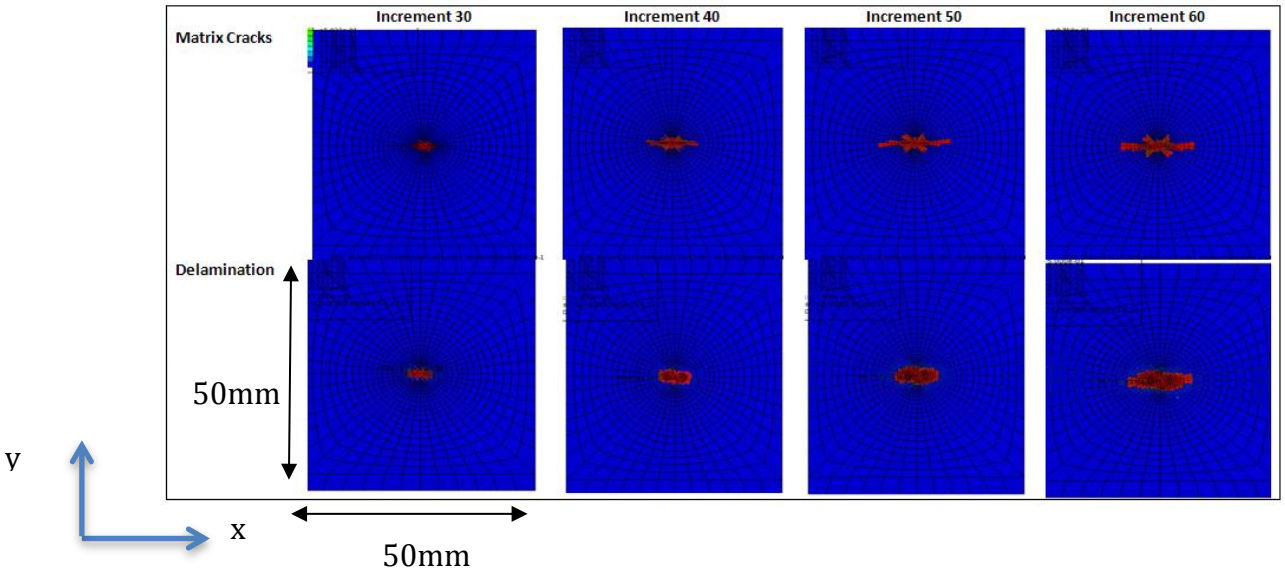

Figure 35 Impact damage occurring at Ply 1 and Interface 1, captured at different impactor displacement increments to demonstrate the relationship between matrix cracks and delamination sizes

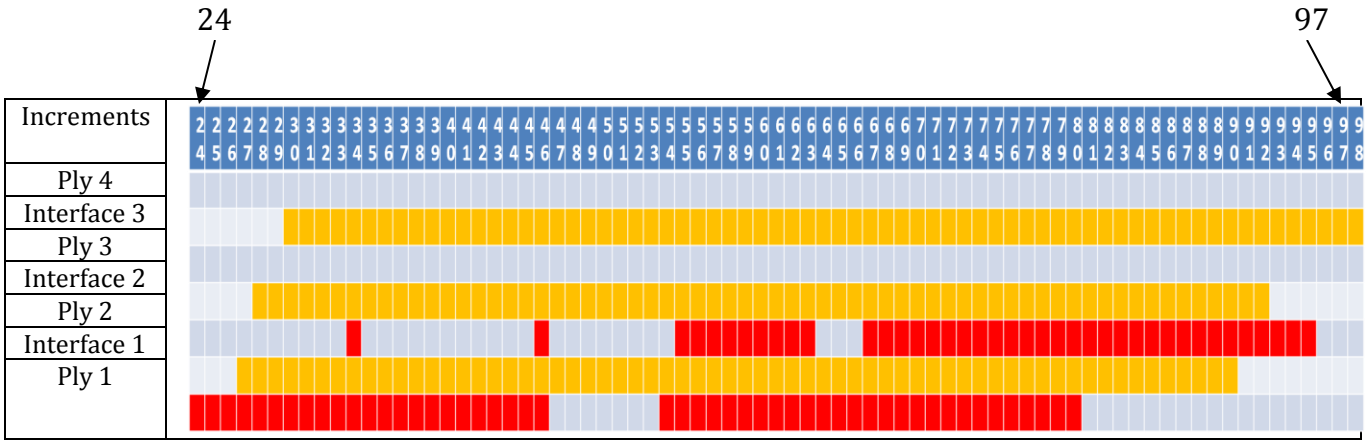

Figure 36 Pictorial representation of impact damage sequence in a $[0/45/90/-45]_s$ layup. Red represents the increments at which matrix crack initiation and growth occurs, yellow represents the increments at which delamination initiation and growth occurs

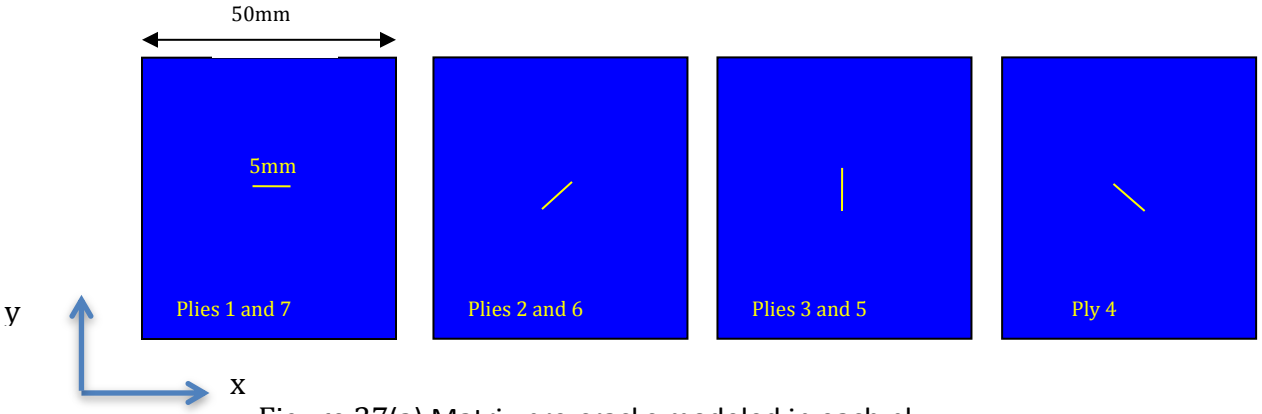

Figure 37(a) Matrix pre-cracks modeled in each ply

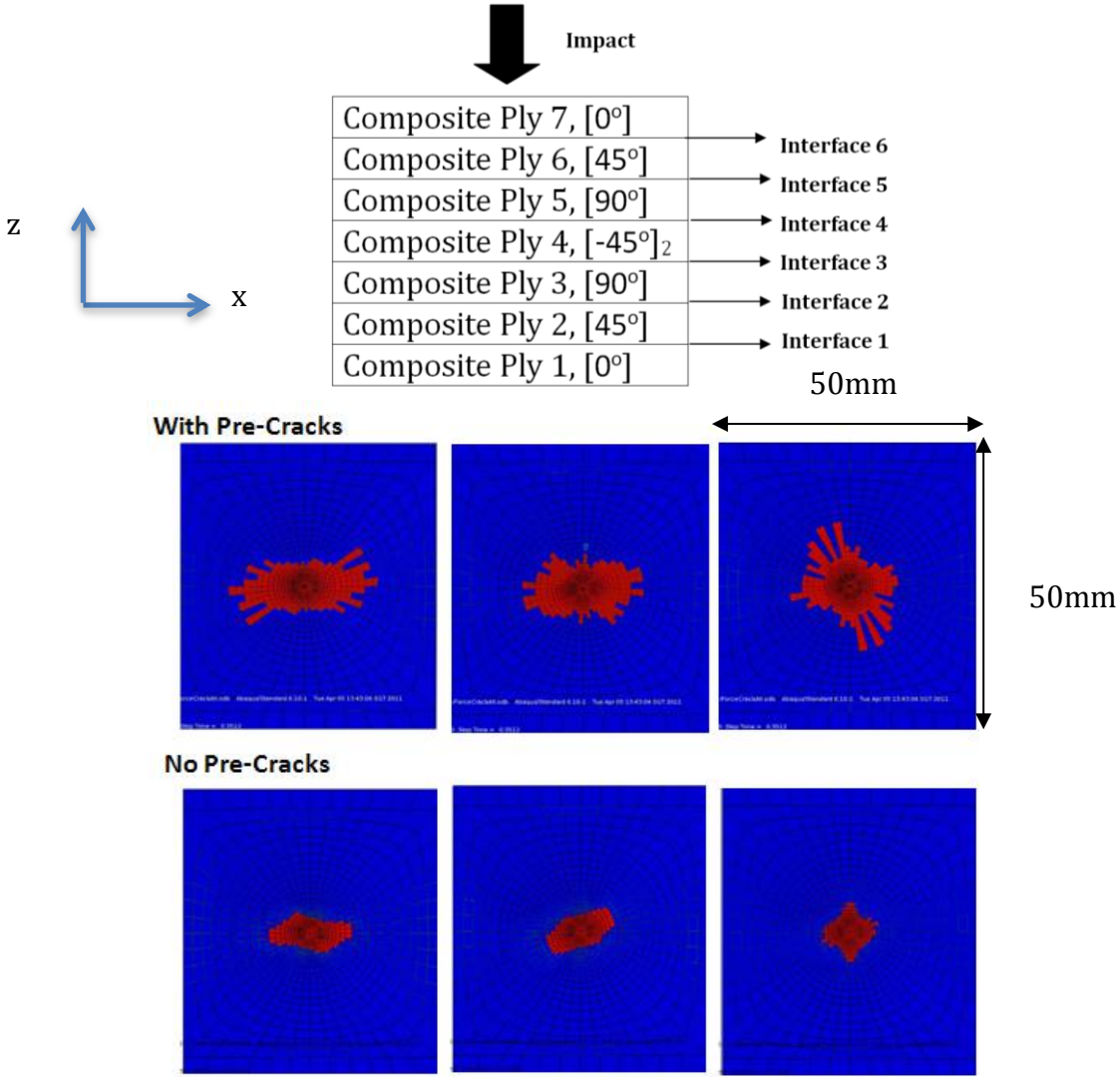

Figure 37(b) Comparison of impact damage predicted by FE models with and without the inclusion of pre-cracks, $[0/45/90/-45]_s$

In order to study the effects of matrix cracks on delamination formation, pre-cracks were included in the composite plies of a laminate with the same stacking sequence as Model A ($[0^o/45^o/90^o/-45^o]_s$). The cracks were 5mm in length, one-tenth of the length of the composite plate, and lie in the direction of the fiber orientation, as shown in Figure 37(a). The delaminations occurred much earlier in the model with pre-cracks, and are larger in size than that in the model without pre-cracks. In the damage sequence mapped out in Figure 36, damage first initiated in the form of matrix cracks in Ply 1 at increment 24. This matrix crack would drive the delamination growth in Interface 1 in the same direction as the matrix crack. Delamination initiated in Interface 1 at increment 27. Figure 36 shows that matrix cracks occurring in Ply 1 are the precursor to delaminations. Since cracks already pre-exist in the model with pre-cracks, the delaminations occurred much earlier in the model with pre-cracks. A possible reason for the larger delamination sizes in the model with pre-cracks is that impact energy that would otherwise have been used in the formation of matrix cracks are used for the formation of delaminations instead, since cracks already pre-exist in the FE model.

4.3 Parametric studies

It has been widely shown by many different studies [23, 55, 64, 164-167] that low-velocity impact damage on CFRP laminates is sensitive to different parameters such as the stacking sequence of the composite laminate, the total thickness of the laminate, the ply thickness, boundary conditions etc. To better understand the effect of each variable on the impact damage pattern of a CFRP laminate subject to impact, parametric studies are carried out. The parameters considered in this study are summarized in Table 5 on the next page. In order to study the effect of decreasing the individual ply thickness on the low-velocity impact damage pattern in a CFRP laminate, Model B is created, in which the individual ply thickness was reduced to 0.03mm, approximately a quarter of the individual ply thickness of Model A. Thin ply laminates are of interest because there have been reports that thin ply laminates demonstrated higher CAI strength compared to standard ply laminates [168, 169]. Model C, with a stacking sequence of $[-45/0/45/90]_{s,}$ was created to study the effect of varying the orientation of the bottommost ply, or the ply farthest from the impact face. Model D was created to study the effect of increasing the totally number of plies in a laminate, Model E was created to study the effect of ply-grouping on the low-velocity impact damage pattern and finally, Model F was created to study the effect of having a small relative angle between each successive ply in the composite laminate.

For all the results presented in this section, only the damage in the bottom half of the laminate (Ply 1 to the mid-ply) is shown as damage in the bottom half is more extensive.

	A	B	C	D	E	F
	Reference case	Thin-ply effect	Surface-ply effect	Number of plies	Ply-grouping	Small relative angle
Ply Thickness	0.125mm	0.07mm	0.125mm	0.125mm	0.125mm	0.125mm
Number of plies	8	16	8	16	16	4
Stacking sequence	$[0/45/90/-45]_s$	$[0/45/90/-45]_{2s}$	$[-45/0/45/90]_s$	$[0/45/90/-45]_{2s}$	$[0_2/45_2/90_2/-45_2]_s$	$[0/10_2/0]$

Table 5 Summary of the specifications of 7 different FE models used in the parametric studies

4.3.1 Thin-ply effect

A thin ply FE model (Model B) with each ply thickness approximately a quarter that of the ply thickness of the reference laminate (Model A) is built to study the effect of ply-thickness on delamination. This thin-ply model bears the stacking sequence $[0/45/90/-45]_{2s}$. Thin ply laminates are of interest because there have been reports that thin ply laminates demonstrate higher CAI strength compared to standard ply laminates. The ply thickness of thin ply laminates generally range between half to a quarter the thickness of standard ply laminates [67, 168-170].

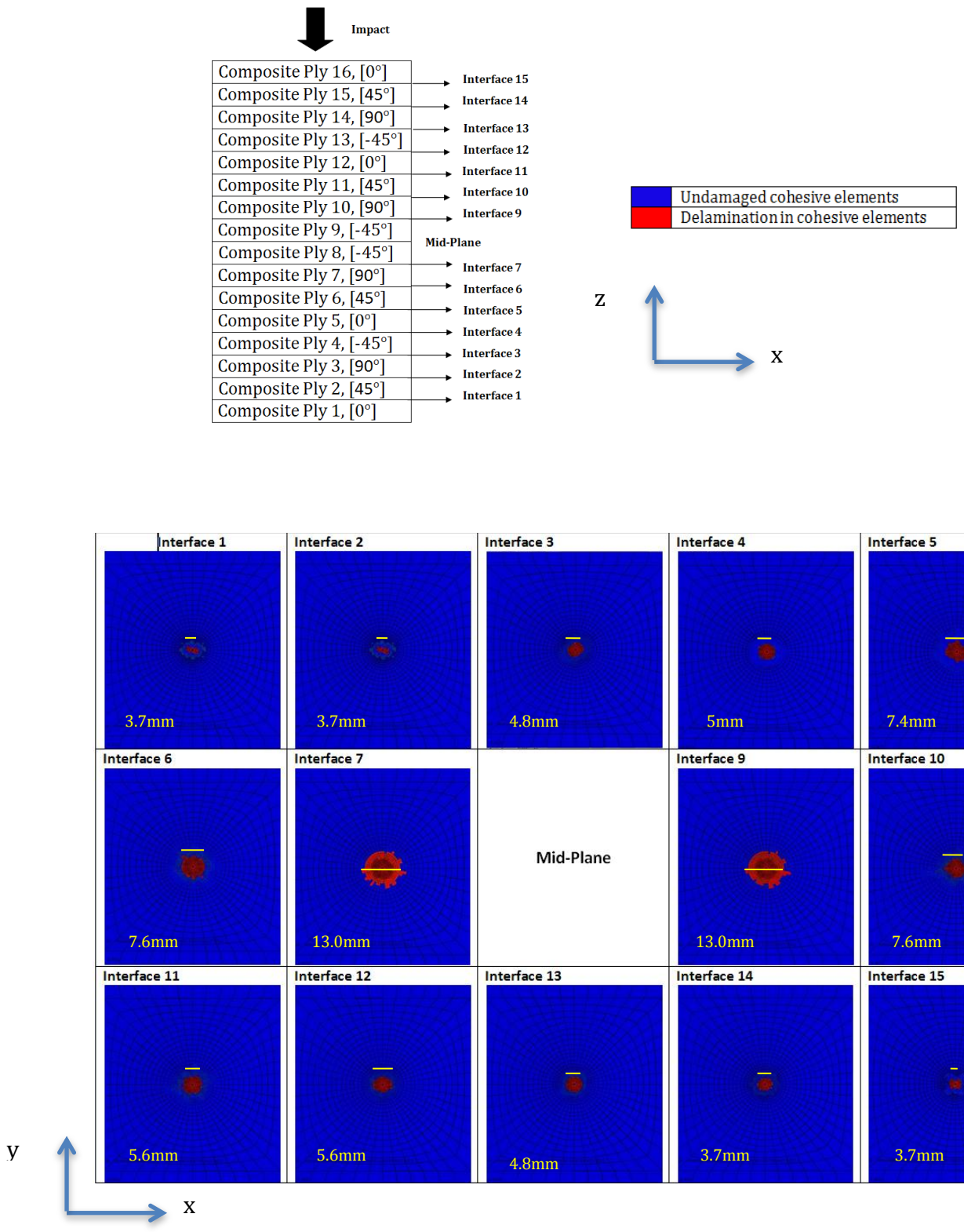

Figure 38 FE prediction of impact damage from Model B

The delamination pattern and damage sequence predicted from the FE simulations for Model B in Figure 38 is markedly different from the delamination pattern and damage sequence predicted in Model A (Figure 34(b)). In Model A, the delamination area was most extensive at the bottommost interface away from the impact face, and the delamination area decreases towards the impact face. However, in Model B, the delamination areas were the smallest at the extreme interfaces (i.e. bottommost interface and impact face interface). The most extensive delamination was observed around the mid-plane.

Various studies on the effect of thin-ply laminate have been conducted by different researchers, and differing results and conclusions were reported. In [171], Stavropoulos et al. reported that an increase in laminate thickness achieved via the use of thicker ply laminates instead of the use of more plies of the same thickness would result in higher CAI strength values. In this study, the thin ply laminates had a ply thickness of 0.125mm while the thick ply laminates had a ply thickness of 0.25mm. In other words, Stavropoulos et al. [171] found that thicker ply laminates have higher CAI strength than thinner ply laminates. On the other hand, Saito et al. [168] reported that thin-ply laminates of 0.038mm ply thickness showed 23% higher CAI strength compared to standard ply laminates of 0.147mm ply thickness. Yokozeki et al. [169] also reported that thin-ply laminates of 0.068mm ply thickness showed an 8% increase in CAI strength compared to standared ply laminates of 0.134mm ply thickness. Sihn et al. [170] performed experimental studies on thin ply laminates of 0.04mm ply thickness and standard ply laminates of 0.14mm ply thickness and reported that the projected delamination sizes for both types of specimens were almost the same. This is in contrast to that reported by Saito et al.[168], where the projected delamination area was found to be larger in thin ply laminates.

The results from Model B are presented in Figure 38. The results seem to concur with the experimental results reported by Saito et al. [168] on several aspects. First, the delaminations are found to be most extensive in the interfaces nearer the midplane. This is in contrast to delaminations in standard ply laminates in which delamination areas generally increase away from the impact face such that the interface furthest away from impact would sustain the largest delamination [163]. Secondly, Saito et al. observed few transverse cracks in thin ply laminates. In the FE model, the matrix cracks were observed only in plies 7-10.

In Section 2.2.1, it has been discussed that there exists a minimum composite ply thickness in order for critical matrix cracks to propagate. This phenomenon could explain the results obtained from Model B. In a standard ply laminate such as Model A, each composite ply thickness exceeded the minimum thickness for critical matric cracks to propagate. Hence matrix cracks were observed at every layer and delaminations occurred at every interface. In thin ply laminates such as Model B, the composite ply thickness was below that of the minimum composite ply thickness for critical matrix cracks propagation, with the exception of the mid-ply where two plies of the same fiber orientation were stacked together. Hence, critical matrix cracks were able to propagate only in the middle layer. Since matrix cracks are the precursor to delamination as discussed in Section 2.2.1, delamination would be most extensive in the interface at the mid-plane.

4.3.2 Surface-ply effect

The surface-ply effect is of interest because there have been studies reporting that laminates containing surface angles of ±45° demonstrated superior impact resistance and improved residual strength as compared to those containing surface angles of 0°[163, 165]. To study the surface-ply effect, Model C is created. Model C is identical to Model A except for a change in the laminate layup. In Model C, the stacking sequence is $[-45^o/0^o/45^o/90^o]_s$. A comparison between the impact damage predicted by both models could be used to study the surface-ply effect, or the effect of placing ±45° plies on the surface compared to having 0° plies on the surface of the laminate.

Hitchen et al. [163] performed experimental studies on the effect of stacking sequence on impact damage. The 16-ply laminates used had stacking sequences of $[45/0/-45/0]_{2s}$ and $[0/45/0/-45]_{2s}$. The researchers reported that the total delamination area in panels with 45° surface plies was smaller than those with 0° surface plies. It was also reported that laminates containing ±45° surface plies displayed superior impact resistance and improved residual strength compared to those with 0° surface plies. The smaller delamination area in laminates with ±45° surface plies as compared to laminates with 0° surface plies was attributed to the higher energy absorbed in delamination initiation for laminates with ±45° surface plies. Less energy is hence available for delamination growth.

The FE results obtained from Model A and Model C are presented in Figure 39. It is evident that the delamination area predicted by Model A is larger and more elongated than that predicted by Model C. However, the matrix cracks occurring in Plies 1, 3 and 4 in Model C seems to be more extensive than that occurring in Model A. The FE results show good agreement with the experimental studies performed by Hitchen et al. in terms of delamination size. However, the experimental matrix damage was not reported.

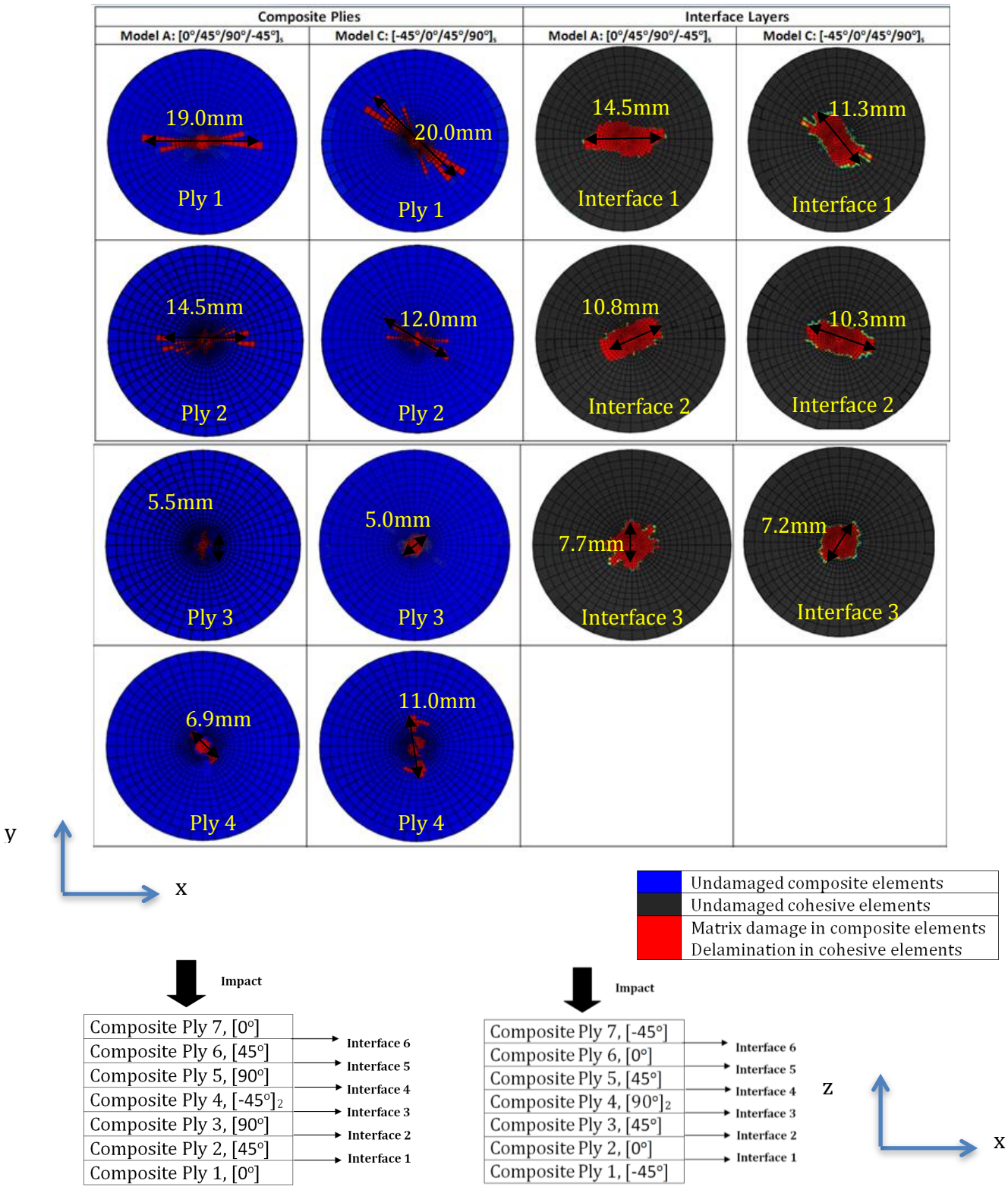

Figure 39 FE prediction of impact damage from Model A and Model C

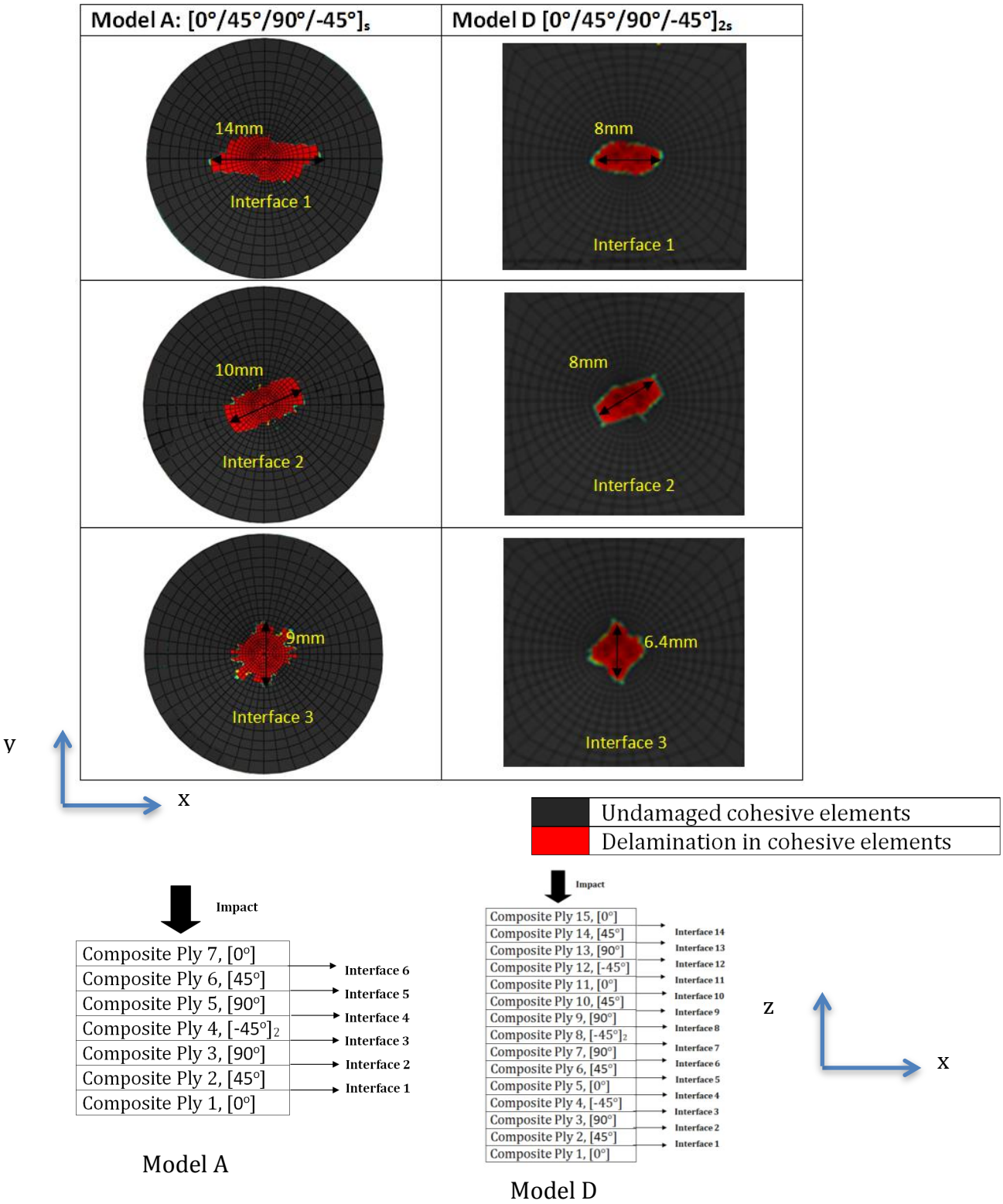

Figure 40 FE prediction of impact damage from Model A and Model D

4.3.3 Effect of laminate thickness

To study the effect of laminate thickness on impact damage, a comparison between the impact damage predicted by Model A and Model D was made. Laminate thickness is achieved via an increase in the total number of plies, with each ply thickness remaining constant. The results are present in Figure 40. Delamination at each interface in Model A was evidently more extensive than that in Model D. This result is in agreement with that reported by Stavropoulos et al. in [171], where the results from a study of the thickness effect on ballistically impacted CFRP laminates were presented. The researchers reported an increased threshold of higher impact energies for damage to initiate as laminate thickness increased, with each ply thickness remaining constant. Hence, thick laminates display a smaller damage size as compared to thin laminates.

4.3.4 Effect of ply-grouping

The impact damage predicted by Models D and E were compared to study the effect of ply-grouping on the shape and size of impact-induced delaminations. The results are presented in Figure 41 below. Model E, with the presence of ply grouping, has six interfaces in which delamination can occur because delamination do not occur between plies of the same fiber orientation as discussed in Section 2.1.3 [18,35,36]. Since Model D has more interfaces in which delamination can occur, the total delamination area in Model D is larger than that in Model E. However, it is observed that the individual delamination areas occurring in the interfaces of Model E are predicted to be larger than those occurring in Model D. This results in Model E having a larger projected delamination area than Model D.

These results are in agreement with that reported by Fuossa et al. in [165]. The researchers studied the effect of ply grouping using two laminates

of layups $[-45_3/0_3/45_3/90_3]_s$ and $[-45/0/45/90]_{3s}$, and found that the laminate with grouped plies had a projected delamination area more than twice that of the laminate without grouped plies. The largest delamination in Model D occurs in Interface 4, with dimensions of 8.4mm, while the largest delamination in Model D occurs in Interface 1, with dimensions of 17.3mm (Figure 41). Assuming the projected delamination area to be of the same size as the largest delamination, the projected delamination area predicted by Model E is 2.1 times that predicted by Model D.

In Section 2.2.1, the role of a bending stiffness mismatch between adjacent composite layers in the formation of delaminations has been discussed. Liu [36] defined a bending mismatch coefficient between adjacent layers of differing fiber orientation, and reported that the greater the bending mismatch coefficient, the greater the size of the delamination. Using this same theory, Fuossa et al. [165] attributed the larger delamination area in the laminate with grouped plies to the increased bending stiffness within the ply group, resulting in an increase in stress concentration at the interfaces. Furthermore, ply grouping reduces the number of interfaces available for delamination. Since delamination serves to absorb energy from an impact, reducing the locations at which delaminations can take place will in turn increase the delamination size at the remaining interfaces.

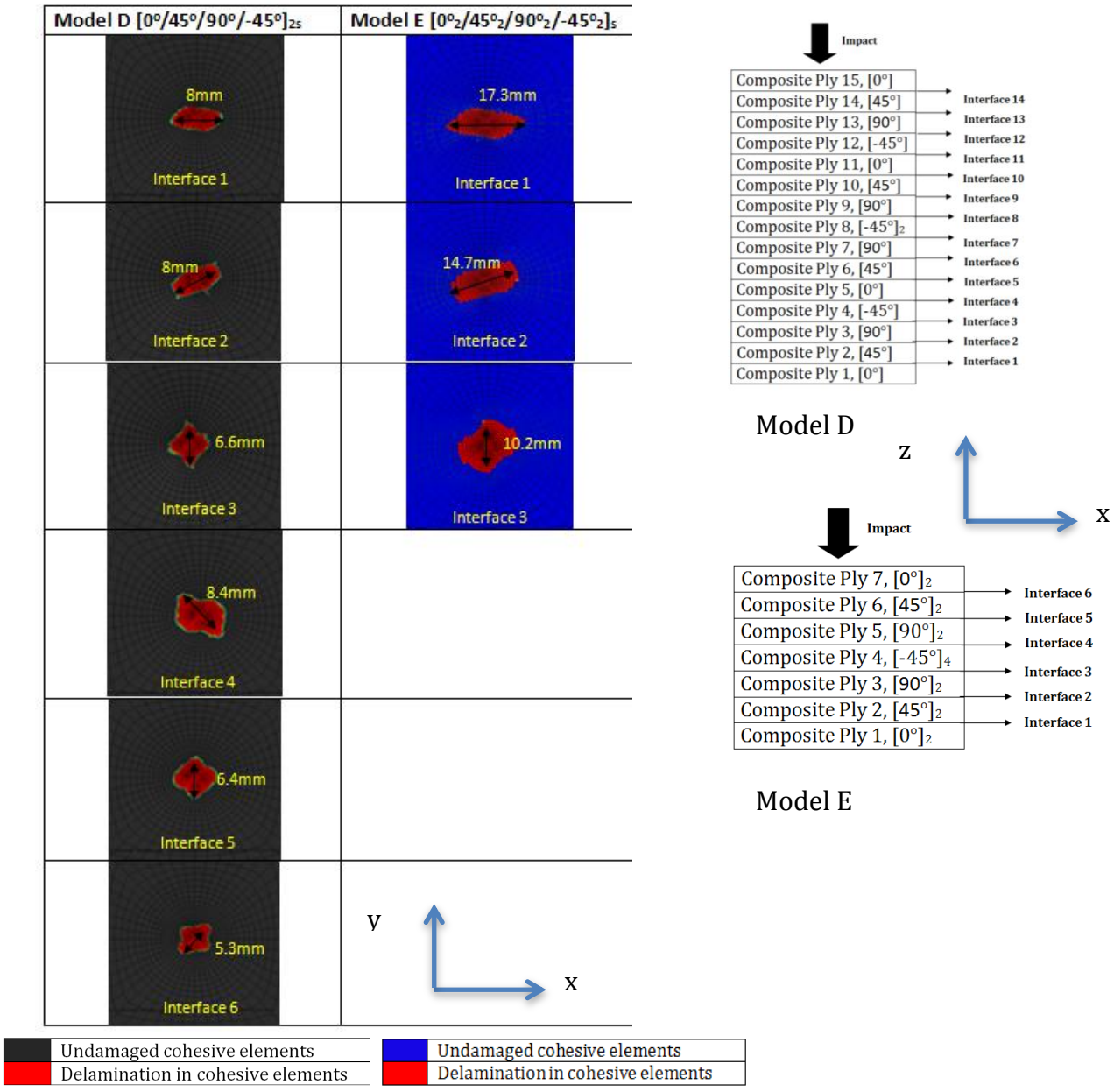

Figure 41 Impact damage prediction of Model D and Model E

4.3.5 Effect of relative angle between fiber orientations of adjacent plies

Model F with a layup of $[0^o/10^o_2/0^o]$ served to investigate the effect of a small relative angle between the fiber orientations of adjacent plies. The results are presented in Figure 42 below. As observed from the results, there exists extensive matrix damage in the composite plies while delamination damage has just begun to initiate in the interface layers. Such a damage profile is significantly different from that observed in Models A-E where the relative angles between the fiber orientations of adjacent plies are all 45^o. In Models A-E, the delamination sizes are always observed to be approximately that of the matrix damage at any particular point of time during the impact process, as presented in Section 4.2.

These findings are in agreement with the experimental findings of Hong et al. [172]. The researchers performed impact experiments on $[0_5/\theta_5/0_5]$ laminates where θ was equal to 0, 15, 30, 45, 60 and 90, and found that the delamination area increased as θ increased, with $\theta=0$ having no delamination at all. The researchers attributed this finding to the fact that delamination areas in a composite laminate subjected to impact is correlated to a bending stiffness mismatch between adjacent plies, and plies with a greater difference in fiber orientation angle would experience a larger bending stiffness mismatch, leading to a larger delamination area. Furthermore, the researchers found that the energy required for delamination initiation increases as θ increases.

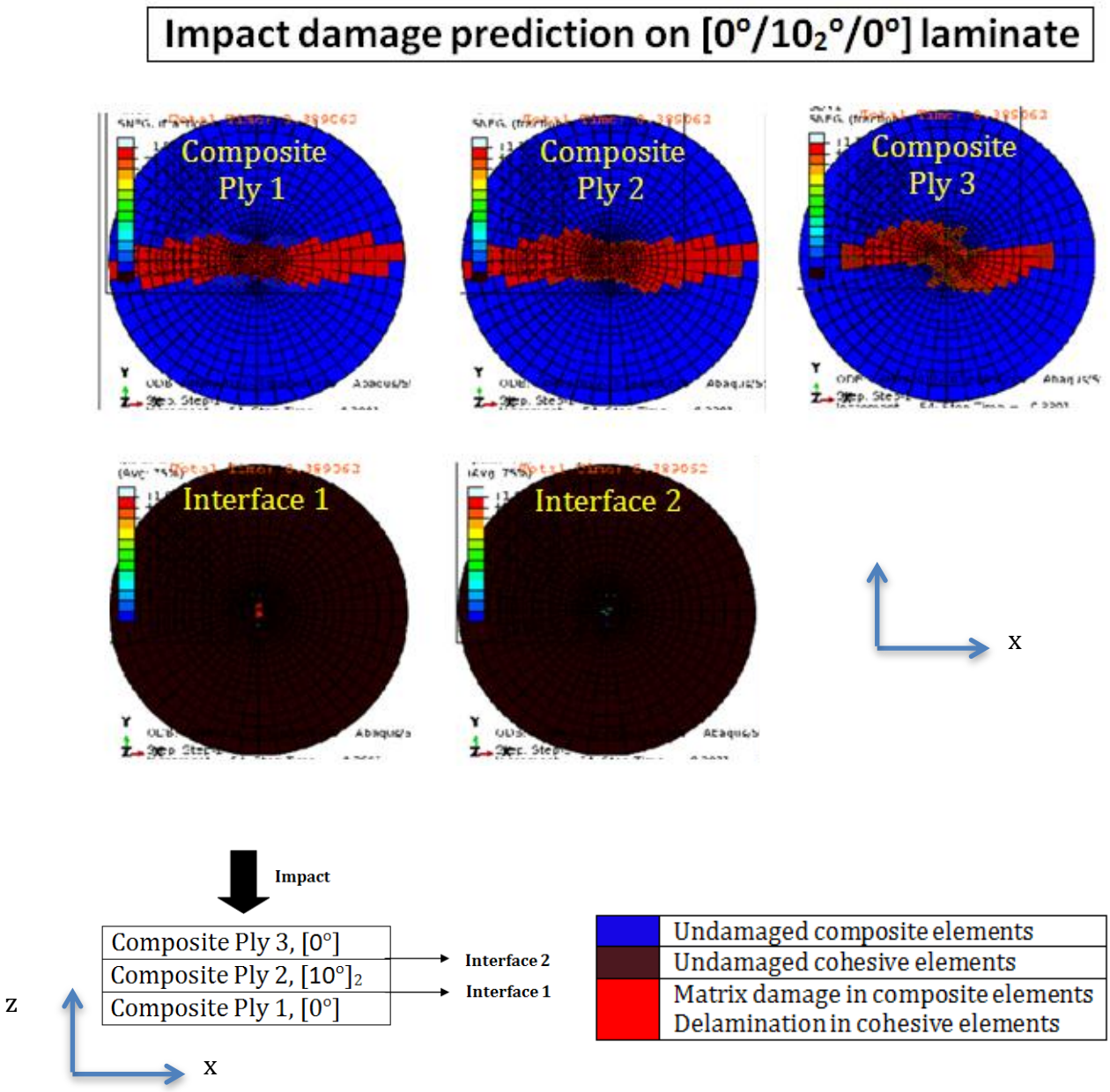

Figure 42 Impact damage prediction for [0/10$_2$/0] layup

4.4 Conclusions

In this chapter, the prediction of progressive damage due to low-velocity impact was presented. Although FE prediction of impact damage is a topic that has received widespread attention and research, developing an FE model for impact is a necessary step towards a holistic integrated FE analysis approach.

Comparisons were performed between the impact damage predicted by the impact FE model developed in this research with experimental impact damage reported in literature. The impact FE model developed has been verified to be capable of predicting impact damage that shows good agreement with experimental impact damage. Furthermore the versatility of the impact FE model in predicting low-velocity impact damage to an acceptable accuracy for several different laminate parameters has also been shown. This is important because an impact FE model capable of predicting impact damage accurately is a prerequisite to an accurate prediction of CAI strength in an integrated FE approach.

The following summarizes the key findings from the parametric studies:

- The low-velocity impact damage pattern observed in CFRP laminates made up of thin plies of ply thickness about half that of standard plies is significantly different from the damage pattern observed in standard ply laminates. In thin ply laminates, delaminations are found to be most extensive in the interfaces nearer the mid-plane. This is in contrast to delaminations in standard ply laminates in which delamination areas generally increase away from the impact face such that the interface furthest from the impact face sustains the largest delamination.

Saito et al. [168] explained that such a unique damage pattern observed in thin ply laminates was due to a ply thickness threshold of 0.04mm in which cracks can propagate. However, in the FE model used in this research, the ply thickness for the thin ply laminate was 0.07mm, exceeding that of the threshold value for crack propagation to occur of 0.04mm proposed by Saito et al. [168]. Despite this, the same phenomenon of delaminations being most extensive in the interfaces nearer the mid-plane was still observed in Model B.

- Composite laminates with 45^{o} surface ply sustains smaller delamination damage and greater matrix cracks as compared to composite laminates with 0^{o} surface ply. If the composite laminates were infinitely large, such a difference in impact damage sustained would not be expected to occur, since the impact area is circular. The impact damage sustained would be the same regardless of surface ply angle. Hence, the observed difference in impact damage sustained between the two laminates, one with 0^{o} surface ply and the other with 45^{o} surface ply, is attributed to the effect of the boundary conditions, which arises because the laminate is sufficiently small.
- Comparing impact damage in thicker laminates made up of a larger number of plies with thinner laminates made up of a smaller number of plies of the same individual ply thickness as the thick laminates, the delamination in each interface predicted by the FE model for the thick laminates was less extensive as compared to that predicted for thinner laminates. Stavropoulos et al. [171] explained that this observation was due to an increased threshold of higher impact energies for damage to initiate with increasing laminate thickness. Furthermore, in laminates where plies of the same orientation are grouped together, the total

delamination area is smaller than that in laminates without the presence of grouped plies, while the projected delamination area is greater than that in laminates without grouped plies. Fuossa et al. [165] attributed the larger delamination area in laminates with grouped plies to the increased bending stiffness within the ply group, resulting in an increased stress concentration at the interfaces. Furthermore, grouped plies reduce the number of interfaces available for delamination, hence increasing the delamination area at the reduced number of interfaces.

- When the relative angle between fiber orientations of adjacent plies are small (in this case a relative angle of 10^{o} was used), delamination due to low-velocity impact was suppressed, while matrix cracks propagated more readily. This is markedly different from the low-velocity impact damage observed in quasi-isotropic laminates, in which delamination sizes are always observed to be approximately the same as the size of the matrix cracks adjacent to the delamination. Hong et al. [172]attributed this finding to the fact that delamination areas in a composite laminate subjected to impact is correlated to a bending stiffness mismatch between adjacent plies, and plies with a smaller difference in fiber orientation angle would experience a smaller bending stiffness mismatch, leading to smaller delamination sizes.

Chapter 5

FINITE ELEMENT SIMULATIONS OF CAI TESTS

Chapter 5 presents stage II of the research, where damage due to low-velocity impact is pre-modeled into the finite element model for the prediction of residual compression after impact (CAI) strength. The CAI test is used to determine residual compressive strength of a laminate subjected to low-velocity impact.

For the prediction of CAI strength from a given impact damage pattern, a study on how the modeling of multiple delaminations found in impact damaged specimens would influence the residual CAI strength predicted is presented in this chapter. This study is aimed at identifying the main causes of the compressive strength reduction in impacted composite plates.

Much research has been done to predict the CAI strength of impact damaged composites. However most attempts at predicting the residual CAI strength [73,173, 174] make the assumptions that delamination shapes and sizes are uniform in each interface, with the delamination shapes simplified to be either circular or elliptical. Another common assumption made in most CAI strength prediction studies is that delamination is the only dominant damage mode leading to the reduction of compressive strength of the composite laminate. The effect of other modes of damage and their interactions in an impacted CFRP laminate on the residual CAI strength is ignored. Such assumptions do not accurately reflect reality.

In this stage of the research, experimental data of the delamination and crack profile of an impact damaged composite obtained by I. Kimpara and H. Saito [3] was modeled approximately into the FE model, and the CAI strength of the experiment and simulation was compared. The main difference distinguishing the approach used in this research for the FE prediction of CAI strength from other commonly used approaches reported in literature is the modeling of non-uniform delaminations representative of experimental impact-induced delaminations and matrix cracks, instead of simply modeling idealized delamination shapes and sizes without modeling the matrix cracks.

The objectives are to determine the dominant damage modes that have an influence on the residual CAI strength, and to ascertain whether matrix cracks play an important role in reducing the compressive strength of the CFRP laminate.

5.1 Finite element models of CAI tests

The FE model used to simulate the CAI test is of the same formulation as the FE model used to simulate impact, as described in Section 3.2. The composite plies were modeled using 3D continuum shell elements SC8R with one element in the thickness direction, while the interface was modeled using a single cohesive element in the thickness direction. Each composite layer is 0.1875mm thick, and each cohesive element is 0.01mm thick. Tie-constraints and surface-to-surface interactions were used in the FE model to prevent the interpenetration of the composite plies. This is demonstrated in Figure 44. The tie constraints used between the composite plies and interface layers would prevent them from interpenetrating each other. In addition, the surface-to-surface interaction between the composite plies would prevent

the cohesive thickness to be of a negative value, thus prevent the composite plies from penetrating each other. The material properties used in the FE model for the prediction of CAI strength are those of T800S/3900-2B, presented in Table 2. These material properties are used in order to compare the simulation results with the experimental results reported by Kimpara et al. [3]. Compression after impact tests are simulated by subjecting the FE model to in-plane compressive loads. To simulate compression, a unit displacement (1mm) in the negative y-direction is prescribed to nodes in the FE model that are lying on the red line shown in Figure 43. Nodes lying along the yellow line shown in Figure 43 are not allowed any translational displacements, i.e. U1= U2 = U3 = 0. Furthermore, nodes lying along the red line are not allowed any rotation about the x-axis. In addition, a small transverse nodal force (simulated by prescribing a displacement of 0.001mm in the out-of-plane direction) is applied at the center of the model to induce local buckling [71].

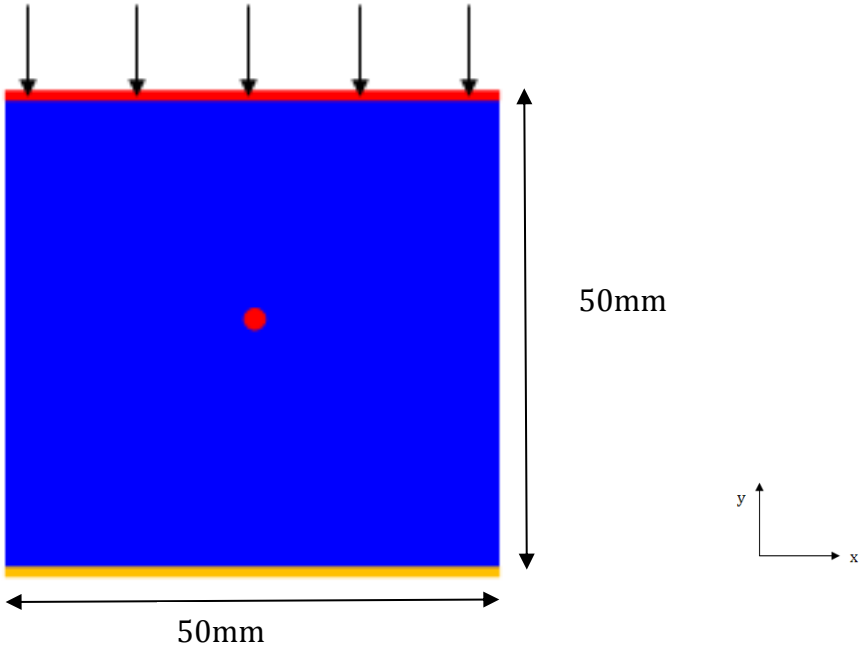

Figure 43 FE model for the prediction of CAI strength. The mesh is not shown in this figure because different meshes are used for this study, and the different meshes are shown in the later part of this chapter.

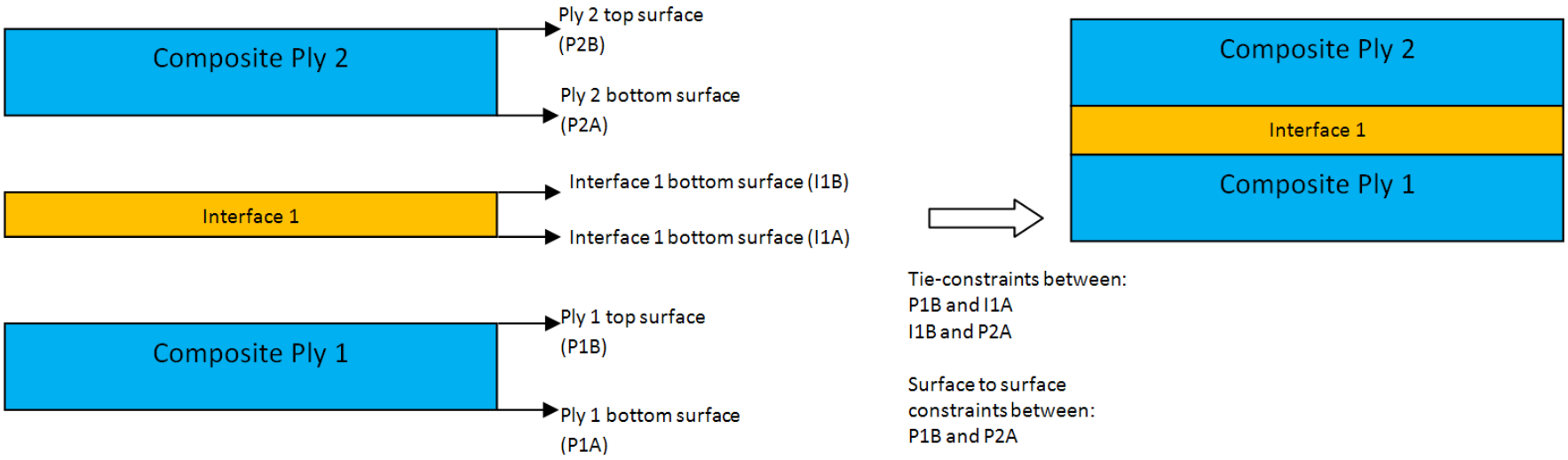

Figure 44 Pictorial representation of constraints used in the FE model to prevent the interpenetration of surfaces

I. Kimpara and H. Saito [3] performed an experimental study on impact damage and the residual CAI strength. In this experiment, a quasi-isotropic CFPR laminate made of the material T800S/3900-2B in a $[-45^o/0^o/45^o/90^o]_{2s}$ stacking sequence was subjected to impact. The impactor used Information on the impact damage incurred is then extracted and a 3D damage distribution map was obtained. More details on the impact stage of the experimental study have been presented in Section 4.1.2 of this thesis. CAI test is then performed on the impacted specimen and the CAI strength is obtained and compared with the compressive strength of an undamaged specimen of the exact same dimensions and layup. The CAI test experimental set-up is shown in Figure 45. The dimensions of the FE models replicate that of the experiment, with a height of 50mm and a width of 43mm. This experiment is used as a reference for the FE models built for the purpose of CAI strength prediction. A comparison of the CAI strength predicted by the different FE models built in this study with the experimental CAI strength is carried out. The experimental CAI strength is reported in Figure 46. As seen, it is approximately half that of the compressive strength of an undamaged specimen.

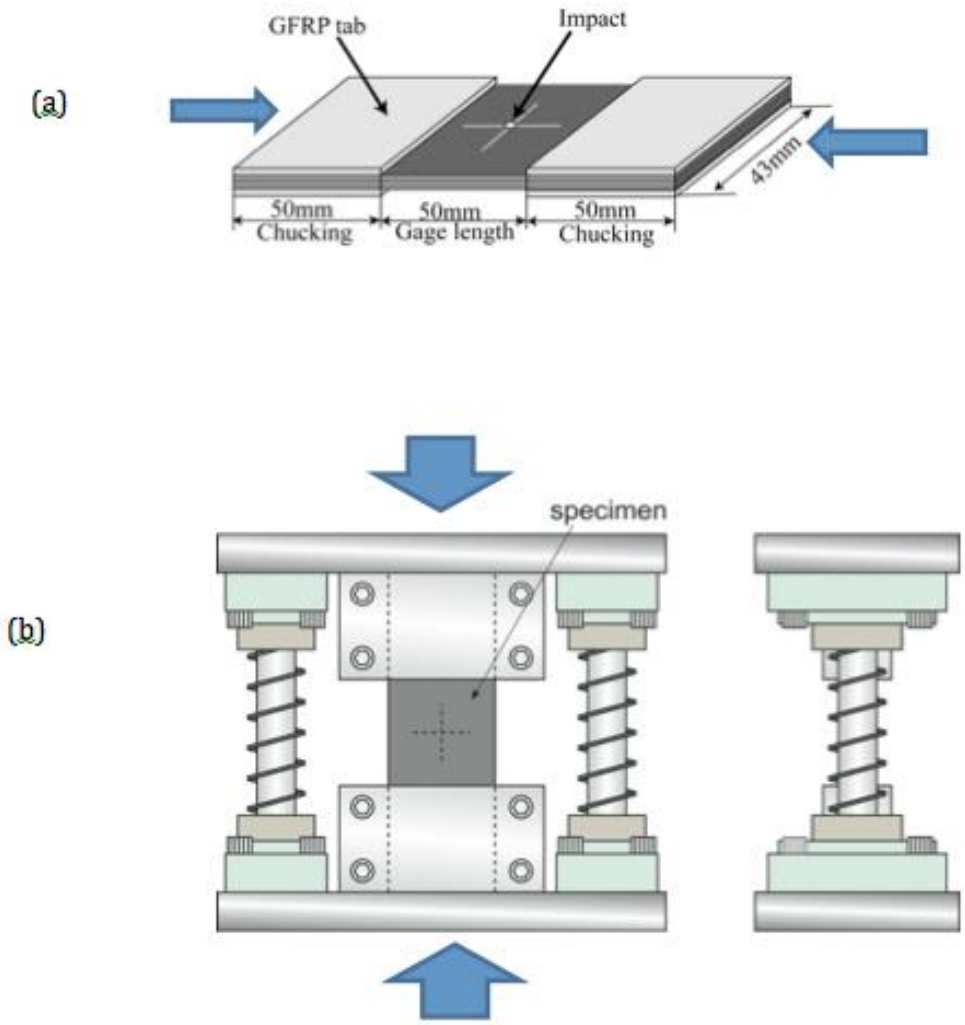

Figure 45 CAI test experimental set-up, obtained from [3]

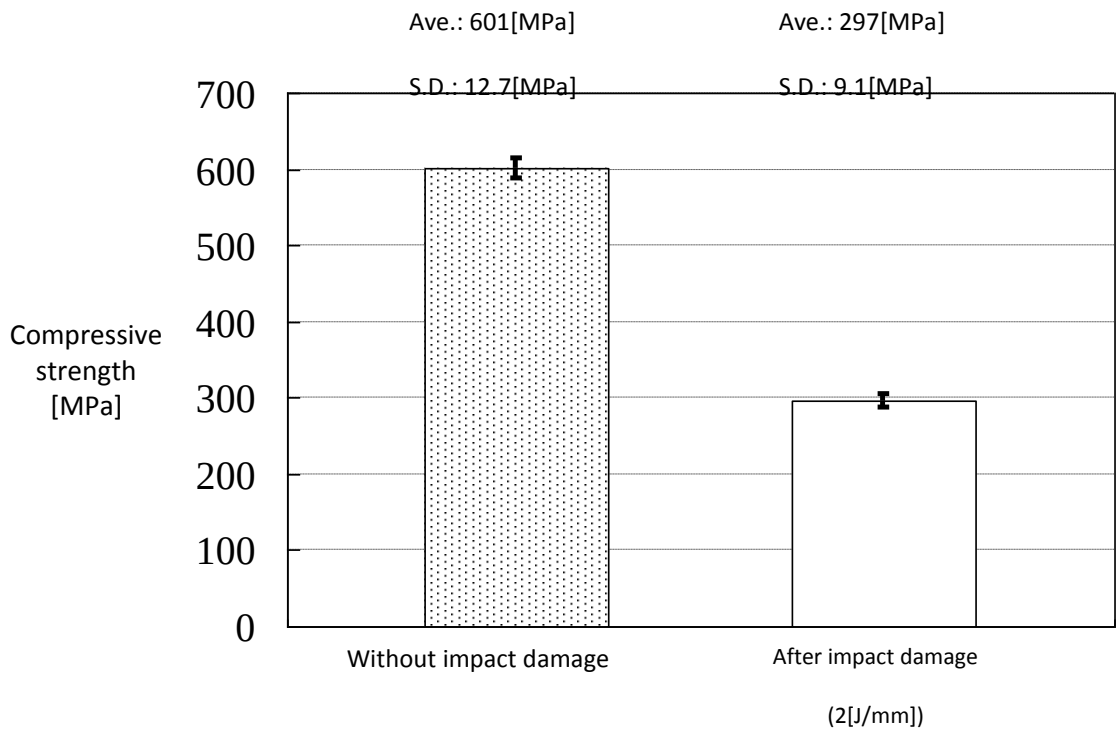

Figure 46 Experimental comparison of the residual CAI strength with compressive strength of an undamaged specimen, obtained from [3]

Seven different FE models, each with varying complexity of impact damage pre-modeled into the models, are used to study how the pre-modeling of different impact damage types and patterns would influence the residual CAI strength predicted by the FE model. The purpose of these models is to determine whether increasing the complexity of the impact damage pre-modeled into the FE model for CAI strength prediction has a significant effect on the CAI strengths predicted. Since the experiment conducted by Kimpara et al. [3] is used as a benchmark to determine the accuracy of the CAI strength predicted by the FE models, the impact damage pre-modeled into the different FE models are modeled based on the impact damage profile extracted from the reference experiment [3], and result from

different ways of approximation of the impact damage observed from the experiment.

The differences between the FE models built in this study for CAI strength prediction lie in the complexity of impact damage that is pre-modeled into them, and can be broadly classified into two categories (Refer to Table 6): Models in which only delaminations are considered (Models A, B, C1, D and E1), and models in which both delaminations and matrix cracks are included (Models C2 and E2). These models can further be classified into two sub-categories: Models in which the delaminations included are of identical shapes and sizes throughout every interface within the model. These models are termed "uniform delamination models". The second sub-category contains models in which the interfaces contain delaminations of different shapes and sizes. These models are termed "non-uniform delamination models". With the exception of Models C1 and C2, all the models have a stacking sequence of $[-45^o/0^o/45^o/90^o]_{2s}$, same as that of the laminate used in the reference experiment.

Models A and B, both with uniform delaminations, are constructed to study the effect of simplified uniform delaminations on the residual CAI strength predicted by the FE models. Model A contains delaminations in every interface that span 16mm in height and 43mm in width, extending through the entire width of the model, seen in Figure 48(a). Model B contains centrally embedded 16mm by 16mm square delaminations in every interface, as seen in Figure 48(b). The dimensions of 16mm was chosen for both Models A and B because the projected delamination observed in the reference experiment [3] covered an approximate area of 16mm by 16mm, as seen in Figure 30(a).

Models C1 and C2 is identical to Model B in terms of the delamination that is pre-included in the model. However, both Models C1 and C2 have a

stacking sequence of $[90^o/0^o]_{4s}$ instead of $[-45^o/0^o/45^o/90^o]_{2s}$. Furthermore, Model C2 contains matrix cracks pre-modeled into it in addition to the centrally embedded square delamination. The purpose of Models C1 and C2 is to study whether matrix crack interactions with delamination have any effect on the predicted CAI strength. The mesh used for Models B, C1 and C2 with centrally embedded square delaminations is made up of regular square elements, as seen in Figure 49. In such a regular mesh, only horizontal and vertical cracks can be pre-modeled into the FE models. Since matrix cracks in each composite ply propagate along the fiber direction of that ply, only 0^o and 90^o cracks can be modeled into the mesh, and hence the stacking sequence of Models C1 and C2 is chosen to be $[90^o/0^o]_{4s}$.

Unlike Models A, B, C1 and C2 which contain identical delaminations at every interface, the delaminations pre-modeled in Models D, E1 and E2 are non-uniform, as seen in Figure 52 and Figure 53 respectively. The delamination in Model D is modeled as closely as possible to those obtained from the experiments conducted by Kimpara et al. [3], while Model E1 contains delaminations which progresses in each interlayer by a rotation of 45^o. The delamination modeled in Model E1 is an approximation of the non-uniform delamination profile observed from the experiments [3]. As seen in Figure 30(b), the delamination profile obtained from the experiments [3] has been reinterpreted in this current thesis where the delaminations can be approximated to progress in each interlayer by a rotation of 45^o. Such an approximate non-uniform delamination profile is hence modeled into Models E1 and E2. The difference between Models E1 and E2 is that Model E2 has matrix cracks pre-modeled into it. Model E2 is constructed to study whether matrix crack interactions with delamination have any effect on the CAI strength predicted.

Delaminations are modeled by degrading the cohesive elements' stiffness to a negligible value, about 10^{-6} times that of the stiffness of an

undamaged cohesive element. For example, to model an embedded square delamination as shown in Figure 48(b), the stiffness of the cohesive elements lying within the area highlighted red in Figure 48(b) are degraded. The material properties of all other cohesive elements remain at their original values. Matrix cracks are modeled by nodes-separation. For example, to create a simple horizontal matrix crack as shown in Figure 47, the laminate is first modeled in two parts. The coinciding nodes at the edges of each part where the matrix crack is not supposed to exist are then merged to become a single node, as seen in Figure 47. The resultant model is a single laminate containing a matrix crack at the location where the nodes remain unconnected.

Type of damage pre-modeled into CAI strength prediction model		
Delaminations only	Uniform Delamination	Model A: Through-width delamination
		Model B: Embedded square delamination
		Model C1: Embedded square delamination, $[90/0]_{4S}$
	Non-Uniform Delamination	Model D: Exact delamination profile as observed in experiments are modeled
		Model E1: Delamination progressing in each interlayer by a rotation of 45^{o}
Delaminations and matrix cracks	Uniform Delamination	Model C2: Embedded square delamination with matrix cracks, $[90/0]_{4S}$
	Non-Uniform Delamination	Model E2: Spiral delamination with matrix cracks

Table 6 Different FE models for CAI strength prediction used in this study. All models have the same stacking sequence as the laminate used in the reference experiment except Models C1 and C2

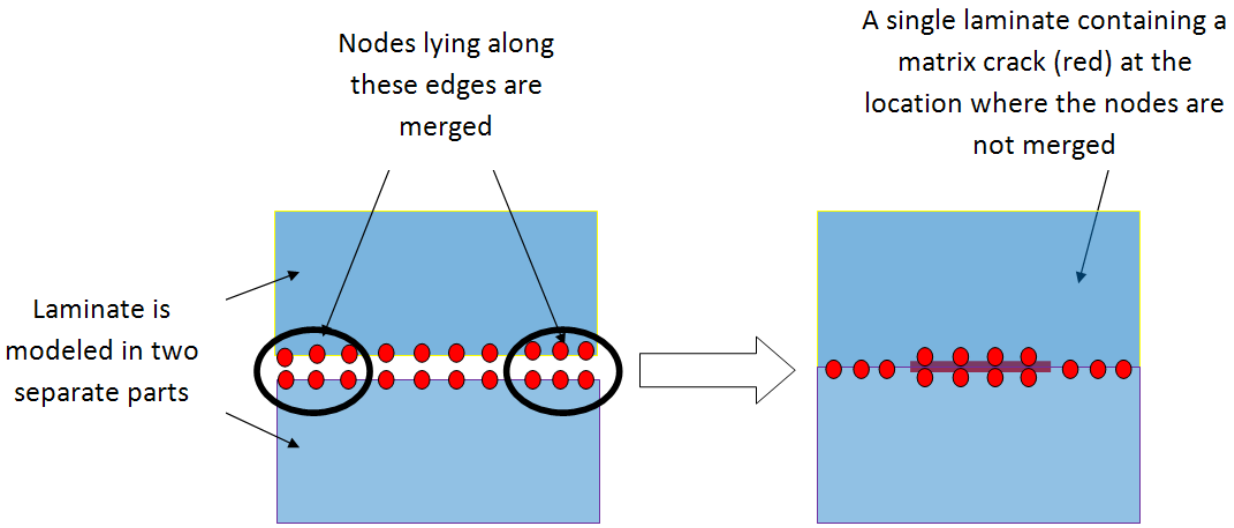

Figure 47 Pictorial representation of how matrix cracks are modeled

5.1.1 Uniform delamination models without matrix cracks

Two simple models (Models A and B) with uniform delamination are constructed; one with through-width delaminations (Figure 48(a)), and the other containing embedded square delaminations (Figure 48(b)). The purpose of these two models is to study the effect of a simplified delamination on the residual CAI strength of the laminate. The dimensions of the models replicate that of the dimensions of the laminates used in the reference experiment, with a height of 50mm and a width of 43mm. In Model A, a delamination 16mm in height and 43mm in width is modeled into The dimensions of the embedded square delaminations are chosen to be 16mm because as presented in Figure 30 in Section 4.1.2, the projected delamination from the reference low-velocity impact experiment covers an area of 16mm by 16mm. Furthermore, in majority of the studies available in literature involving the prediction of CAI, the delaminations shapes and sizes are simplified to be the same in every interface, and the delamination sizes are approximated to be that of the overall projected delamination area as observed in experiments.

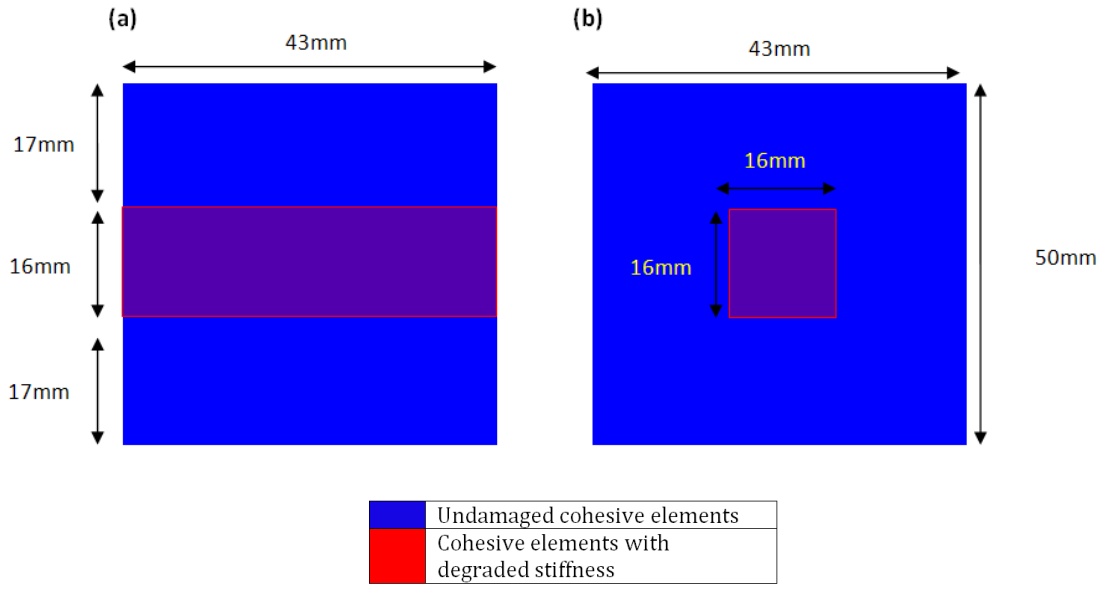

Figure 48 Uniform delamination models with (a) through-width delaminations and (b) embedded square delaminations

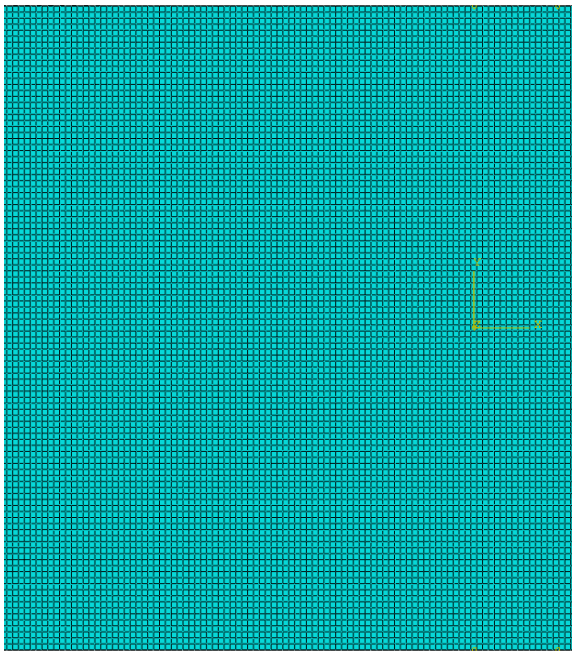

Figure 49 Mesh used for Models A, B, C1, C2 and D

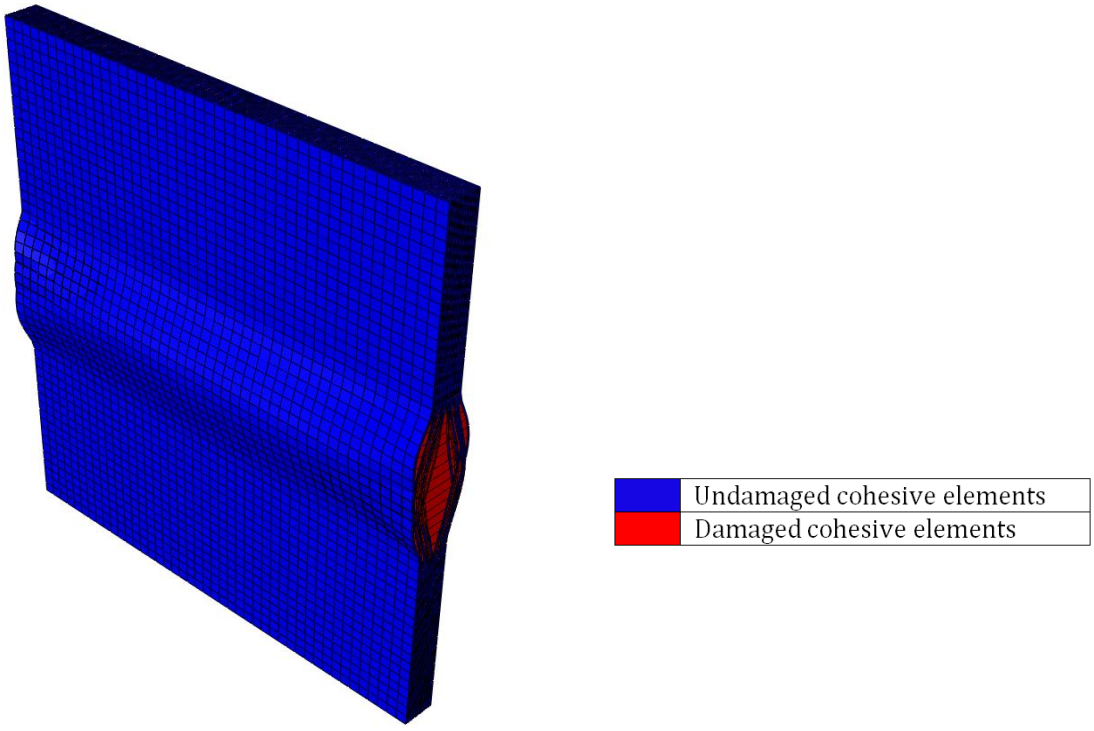

Figure 50 Buckled shape for Model A

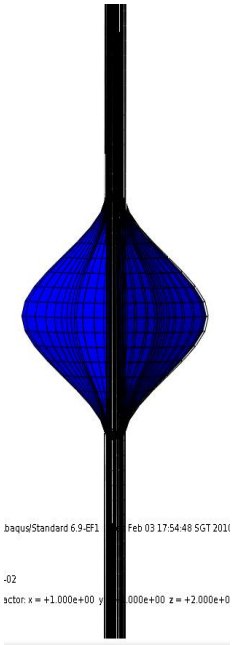

Figure 51 y-z view of buckled shape for Model B, with magnification of 20 times in the z direction

An undamaged FE model with material properties that are those of T800S/3900-2B (Table 2) predicts a compressive strength of approximately 580MPa. This is in close agreement with the experimental value of 601MPa as reported in Figure 46. Model A (uniform through-width delamination) predicts a CAI strength value of approximately 20MPa. The CAI strength predicted by Model B (uniform embedded square delamination) is approximately 250MPa, which is a little less than half that of the predicted undamaged compressive strength. This prediction is in closer agreement with the experimental CAI strength of 297MPa (Figure 46) than that obtained from Model A. Figure 50 above shows the final result of the buckled Model A. Figure 51 shows the buckled shape of Model B, with a magnification of 20 times in the z-direction, so that the bulge due to the locally buckled area at the centrally embedded delamination is made obvious.

5.1.2 Non-uniform delamination model without matrix cracks

It has been reported in [173] that the reduction in the CAI strength is dependent on various characteristics of the delamination, such as the size, the shape, the area and the position of the delamination. Furthermore, Obdržálek et al. recently performed a study on the applicability of simple delamination shapes in buckling analyses [74], and concluded that a representation of the shape of the delaminations that is as precise as possible is necessary for accurate analyses of the buckling and post-buckling behavior of delaminated plates. In this study by Obdržálek et al. [74], the authors concluded that the elliptic representation of an irregular shape of delamination may result in the reduction of the CAI strength predicted by more than 20%, as compared to the prediction obtained by considering the irregular shape of delamination as observed in experiments. As reported in Section 5.1.1,

Model B with the uniform embedded square delamination predicted a CAI strength of 250. As compared to the experimental CAI strength obtained by Kimpara et al. [3] of 297MPa, the simplified uniform square delaminations resulted in the reduction of the CAI strength prediction of more than 15%. In view of these conclusions, non-uniform delamination models containing delamination profiles representing that obtained from the reference experiment are created.

Model D contains the approximate delamination profile modeled as closely as possible to those obtained in the reference experiment. The delamination shapes, sizes and locations that are modeled in each interface in Model D represents the delaminations observed in the impact experiment as precisely as possible. This is done by superimposing the delamination profile obtained from the experiment over the FE mesh, as demonstrated in Figure 52. For example, to model the delamination in interface 15, the stiffness of the cohesive elements that are contained within the dark orange area in Figure 52 is degraded. To model the delamination in interface 12, the stiffness of the cohesive elements contained in the blue area is degraded.

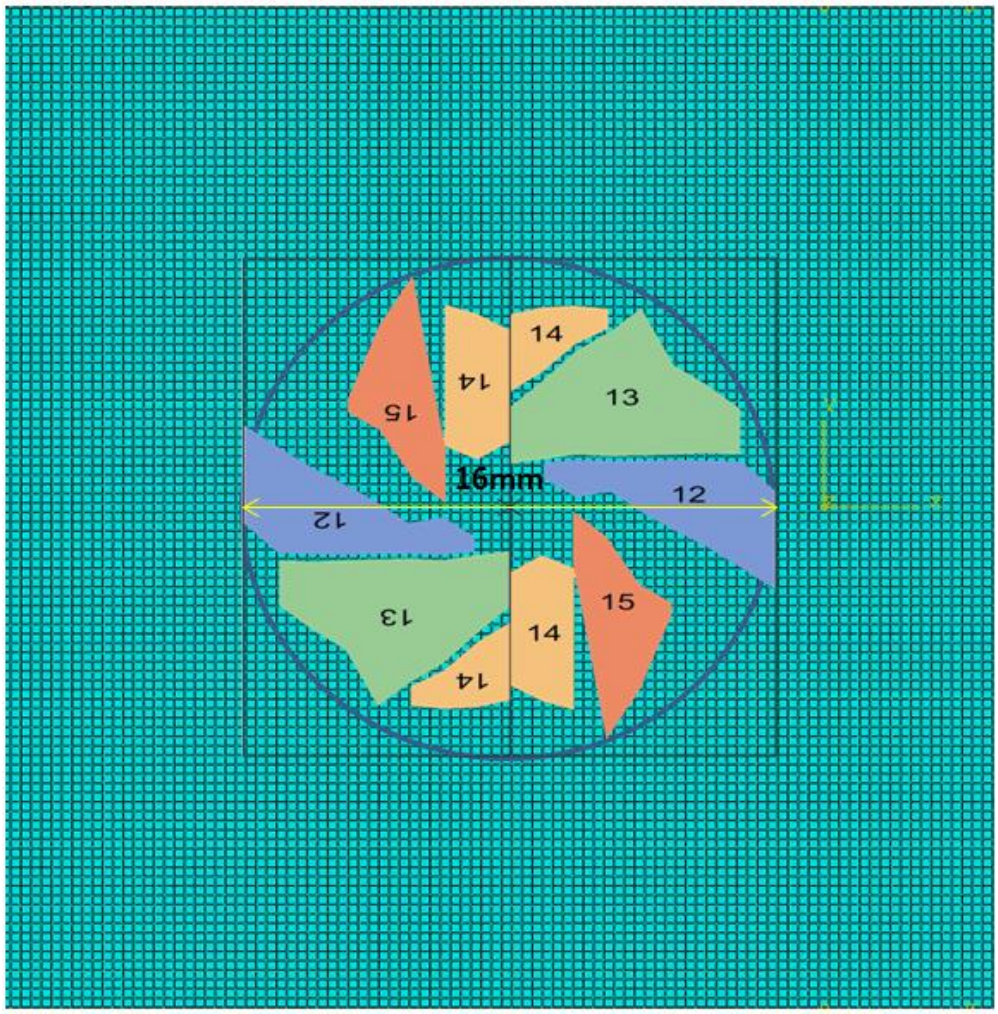

	Undamaged cohesive elements
	Experimental delamination area in Interface 12
	Experimental delamination area in Interface 13
	Experimental delamination area in Interface 14
	Experimental delamination area in Interface 15

Figure 52 Pictorial representation of how delaminations are modeled in Model D

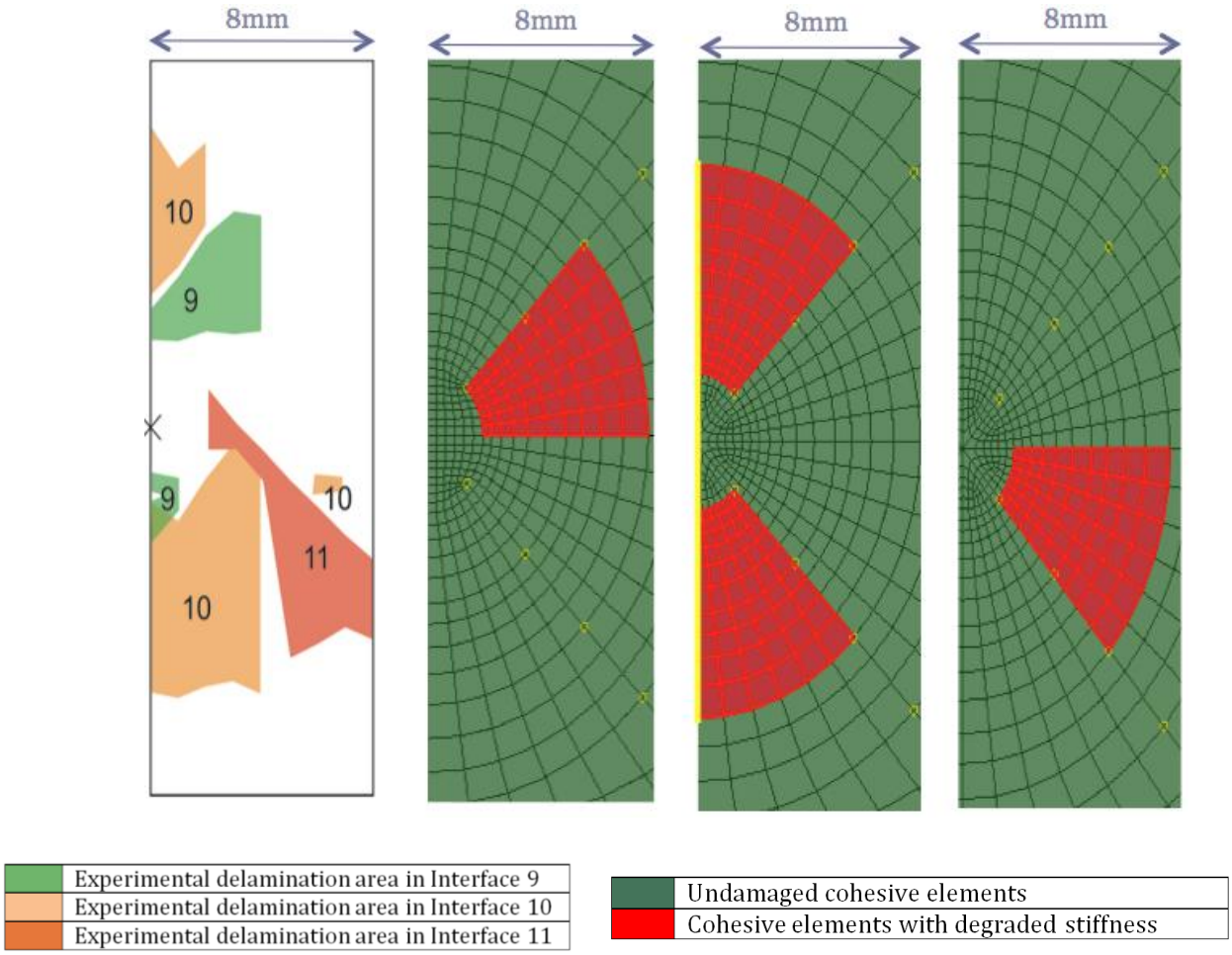

Figure 53 Pictorial representation of how delaminations are modeled in Models E1 and E2.

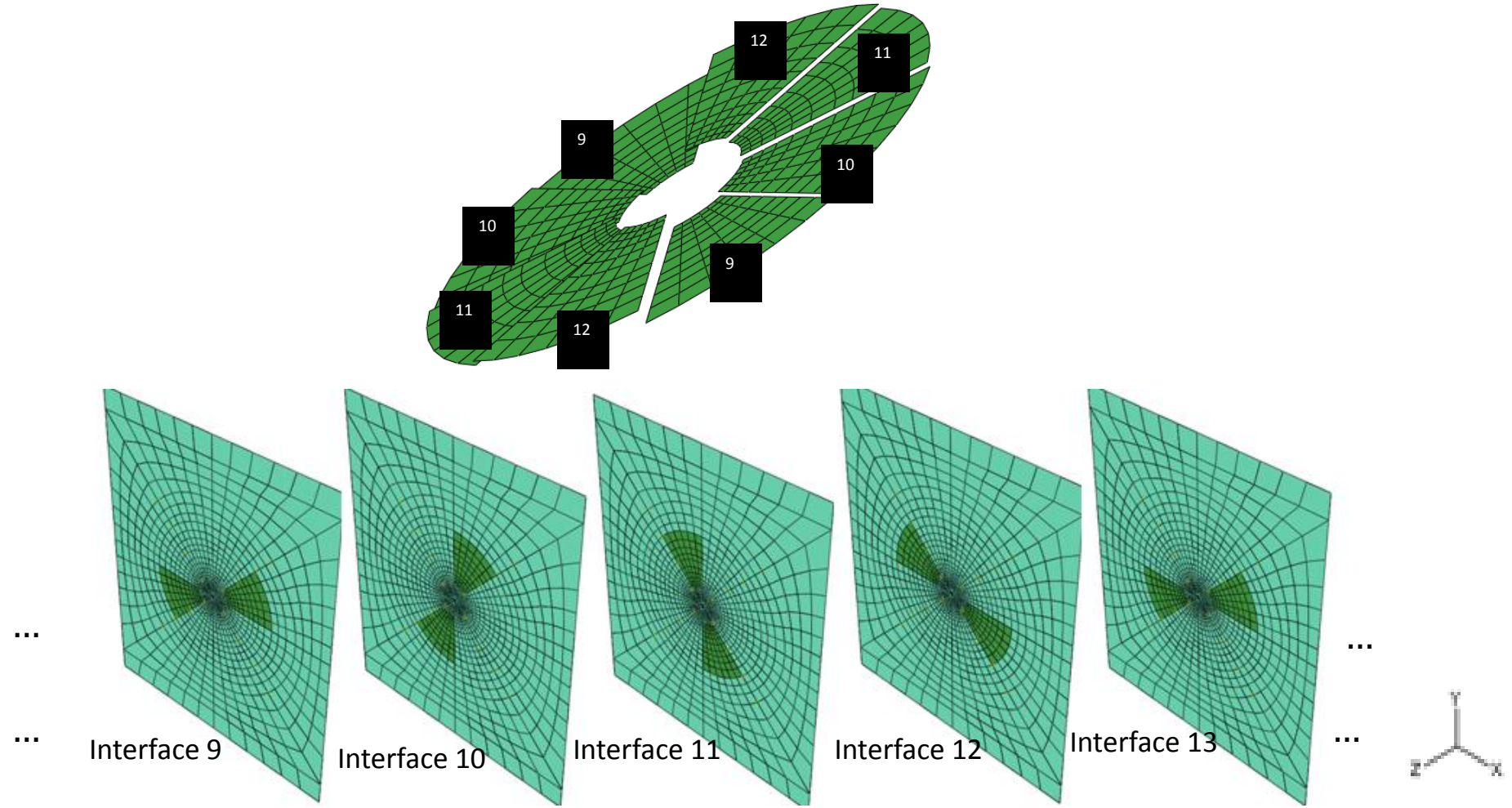

Figure 54 Modeling of spiral shaped delaminations progressing at 45^{o} units as observed in the reference experiment in Models E1and E2

I. Kimpara and H. Saito concluded from their experiments that 'a spiral-shape delamination progressed in each inter-layer, and their progress direction was rotated by a unit of 45 degrees. Transverse cracks progressed from the edge of delamination.' [3] (Figure 27) Model E1 is created to represent this experimental finding of delamination progression in each interface, with a unit rotation of 45^{o} in a simplified manner, instead of modeling the exact delamination profile as observed in experiments, as what was done in Model D. The purpose of this is to study the amount of damage details required in order to achieve an accurate CAI strength prediction. As shown in Figure 53 and Figure 54, Model E1 contains delaminations of the same shape and size at each interface, but the delaminations are interspersed at different locations in each interface. Figure 53 shows how the delaminations size and locations observed in the experiment are approximated and modeled into Model E1. Figure 54, consisting five successive cohesive layers, shows how the spiral shape delamination progressing at 45^{o} units as observed in the experiment was modeled. The overall projected delamination area is idealized to be a circular area of diameter 16mm. The circular area is divided into 8 equal sections, and the experimental delaminations were approximated to fit into any of the sections that best represent the location of the delamination. The section that best fits the location of the experimental delamination observed will be the section in which the cohesive element stiffness is degraded to model delamination in the FE model.

Unexpectedly, the CAI strength predicted by Model D and Model E1 are exactly the same as the compressive strength predicted by the undamaged model. The buckled shape for Models D and E1 is also the same as that for the undamaged model, seen in Figure 55. It is hence hypothesized that in addition to delaminations, matrix cracks are important contributing factors to the reduced compressive strength.

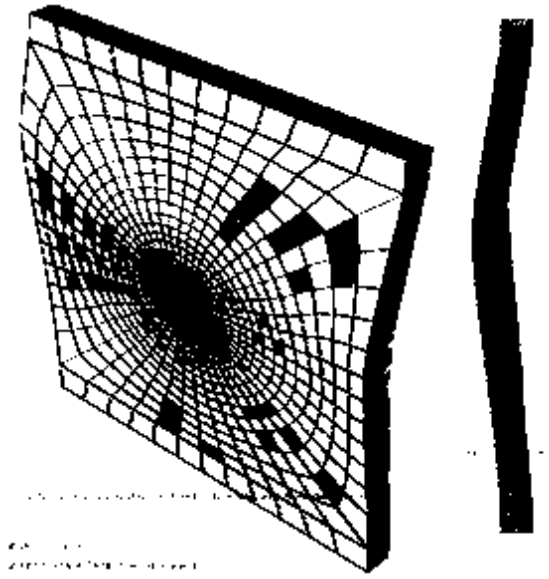

Figure 55 Buckled shape for undamaged model. The same buckled shape is obtained from Models D and E1.

5.1.3 Uniform delamination model with matrix cracks

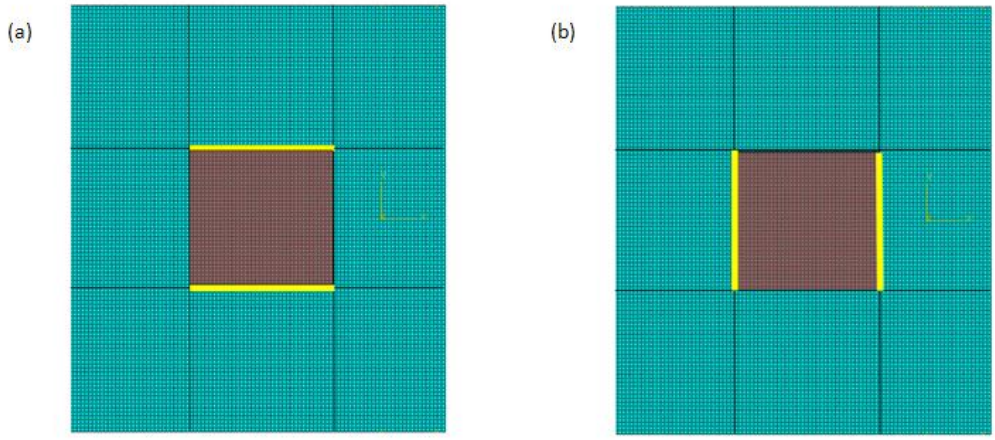

Figure 56 Delaminations located in the shaded region in the center of the composite plates, with (a) horizontal 0^o matrix cracks (yellow) and (b) vertical 90^o matrix cracks

Models C1 and C2 are made of the same mesh as Model B, and both models contain embedded square delaminations of the same dimensions. However, the stacking sequence of Model E is $[90/0]_{4S}$. This is because in such a regular mesh comprised of rectangular elements, only horizontal and vertical matrix cracks can be modeled using the technique described in Section 5.1 and Figure 47. Horizontal cracks are modeled into composite plies oriented in the 0^o direction while vertical cracks are modeled into composite plies oriented in the 90^o direction.

An undamaged model with a $[90/0]_{4S}$ layup predicts a compressive strength of approximately 970MPa. Model C1 (embedded square delaminations without matrix cracks) predicts a compressive strength of approximately 400MPa while Model C2 (with matrix cracks) predicts a slightly lower compressive strength of approximately 360MPa. As observed in Figure 57, the matrix cracks allow for easier lateral deflection of each composite ply, leading to a reduced CAI strength. In the case of a model with only uniform delamination (Models A and B), such lateral displacement of the composite plies are not inhibited, leading to the prediction of a CAI strength that is almost half that of the undamaged model. However, when non-uniform delaminations, which are more representative of realistic delaminations induced by impact, are modeled instead (Models D and E1), there is an inhibition of such lateral displacement of the composite plies, resulting in a high CAI strength predicted. In fact, the CAI strength predicted by Models D and E1 in this study is exactly the same as that of an undamaged model. These results support the hypothesis that the inclusion of cracks is of great significance in models where a realistic representation of damage is desired.

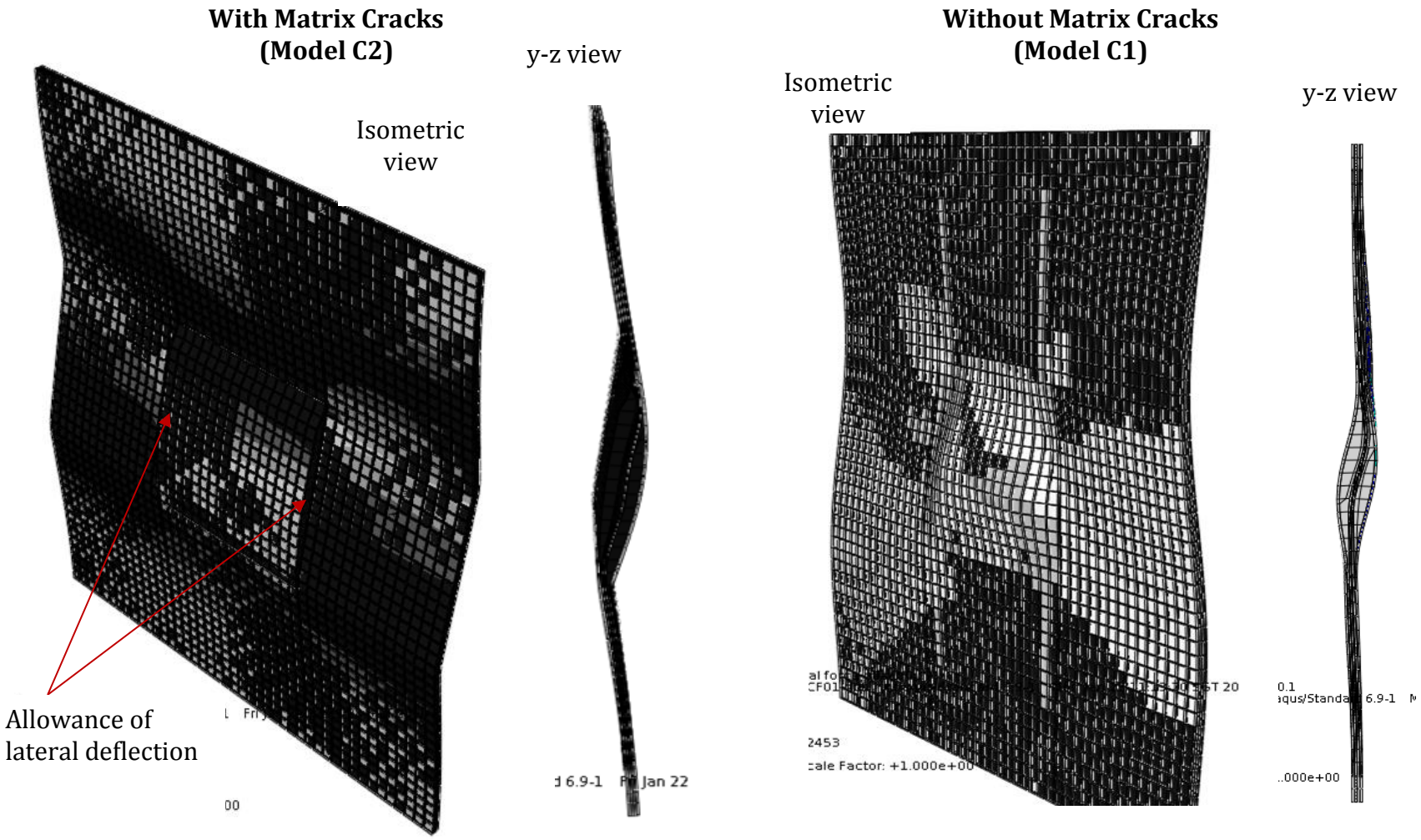

Figure 57 FE results obtained for (a) Model C2 and (b) Model C1

5.1.4 Non-uniform delamination model with matrix cracks

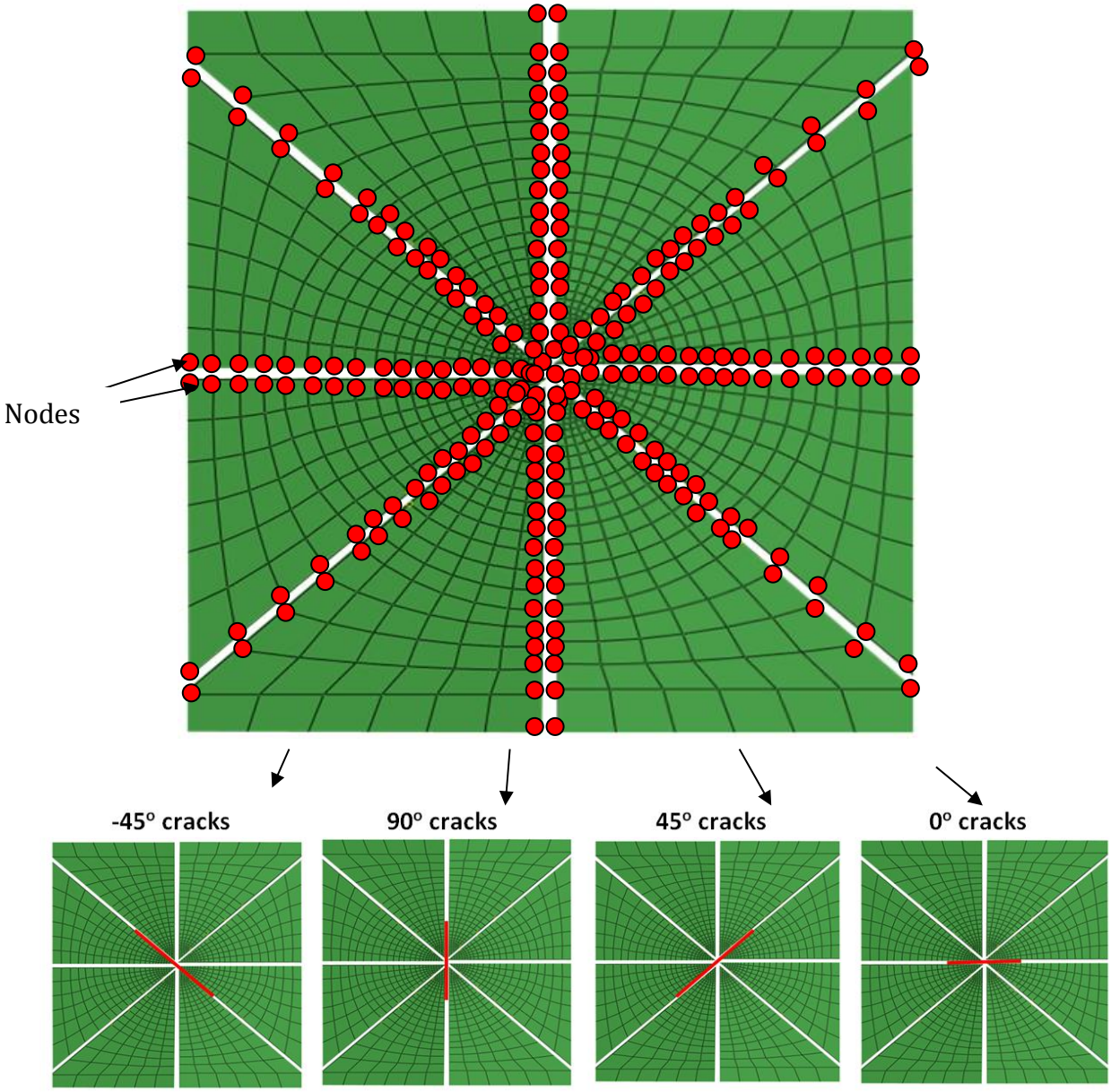

Figure 58(a) Pictorial representation of matrix crack modeling. The red lines represent the cracks, where the nodes are not merged.

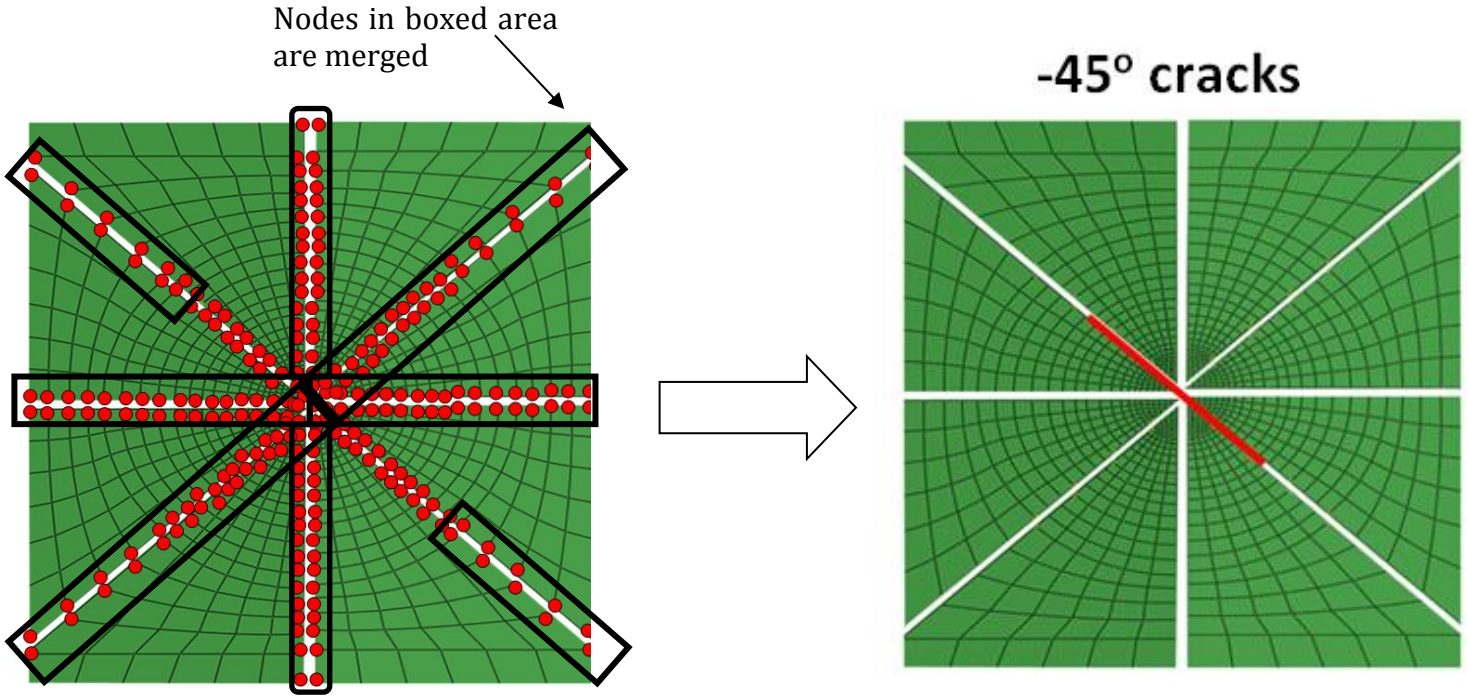

Figure 58(b) Detailed example of how a -45° crack is modeled in a composite ply

For example, in order to model a matrix crack oriented in the ±45^{o} direction, the mesh as seen in Figure 58 is employed. The composite ply is modeled using eight separate parts as seen in Figure 58. The coinciding nodes at which cracks do not exist are then merged.

The cross-sectional damage information in the y-z plane (Figure 59(a) and (b)) is carefully compared with the delamination profiles (Figure 30) obtained in the x-y plane to determine the matrix crack locations by superposing the two damage information together. The method in which this is done is presented in Figure 59(c). As seen in Figure 59(c), a mesh is drawn onto the delamination profile for Interfaces 3 and 4. Eight units, each 1mm in width, are drawn in the x-direction. This is done because the laminate is cut into multiple cross-sections of 1mm thickness to obtain the internal impact damage information. 25 units are drawn in the y-direction. This corresponds to the same 25 units that can be observed in the y-direction in the y-z cross sections. Any red lines cutting across layers 3 or 4 are then superposed into the mesh drawn in the delamination profile. The 8 units drawn in the x-direction and 25 units drawn in the y-direction would aid in locating the positions of the cracks.

Using this method of determining the location and length of the matrix cracks, the matrix cracks profile is included into the delamination profile in Figure 60. Large matrix cracks having the same size as the delaminations adjacent to the cracks are found to lie in the fiber direction. Other smaller matrix cracks of less than 1mm in length are found in various other places. In the modeling of the matrix cracks, only the large matrix cracks are modeled in Model E2. The direction of the crack modeled in each composite ply was the same as the direction of the crack observed from the experiment [3].

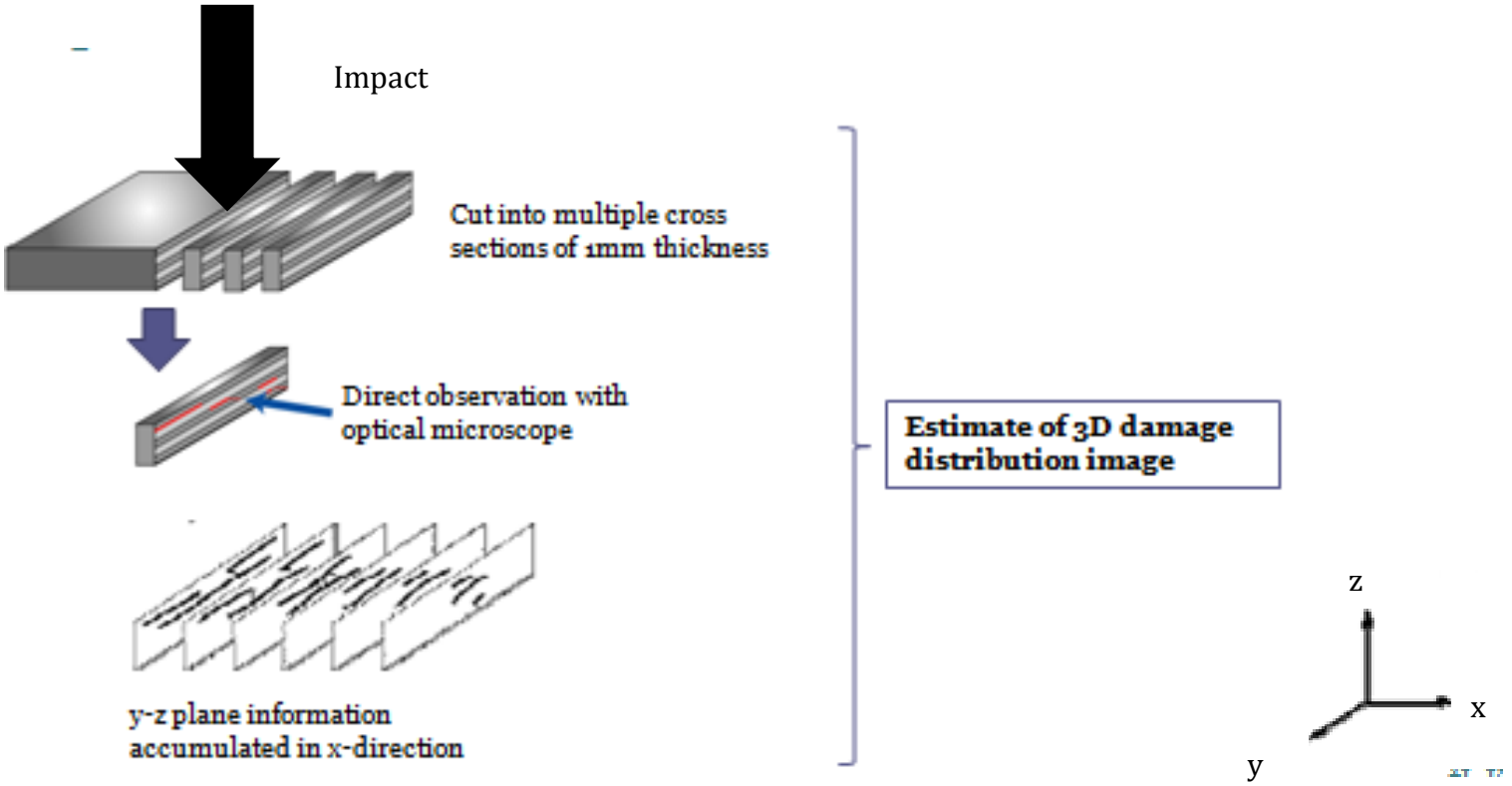

Figure 59(a) Methodology of characterization of impact damage in the y-z plane of the laminate, obtained from [3]

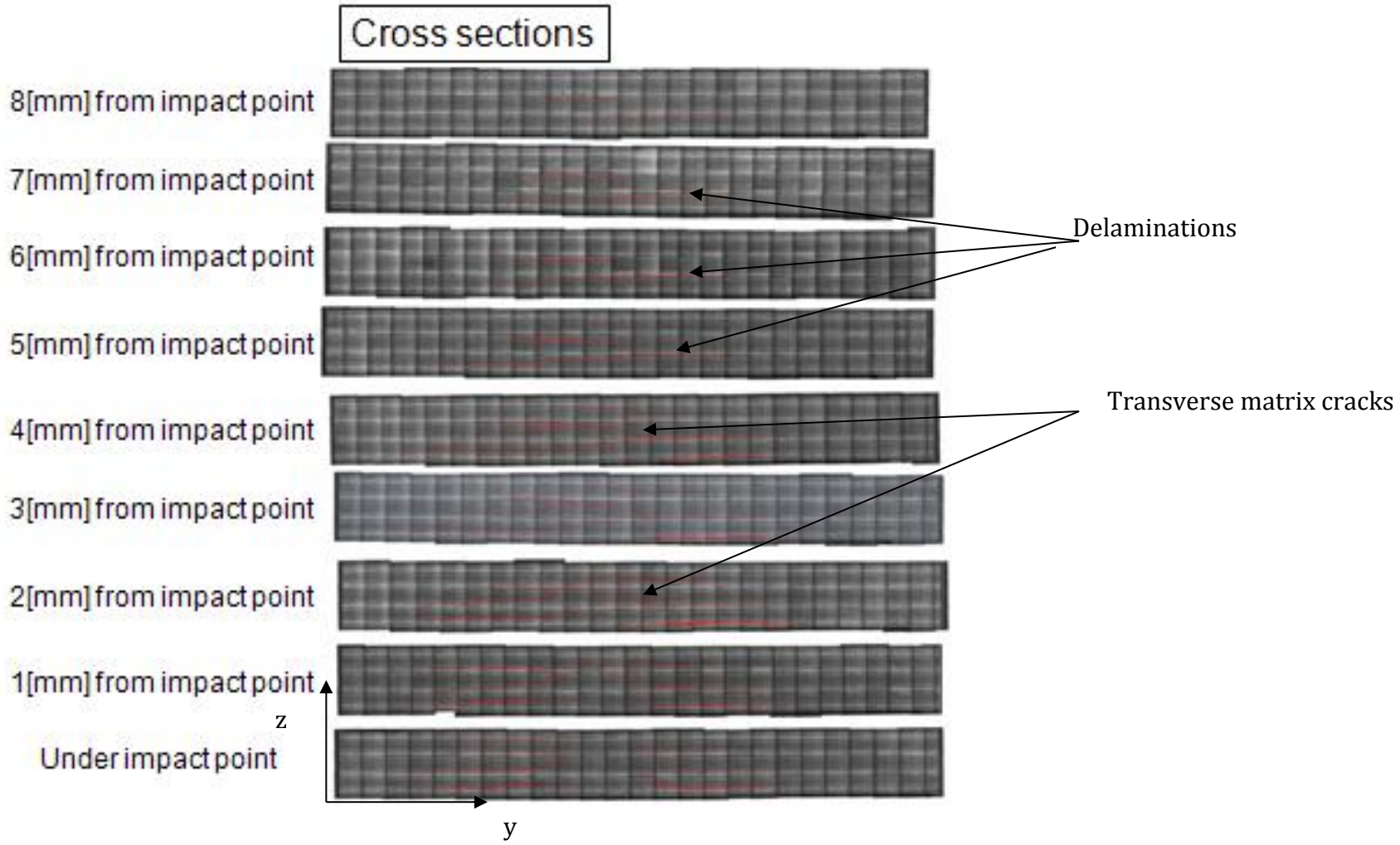

Figure 59(b) Experimental results obtained from [3]. Cross sections provide matrix cracks and delamination damage information

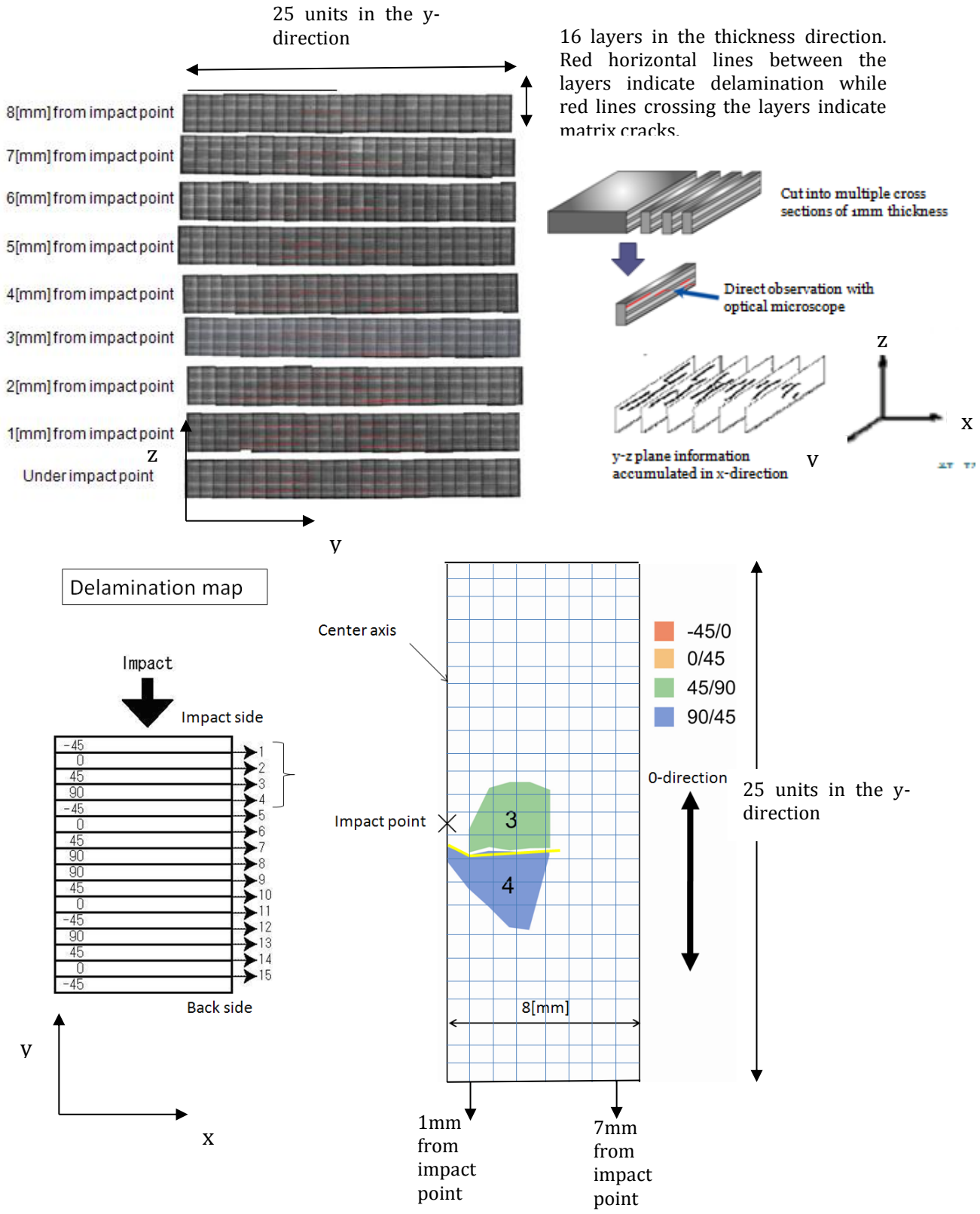

Figure 59(c) Pictorial representation of how the experimental data obtained from [3] is superimposed to determine the matrix crack locations

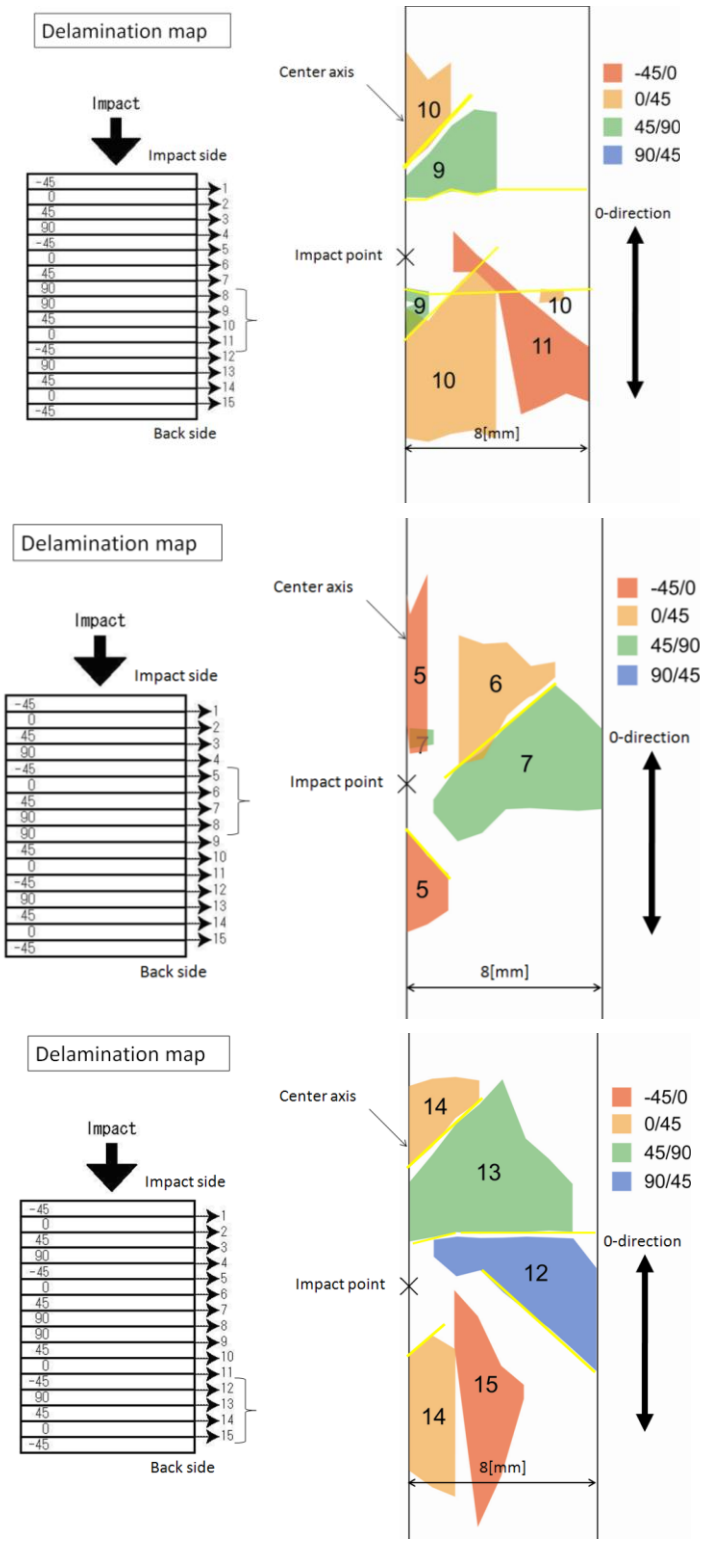

Figure 60 Representation of matrix cracks in yellow

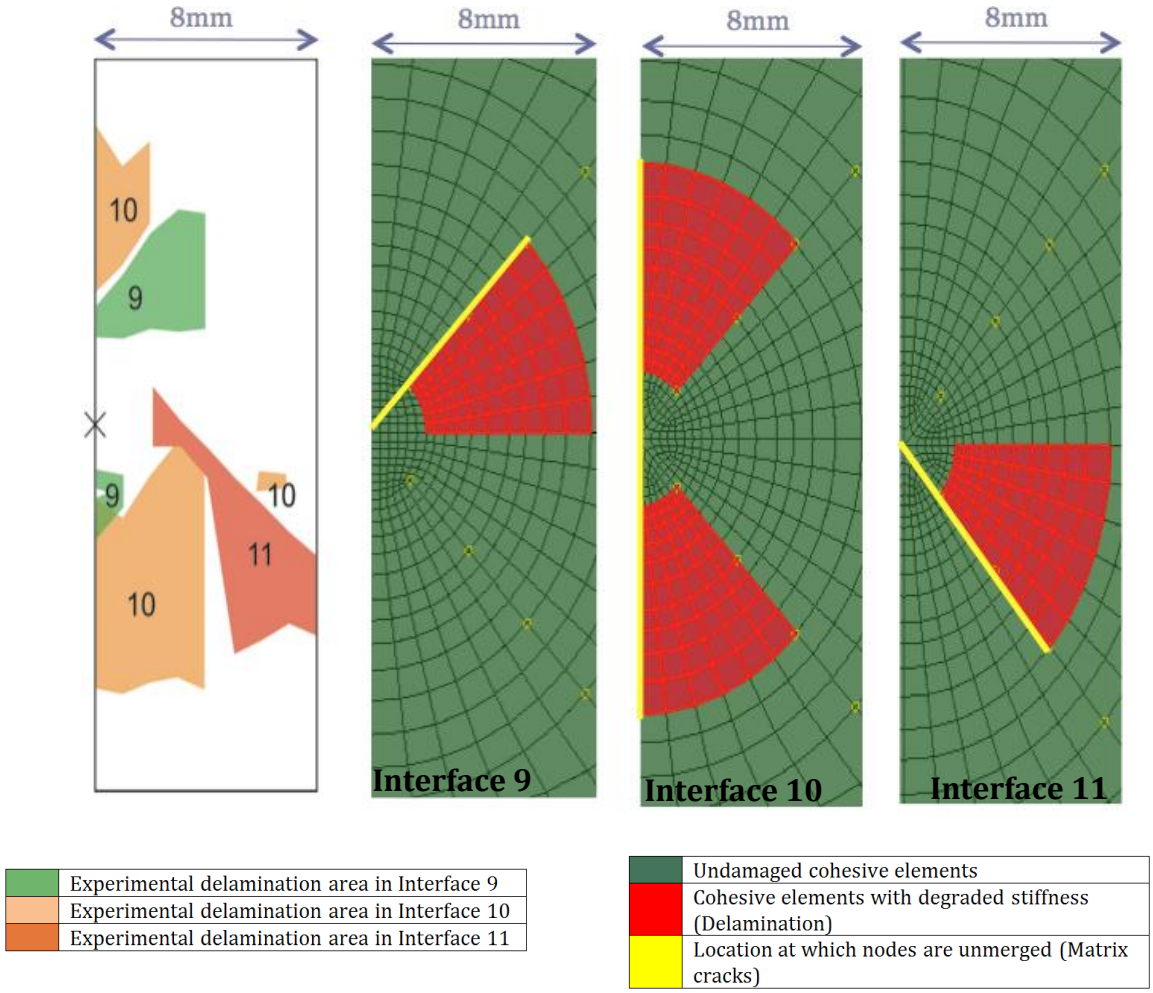

Figure 61 Example of the approximation of delamination (red) and matrix crack (yellow) size and position from experimental result into Model E2

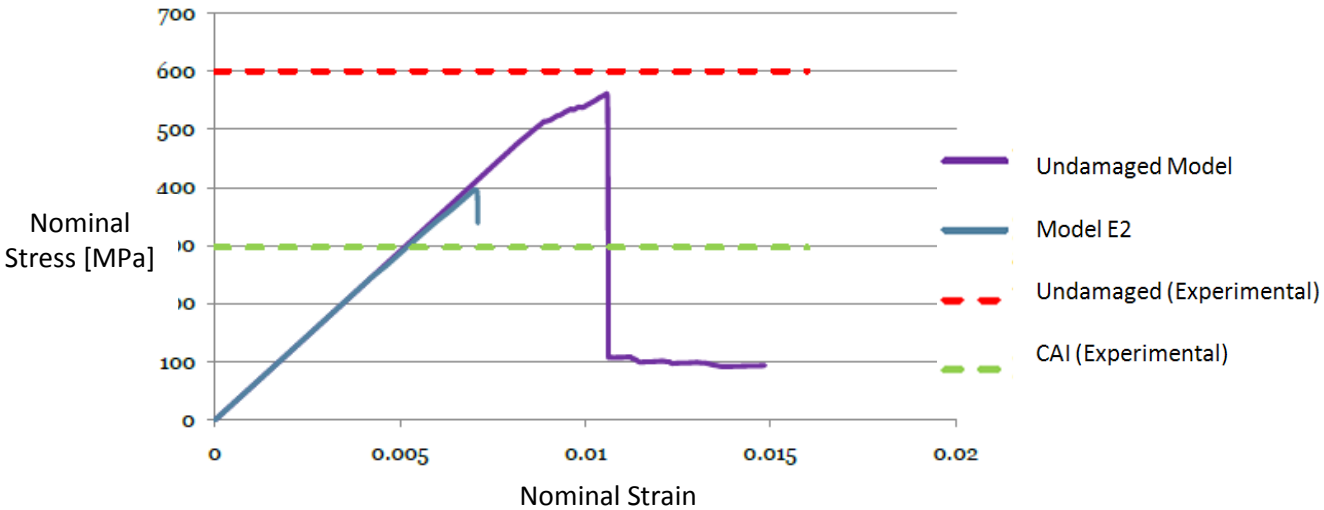

Figure 62 Stress-strain curve comparing experimental results to FE results

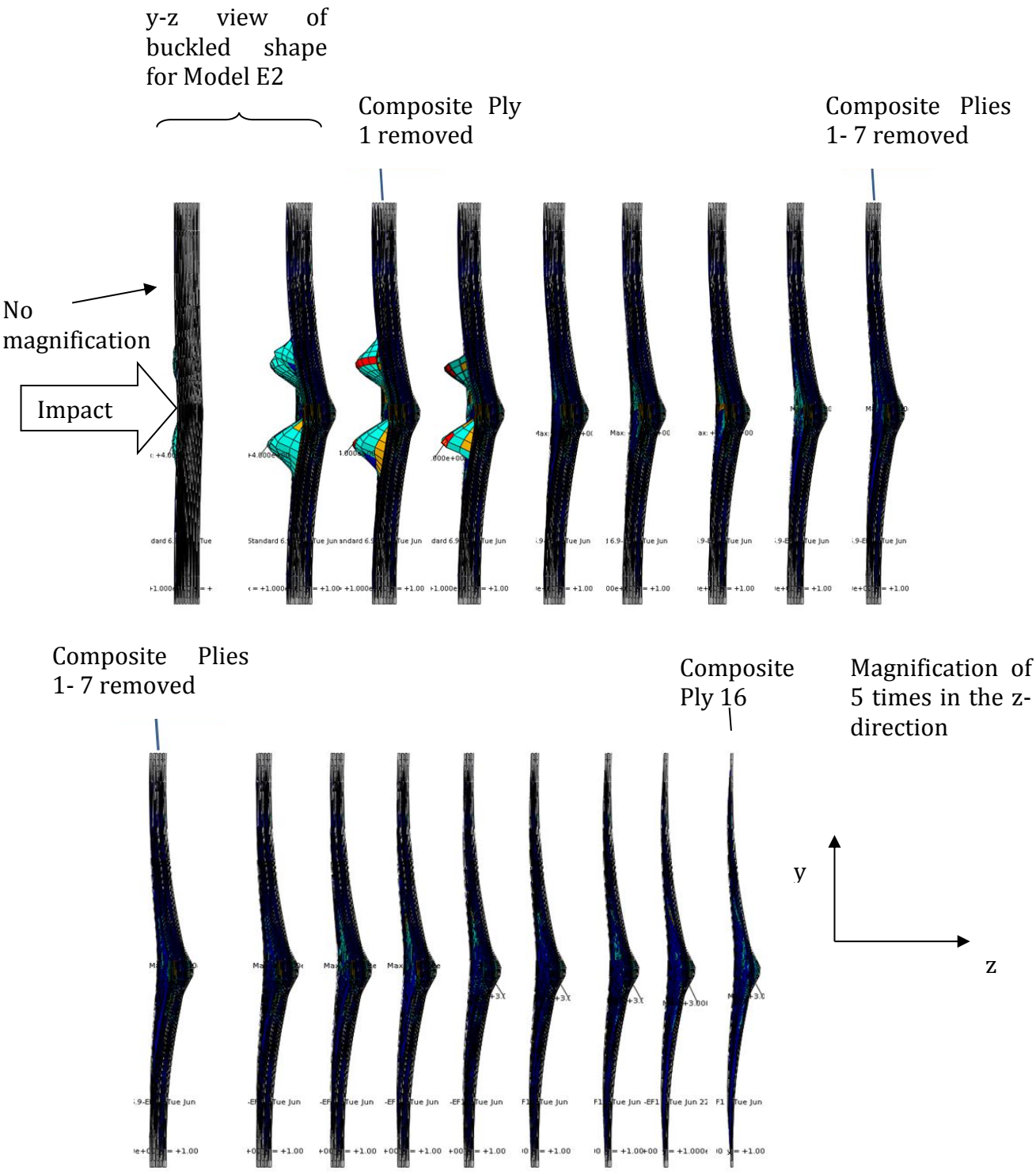

Figure 63 y-z view of buckled Model E2, with each composite ply removed successfully to reveal the buckled shape of each composite ply

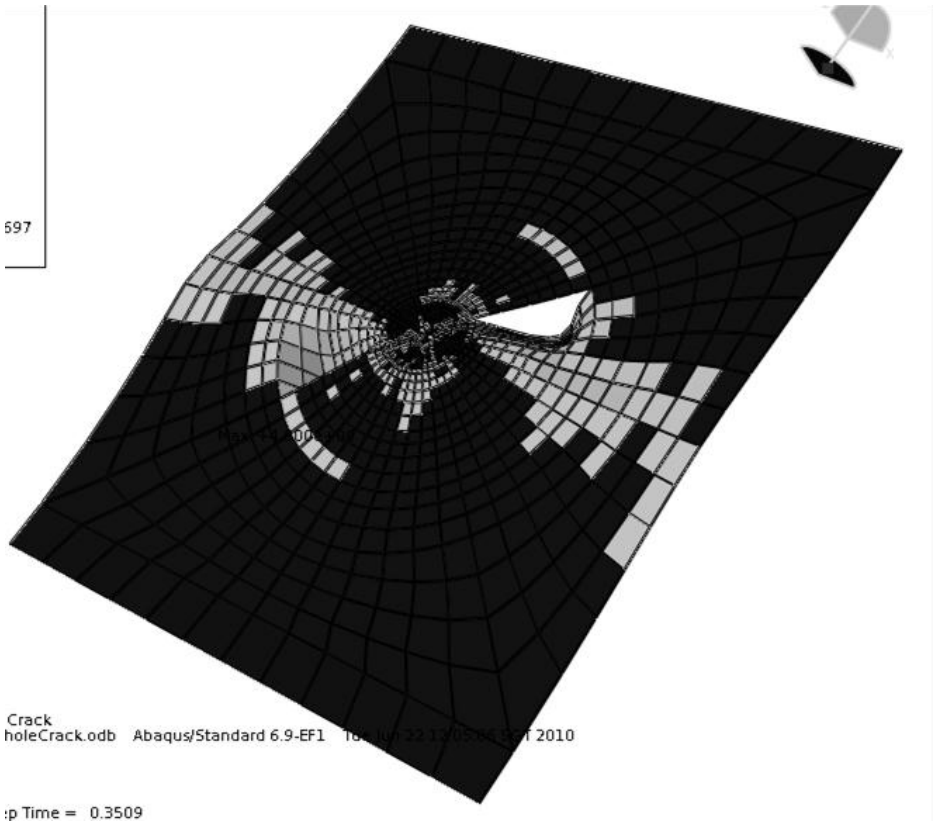

Figure 64 Composite Ply 3 of Model E2, showing that the 45^{o} crack pre-modeled allows for the lateral deflection of the ply under compression

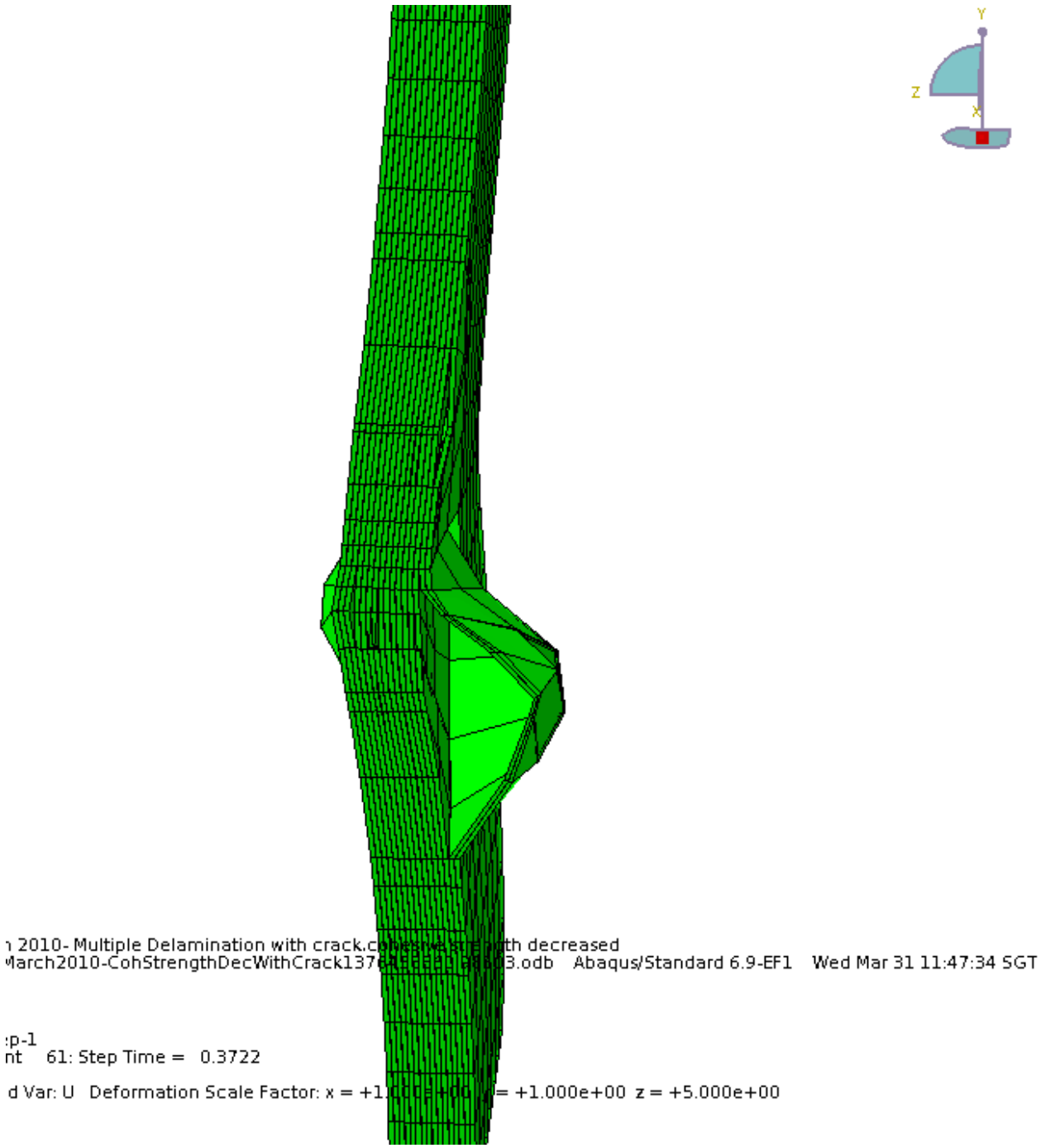

Figure 65 Cut view of the FE results from Model E2, showing that interpenetration of the composite plies does not occur

Figure 62 shows a comparison between the experimental results and the results predicted by the FE model. The nominal stress plotted in the y-axis is obtained by dividing the compressive load applied by the cross-sectional area over which the load is applied. While Model E1, which contains the exact delamination as Model E2, predicted a CAI strength that is identical to the compressive strength predicted by the undamaged model, Model E2 predicted a CAI strength of approximately 400MPa after cracks are included in the model. As stated previously, the buckled shape of Model E1 is identical to that of an undamaged model, as shown in Figure 55. The buckled shape of Model E2 is shown in Figure 63. As seen in Figure 63, composite plies 1, 2 and 3 (nearest the impact face) buckles the most extensively. Figure 64 shows that the 45^{o} matrix crack pre-modeled into Model E2 allows the lateral deflection of the composite ply to occur. Figure 65 shows a cut cross-sectional view of the buckled Model E2, proving that interpenetration of the composite plies does not occur.

This result confirms that modeling delaminations alone are insufficient for an accurate prediction of CAI strength; the modeling of matrix cracks is critical in obtaining a more accurate CAI strength prediction.

5.2 Parametric studies

A parametric study where the delamination sizes and crack lengths were varied was carried out. Three different crack lengths and delamination sizes were considered, and nine cases were tested in all. Figure 66 below summarizes the nine different cases of the parametric study.

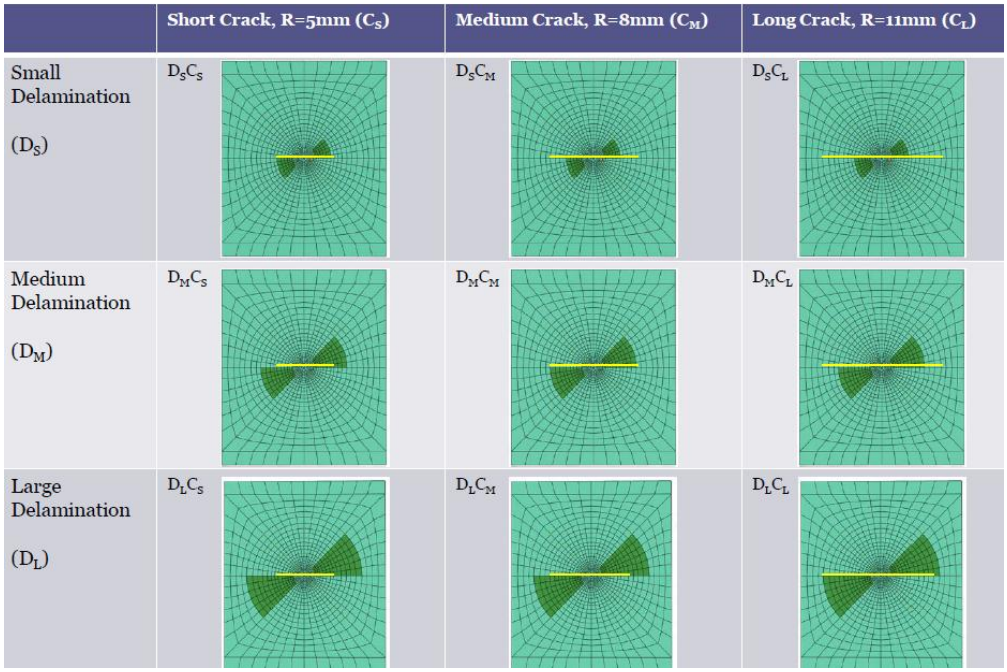

Figure 66 Summary of the nine cases considered in the parametric study

A delamination of radius 5mm is termed 'small delamination' (D_S), a delamination of radius 8mm is termed 'medium delamination' (D_M) and a delamination of radius 11mm is termed 'large delamination' (D_L). The medium delamination size roughly equals the size of the delamination observed in the experiment. Similarly, a crack of radius 5mm is termed 'small

crack (C_S)' and so on. The case with a delamination size and crack length of 8mm (D_MC_M) is the same model as Model E2 used in Section 5.1.4.

For the FE models containing a small delamination (Models D_SC_S, D_S,C_M and D_SC_L), a variation in crack length did not have any effect on the predicted CAI strength, which remained constant at 480MPa. When the delamination size was increased to a medium delamination of radius 8mm, the predicted CAI strength decreased in general. For the cases with medium delamination (Models D_MC_S, D_M,C_M and D_MC_L), Model D_MC_S predicted a CAI strength of 440MPa while Models D_M,C_M and D_MC_L predicted identical CAI strength of 400MPa. The FE models containing a large delamination predicted different CAI strengths for all three different crack lengths. The results are summarized in Table 7 below, together with Figure 67 and Figure 68.

	Short Crack, R=5mm (C_S)	Medium Crack, R=8mm (C_M)	Long Crack, R=11mm (C_L)
Small Delamination (D_S)	~480MPa	~480MPa	~480MPa
Medium Delamination (D_M)	~440MPa	~400MPa	~400MPa
Large Delamination (D_L)	~420MPa	~320MPa	~300MPa

Table 7 Summary of CAI predicted in the parametric study

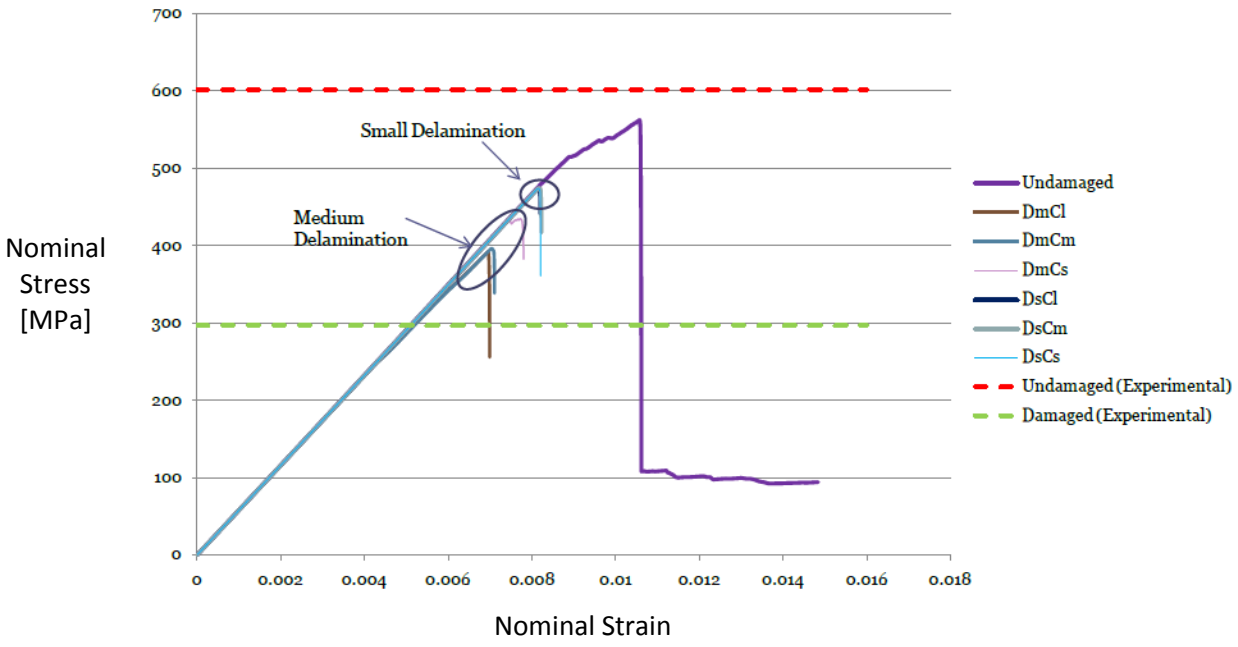

Figure 67 Stress- strain curve from parametric study, showing the CAI strengths for models with medium and small delaminations

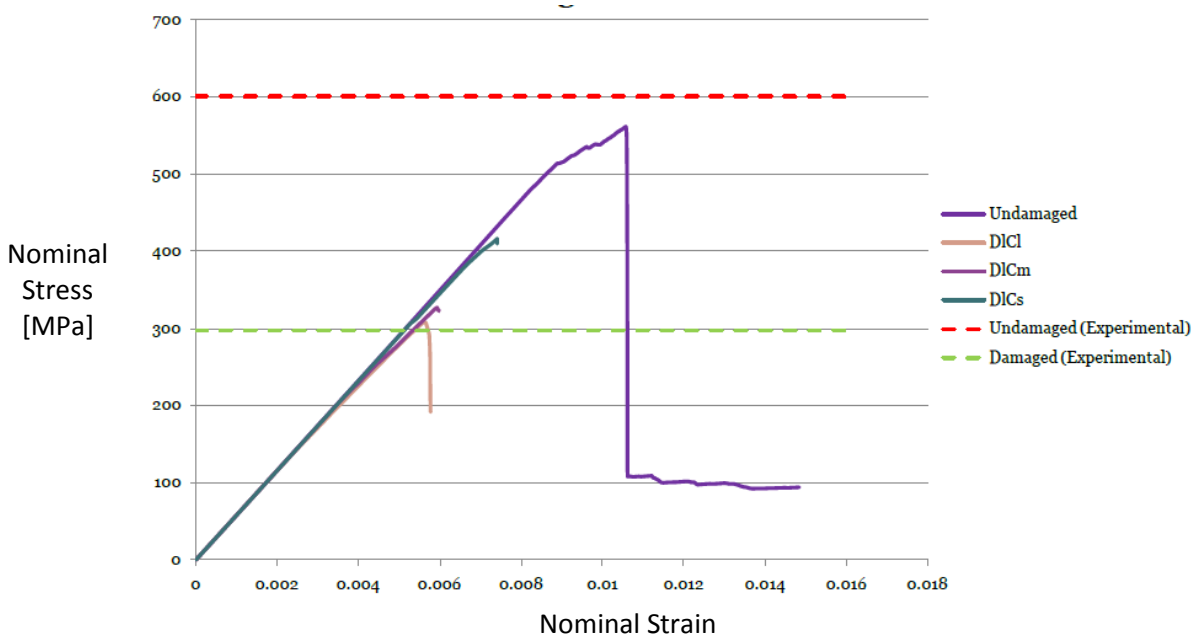

Figure 68 Stress-strain curve from parametric study, showing the CAI strengths for models with large delaminations

It can be concluded from the results that a combination of the sizes of both the delamination area and the matrix crack modeled in the FE model affects the prediction of CAI strength. The modeling of matrix cracks in the CAI strength prediction models is crucial because the cracks allow for the lateral displacement of the delaminated areas, permitting local buckling to take place. As demonstrated by the results, the cracks make a difference only up to a length identical to the size of the delamination. Any extension in crack length beyond the delaminated area will have no effect on the CAI strength predicted because in the undelaminated regions, there is no need for any allowance of lateral displacements of the individual plies.

5.3 Conclusion

Studies performed in this chapter have demonstrated the effect of the modeling complexity of the impact damage in the CAI strength prediction model on the accuracy of CAI strength prediction. It has been shown that the CAI strength obtained from FE models with multiple delaminations alone do not compare well with the experimental results, while models with multiple delaminations and matrix cracks provide a better prediction. Hence, the widespread acceptance that delamination is the major damage mechanism which causes the compressive strength of a composite laminate to decrease might be flawed. The following lists the main conclusions that can be drawn from this chapter:

1. The idealization of delamination shape and sizes to be uniform throughout the interfaces in FE models for CAI strength prediction allows for the lateral deflection of the laminate under compression. In laminates containing delaminations of the same shape and size, lateral deflection at the delaminated areas is not inhibited, hence even when matrix cracks are not modelled, a CAI strength that is lower than the compressive strength of the undamaged material can be predicted. However, such an idealization of delamination shapes and sizes is not an accurate representation of a real-case scenario.
2. The modeling of non-uniform delaminations representative of experimental impact-induced delaminations alone would lead to the prediction of an overly high CAI strength.
3. The modelling of matrix cracks is critical for the accurate prediction of the CAI strength of an impact damaged laminate if the delaminations modelled are to be realistic (non-uniform delaminations). This is because the matrix cracks would allow for the lateral deflection of the laminate under compression. It can also be concluded that matrix

cracks formed due to an impact event plays an important role in reducing the CAI strength of a composite plate.

4. From the parametric studies performed, it has been found that while matrix cracks play an important role in reducing the CAI strength of a composite plate, the delamination area is the limiting factor for crack length variation to have an effect on the CAI strength. Any extension in crack length beyond the delaminated area will have no effect on the CAI strength because in the undelaminated regions, there is no need for any allowance of lateral displacements of the individual plies. It can hence be concluded that matrix cracks play a crucial role in reducing the CAI strength of a composite plate only when the cracks lie within the delaminated area of the composite plate.

Chapter 6

INTEGRATED FE ANALYSIS FROM LOW-VELOCITY IMPACT TO CAI STRENGTH PREDICTION

This chapter presents the third and final stage of this research, which is the integrated approach in which the FE simulation for low-velocity impact is integrated with the FE simulation for the prediction of CAI strength. Such an integrated approach would allow for the direct prediction of CAI strength from the same impact damaged model without having to pre-include an idealized damage pattern into the CAI strength prediction model.

The purpose of this stage of the research is to enable the virtual testing of composites to be performed more efficiently. By having an integrated approach, the entire process, from impact damage to the residual CAI strength prediction, can ideally be captured in one seamless computational analysis procedure. Typically, the analysis of low-velocity impact and the residual CAI strength prediction is performed in two separate steps, involving cutting the impact damaged specimens to derive the impact damage profile and then idealizing the impact damage in the subsequent FE model for CAI strength prediction.

Chapter 5 established the importance of modeling matrix cracks in a CAI strength prediction model in addition to the modeling of the multiple delaminations induced by low-velocity impact. However, modeling the impact induced damage into the CAI strength prediction model can be a time-consuming and challenging process. This is due to the fact that low-velocity impact damage is rather complex, with different shapes and sizes of delaminations occurring at different interfaces, and different sizes and

directions of matrix cracks occurring in each ply. Furthermore, low-velocity impact damage is influenced by different parameters such as the ply layup, the thickness of the plies and the boundary conditions etc. A change in any parameter would lead to a different impact damage pattern and subsequently a different CAI strength.

Chapter 4 has sought to prove the versatility of the impact FE model created in this research in predicting low-velocity impact damage to an acceptable level of accuracy for several different impact scenarios. This impact FE model can hence be used in this integrated FE analysis for the prediction of CAI strength.

6.1 Description of integrated FE analysis

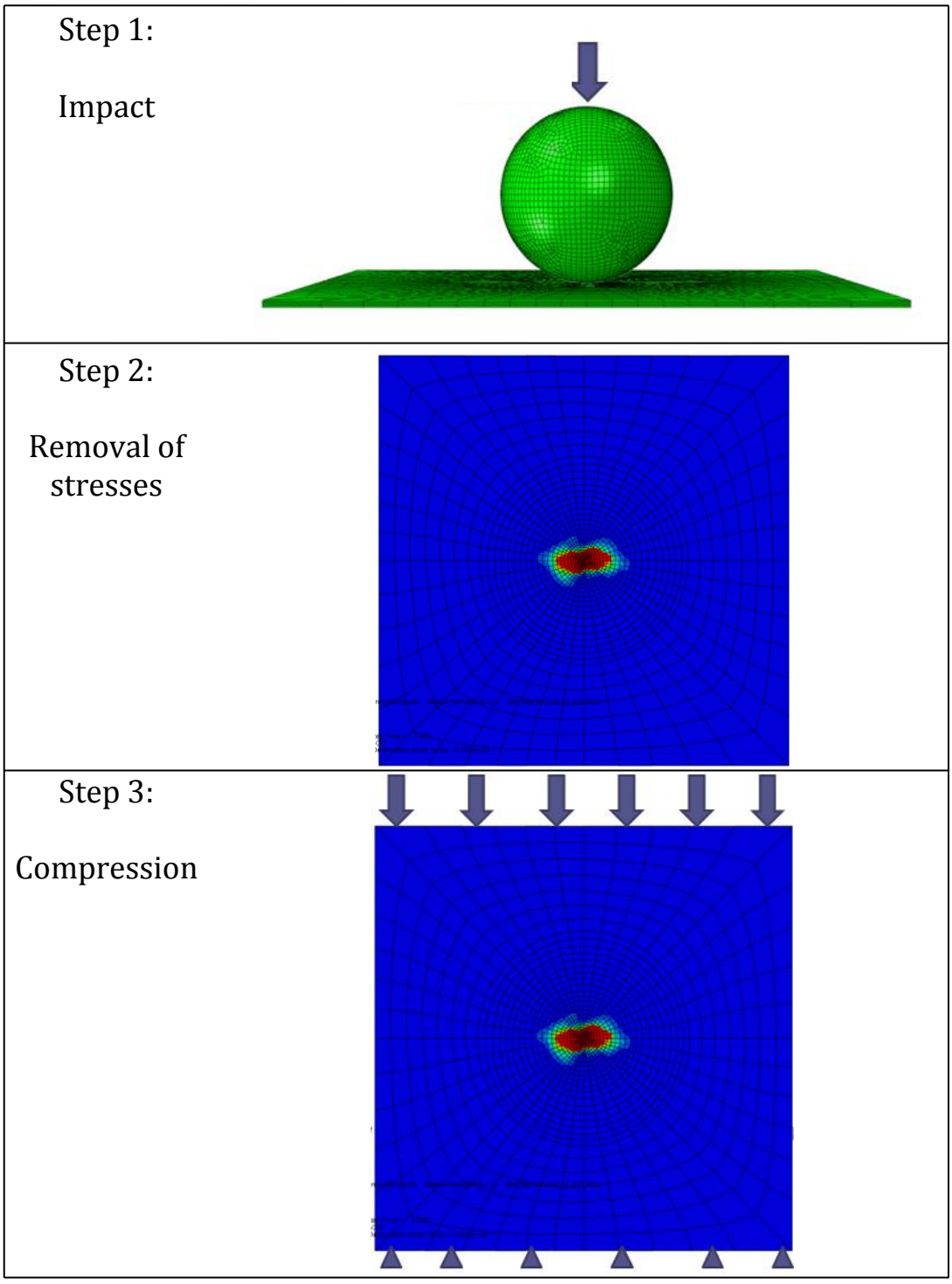

Figure 69 Steps in the integrated FE analysis

The FE model used for the integrated FE analysis simulates the laminate used in the experiment of Kimpara et al. [3], with a layup of $[-45^o/90^o/45^o/0^o]_{2s}$. The experiment was described in Section 4.1.2.

In the first step of the integrated FE analysis, low-velocity impact is simulated. The FE model used for the simulation of low-velocity impact is identical to that described in Section 4.1.2, and the results obtained by the FE model is presented in Figure 31. Restart output requests for the impact FE analysis has to be fielded in this first step of the integrated FE analysis. This restart information would be required in the import of damage information from the impact model to the CAI strength prediction model. In this model, restart information is requested every 10 increments in the FE analysis. A force-displacement curve for the impacted composite laminate is then plotted, as shown in Figure 70. The force plotted in the y-axis is the force exerted by the impactor on the composite laminate in the thickness direction. This force is caused by the displacement prescribed to the impactor, simulating quasi-static impact. As described in Section 3.2, the impactor is modeled as a rigid body with infinite stiffness, and is constrained to move only in the z-direction, or the thickness direction of the laminate. The impact process is modeled by prescribing a displacement instead of a velocity to the impactor since low-velocity impact can be considered a quasi-static process [12]. The displacement plotted in the x-axis of the force-displacement curve (Figure 70) is the z-direction displacement of the impactor, which is equivalent to the displacement of the point on the laminate that is in direct contact with the impactor. The area under the force-displacement curve would be equivalent to the impact energy.

The equation of the force-displacement curve plotted can be obtained using Microsoft Excel, as shown in Figure 70. A simple Matlab code written for this research is then used to determine the displacement at a particular impact energy of interest. However, in this impact case, the maximum impact

energy attained by the FE model was 1.2J, which corresponded with an impactor displacement of 1.42mm. In other words, at a displacement of 1.42mm along the x-axis of the force-displacement curve presented in Figure 70, the area under the curve is equivalent 1.2J. The reason that maximum impact energy attained by the FE model is only 1.2J is expounded in Section 6.2. The post-impact damage state at this particular displacement of 1.42mm is then obtained from the impact FE simulation of the laminate with a stacking sequence of $[-45^o/90^o/45^o/0^o]_{2s}$. The impact damage obtained due to the impact energy of 1.2J has been presented in Figure 31.

During a low-velocity impact event, the impactor velocity at the point of impact is gradually reduced as its movement is opposed by the deforming composite laminate. This deceleration is associated with a reaction force on the impactor. At this point of time, stresses are induced in the composite laminate. The kinetic energy of the impactor is transferred to the laminate and stored temporarily as elastic strain energy. If the local strength of the material is reached, part of this energy would be dissipated through irreversible impact damage. After the impactor velocity reaches zero, the major part of the accumulated elastic strain energy is then transferred back to the impactor which accelerates away from the specimen. However, since low-velocity impact is simulated as a quasi-static process by prescribing a displacement instead of a velocity to the impactor, the process in which the impactor accelerates away from the laminate is not captured in this FE simulation. This process is simulated in the second step of this integrated FE analysis by removing the stresses in the damaged model, retaining only the damage information such as the matrix cracks, delaminations and fiber failure. The laminate thus returns to its original position.

In the final step of the integrated FE analysis, the damaged model after stress release was compressed to obtain the resultant CAI strength.

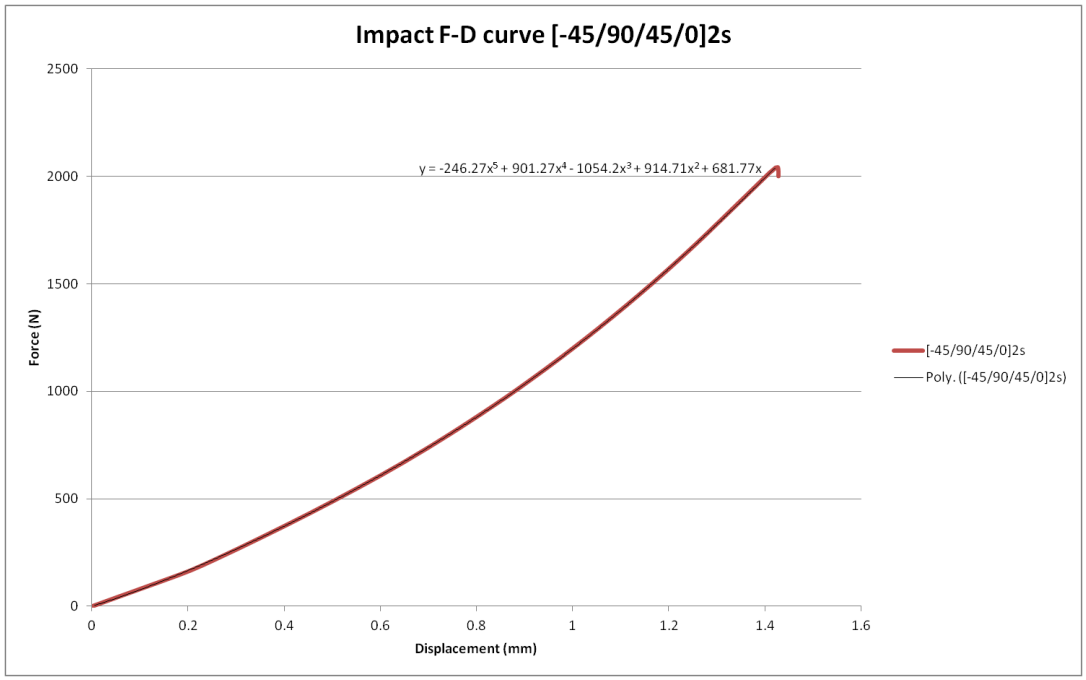

Figure 70 Force-displacement curve for impact on a $[-45/90/45/0]_{2s}$ laminate

6.2 Results and discussions

As seen in Figure 71, the CAI strength predicted by the integrated FE analysis is approximately 430MPa. This is almost 40% above the experimental value. An obvious reason for this over prediction of CAI strength value by the integrated model is that the integrated model was prescribed an energy of 1.2J, while the experimental impact energy was 6J. In all the impact simulations run in this current research, the area under the force-displacement curve would correspond to an impact energy of approximately 0.4J/mm. Herein lies the shortfall of the current impact FE model. In this current impact model, the simulation will not converge once a drop in force is experienced, as shown in the impact force-displacement curve in Figure 70. The divergence is due to an out-of-plane hourglassing effect, in which the elements distort in a manner where the strains calculated at all integration points are zero, leading to an uncontrolled distortion of the mesh without stresses to resist the distortion. This problem could be solved by using solid elements instead of continuum shell elements. However, impact of a thin laminate would involve high levels of bending, and to accurately model bending dominated loading of a model meshed with solid elements, more than three elements in the thickness direction has to be employed to overcome the shear-locking effect that solid elements display under bending. The extensive number of solid elements would increase computational costs significantly. An FE model of a laminate of the same layup of $[-45^{o}/90^{o}/45^{o}/0^{o}]_{2s,}$ was built using 3 solid elements per ply in the thickness direction. However, after two weeks of runtime, the impact simulation only attained an impactor displacement of 0.5mm. The FE model meshed using solid elements was hence pursued no further as the runtime was unacceptably long.

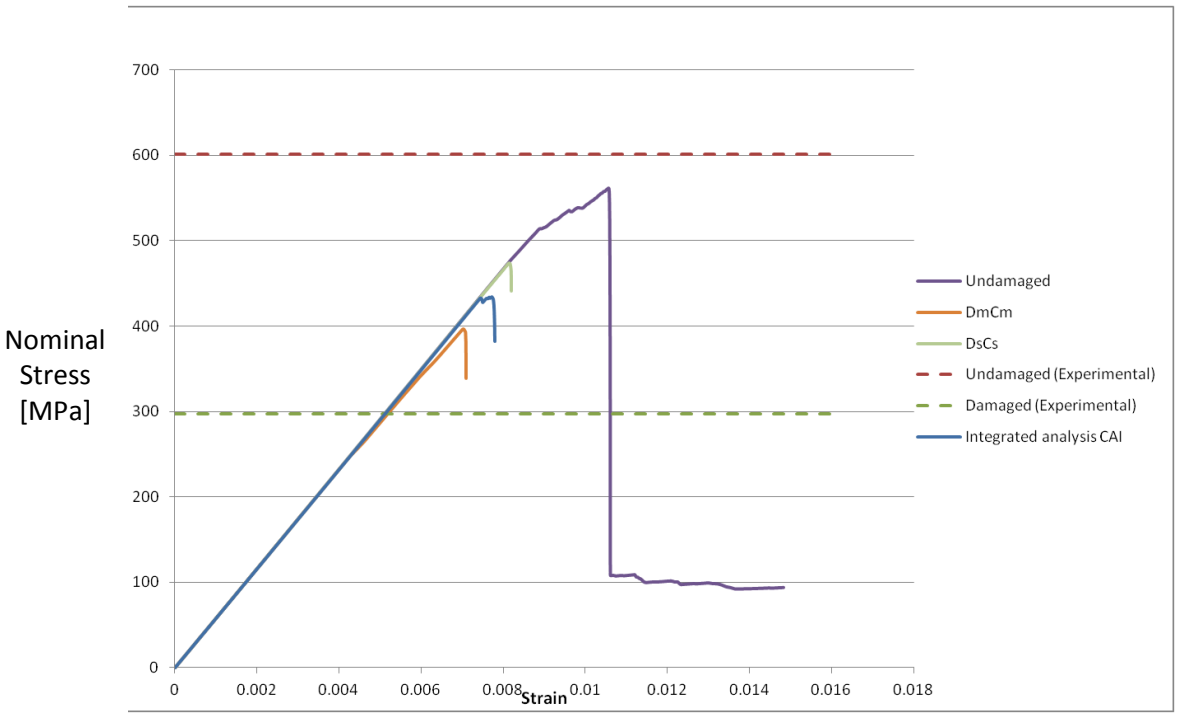

Figure 71 Stress-strain curve comparing the CAI strength predicted using the integrated FE approach with that predicted using the CAI strength prediction model with pre-modeled delaminations and cracks

As reported in Figure 71, the compressive strength of an undamaged laminate predicted by the FE model is approximately 570MPa, an underestimation of close to 5% as compared to the experimental value. A possible cause of the underestimation might be the way damage is modeled in the FE model, described in Section 3.1.1.2. Once an element is deemed to have completely failed, the material properties are degraded to zero. However, in a real-case scenario, a failed material would still be able to withstand and transfer loads in compression instead of having totally degraded material properties.

It has been reported in various studies regarding thin ply composites that reducing the thickness of the composite ply would improve the impact damage resistance properties of the laminates and lead to an increase in the CAI strength. In [63], Saito et al. investigated on the effect of ply-thickness on impact damage morphology in CFRP laminates. The laminates used were of layups $[45^o/0^o/-45^o/90^o]_{3s}$ for the laminates with a standard thickness of 0.147mm per ply, and $[45^o/0^o/-45^o/90^o]_{12s}$ for the thin ply laminates, of 0.038mm per ply. They reported an increase in CAI strength of 23% for the thin-ply laminates. In [169], Yokozeki et al. studied the strength and damage resistance properties of thin-ply composite laminates under impact. The thin-ply prepregs used in this study was approximately half the thickness of that of the prepregs with standard thickness. The laminate layups used were $[45^o/0^o/-45^o/90^o]_{2s}$ for the standard laminates, and $[45^o/0^o/-45^o/90^o]_{4s}$ for the thin-ply laminates. An eight percent increase in CAI strength in the thin-ply laminate was reported.

In order to check if the integrated FE model is capable of predicting an increase in CAI strength of a thin-ply laminate, the CAI strength of two other composite layups were predicted using the integrated FE model. The first had a layup of $[0^o/45^o/90^o/-45^o]_s$ (Model A in Section 4.3), with a thickness of 0.125mm per ply and a total ply thickness of 1.07mm inclusive of cohesive ply thicknesses. The second had a layup of $[0^o/45^o/90^o/-45^o]_{2s}$ (Model B in Section 4.3) with a ply thickness of 0.07mm, more than half that of the first model. Both models were subject to an impact energy of 0.42J. The CAI strength predicted for the first model was approximately 240MPa, while that predicted for the thin-ply model was approximately 270MPa. The thin-ply Model, Model B, predicted a CAI strength that is 12.5% more than that predicted by Model A. This is in closer agreement to the results reported by Yokozeki et al [169], who reported an 8% increase in CAI strength of thin ply laminates as compared to the CAI strength of standard ply laminates. In their

study, the thin ply laminates used were approximately half the thickness of standard ply laminates.

To the author's knowledge, the only report found in literature on the simulation of impact tests followed by CAI tests consecutively was written by González et al. in their paper "Simulation of drop-weight impact and compression after impact tests on composite laminates" [175] published in 2012. In this paper, the researchers presented their finite element simulations of two standardized and sequential tests, the impact and compression after impact tests, performed on composite laminates. The main differences between their work and the current FE model presented are summarized as follows:

- Impact was assumed to be a quasi-static event in the FE model used in this research, which could be modelled using Abaqus/Standard. The impact event was simulated by prescribing a displacement to the impactor. However, the impact event was modelled using Abaqus/Explicit in González et al.'s FE model, and the impactor was assigned an initial velocity instead of a displacement. In this research, the impact event was modeled as a quasi-static process using Abaqus/Standard instead of using Abaqus/Explicit in order to reduce the runtime of the simulations. Generally, the use of Abaqus/Explicit is computationally more expensive than Abaqus/Standard.
- In González et al.'s FE model, a regular mesh with identical elements was used to model the laminate around the locus of impact. The researchers recognized the fact that the use of in-plane structured meshes oriented with the fiber direction poses clear advantages, but has chosen not to use meshes oriented with the fiber direction in order to achieve a well-balanced compromise of required and available computer resources. In the FE model used in this research, the biased mesh used in which the elements were arranged in a

circular manner outward (Figure 18) was structured in such a way that the edges of the elements correspond to the fiber orientation for improved prediction of the matrix crack paths. A biased mesh was chosen such that the elements near the point of impact are smaller in size compared to the elements at the edges of the laminate. Such a mesh serves to save on the computation runtime.

- The interlaminar damage model used for the prediction of delamination initiation and growth is the same in both FE models, where the constitutive law enforces a linear softening relationship between the traction and separation at the interface. The constitutive law is based on the B-K criterion described in Section 3.1.1.2. However, the intralaminar damage model used in González et al.'s FE model is superior to that used in the FE model of this research because González et al.'s model accounts for crack-closure effect under load reversal conditions. In their FE model, damage caused by tension loads is tracked separately from damage caused by compression loads through the use of different degradation factors. However, their paper does not detail how the crack closure effects are being accounted for.
- Impact and CAI test simulations carried out by González et al. were performed on 32-ply laminates. The simulations were performed using multiple processors on separate computers, in which Abaqus/Explicit automatically breaks the FE model into separate domains and assigns each domain to a processor such that analysis is carried out independently in each domain. At the end of the analysis, the individual files are merged together automatically. Each simulation is run parallelly in a total of six linked computers, each with 8GB RAM and four processors of 2.4GHz. The total runtime analysis of the impact and CAI tests is reported to range between twelve to fifteen days. The FE simulations reported in this thesis are

run using a single computer with 48GB RAM and 12 processors of 3.46GHz. The total runtime for a 16-ply laminate was an average of about two days. The significantly longer simulation runtime for González et al.'s model was due mainly to the fact that Abaqus/Explicit, in which very small time increments of order 1e-9s are required, was used to run the simulation. However a low-velocity impact event is considered long in time, of the order 5e-3s. Hence, a large amount of increments are required before the simulation is complete. The advantage of using Abaqus/Explicit in González et al.'s model is that it enables the researchers to study the impact event in great detail, such as the comparison of numerical and experimental impact force versus time curve. This model also allows for the study of the energy dissipated in relation to each different damage mode occurring in the laminate due to an impact event, because in this model, the researchers could split the entire energy of the system into different energy components such that the role each damage mode plays at any time of the impact event can be identified. Such studies would enable the researchers to have a better understanding of the behaviour of a composite laminate under impact. While the FE model devised in this current research is incapable of studying the impact event to such details, an advantage of the FE model used in this thesis over the FE model devised by González et al. is the short simulation run-time. To this effect, these two integrated FE models could complement each other. When the priority of the researcher is to better understand the damage process occurring during an impact event, González et al.'s integrated FE model could be used; when the priority of the researcher is to predict the CAI strength value due to an impact event, the FE model devised in this research could be used.

6.3 Conclusions

In Chapter 6, an integrated approach which integrates the FE simulation for low-velocity impact with the FE simulation for the prediction of CAI strength was presented. The feasibility of capturing the entire process of low-velocity impact damage and the residual CAI strength prediction in one seamless computational analysis procedure without having to pre-include an idealized damage pattern into the CAI strength prediction model has been proven.

The following points summarize the key features of the integrated model:

- The integrated FE analysis consists of three steps. In the first step, low-velocity impact is simulated. Force and displacement data is extracted from this step, and a force-displacement curve for the impacted composite laminate is plotted.
- The equation of the force-displacement curve is obtained using Microsoft Excel. The area under the force-displacement curve is equivalent to the impact energy, and a Matlab code is used to determine the displacement at a particular impact energy of interest.
- The second step of the integrated FE analysis involves the removal of stresses in the damaged model, retaining only the damage information. This step accounts for the acceleration of the impactor away from the laminate that is not captured in this quasi-static FE simulation.
- The final step of the integrated FE analysis simulates the compression of the impact-damaged laminate, predicting the resultant CAI strength.

While the feasibility of capturing the entire process of low-velocity impact to CAI strength prediction in one seamless computational analysis

procedure without having to pre-include an idealized damage pattern into the CAI strength prediction model has been proven, this integrated FE model is limited by a shortfall in the current impact FE model. Currently, the integrated FE model can only be applied in low-velocity impact cases with impact energy up to 0.4J/mm. To improve on the integrated FE model, solid elements with more than three elements in the thickness direction have to be employed. However solid elements were not used in this study because of the large computational demands.

Chapter 7

CONCLUSIONS AND RECOMMENDATIONS FOR FUTURE WORK

A novel integrated finite element analysis approach for the prediction of compression after impact (CAI) strength of CFRP laminates has been presented in this thesis. In this approach, an impact FE analysis is first performed to predict the progressive impact damage incurred in a CFRP laminate due to low-velocity impact. Subsequently, the same impact damaged FE model is compressed to obtain the resultant CAI strength value.

Running simulations of impact followed by simulations of CAI tests consecutively would lead to a more realistic prediction of the CAI strength, as compared to the CAI strength predicted from models with idealistic delamination patterns pre-modeled into the CAI strength prediction model. A reliable FE model for the consecutive simulation of impact damage due to low-velocity impact and CAI tests is critical and of great interest because it would be a less expensive avenue for designers as opposed to experimental tests.

This approach is still in its infancy stage, and with further research, it has the potential to be developed into a CAI strength prediction tool that allows for the user to obtain a predicted CAI strength value by specifying the impact energy, together with the composite laminate parameters and boundary conditions.

7.1 Conclusions

The following conclusions can be drawn from this research:

- Stage I of this research involves the development of an impact FE model with the capability of predicting progressive impact damage to an acceptable accuracy. Even though FE prediction of impact damage is a topic that has received widespread attention and research, developing an FE model for impact is mandatory in this current research in order for the integrated FE analysis approach to be implemented.
- Chapter 3 has shown that a hybrid maximum-stress and Tsai-Wu failure criterion, or a Hashin failure criterion works well for the prediction of in-plane damage initiation. The cohesive elements available in Abaqus, which predict damage initiation using a quadratic failure criterion, are used in the modeling of delaminations. It has been shown that a linear softening law has to be implemented in the modeling of damage progression in order for the FE model to provide an accurate impact damage prediction.
- A mesh composed of smaller elements around the point of impact and larger elements towards the edge of the model has been proven to be computationally more efficient than a mesh composed of uniform elements.
- In chapter 4, the impact FE model developed has been verified to be capable of predicting impact damage to an acceptable level of accuracy via a qualitative comparison of the impact damage prediction to experimental impact damage reported in literature. Furthermore the versatility of the impact FE model in predicting low-velocity impact damage to an acceptable accuracy for several different laminate parameters has also been proven. This is important because an impact FE model capable of predicting impact

damage accurately is a prerequisite to an accurate prediction of CAI strength in this integrated FE approach proposed.

- Chapter 5 concludes that the modeling of matrix cracks is critical for the accurate prediction of the CAI strength of an impact damaged laminate, if the delaminations modeled are to be representative of impact damage induced delaminations that occur in real case scenarios. It has also been established in this chapter that the matrix cracks formed due to an impact event plays a crucial role in reducing the CAI strength of a composite laminate; delamination alone is not the major damage mechanism that reduces the compressive strength of a composite laminate.
- Parametric studies performed in Chapter 5 has shown that while matrix cracks play an important role in reducing the CAI strength of a composite laminate, the delamination area is the limiting factor for matrix crack length variation to have an effect on the CAI strength. Any extension in crack length beyond the delaminated area will have no effect on the CAI strength. It can hence be concluded that matrix cracks play a crucial role in reducing the CAI strength of a composite plate only when the cracks lie within the delaminated area of the composite plate.
- The import analysis function available in Abaqus has been proven to be a viable method used in integrating the FE impact analysis together with the CAI strength prediction analysis. However, due to the fact that the impact analysis is a quasi-static analysis simulated by prescribing a displacement to the impactor, an intermediate step has to be implemented to release all the stresses in the impacted FE model and to return the out-of-plane displacement of the laminate to zero, retaining only the damage information such as the matrix cracks,

delaminations and fiber failure. This would prevent global buckling of the laminate in the CAI strength prediction step.

7.2 Recommendations and future work

The recommendations for future research are summarized below:

- In the integrated FE analysis presented in this thesis, an intermediate step in which the stresses and out-of-plane displacement are reduced to zero was implemented. As a result, the impact damaged FE model on which the CAI test was performed contained only damage information such as the matrix cracks and delaminations, disregarding any permanent indentation that might be present in a real-case scenario. Post-impact permanent indentation has been successfully modeled by various researchers and presented in [66, 70, 176]. These models that could capture post-impact permanent indentation could be implemented in the current integrated FE model, in order for a more realistic impact damage and hence a more accurate value of CAI strength to be predicted.
- In the early stages of this research, a fiber kinking model proposed by Pinho et. al. [118, 134] was implemented in the FE model. However, the implementation of this fiber kinking model had no effect on the impact and CAI strength results. This is due to the fact that in this model, the fiber misalignment angle is deduced by solving an iterative equation involving X_C, and this would yield the same result as the direct usage of X_C in a failure criterion, which is used in the current model. In the current model, the material properties of the composite plies are degraded to zero once the material fails. However, this does

not accurately represent a real-case scenario of compressive failure since the failed material would still be able to carry and transfer some loads under compression. Hence, the FE model would tend to provide an under prediction of CAI strength. The amount of residual stress that a failed material can carry under compression is still uncertain, and further research could be carried out in this area to be implemented in the FE model to enable a higher accuracy of CAI strength prediction.

- In this study, the efficacy of the integrated FE model has been proven through qualitative comparisons of impact damage and CAI strengths with experiments. Subsequently, quantitative verification of the model could be performed by specifying the same impact energy used in experiments to the FE model. In order to do so, solid elements have to be employed and high computational costs would be incurred.
- This integrated FE model has the potential to be sufficiently versatile in terms of enabling users to study the effect of different impact parameters on the CAI strength and to better understand how each impact parameter affects the damage tolerance of composite laminates. For example, laminate parameters such as the thickness of the laminate, the boundary conditions and the ply sequence and impact parameters such as impact energy and impact location [82] could be varied and the resultant CAI strength predicted could be compared.

References

1. Papanicolaou, G.C. and C.D. Stavropoulos, *NEW APPROACH FOR RESIDUAL COMPRESSIVE STRENGTH PREDICTION OF IMPACTED CFRP LAMINATES.* Composites, 1995. **26**(7): p. 517-523.
2. Soutis, C. and P.T. Curtis, *Prediction of the post-impact compressive strength of CFRP laminated composites.* Composites Science and Technology, 1996. **56**(6): p. 677-684.
3. Kimpara, I. and H. Saito. *Integrated experimental characterization of post-impact fatigue behaviour of CFRP laminates*. in *The 9th Japan International SAMPE Symposium & Exhibition (JISSE-9)*. 29th Nov-2nd Dec 2005. Tokyo (Big Sight), Japan, S7-04.
4. Wang, H., P.H. Chen, and Z. Shen, *Experimental studies on compression-after-impact behavior of quasi-isotropic composite laminates.* Science and Engineering of Composite Materials, 1997. **6**(1): p. 19-35.
5. Ishikawa, T., *Some experimental findings in compression-after-impact (CAI) tests of CF/PEEK (APC-2) and conventional CF/epoxy flat plates.* Composites Science and Technology, 1995. **55**(4): p. 349-363.
6. Lee, J. and C. Soutis, *Prediction of impact-induced fibre damage in circular composite plates.* Applied Composite Materials, 2005. **12**(2): p. 109-131.
7. Bland, P.W. and J.P. Dear, *Observations on the impact behaviour of carbon-fibre reinforced polymers for the qualitative validation of models.* Composites Part a-Applied Science and Manufacturing, 2001. **32**(9): p. 1217-1227.
8. Siow, Y.P. and V.P.W. Shim, *An experimental study of low velocity impact damage in woven fiber composites.* Journal of Composite Materials, 1998. **32**(12): p. 1178-1202.
9. Xiong, Y., *A PREDICTION METHOD FOR THE COMPRESSIVE STRENGTH OF IMPACT DAMAGED COMPOSITE LAMINATES.* Composite Structures, 1995. **30**(4): p. 357-367.
10. Sekine, H., N. Hu, and M.A. Kouchakzadeh, *Buckling analysis of elliptically delaminated composite laminates with consideration of partial closure of delamination.* Journal of Composite Materials, 2000. **34**(7): p. 551-574.
11. Habib, F.A., *A new method for evaluating the residual compression strength of composites after impact.* Composite Structures, 2001. **53**(3): p. 309-316.
12. Mishra, A. and N.K. Naik, *Failure initiation in composite structures under low-velocity impact: Analytical studies.* Composite Structures, 2010. **92**(2): p. 436-444.

13. Rhead, A.T., R. Butler, and N. Baker, *Analysis and Compression Testing of Laminates Optimised for Damage Tolerance.* Applied Composite Materials, 2011. **18**(1): p. 85-100.
14. Chen, H.R. and X.N. Sun, *Residual compressive strength of laminated plates with delamination.* Composite Structures, 1999. **47**(1-4): p. 711-717.
15. Hu, N., Fukunaga, H., Sekine, H., Ali, K. M. *Compressive buckling of laminates with an embedded delamination.* Composites Science and Technology, 1999. **59**(8): p. 1247-1260.
16. Liu, D. and L.E. Malvern, *MATRIX CRACKING IN IMPACTED GLASS/EPOXY PLATES.* Journal of Composite Materials, 1987. **21**(7): p. 594-609.
17. Schultheisz, C.R. and A.M. Waas, *Compressive failure of composites .1. Testing and micromechanical theories.* Progress in Aerospace Sciences, 1996. **32**(1): p. 1-42.
18. Nguyen, M.Q., Elder, D. J., Bayandor, J., Thomson, R. S., Scott, M. L., *A review of explicit finite element software for composite impact analysis.* Journal of Composite Materials, 2005. **39**(4): p. 375-386.
19. Waas, A.M. and C.R. Schultheisz, *Compressive failure of composites .2. Experimental studies.* Progress in Aerospace Sciences, 1996. **32**(1): p. 43-78.
20. Malvern, L.E., N. Takeda, and R.L. Sierakowski, *Microscopic observations of cross sections of impacted composite laminates.* Journal of Composites Technology & Research, 1982. **4**(2): p. 40-44.
21. Gibson, R.F., *Principles of composite material mechanics*. 1994, New York: McGraw-Hill.
22. Baker, A., S. Dutton, and D. Kelly, *Composite materials for aircraft structures*. AIAA Education Series, ed. J.A. Schetz. 2004, Reston, VA: American Institute of Aeronautics and Astronautics.
23. Cantwell, W.J. and J. Morton, *The impact resistance of composite materials - a review.* Composites, 1991. **22**(5): p. 347-362.
24. Kumar, P. and B. Rai, *DELAMINATIONS OF BARELY VISIBLE IMPACT DAMAGE IN CFRP LAMINATES.* Composite Structures, 1993. **23**(4): p. 313-318.
25. Nakamura, T. and L.C. Wu, *Effects of ply-arrangement on compressive failure of layered structures.* Engineering Fracture Mechanics, 2000. **67**(5): p. 421-443.
26. Fawcett, A.J. *Damage tolerance and the composite airframe*. [cited 2012 5.5.]; Available from: http://www.niar.wichita.edu/niarworkshops/Portals/0/Thursday_1015_Fawcett.pdf.
27. de Freitas, M. and L. Reis, *Failure mechanisms on composite specimens subjected to compression after impact.* Composite Structures, 1998. **42**(4): p. 365-373.

28. Donadon, M.V., Iannucci, L., Falzon, B. G., Hodgkinson, J. M., de Almeida, S. F. M., *A progressive failure model for composite laminates subjected to low velocity impact damage.* Computers & Structures, 2008. **86**(11-12): p. 1232-1252.
29. Davies, G.A.O. and R. Olsson, *Impact on composite structures.* Aeronautical Journal, 2004. **108**(1089): p. 541-563.
30. Abrate, S., *Impact on Laminated Composite Materials.* Applied Mechanics Reviews, 1991. **44**(4): p. 155-190.
31. Kortschot, M.T. and C.J. Zhang, *CHARACTERIZATION OF COMPOSITE MESOSTRUCTURES AND DAMAGE BY DE-PLY RADIOGRAPHY.* Composites Science and Technology, 1995. **53**(2): p. 175-181.
32. Christensen, R.M. *Failure Theory for Materials Science and Engineering*. 18.11.2010 [cited 2011 05.01]; Available from: www.failurecriteria.com.
33. Richardson, M.O.W. and M.J. Wisheart, *Review of low-velocity impact properties of composite materials.* Composites Part a-Applied Science and Manufacturing, 1996. **27**(12): p. 1123-1131.
34. Lee, S.-W.R. and C.T. Sun, *A Quasi-Static Penetration Model for Composite Laminates.* Journal of Composite Materials, 1993. **27**(3): p. 251-271.
35. Cui, W.C. and M.R. Wisnom, *A COMBINED STRESS-BASED AND FRACTURE-MECHANICS-BASED MODEL FOR PREDICTING DELAMINATION IN COMPOSITES.* Composites, 1993. **24**(6): p. 467-474.
36. Liu, D.H., *IMPACT-INDUCED DELAMINATION - A VIEW OF BENDING STIFFNESS MISMATCHING.* Journal of Composite Materials, 1988. **22**(7): p. 674-692.
37. Iannucci, L., *Dynamic delamination modelling using interface elements.* Computers & Structures, 2006. **84**(15-16): p. 1029-1048.
38. Davies, G.A.O. and X. Zhang, *IMPACT DAMAGE PREDICTION IN CARBON COMPOSITE STRUCTURES.* International Journal of Impact Engineering, 1995. **16**(1): p. 149-170.
39. Sanchu-Saez, S., *Compression after impact of thin composite laminates.* Composites Science and Technology, 2005. **65**(13): p. 1911-1919.
40. Cartie, D.D.R. and P.E. Irving, *Effect of resin and fibre properties on impact and compression after impact performance of CFRP.* Composites Part a-Applied Science and Manufacturing, 2002. **33**(4): p. 483-493.
41. Bouvet, C., Castanie, B., Bizeul, M. , Barrau, J., *Low velocity impact modeling in laminate composite panels with discrete interface elements.* International Journal of Solids and Structures, 2009. **46**: p. 2809-2821.
42. Allix, O. and L. Blanchard, *Mesomodeling of delamination: towards industrial applications.* Composites Science and Technology, 2006. **66**(6): p. 731-744.

43. Baker, A.A., R. Jones, and R.J. Callinan, *DAMAGE TOLERANCE OF GRAPHITE EPOXY COMPOSITES.* Composite Structures, 1985. **4**(1): p. 15-44.
44. Jones, R., Paul, J., Tay, T. E., Williams, J. F., *ASSESSMENT OF THE EFFECT OF IMPACT DAMAGE IN COMPOSITES - SOME PROBLEMS AND ANSWERS.* Composite Structures, 1988. **10**(1): p. 51-73.
45. Zhou, G. and L.A. Rivera, *Investigation for the reduction of in-plane compressive strength in preconditioned thin composite panels.* Journal of Composite Materials, 2005. **39**(5): p. 391-422.
46. Hull, D. and Y.B. Shi, *DAMAGE MECHANISM CHARACTERIZATION IN COMPOSITE DAMAGE TOLERANCE INVESTIGATIONS.* Composite Structures, 1993. **23**(2): p. 99-120.
47. Boll, D.J., Bascom, W. D., Weidner, J. C., Murri, W. J., *A MICROSCOPY STUDY OF IMPACT DAMAGE OF EPOXY-MATRIX CARBON-FIBER COMPOSITES.* Journal of Materials Science, 1986. **21**(8): p. 2667-2677.
48. Srinivasan, K., Jackson, W. C., Smith, B. T., Hinkley, J. A., *CHARACTERIZATION OF DAMAGE MODES IN IMPACTED THERMOSET AND THERMOPLASTIC COMPOSITES.* Journal of Reinforced Plastics and Composites, 1992. **11**(10): p. 1111-1126.
49. Zhou, G., J.C. Lloyd, and J.J. McGuirk, *Experimental evaluation of geometric factors affecting damage mechanisms in carbon/epoxy plates.* Composites Part a-Applied Science and Manufacturing, 2001. **32**(1): p. 71-84.
50. Chaturvedi, S.K. and R.L. Sierakowski, *EFFECTS OF IMPACTOR SIZE ON IMPACT DAMAGE-GROWTH AND RESIDUAL PROPERTIES IN AN SMC-R50 COMPOSITE.* Journal of Composite Materials, 1985. **19**(2): p. 100-113.
51. Ishai, O. and A. Shragai, *EFFECT OF IMPACT LOADING ON DAMAGE AND RESIDUAL COMPRESSIVE STRENGTH OF CFRP LAMINATED BEAMS.* Composite Structures, 1990. **14**(4): p. 319-337.
52. Davies, G.A.O. and J. Ankersen, *Virtual testing of realistic aerospace composite structures.* Journal of Materials Science, 2008. **43**(20): p. 6586-6592.
53. Olsson, R., *Analytical model for delamination growth during small mass impact on plates.* International Journal of Solids and Structures, 2010. **47**(21): p. 2884-2892.
54. Abrate, S., *Modeling of impacts on composite structures.* Composite Structures, 2001. **51**(2): p. 129-138.
55. Gonzalez, E.V., Maimi, P., Camanho, P. P., Lopes, C. S., Blanco, N., *Effects of ply clustering in laminated composite plates under low-velocity impact loading.* Composites Science and Technology, 2011. **71**(6): p. 805-817.

56. Huang, K.Y., A. de Boer, and R. Akkerman, *Analytical Modeling of Impact Resistance and Damage Tolerance of Laminated Composite Plates.* Aiaa Journal, 2008. **46**(11): p. 2760-2772.
57. Williams, K.V. and R. Vaziri, *Application of a damage mechanics model for predicting the impact response of composite materials.* Computers & Structures, 2001. **79**(10): p. 997-1011.
58. Finn, S.R., Y.F. He, and G.S. Springer, *DELAMINATIONS IN COMPOSITE PLATES UNDER TRANSVERSE STATIC LOADS - EXPERIMENTAL RESULTS.* Journal of Reinforced Plastics and Composites, 1992. **11**(11): p. 1196-1238.
59. Finn, S.R. and G.S. Springer, *DELAMINATIONS IN COMPOSITE PLATES UNDER TRANSVERSE STATIC OR IMPACT LOADS - A MODEL.* Composite Structures, 1993. **23**(3): p. 177-190.
60. de Moura, M. and A.T. Marques, *Prediction of low velocity impact damage in carbon-epoxy laminates.* Composites Part a-Applied Science and Manufacturing, 2002. **33**(3): p. 361-368.
61. Choi, H.Y., R.J. Downs, and F.K. Chang, *A NEW APPROACH TOWARD UNDERSTANDING DAMAGE MECHANISMS AND MECHANICS OF LAMINATED COMPOSITES DUE TO LOW-VELOCITY IMPACT .1. EXPERIMENTS.* Journal of Composite Materials, 1991. **25**(8): p. 992-1011.
62. Choi, H.Y., H.Y.T. Wu, and F.K. Chang, *A NEW APPROACH TOWARD UNDERSTANDING DAMAGE MECHANISMS AND MECHANICS OF LAMINATED COMPOSITES DUE TO LOW-VELOCITY IMPACT .2. ANALYSIS.* Journal of Composite Materials, 1991. **25**(8): p. 1012-1038.
63. Saito, H., Morita, M., Kawabe, K., Kanesaki, M., Takeuchi, H., Tanaka, M., Kimpara, I.., *Effect of ply-thickness on impact damage morphology in CFRP laminates.* Journal of Reinforced Plastics and Composites, 2011. **30**: p. 1097-1106.
64. Lopes, C.S., Camanho, P. P., Gurdal, Z., Maimi, P., Gonzalez, E. V., *Low-velocity impact damage on dispersed stacking sequence laminates. Part II: Numerical simulations.* Composites Science and Technology, 2009. **69**(7-8): p. 937-947.
65. Lopes, C.S., Seresta, O., Coquet, Y., Gurdal, Z., Camanho, P. P., Thuis, B., *Low-velocity impact damage on dispersed stacking sequence laminates. Part I: Experiments.* Composites Science and Technology, 2009. **69**(7-8): p. 926-936.
66. Faggiani, A. and B.G. Falzon, *Predicting low-velocity impact damage on a stiffened composite panel.* Composites Part a-Applied Science and Manufacturing, 2010. **41**(6): p. 737-749.
67. Yokozeki, T., Kuroda, A., Yoshimura, A., Ogasawara, T., Aoki, T.., *Damage characterization in thin-ply composite laminates under out-of-plane transverse loadings.* Composite Structures, 2010. **93**: p. 49-57.

68. Aoki, Y., H. Suemasu, and T. Ishikawa, *Damage propagation in CFRP laminates subjected to low velocity impact and static indentation.* Advanced composite materials, 2007. **16**: p. 45-61.
69. Sun, C.T. and C.J. Jih, *Quasi-static modeling of delamination crack propagation in laminates subjected to low-velocity impact.* Composites Science and Technology, 1995. **54**: p. 185-191.
70. Abdallah, E.A., *Experimental analysis of damage creation and permanent indentation on highly oriented plates.* Composites Science and Technology, 2009. **69**(7-8): p. 1238-1245.
71. Whitcomb, J.D., *Analysis of a laminate with a postbuckled embedded delamination.* Journal of Composite Materials, 1992. **26**: p. 1523-1535.
72. Pavier, M.J. and M.P. Clarke, *Finite element prediction of the post-impact compressive strength of fibre composites.* Composite Structures, 1996. **36**(1-2): p. 141-153.
73. Suemasu, H., T. Irie, and T. Ishikawa, *Buckling and post-buckling behavior of composite plates containing multiple delaminations.* Journal of Composite Materials, 2009. **42**: p. 191-202.
74. Obdrzalek, V. and J. Vrbka, *On the applicability of simple shapes of delaminations in buckling analyses.* Composites Part B-Engineering, 2011. **42**(3): p. 538-545.
75. Craven, R., L. Iannucci, and R. Olsson, *Delamination buckling: A finite element study with realistic delamination shapes, multiple delaminations and fibre fracture cracks.* Composites Part a-Applied Science and Manufacturing, 2010. **41**(5): p. 684-692.
76. Dost, E.F., L.B. Icewicz, and J.H. Goose, *Sublaminate stability based modeling of impact-damaged composite laminates.* 3rd Tech. Conf. of Am. Soc. for Composites, 1988. **Technical Publication Co.** : p. 354-363.
77. Shivakumar, K.N. and J.D. Whitcomb, *BUCKLING OF A SUBLAMINATE IN A QUASI-ISOTROPIC COMPOSITE LAMINATE.* Journal of Composite Materials, 1985. **19**(1): p. 2-18.
78. Avery, W.B., *A semi-discrete approach to modeling post-impact compression strength of composite laminates.* In: Proc. of 21st Inter. SAMPE Technical Conference, 1989: p. 141-151.
79. Kassapoglou, C., *Compression strength of composite sandwich structures after barely visible impact damage.* Journal of Composites Technology & Research, 1996. **18**(4): p. 274-284.
80. Gottesman, T., *RESIDUAL STRENGTH OF IMPACTED COMPOSITES - ANALYSIS AND TESTS.* Journal of Composites Technology & Research, 1994. **16**(3): p. 244-255.
81. Chen, P.H., Z. Shen, and J.Y. Wang, *A new method for compression after impact strength prediction of composite laminates.* Journal of Composite Materials, 2002. **36**(5): p. 589-610.

82. Malhotra, A., F.J. Guild, and M.J. Pavier, *Edge impact to composite laminates: experiments and simulations.* Journal of Materials Science, 2008. **43**(20): p. 6661-6667.
83. Breen, C., F. Guild, and M. Pavier, *Impact damage to thick carbon fibre reinforced plastic composite laminates.* Journal of Materials Science, 2006. **41**(20): p. 6718-6724.
84. Short, G.J., F.J. Guild, and M.J. Pavier, *Delaminations in flat and curved composite laminates subjected to compressive load.* Composite Structures, 2002. **58**(2): p. 249-258.
85. Short, G.J., F.J. Guild, and M.J. Pavier, *Post-impact compressive strength of curved GFRP laminates.* Composites Part a-Applied Science and Manufacturing, 2002. **33**(11): p. 1487-1495.
86. Kim, S.J., N.S. Goo, and T.W. Kim, *The effect of curvature on the dynamic response and impact-induced damage in composite laminates.* Composites Science and Technology, 1997. **57**(7): p. 763-773.
87. Palazotto, A., *IMPACT RESPONSE OF GRAPHITE EPOXY CYLINDRICAL PANELS.* Aiaa/Asme/Asce/Ahs/Acs 32nd Structures, Structural Dynamics, and Materials Conference, a Collection of Technical Papers,, Pts 1-4: Pt 1 : Materials, Engineering Optimization, Works in Progress ; Pt 2, Structures and Design ; Pts 3-4 : Structural Dynamics, 1991: p. 1130-1136.
88. Reddy, Y.S.N. and J.N. Reddy, *LINEAR AND NONLINEAR FAILURE ANALYSIS OF COMPOSITE LAMINATES WITH TRANSVERSE-SHEAR.* Composites Science and Technology, 1992. **44**(3): p. 227-255.
89. Turvey, G.J. and M.Y. Osman, *EXACT AND APPROXIMATE LINEAR AND NONLINEAR INITIAL FAILURE ANALYSIS OF LAMINATED MINDLIN PLATES IN FLEXURE*. Composite Structures 5, ed. I.H. Marshall. 1989. 133-171.
90. Sandhu, R.S., *A survey of failure theories of isotropic and anisotropic materials.* Technical Report, AFFDL-TR-72-71.
91. Jenkins, C.F., *Report on materials of construction used in aircraft and aircraft engines.* Great Britain Aeronautical Research Committee, 1920.
92. Waddoups, M.E., *Advanced composite material mechanics for the design and stress analyst.* General Dynamics, Fort Worth Division Report FZM-4673, Fort Worth, TX, 1967.
93. Hart-Smith, L.J., *Predictions of the original and truncated maximum-strain failure models for certain fibrous composite laminates.* Composites Science and Technology, 1998. **58**(7): p. 1151-1178.
94. Hart-Smith, L.J., *Predictions of a generalized maximum-shear-stress failure criterion for certain fibrous composite laminates.* Composites Science and Technology, 1998. **58**(7): p. 1179-1208.
95. Hill, R., *A theory of the yielding and plastic flow of anisotropic materials.* Proceedings of the Royal Society of London, Series A, 1948. **193**: p. 281-297.

96. Azzi, V.D. and S.W. Tsai, *Anisotropic strength of composites.* Experimental Mechanics, 1965. **5**(9): p. 283-288.
97. Hoffman, O., *The brittle strength of orthotropic materials.* Journal of Composite Materials, 1967. **1**: p. 200-206.
98. Tsai, S.W. and E.M. Wu, *A general theory of strength for anisotropic materials.* Journal of Composite Materials, 1971. **5**(1): p. 58-80.
99. Gol'denblat, I.I. and V.A. Kopnov, *Strength of glass reinforced plastics in the complex stress state.* Polymer Mechanics, 1966. **1**: p. 56-60.
100. Hashin, Z., *Analysis of composite materials- a survey.* Journal of Applied Mechanics, 1983. **50**: p. 481-505.
101. Wu, E.M., *Optimal experimental measurements of anisotropic failure tensors.* Journal of Composite Materials, 1972. **6**: p. 472-489.
102. Tsai, S.W. and H.T. Hahn, *Introduction to composite materials*. 1980, Lancaster, PA: Technomic Publishing Co.
103. Hashin, Z. and A. Rotem, *A fatigue failure criterion for fiber-reinforced materials.* Journal of Composite Materials, 1973. **7**: p. 448-464.
104. Rotem, A. and Z. Hashin, *Failure modes of angle ply laminates.* Journal of Composite Materials, 1975. **9**: p. 191-206.
105. Hashin, Z., *Failure criteria for unidirectional fiber composites.* Journal of Applied Mechanics, 1980. **47**: p. 329-334.
106. Sandhu, R.S., *Non-linear behaviour of unidirectional and angle ply laminates.* AIAA Journal of Aircraft, 1974. **13**: p. 104-111.
107. Wolfe, W.E. and T.S. Butalia, *A strain-energy based failure criterion for non-linear analysis of composite laminates subjected to biaxial loading.* Composites Science and Technology, 1998. **58**(7): p. 1107-1124.
108. Butalia, T.S. and W.E. Wolfe, *A strain-energy-based non-linear failure criterion: comparison of numerical predictions and experimental observations for symmetric composite laminates.* Composites Science and Technology, 2002. **62**(12-13): p. 1697-1710.
109. Huang, H.S., G.S. Springer, and R.M. Christensen, *Predicting failure in composite laminates using dissipated energy.* Journal of Composite Materials, 2003. **37**(23): p. 2073-2099.
110. Lee, J.D., *Three dimensional finite element analysis of damage accumulation in composite laminate.* Computers & Structures, 1982. **15**(3): p. 335-350.
111. Ochoa, O.O. and J.J. Engblom, *ANALYSIS OF PROGRESSIVE FAILURE IN COMPOSITES.* Composites Science and Technology, 1987. **28**(2): p. 87-102.
112. Bakuckas Jr., J.G., *Computational methodology to predict damage growth in unidirectional composites-I. Theoretical formulation and numerical implementation.* Engineering Fracture Mechanics, 1995. **52**(5): p. 937-951.
113. Mahishi, J.M. and D.F. Adams, *Micromechanical predictions of crack initiation, propagation, and crack growth resistance in*

boron/aluminium composites. Journal of Composite Materials, 1982. **16**: p. 457-469.
114. Tan, S.C., *A PROGRESSIVE FAILURE MODEL FOR COMPOSITE LAMINATES CONTAINING OPENINGS.* Journal of Composite Materials, 1991. **25**(5): p. 556-577.
115. Pal, P. and C. Ray, *Progressive failure analysis of laminated composite plates by finite element method.* Journal of Reinforced Plastics and Composites, 2002. **21**(16): p. 1505-1513.
116. Prusty, B.G., *Progressive failure analysis of laminated unstiffened and stiffened composite panels.* Journal of Reinforced Plastics and Composites, 2005. **24**(6): p. 633-642.
117. Tan, S.C. and J. Perez, *PROGRESSIVE FAILURE OF LAMINATED COMPOSITES WITH A HOLE UNDER COMPRESSIVE LOADING.* Journal of Reinforced Plastics and Composites, 1993. **12**(10): p. 1043-1057.
118. Pinho, S.T., L. Iannucci, and P. Robinson, *Physically based failure models and criteria for laminated fibre-reinforced composites with emphasis on fibre kinking. Part II: FE implementation.* Composites Part a-Applied Science and Manufacturing, 2006. **37**(5): p. 766-777.
119. Vinson, J.R. and R.L. Sierakowski, *The behavior of structures composed of composite materials*. 1987, Dordrecht: Martinus Nijhoff Publishers.
120. Greif, R. and E. Chapon, *INVESTIGATION OF SUCCESSIVE FAILURE MODES IN GRAPHITE EPOXY LAMINATED COMPOSITE BEAMS.* Journal of Reinforced Plastics and Composites, 1993. **12**(5): p. 602-621.
121. Kim, Y., J.F. Davalos, and E.J. Barbero, *Progressive failure analysis of laminated composite beams.* Journal of Composite Materials, 1996. **30**(5): p. 536-560.
122. Reddy, Y.S. and J.N. Reddy, *Three-dimensional finite element progressive failure analysis of composite laminates under axial tension.* Journal of Composites Technology & Research, 1993. **15**(2): p. 73-87.
123. Tan, S.C. and R.J. Nuismer, *A THEORY FOR PROGRESSIVE MATRIX CRACKING IN COMPOSITE LAMINATES.* Journal of Composite Materials, 1989. **23**(10): p. 1029-1047.
124. Shokrieh, M.M. and L.B. Lessard, *Progressive fatigue damage modeling of composite materials, part I: Modeling.* Journal of Composite Materials, 2000. **34**(13): p. 1056-1080.
125. Shokrieh, M.M. and L.B. Lessard, *Progressive fatigue damage modeling of composite materials, part II: Material characterization and model verification.* Journal of Composite Materials, 2000. **34**(13): p. 1081-1116.
126. Tserpes, K.I., P. Papanikos, and T. Kermanidis, *A three-dimensional progressive damage model for bolted joints in composite laminates subjected to tensile loading.* Fatigue & Fracture of Engineering Materials & Structures, 2001. **24**(10): p. 663-675.

127. Reddy, Y.S.N., C.M.D. Moorthy, and J.N. Reddy, *Non-linear progressive failure analysis of laminated composite plates.* International Journal of Non-Linear Mechanics, 1995. **30**(5): p. 629-649.
128. Talreja, R., *A CONTINUUM-MECHANICS CHARACTERIZATION OF DAMAGE IN COMPOSITE-MATERIALS.* Proceedings of the Royal Society of London Series a-Mathematical Physical and Engineering Sciences, 1985. **399**(1817): p. 195-216.
129. Talreja, R., *TRANSVERSE CRACKING AND STIFFNESS REDUCTION IN COMPOSITE LAMINATES.* Journal of Composite Materials, 1985. **19**(4): p. 355-375.
130. Ladeveze, P. and E. Ledantec, *DAMAGE MODELING OF THE ELEMENTARY PLY FOR LAMINATED COMPOSITES.* Composites Science and Technology, 1992. **43**(3): p. 257-267.
131. Coutellier, D. and P. Rozycki, *Multi-layered multi-material finite element for crashworthiness studies.* Composites Part a-Applied Science and Manufacturing, 2000. **31**(8): p. 841-851.
132. Johnson, A.F., *Modelling fabric reinforced composites under impact loads.* Composites Part a-Applied Science and Manufacturing, 2001. **32**(9): p. 1197-1206.
133. Williams, K.V., R. Vaziri, and A. Poursartip, *A physically based continuum damage mechanics model for thin laminated composite structures.* International Journal of Solids and Structures, 2003. **40**(9): p. 2267-2300.
134. Pinho, S.T., L. Iannucci, and P. Robinson, *Physically-based failure models and criteria for laminated fibre-reinforced composites with emphasis on fibre kinking: Part I: Development.* Composites Part a-Applied Science and Manufacturing, 2006. **37**(1): p. 63-73.
135. Krueger, R., *The virtual crack closure technique: history, approach and applications.* NASA/CR-2002-211628, 2002.
136. Camanho, P.P., C.G. Dávila, and D.R. Ambur, *Numerical simulation of delamination growth in composite materials.* NASA/TP-2001-211041, 2001.
137. Davidson, B.D., *AN ANALYTICAL INVESTIGATION OF DELAMINATION FRONT CURVATURE IN DOUBLE CANTILEVER BEAM SPECIMENS.* Journal of Composite Materials, 1990. **24**(11): p. 1124-1137.
138. Dugdale, D., *Yielding of steel sheets containing slits.* Journal of the Mechanics and Physics of Solids, 1960. **8**(2): p. 100-104.
139. Barenblatt, G.N., *The mathematical theory of equilibrium cracks in brittle fracture.* Advances in applied mechanics, 1962. **7**.
140. Tay, T.E., *Characterization and analysis of delamination fracture in composites: An overview of developments from 1990 to 2001.* Applied Mechanics Reviews, 2003. **56**(1): p. 1-32.

141. Schellekens, J.C.J. and R. De Borst, *On the numerical modelling of edge delamination in composites.* Key engineering materials, 1996. **120-121**: p. 131-160.
142. Collombet, F., J. Bonini, and J.L. Lataillade, *A three-dimensional modelling of low velocity impact damage in composite laminates.* International Journal for Numerical Methods in Engineering, 1996. **39**(9): p. 1491-1516.
143. Lo, D.C., *Modelling of damage evolution in thick laminates subjected to low velocity impact.* Mechanics of Thick Composites, Applied Mechanics Division ASME Summer Annual Meeting, 1993. **AMD-Vol 162**: p. 137-150.
144. Li, D.S. and M.R. Wisnom, *MODELING DAMAGE INITIATION AND PROPAGATION IN COMPOSITES USING INTERFACE ELEMENTS*. Computer Aided Design in Composite Material Technology Iv, ed. W.R. Blain and W.P. deWilde. 1994. 213-220.
145. Wisheart, M. and M.O.W. Richardson, *The finite element analysis of impact induced delamination in composite materials using a novel interface element.* Composites Part a-Applied Science and Manufacturing, 1998. **29**(3): p. 301-313.
146. *Abaqus Analysis User's Manual*. Version 6.10 2011.
147. Chang, F.K. and K.Y. Chang, *A PROGRESSIVE DAMAGE MODEL FOR LAMINATED COMPOSITES CONTAINING STRESS-CONCENTRATIONS.* Journal of Composite Materials, 1987. **21**(9): p. 834-855.
148. Ridha, M., C.H. Wang, and T.E. Tay, *Modelling complex progressive failure in notched composite laminates with varying stacking sequences (Unpublished)*. 2013.
149. Tay, T.E., *Progressive failure analysis of composites.* Journal of Composite Materials, 2008. **42**(18): p. 1921-1966.
150. Camanho, P.P., C.G. Davila, and S.T. Pinho, *Fracture analysis of composite co-cured structural joints using decohesion elements.* Fatigue & Fracture of Engineering Materials & Structures, 2003. **27**: p. 745-757.
151. Benzeggagh, M.L. and M. Kenane, *Measurement of mixed-mode delamination fracture toughness of unidirectional glass/epoxy composites with mixed-mode bending apparatus.* Composites Science and Technology, 1996. **56**(4): p. 439-449.
152. Brewer, J.C. and P.A. Lagace, *QUADRATIC STRESS CRITERION FOR INITIATION OF DELAMINATION.* Journal of Composite Materials, 1988. **22**(12): p. 1141-1155.
153. Graca-e-Costa, R., *A non-iterative approach for the modelling of quasi-brittle materials.* International Journal of Fracture, 2012. **178**(1-2): p. 281-298.
154. Alfano, G. and M.A. Crisfield, *Finite element interface models for the delamination analysis of laminated composites: Mechanical and*

computational issues. International Journal for Numerical Methods in Engineering, 2001. **50**(7): p. 1701-1736.
155. Yokozeki, T., T. Ogasawara, and T. Ishikawa, *Nonlinear behavior and compressive strength of unidirectional and multidirectional carbon fiber composite laminates.* Composites Part a-Applied Science and Manufacturing, 2006. **37**(11): p. 2069-2079.
156. Davidson, B.D. and F.O. Sediles, *Mixed-mode I-II-III delamination toughness determination via a shear-torsion-bending test.* Composites Part a-Applied Science and Manufacturing, 2011. **42**(6): p. 589-603.
157. Turon, A., *An engineering solution for mesh size effects in the simulation of delamination using cohesive zone models.* Engineering Fracture Mechanics, 2007. **74**(10): p. 1665-1682.
158. Camanho, P.P., C.G. Davila, and M.F.S.F. De Moura, *Numerical simulation of mixed-mode progressive delamination in composite materials.* Journal of Composite Materials, 2003. **37**(16): p. 1415-1438.
159. Hojo, M., *Mode I delamination fatigue properties of interlayer-toughened CF/epoxy laminates.* Composites Science and Technology, 2006. **66**(5): p. 665-675.
160. Guild, F.J., P.J. Hogg, and J.C. Prichard, *A MODEL FOR THE REDUCTION IN COMPRESSION STRENGTH OF CONTINUOUS FIBER COMPOSITES AFTER IMPACT DAMAGE.* Composites, 1993. **24**(4): p. 333-339.
161. Las, V. and R. Zemcik, *Progressive damage of unidirectional composite panels.* Journal of Composite Materials, 2008. **42**(1): p. 25-44.
162. Li, C.F., *Low-velocity impact-induced damage of continuous fiber-reinforced composite laminates. Part 1. An FEM numerical model.* Composites Part a-Applied Science and Manufacturing, 2002. **33**(8): p. 1055-1062.
163. Hitchen, S.A. and R.M.J. Kemp, *The effect of stacking sequence on impact damage in a carbon fiber/epoxy composite.* Composites, 1995. **26**: p. 207-214.
164. Amaro, A.M., *The influence of boundary conditions on low-velocity impact composite damage.* Strain, 2011. **47**: p. 220-226.
165. Fuossa, E., P.V. Straznicky, and C. Poon, *Effects of stacking sequence on the impact resistance in composite laminates- Part 1: Parametric study.* Composite Structures, 1998. **41**: p. 67-77.
166. Hoppel, C.P.R. and S.J. De Teresa, *Effect of angle-ply orientation on compression strength of composite laminates.* 15th U.S. Army Symposium on Solid Mechanics, Myrtle beach, SC, April 12-14, 1999. **UCRL-JC-131920**.
167. !!! INVALID CITATION !!!
168. Saito, H., *Effect of ply-thickness on impact damage morphology in CFRP laminates.* Journal of Reinforced Plastics and Composites, 2011. **30**(13): p. 1097-1106.

169. Yokozeki, T., Y. Aoki, and T. Ogasawara, *Experimental characterization of strength and damage resistance properties of thin-ply carbon fiber/toughened epoxy laminates.* Composite Structures, 2007. **82**: p. 382-389.
170. Sihn, S., *Experimental studies of thin-ply laminated composites.* Composites Science and Technology, 2007. **67**: p. 996-1008.
171. Stavropoulos, C.D. and G.C. Papanicolaou, *Effect of thickness on the compressive performance of ballistically impacted carbon fibre reinforced plastic (CFRP) laminates.* Journal of Materials Science, 1997. **32**: p. 931-936.
172. Hong, S. and D. Liu, *ON THE RELATIONSHIP BETWEEN IMPACT ENERGY AND DELAMINATION AREA.* Experimental Mechanics, 1989. **29**(2): p. 115-120.
173. Hwang, S.F. and C.P. Mao, *Failure of delaminated carbon/epoxy composite plates under compression.* Journal of Composite Materials, 2001. **35**: p. 1634-1653.
174. Suemasu, H., *A numerical study on compressive behavior of composite plates with multiple circular delaminations considering delamination propagation.* Composites Science and Technology, 2008. **68**: p. 2562-2567.
175. Gonzalez, E.V., *Simulation of drop-weight impact and compression after impact tests on composite laminates.* Composite Structures, 2012. **94**(11): p. 3364-3378.
176. Bouvet, C., S. Rivallant, and J.J. Barrau, *Low velocity impact modeling in composite laminates capturing permanent indentation.* Composites Science and Technology, 2012. **72**(16): p. 1977-1988.